A NUMERICAL BOUNDARY INTEGRAL EQUATION METHOD FOR TRANSIENT MOTIONS

Thesis by

David Martin Cole

In Partial Fulfillment of the Requirements

for the Degree of

Doctor of Philosophy

California Institute of Technology

Pasadena, California

1980

(Submitted May 28, 1980)

ACKNOWLEDGEMENTS

It is nearly impossible to state the extent to which I have been influenced by the various people with whom I have worked and played as a graduate student. A list of these people would certainly fill several pages. Rather than compiling such an inventory, I would like to thank the past and present faculty and students of the Caltech Seismological Laboratory, a community of scientists, scholars, teachers and friends, for their support and inspiration during the years that I have spent there.

My associations with Bernard Minster and David Harkrider have been especially valuable to me. Dan Kosloff introduced me to the ideas of numerical analysis and was involved in the initial stages of this work.

Donna Lathrop did an excellent job of typing the difficult material presented here.

Financial support was provided in part by the National Science Foundation under contract number EAR-7622624. Additional support was provided by the Advanced Research Projects Agency of the Department of Defense and was monitored by the Air Force Office of Scientific Research under contract number F49620-77-C-0022.

ABSTRACT

This thesis presents the results of a study of a numerical technique for the solution of initial-boundary value problems of linear elastodynamics. The numerical method is based on a boundary integral equation (BIE) formulation of the mechanics of bodies of arbitrary shape. These integral equations are discretized and a time stepping technique is used to solve the resulting system of linear algebraic equations.

The theoretical basis of the continuous problem and the general interpolation and discretization scheme are described in Chapter 1. The problem is then specialized to the two-dimensional case of antiplane strain and most subsequent calculations and discussions take place in this context. The performance of the numerical method depends entirely on the interpolation scheme used, and on the manner in which boundary shapes are approximated.

The consequences of particular interpolation schemes for boundary value problems on a half-plane are discussed in Chapter 2. The results of several numerical calculations are compared with exact, or much more accurate solutions. This chapter also presents a comparison of the performance of the numerical BIE method with the performance of other specialized numerical procedures which have been used previously for problems of this nature. The BIE method yields results which are as accurate, or more accurate than the other methods for given discretization parameters.

The method is applied to basic boundary value problems for curved symmetric and nonsymmetric boundaries in Chapter 3. The

solutions obtained there are again compared to more accurate or exact solutions produced by independent methods. The general dependence of errors on discretization parameters is discussed.

Chapter 4 gives the solution of a problem in which a Love wave propagates through a limited region of laterally varying structure. The time stepping nature of the BIE method makes feasible certain rearrangements of the numerical equations which yield a representation of the mechanical system in which the incident, unperturbed Love wave arises as an inhomogeneous term. Solution of this localized numerical equation then yields an intermediate variable, the change in the traction boundary value of the layered space surface, which is used to evaluate the scattered displacement wave.

The performance characteristics and unusual properties of the time stepping BIE method are summarized in the General Summary. The appendices deal with several subjects. Appendix A gives an evaluation of singular integrals arising in the general continuous integral equation formulation. Appendix B gives a body force equivalent of nonequilibrium static initial values. Appendix C discusses the convergence and stability of solutions obtained using a particular interpolation scheme. Appendix D contains FORTRAN subroutines used in evaluating discrete kernels for the antiplane strain case. Appendix E gives the solution to a diffraction problem which is used to evaluate errors in a BIE solution of the same problem which is given in Chapter 3.

TABLE OF CONTENTS

		Page
ACKNOWLEDGEMENTS		ii
ABSTRACT		iii
GENERAL INTRODUCTION		1
Chapter 1.	THE BIE FORMALISM	10
	1. Introduction	10
	2. Analytic Boundary Integral Equations	13
	3. Numerical Approximation of the BIE	20
Chapter 2.	ANTIPLANE STRAIN TRACTION INTERPOLATION	26
	1. Introduction	26
	2. A Simple Traction Interpolator	35
	3. Comparison to Other Methods	62
Chapter 3.	GENERAL BOUNDARY SHAPES IN ANTIPLANE STRAIN	72
	1. Introduction	72
	2. Diffraction by a Circular Cavity	80
	3. Evaluation of Tractions on a Circle	92
	4. Evaluation of Tractions on Nonsymmetric Boundary	95
Chapter 4.	LOVE WAVE WITH TOPOGRAPHY	108
	1. Introduction	108
	2. Analytic Composite BIE	114
	3. Numerical Composite BIE	123
	4. Numerical Representation of Topography	132
	5. Solution Processes	139
	6. Solution for a Rectangle	141
GENERAL SUMMARY		151
REFERENCES		157
APPENDIX A	EVALUATION OF SINGULAR INTEGRALS	162
APPENDIX B	TREATMENT OF INITIAL VALUES	168
APPENDIX C	CONVERGENCE OF D_o FOR THE FUNDAMENTAL BOUNDARY VALUE PROBLEMS FOR THE HALF PLANE	173

Page

APPENDIX D ALGEBRAIC RELATIONS FOR CALCULATING DISCRETE KERNELS 185

APPENDIX E DIFFRACTED SH WAVES DUE TO A LINE SOURCE ON A CIRCULAR CAVITY WALL. 195

GENERAL INTRODUCTION

The increasing use of seismic wave modeling techniques for investigations of earth structure, seismic risk assessment, and mineral exploration has emphasized the inadequacies in currently available mathematical methods for dealing with wave propagation problems in irregular media. One area in which the need for new and more versatile tools is particularly pronounced is the situation in which waves encounter material irregularities of size approximately equal to the incident wavelengths.

The well-developed finite difference and finite element methods provide a means of solving some of these problems. These techniques have the advantages that they are limited in accuracy only by the grid size used, they are not restricted to a narrow class of materials, and computer software already exists for general types of applications. They have some inherent limitations, in that it is not feasible to use them to model wave propagation over distances very large compared to the wavelengths of interest. This is due to limitations of computer size and speed, and the dispersive properties of the numerical schemes. There are also difficulties in the accurate representation of material boundaries (cf., Boore (1970)).

Methods based on geometric ray theory are useful in cases where the wavelengths are fairly short (Hong (1978)). They are not applicable when the wavelengths are of the same size as the irregular body. There is also a considerable problem in the calculation of ray paths. Methods based on the Kirchhoff formulae (Berryhill (1979),

Scott and Helmberger (1980)) may give an improvement over ray methods for longer wavelengths. They have the fundamental limitation that unknown boundary values are estimated on the basis of analogy with ray theory, rather than by calculation.

The numerical method presented here is intended to provide an alternative problem solving approach which is complementary to currently used analytic wave propagation theories. The propagation problems to which the method is applicable may, in a broad sense, be considered as scattering problems. This problem class includes the interaction of specified waves with a small number of localized irregularities. The waves may propagate in a homogeneous medium or they may propagate in waveguides. The method is applicable over a broad range of periods. It is limited at the short period end of the seismic spectrum by economic considerations.

The technique is based on a formulation in which the propagation properties of the medium are represented by Green's tensors, the responses of the medium to concentrated forces. As such, it is readily combined with analytic methods which use Green's solutions to evaluate waves emanating from sources in a regular structure. The numerical method discussed here falls naturally into the class of boundary integral equation (BIE) methods (Cruse and Rizzo (1975)). These techniques formulate the laws of motion of linear continua as multi-dimensional linear integral equations over the boundaries of continuous bodies. The kernels in these integral equations are Green's functions of the partial differential equations governing the motion of the medium

and they usually possess integrable singularities. The unknown and specified dynamic variables appearing in the integral equations are the natural boundary values for the problem considered. In the case of elastodynamics these are the boundary values of displacement and traction.

The method considered here differs in a fundamental way from previous developments on this topic because of the nature the Green's function used. The integral equations are solved using a time stepping method, thus the kernels of the integral equations are solutions of hyperbolic systems of partial differential equations and possess propagating singularities. Previous BIE calculations have mainly involved equations with kernels which are Green's solutions for elliptic or parabolic partial differential equations, and the kernels are singular at only a single point. The presence of propagating singularities in the kernels has a significant effect on the overall structure of the method, particularly in the selection of interpolation schemes. It has been found that low order interpolation gives better numerical performance than high order interpolation. The opposite is true for kernels derived from parabolic or elliptic equations. This result may be understood by noting that low order interpolation in this case preserves the impulsive nature of the kernel, while still removing the singularities. It is necessary to average out the singularities of the kernels in some manner before any numerical calculations can be attempted.

Because the solution process is carried out in the time domain, the linear equations resulting from the discretization process have properties corresponding to the causality properties of the medium. For sufficiently short time steps the linear algebraic system may be solved by back-substitution. For any reasonable size of time step the bandwidth of the algebraic system is small.

Because the mechanical system is described by boundary integral equations, the number of spatial coordinates to be dealt with in a problem is smaller by one than the number of spatial coordinates required to describe the boundaries of homogeneous subregions of the medium. This reduces the number of dynamic variables in the problem, as compared with finite difference and finite element methods. This reduction in size of the numerical problem is partly illusory because the BIE formulation of the problem is not localized in time and space, i.e. large portions of the total time history of each dynamic variable are used in each time step of the solution process.

The time translation invariance of the governing system of differential equations appears in the analytic integral equation formulation. The integrals over time are of a convolution form. In the discretized equations these integrals become discrete convolutions and techniques developed for the manipulation and analysis of time series may sometimes be used to great advantage. If the medium possess spatial translation symmetries, discrete Fourier transform methods may also be applied spatially.

The simplicity of the solution method and the ability to economically manipulate the numerical operators make feasible extensive rearrangements of the discretized equations. By rearranging and partially solving the numerical equations one obtains the possibility of combining the numerical BIE technique with continuous analytic methods for problems involving localized irregularities. These rearrangements can generally be interpreted as the numerical calculation of Green's functions for a composite medium with particular boundary conditions, with the additional specialization that source and receiver points lie only on a particular material boundary.

An important disadvantage of the time domain BIE method is that it requires rather large amounts of computer storage for discrete kernels and dynamic variables. Some of the calculations described here required a megabyte or more of storage at some steps. This sort of calculation is most readily carried out on computers with large semiconductor memories and large amounts of virtual memory on disc. The BIE technique does not provide significantly improved accuracy, compared to finite difference or finite element methods. The rules of thumb applied to those methods are generally close to those which are applicable to the BIE method. It should be noted, however, that the techniques are fundamentally different in that the BIE method deals exclusively with boundary values as unknown quantities and thus comparisions of accuracy between BIE methods and volume gridding methods are not easily made. The strength of the method lies primarily in its simplicity and the ease of combination with analytic methods.

It can also be combined with the more general volume-gridding methods. No problems of this sort have been attempted here, but a few examples with BIEs corresponding to elliptic differential equations exist in the literature (cf., Zienkiewicz (1977), Chapter 23).

Chapter 1 consists of a description of the general elastodynamic BIE for continuous variables and an introduction to the interpolation and discretization method for the antiplane strain case. Some general properties of the discrete system of equations are discussed there. Appendix A discusses the treatment of singular integrals in the analytic equations. Appendix B discusses modifications of the analytic formulae which are necessary for the use of nonequilibrium static initial values.

Chapter 2 contains a detailed discussion of the motivation for the traction interpolator used here. The traction interpolator which has been found to give the best all around results is the simplest possible. It is piecewise constant in space and time. This chapter gives a quantitative evaluation of the errors encountered in the solution of displacement or traction boundary value problems on a half plane. It also contains a comparison of the performance of the BIE technique with other more specialized numerical methods of treating these problems. The stability of convergence of the method for these problems is discussed in Appendix C.

Chapter 3 discusses the motivation behind the choice of displacement interpolators used here and has numerical examples which indicate the performance of the method for symmetric and nonsymmetric

curved boundaries. A particularly important problem in this chapter involves the solution of a diffraction problem around a circular cavity. The analytic solution is nontrivial and it is discussed in detail in Appendix E. The successful numerical solution of the problem requires the accurate cancellation of disturbances which may be thought of as propagating acausally across the interior of the cavity. This problem is considered to be a sensitive test of the method. The errors due to poor approximation of boundary shapes are discussed here. It is shown that, while the errors may be large at sharp corners, accurate results may still be obtained along portions of the boundary which are well represented. Possible improvements to the displacement interpolator are suggested on the basis of results from this chapter.

Chapter 4 deals with a practical problem in seismology, the interaction of Love waves with a finite length step increase in the thickness of the surface layer. The relationship between the analytic mode theory of the guided wave and the analytic and numerical BIE representations of the medium is discussed in detail. The system of numerical BIEs is then rearranged into a form in which the incident Love wave, which develops in the uniformly layered portion of the medium, appears as a separate inhomogeneous term of a composite BIE. An analytically evaluated waveform is substituted for this term. The remaining steps to reach a solution are straightforward. This problem serves to illustrate the ease with which the BIE method can be integrated with available analytic methods for the solution of problems

to which neither is applicable alone. Methods for treating related lateral heterogeneity problems are suggested.

A General Summary is included which gives a synopsis of the performance characteristics and unusual properties of the antiplane strain BIE technique. It also gives suggestions for extension of the method to other problems.

This thesis has some important omissions. There is no attempt to treat here the general analytic theory of elastodynamic BIEs. Some of the theory of integral equations for time harmonic motions is given in textbooks on potential theory and integral equations. Kupradze (1963) gives proofs of the uniqueness and existence of solutions for integral equations closely related to the time harmonic elastic BIEs. It is assumed here that solutions to the time domain integral equations exist, are unique and are exactly equivalent to solutions which can be obtained from partial differential equation formulations. There is no evidence to the contrary of which the author is aware.

A more important omission is the complete absence of truly elastic numerical calculations. All numerical examples given deal with two-dimensional SH, or antiplane strain, motions. Since mode conversions between dilatational and shear waves occur only at material boundaries in piecewise homogeneous media, the requirements of accuracy of the numerical method may be greater for the general elastic case than the interpolation method presented here can satisfy.

No mixed-type boundary value problems are discussed here. The time domain BIE method is particularly well suited for the solution of fracture propagation problems. A number of numerical experiments in this area have been carried out for mode III cracks and the ability of the technique to mimic analytic solutions to representative problems has been partially verified.

Chapter 1

THE BIE FORMALISM

1. Introduction

Many of the boundary value problems in geophysics and engineering involve bodies whose geometries preclude the construction of analytical solutions. In such cases it is often necessary to resort to numerical techniques. The most commonly used numerical methods, finite differences and finite elements, require a computational grid which fills the solution domain and is fine enough to resolve the features of interest in the solution. Large domains place strong constraints on the resolution of solutions which may be achieved in practice.

Many problems of interest involve the solution of a system of linear partial differential equations for which a surface integral representation exists. In this form the solution at an interior point of a homogeneous body is written as a quadrature of the physically relevant boundary values, initial values, and interior sources with a singular solution of the system of differential equations. In general, the boundary values will not all be known, and unless the singular solution used coincides with the Green's tensor for the problem, such an integral representation is merely another statement of the problem.

Through a limiting process these integral representations may be converted into integral equations involving only the boundary values, initial values, and interior sources. This integral equation form is an equally valid statement of the problem and has the advantage that the only unknown quantities are boundary values, since the interior sources

and initial values are usually specified. The boundary value problem is formulated directly in terms of boundary values and the solution at interior points need not be considered, although it may be evaluated at these points directly from the integral representation, once the boundary integral equations (BIE) have been solved. In many geophysical modeling problems this is not necessary, since physical observations are often confined to boundaries.

The purpose of this chapter is to present a formalism for the reduction of the BIE for linear elastodynamics to algebraic relations among the boundary values at a finite set of space and time points. These algebraic relations can then be used in a time stepping algorithm to obtain approximate solutions for any boundary value—initial value problem involving the elastic body for which they were formulated.

The advantages of the BIE method lie primarily in the reduction of the number of spatial dimensions of the problem by one and by formulating the problem directly in terms of the boundary values. Since one discretizes only the boundary of the body, the number of unknown variables in the numerical problem is appropriately reduced and the problem of creating acceptable space filling three-dimensional grids is eliminated. In addition, an infinite homogeneous exterior domain may be included through a BIE on its interior surface; this is a "transparent" boundary condition. Infinite boundaries must still be truncated unless suitably vanishing Green's tensors are available.

Numerical BIE methods have been successfully applied to problems resulting from elliptic and parabolic type partial differential equa-

tions. These applications include problems from elastostatics, time harmonic elastodynamics, elastoplasticity, heat flow, electromagnetic scattering, and others. A representative collection of papers may be found in Cruse and Rizzo (1975). The BIE approach is generally found to be competitive with volume gridding methods for problems to which both are applicable. A few problems arising from hyperbolic differential equations have also been treated. Das (1976) and Das and Aki (1977) solve an elastodynamic BIE on a line in two-dimensional fracture dynamics problems. Mitzner (1967) and Friedman and Shaw (1962) treat two-dimensional problems with special boundary conditions. These studies use a time stepping approach, but do not consider a sufficiently general problem to be widely useful. Transient elastic wave propagation problems have been treated by Cruse (1968), solving elliptic BIE problems in the Laplace transform domain and inverting the Laplace transform to obtain time domain solutions. This approach does not take advantage of the causal properties of the time dependent Green's tensors and requires the solution of a full matrix equation for each value of the transform variable. The time domain approach taken here permits the development of an explicit stepping scheme and hence greater economy in the calculation of numerical solutions.

The remainder of this chapter consists of two sections. The second section contains a derivative of the time dependent displacement BIE for elastodynamics. In the third section a discretization scheme for the BIE is developed in the context of interpolation functions, and general features desired in an interpolation scheme are discussed for the antiplane strain case.

2. Analytic Boundary Integral Equations

The equations of motion of isotropic linearized elasticity are:

$$\rho \frac{\partial^2}{\partial t^2} u_i = \sigma_{ij,j} + f_i \tag{1.1}$$

$$\sigma_{ij} = C_{ijk\ell}\, u_{k,\ell} \tag{1.2}$$

$$C_{ijk\ell} = \lambda\delta_{ij}\delta_{k\ell} + \mu(\delta_{ik}\delta_{j\ell} + \delta_{i\ell}\delta_{jk})$$

Here λ and μ are the Lamé constants, ρ is the density, and σ_{ij} are the Cartesian stress components. δ_{ij} is the Kronecker delta, and summation over repeated indices is assumed unless otherwise indicated. $\underline{f}$ is the body force density, and $u_{k,\ell} = \partial/\partial x_\ell\, u_k$.

Consider the motion of a homogeneous body B with interior B' and piecewise Liapunov boundary ∂B (e.g., Kupradze, 1963, p. 86) with normal $\underline{n}$ for times $t \geq 0$. The body forces $\underline{f}$, and initial values $\underline{u}(\underline{r},t)$ and $\partial/\partial t\ \underline{u}(\underline{r},t)$ at $t = 0$ are specified for $\underline{r} \in B$. In addition, there will be conditions which the boundary values $\underline{u}(\underline{r},t)$ and $\underline{\tau}(\underline{r},t) = \underline{\underline{\sigma}} \cdot \underline{n}$ at $\underline{r} \in \partial B$ must satisfy. (For a well-posed problem these conditions will not specify $\underline{u}$ and $\underline{\tau}$ completely.)

A fundamental solution $G_{ij}(\underline{r},t;\underline{r}_o,t_o)$ of equation (1.1) is defined by

$$\rho \frac{\partial^2}{\partial t_o^2} G_{ij} = C_{ipqs}\, G_{qj,s_o p_o} + \delta_{ij}\, \delta(t-t_o)\delta(\underline{r}-\underline{r}_o) \tag{1.3}$$

for $\underline{r}$, $\underline{r}_o \in B'$, where $f_{,s_o}$ denotes differentiation with respect to the s_o-component of $\underline{r}_o$, the source coordinate. $\underline{\underline{G}}$ also has the causality property

$$G_{ij}(\underline{r},t;\underline{r}_o,t_o) \equiv 0 \ , \quad \alpha(t-t_o) < |\underline{r}-\underline{r}_o| \tag{1.3a}$$

and the time translation property

$$G_{ij}(\underline{r},t+t_1;\underline{r}_o,t_o+t_1) = G_{ij}(\underline{r},t;\underline{r}_o,t_o) \tag{1.3b}$$

where $\alpha = ((\lambda+2\mu)/\rho)^{1/2}$ and $\beta = (\mu/\rho)^{1/2}$ are the compressional and shear wave velocities, respectively.

From equations (1.1) and (1.3) one may obtain (see e.g., de Hoop, 1958 or Archambeau and Minster, 1977. Wheeler and Sternberg, 1968, give a precise treatment.)

$$\begin{aligned} \underline{u}(\underline{r},t) = & \int_{t_o=0}^{\infty} \oint_{\partial B} \{\underline{\underline{G}}\cdot\underline{\tau}(\underline{r}_o,t_o) - \underline{u}(\underline{r}_o,t_o)\cdot\underline{\underline{K}}\cdot\underline{n}\}\, dS_o dt_o \\ & + \int_B \rho \left\{\underline{\underline{G}}\cdot\frac{\partial}{\partial t_o}\underline{u}(\underline{r}_o,t_o) - \underline{u}\cdot\frac{\partial}{\partial t_o}\underline{\underline{G}}\right\}\Bigg|_{t_o=0} dV_o \\ & + \int_{t_o=0}^{\infty}\int_B \underline{\underline{G}}\cdot\underline{f}(\underline{r}_o,t_o)dV_o dt_o \end{aligned} \tag{1.4}$$

for $\underline{r} \in B'$. If $r \notin B$, the left-hand side of equation (1.4) is zero. Here, $\underline{n}(\underline{r}_o)$ and dS_o are the outward normal and surface elements of ∂B at $\underline{r}_o$, dV_o is the volume element, and $K_{ijk} = C_{ijrs}G_{rk,s}$ is the stress field associated with $\underline{\underline{G}}$. $\underline{u}\cdot\underline{\underline{K}}\cdot\underline{n} = u_i K_{ijk} n_j \hat{e}_k$.

The second integral in equation (1.4) contains the influence of initial values and the third gives the effect of body forces acting in B'. These two integrals are assumed to be known, and will henceforth be represented by the vector $\underline{F}(r,t)$, which can often be interpreted as an

"infinite space" solution to the body force–initial value problem. A brief discussion of analytic methods for simplifying initial value problems is given in Appendix B. The first integral contains the effect of the boundary values $\underline{u}$ and $\underline{\tau}$ and is of primary interest here, since the boundary values will be regarded as the basic unknown quantities in the problem; if they were known, the displacement at a point $\underline{r} \in B'$ could be calculated directly from equation (1.4).

If $\underline{r} \to \partial B$ in equation (1.4), one obtains an integral equation over ∂B and $t > 0$ involving only the boundary values $\underline{u}$ and $\underline{\tau}$ and the known vector $\underline{F}$. In doing this there is a difficulty arising from the singularities of $\underline{\underline{G}}$ as $\underline{r} \to \underline{r}_0$. Before evaluating the contribution of the singularities to the surface integrals, it is necessary to become more specific about the choice of $\underline{\underline{G}}$.

Up to this point the only restrictions placed on $\underline{\underline{G}}$ are those provided by equations (1.3, 1.3a, and 1.3b) which apply in B'. These conditions are insufficient to uniquely specify $\underline{\underline{G}}$ in B, although equation (1.4) holds for any tensor satisfying them. In particular, they are insufficient to uniquely specify the singularities of $\underline{\underline{G}}$ as $\underline{r} \to \underline{r}_0$ for $\underline{r}_0 \in \partial B$, since they do not exclude solutions of equation (1.3) which contain image sources outside B. In the numerical examples to follow, the infinite space Green's tensor is used for $\underline{\underline{G}}$, so the BIE derived here will use that tensor. This choice is arbitrary and for some problems it may be advantageous to use other tensors. For example, Das and Aki (1977) use a half-plane Green's tensor, and their BIE is of a slightly different form from that obtained here.

The infinite space Green's tensor is (Wheeler and Sternberg, 1968)

$$4\pi\rho G_{ij}(\underline{r},t;\underline{r}_o,0) = \left\{\frac{3y_iy_j}{y^3} - \frac{\delta_{ij}}{y}\right\}\int_{1/\alpha}^{1/\beta} p\delta(t-py)dp$$

$$+ \frac{y_iy_j}{y^3}\left[\frac{1}{\alpha^2}\delta(t-y/\alpha) - \frac{1}{\beta^2}\delta(t-y/\beta)\right]$$

$$+ \frac{\delta_{ij}}{y\beta^2}\delta(t-y/\beta) \qquad (1.4a)$$

where $y_i = x_{i_o} - x_i$, $y = |\underline{y}|$.

The associated stress field is

$$4\pi K_{ijk} = 4\pi C_{ijrs}G_{rk,s_o}$$

$$= -6\beta^2\left[\frac{5y_iy_jy_k}{y^5} - \frac{\delta_{ij}y_k + \delta_{ik}y_j + \delta_{jk}y_i}{y^3}\right]\int_{1/\alpha}^{1/\beta} p\delta(t-py)dp$$

$$+ 2\left[\frac{6y_iy_jy_k}{y^5} - \frac{\delta_{ij}y_k + \delta_{ik}y_j + \delta_{jk}y_i}{y^3}\right]\left[\delta(t-y/\beta) - \left(\frac{\beta}{\alpha}\right)^2\delta(t-y/\alpha)\right]$$

$$+ 2\frac{y_iy_jy_k}{y^4\beta}\left[\dot{\delta}(t-y/\beta) - \left(\frac{\beta}{\alpha}\right)^3\dot{\delta}(t-y/\alpha)\right]$$

$$- \frac{y_k\delta_{ij}}{y^3}\left[1 - 2\left(\frac{\beta}{\alpha}\right)^2\right]\left[\delta(t-y/\alpha) + \frac{y}{\alpha}\dot{\delta}(t-y/\alpha)\right]$$

$$- \frac{\delta_{ik}y_j + \delta_{jk}y_i}{y^3}\left[\delta(t-y/\beta) + \frac{y}{\beta}\dot{\delta}(t-y/\beta)\right] \qquad (1.4b)$$

As $y \to 0$, $\underline{\underline{G}}$ and $\underline{\underline{K}}$ become infinite and asymptotically behave like sums of functions of the form $y^{-n}(\frac{\partial}{\partial t})^m \delta(t)$, with $n = 2,1,0,-1\cdots$ and $m = 0,1,2\cdots$.

We will evaluate the contributions of the singularities in equation (1.4) as $\underline{r} \to \underline{r}_1 \in \partial B$ by isolating the singularity and replacing the full integrals over ∂B by their principal values. Let $C(\underline{r}_1,\varepsilon)$ be a cylinder of radius ε centered on $\underline{r}_1$ with generator parallel to $\underline{n}(\underline{r}_1)$ (see Figure 1.1a). The intersection of ∂B with $C(\underline{r}_1,\varepsilon)$ is a disc about $\underline{r}_1$ denoted by $S(\underline{r}_1,\varepsilon)$. The first term of the surface integral in equation (1.4) may be written as the sum of an integral over $S(\underline{r}_1,\varepsilon)$ and an integral over the remainder of ∂B:

$$\lim_{\underline{r}\to\underline{r}_1 \in \partial B} \oint_{\partial B} \underline{\tau}(\underline{r}_0,t_0) \cdot \underline{\underline{G}}(\underline{r},t;\underline{r}_0,t_0)dS_0$$

$$= \lim_{\underline{r}\to\underline{r}_1} \left\{ \int_{S(\underline{r}_1,\varepsilon)} \underline{\tau} \cdot \underline{\underline{G}}\, dS_0 + \int_{\partial B - S(\underline{r}_1,\varepsilon)} \underline{\tau} \cdot \underline{\underline{G}}\, dS_0 \right\}$$

and likewise for the displacement integral. As $\varepsilon \to 0$, the second integral on the right becomes a principal value and the first gives the contribution of the singularity. The singular parts of the integrals are then the ordered limits

$$S\underline{\tau}(\underline{r}_1,t) = \lim_{\varepsilon\to 0} \lim_{\underline{r}\to\underline{r}_1} \int_{t_0=0}^{\infty} \int_{S(\underline{r}_1,\varepsilon)} \underline{\underline{G}}(\underline{r},t;\underline{r}_0,t_0)$$

$$\cdot \underline{\tau}(\underline{r}_0,t_0)dS_0dt_0 \qquad (1.5)$$

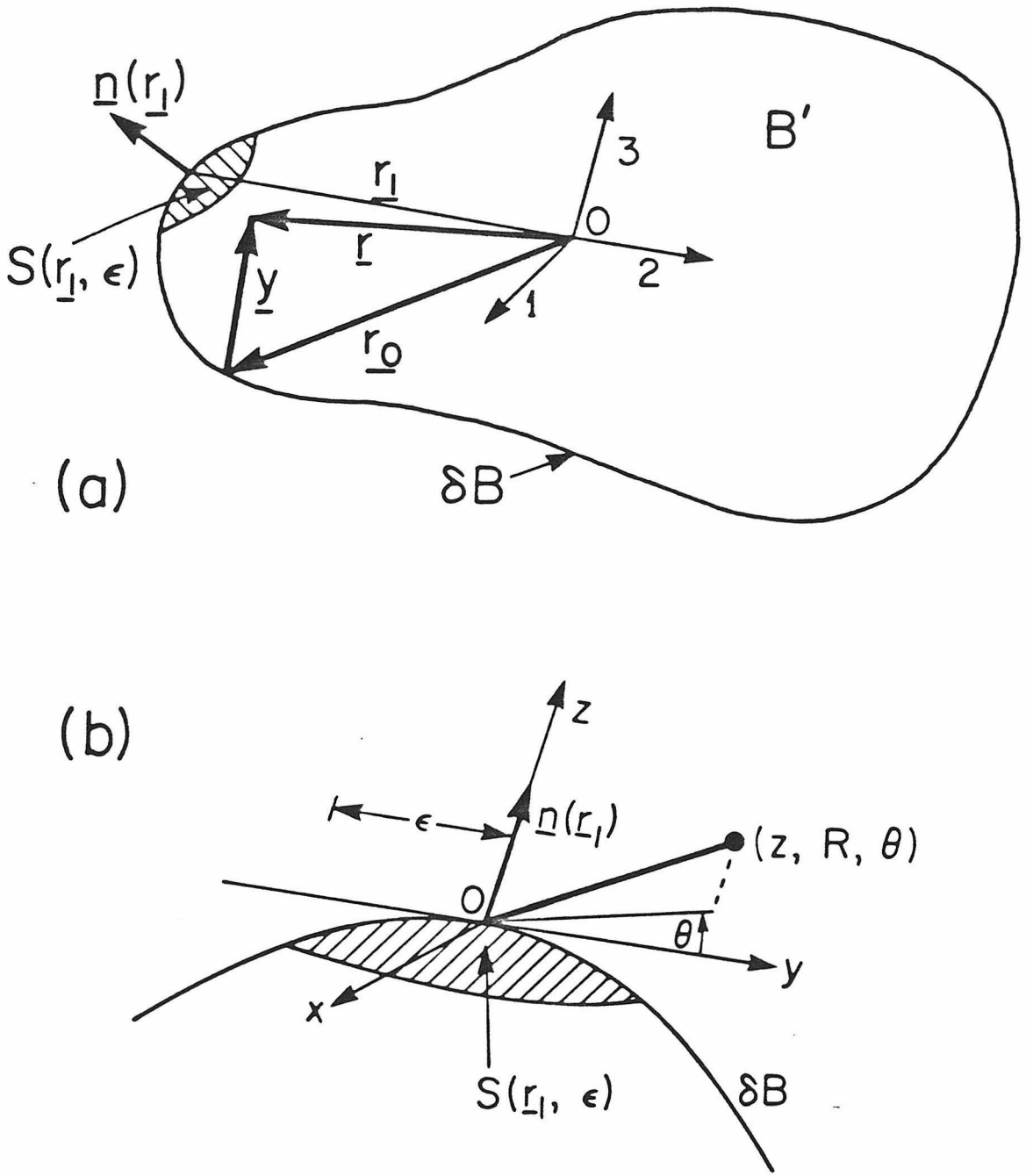

Figure 1.1. (a) A homogeneous elastic body B with surface B. The cap $S(\underline{r}_1, \epsilon)$ contains the singular part of a surface integral and is described in the local coordinate system (b).

$$S\underline{u}(\underline{r}_1,t) = \lim_{\varepsilon\to 0} \lim_{\underline{r}\to\underline{r}_1} \int_{t_o=0}^{\infty} \int_{S(\underline{r}_1,\varepsilon)} \underline{u}(\underline{r}_o,t_o)\cdot\underline{\underline{K}}(\underline{r},t;\underline{r}_o,t_o) \cdot \underline{n}(\underline{r}_o)dS_o dt_o \tag{1.6}$$

It is shown in Appendix A that

$$S\underline{\tau}(\underline{r}_1,t) = 0$$

$$S\underline{u}(\underline{r}_1,t) = -\frac{1}{2}\,\underline{u}(\underline{r}_1,t)$$

if ∂B is sufficiently smooth at $\underline{r}_1$, and $\underline{u}$ and $\underline{\tau}$ also satisfy smoothness conditions at $\underline{r}_1$. Hence, the BIE is

$$\frac{1}{2}\,\underline{u}(\underline{r},t) = \int_{t_o=0}^{\infty} P \int_{\partial B} \{\underline{\tau}\cdot G - \underline{u}\cdot\underline{\underline{K}}\cdot\underline{n}\}dS_o t_o + \underline{F}(\underline{r},t) \tag{1.7}$$

for $t \geq 0$, $\underline{r} \in \partial B$, where $\underline{\underline{G}}$ and $\underline{\underline{K}}$ are the infinite space Green's tensor and its associated stress field. It might be noted that this equation is also valid for any tensor whose singularities are the same as those treated in ∂B here, and which satisfies equations (1.3), (1.3a), and (1.3b) in the interior B'.

Two-dimensional problems may be considered as a special case of equation (1.7) by carrying out the integration on the right side of equation (1.7) over the translation axis. The two-dimensional BIE is of the same form and, in particular, the effect of the singularity in modifying the form of the equation is exactly the same.

In general, one will wish to solve equation (1.7) for $\underline{u}$ or $\underline{\tau}$, or both subject to some constraint, for $\underline{r} \in \partial B$ and $t > 0$. For example, if B is to be in contact with another medium, the boundary conditions of continuous tractions and displacements across ∂B might be applied and the equations of motion of the contacting medium provide a constraint on $\underline{u}$ and $\underline{\tau}$ in equation (1.7). For a piecewise homogeneous linear elastic region one may obtain a set of coupled equations like equation (1.7) over the various boundaries of the medium. The coupling of the equations takes place at common boundaries of the homogeneous subregions. For mixed type boundary value problems in which some components of $\underline{u}$ and/or $\underline{\tau}$ are explicitly given at each point of ∂B, equation (1.7) would be solved for the unknown components at each point.

3. Numerical Approximation of the BIE

We now wish to approximate the BIE (1.7) for $\underline{r} \in \partial B$, $t \in [0,T]$ by a finite system of algebraic equations amenable to solution by digital computers. This will be done by restricting the set of functions admitted as approximate solutions of equation (1.7) to superpositions from a finite set of functions and by applying equation (1.7) at only a finite number of points sufficient to yield a solution for the expansion coefficients.

The development in this section will be specialized to the two-dimensional case of antiplane strain which is simpler because only one component each of displacement and traction is nonzero. The generalization of this formalism to the plane strain and three-dimensional cases is straightforward. For the antiplane strain case:

$$u_1 = u_2 \equiv 0$$

$$\sigma_{11} = \sigma_{22} = \sigma_{33} = \sigma_{12} \equiv 0$$

$$u_3 = u(x_1, x_2, t)$$

$$\underline{\tau} = \underline{\underline{\sigma}} \cdot \underline{n} = \hat{e}_3 \tau(x_1, x_2, t)$$

Equations (1.1) and (1.2) then reduce to

$$\rho \frac{\partial^2}{\partial t^2} u = \mu(u_{,11} + u_{,22}) + f(x_1, x_2, t) \tag{1.8}$$

The infinite space Green's function is

$$G(\underline{r}, t; \underline{r}_o, t_o) = \frac{1}{2\pi\mu} \frac{H(t-t_o - y/\beta)}{[(t-t_o)^2 - y^2/\beta^2]^{1/2}} \tag{1.8a}$$

$H(t)$ is the Heaviside function, β is the shear velocity, and

$$y = |\underline{r}_o - \underline{r}| = [(x_1 - x_{1o})^2 + (x_2 - x_{2o})^2]^{1/2}$$

The BIE is now on a curve ∂B in the x_1-x_2 plane:

$$\frac{1}{2} u(\underline{r}, t) = \int_{t_o=0}^{\infty} P \int_{\partial B} [G\tau(\underline{r}_o, t_o) - u\underline{K} \cdot \underline{n}] \, dS_o dt_o + F(\underline{r}, t) \tag{1.9}$$

Let $\partial B^* = \{\underline{r}_j, j=1, \cdots, J\} \varepsilon \partial B$ be a discrete set of points (nodes) and let $T_N^* = \{t_n; t_n = n\Delta t, n=1, \cdots, N\}$ be a set of equally spaced times with $t_N = T$. The approximations of displacements and tractions on ∂B are, respectively, $u^*(\underline{r}, t)$ and $\tau^*(\underline{r}, t)$. A convenient and intuitively useful way of representing u^* and τ^* is through interpolation functions:

$$u^*(\underline{r},t) = \sum_j \sum_n U_j^n(\underline{r},t)\ u_j^n \tag{1.10}$$

$$\tau^*(\underline{r},t) = \sum_j \sum_n T_j^n(\underline{r},t)\ \tau_j^n \tag{1.11}$$

where u_j^n and τ_j^n are the expansion coefficients. (The indices j and n in this section refer to nodes and times, and not to Cartesian components as in the previous section.) The expansion coefficients are intended to represent the boundary values through the conditions

$$U_j^n(\underline{r}_i,t_m) = \delta_{ij}\delta_{mn}$$

$$T_j^n(\underline{r}_i,t_m) = \delta_{ij}\delta_{mn}$$

for every $\underline{r}_i \in \partial B^*$, $t_m \in T_N^*$. Then

$$u^*(\underline{r}_i,t_m) = u_i^m \tag{1.11a}$$

$$\tau^*(\underline{r}_i,t_m) = \tau_i^m \tag{1.11b}$$

Substitution of u^* and τ^* for u and τ in equation (1.9) for each $\underline{r}_j \in \partial B^*$ and $t_n \in T_N^*$ yields a system of algebraic equations:

$$u_j^n = \sum_{m=1}^{N} \sum_{j=1}^{J} \{DG_{ji}^{nm}\ \tau_i^m - DK_{ji}^{nm}\ u_i^m\} + 2F(\underline{r}_j,t_n) \tag{1.12}$$

$$j=1,\cdots,J \quad ; \quad n=1,\cdots,N$$

where

$$DG_{ji}^{nm} = 2 \int_{t_o=0}^{\infty} P \int_{\partial B} G(\underline{r}_j,t_n;\underline{r}_o,t_o)\ T_i^m(\underline{r}_o,t_o)\ dS_o dt_o \tag{1.13}$$

$$DK_{ji}^{nm} = 2 \int_{t_o=0}^{\infty} P \int_{\partial B} \underline{n} \cdot \underline{\nabla}_o G(\underline{r}_j, t_n; \underline{r}_o, t_o)\, U_i^m(\underline{r}_o, t_o) dS_o dt_o \qquad (1.14)$$

In general, there will be J equations (1.12) and J boundary conditions for each time level n. The system of equations (1.12) will be solved by time stepping, i.e., set $n = 1$, solve for the unknown coefficients in (1.12), then set $n = 2, \cdots$. The nature of the algebraic system to be solved at each time step will be determined by the type of boundary condition used and by the interpolation scheme used. In particular, as will be seen, the overall scheme may be made implicit or explicit, depending on the type of interpolation and computational grid used.

At first sight it might appear that there are N^2J^2 discrete kernels DG_{ji}^{nm} and DK_{ji}^{nm} to be calculated. However, if the interpolation functions are assigned time translation properties similar to those of the Green's function, the number of discrete kernels required is NJ^2 in all cases. Suppose that

$$U_i^m(\underline{r},t) = U_i^{m+\ell}(\underline{r},t+\ell\Delta t)$$

$$T_i^m(\underline{r},t) = T_i^{m+\ell}(\underline{r},t+\ell\Delta t) \qquad (1.15)$$

Then from property (3b) of the Green's function one easily obtains

$$DG_{ji}^{nm} = DG_{ji}^{n+\ell\ m+\ell}$$

$$DK_{ji}^{nm} = DK_{ji}^{n+\ell\ m+\ell} \qquad (1.16)$$

Hereafter the upper (time) indices of DG_{ji}^{nm} will be written unambiguously as DG_{ji}^{n-m} and likewise for DK_{ji}^{n-m}. The causality properties of the Green's function also causes some of the discrete kernels to be zero; if it is required that

$$U_j^n(\underline{r},t) = 0 \qquad t < t_n - p\Delta t \quad \text{or} \quad |\underline{r}-\underline{r}_j| > a$$

$$T_j^n(\underline{r},t) = 0 \qquad t < t_n - q\Delta t \quad \text{or} \quad |\underline{r}-\underline{r}_j| > b \tag{1.17}$$

the discrete kernels will also be causal. Under these circumstances the interpolator U_j^n does not transmit information about the motion at $(\underline{r}_j,t_n)$ to points lying outside a semi-infinite spacetime cylinder of radius "a" centered on $\underline{r}_j$ with generator parallel to the time axis and extending from $t = \infty$ to $t = t_n - p\Delta t$. T_j^n is similarly causal. Then since $G(\underline{r},t;\underline{r}_o,t_o) \equiv 0$ for $\beta(t-t_o) < |\underline{r}-\underline{r}_o|$ one obtains the analogous relations

$$DK_{ji}^{n-m} = 0 \qquad n - m - p < (|\underline{r}_i-\underline{r}_j| + a)/\beta\Delta t$$

$$DG_{ji}^{n-m} = 0 \qquad n - m - q < (|\underline{r}_i-\underline{r}_j| + b)/\beta\Delta t \tag{1.18}$$

Relations such as equation (1.17) can thus be used to make the scheme implicit or explicit. For the three-dimensional case a similar result is obtained from the causality condition, equation (1.3a). If an infinite space three-dimensional Green's tensor is used, there is the possibility of an additional relation corresponding to quiescence after passage of the shear wave.

The properties represented by equations (1.16) and (1.18) are discrete analogs of the properties of the analytic Green's function. The spatial translation-rotation symmetries of the free space Green's function are not usually present in the discrete versions because the node numbering scheme will not in general correspond to uniform increments of distance, and because of the surface orientation involved in the integrals of equations (1.13) and (1.14). Exceptions to this exist, for example, in uniformly gridded planes and cylinders. In such cases the spatial symmetries of the discrete kernels permit the use of techniques associated with the discrete Fourier transform in carrying out algebraic manipulations.

The problem of creating an accurate method of solving antiplane elasticity problems is now reduced to the problem of selecting interpolation functions that cause solutions of equation (1.12) to represent accurately the motion of the body.

The process of selecting the interpolators U_j^n and T_j^n will be carried out in two stages. First, interpolation schemes for the traction will be discussed in Chapter 2. The results of this development will then be used to select an interpolator for the displacement in Chapter 3.

Chapter 2

ANTIPLANE STRAIN TRACTION INTERPOLATION

1. Introduction

In this chapter the problem of discretizing the antiplane strain BIE (1.9) is considered for the case of a half plane. Let B be the region $x_2 \geq 0$. ∂B is then the line $x_2 = 0$ and the analytic and discrete BIEs are, respectively,

$$u(x_1,t) = \frac{1}{\pi\mu} \int_{t_o=0}^{t} \int_{x_o=-\infty}^{\infty} \frac{H((t-t_o) - |x_1 - x_o|)/\beta}{[(t-t_o)^2 - (x_1-x_o)^2/\beta^2]^{\frac{1}{2}}}$$

$$\cdot \tau(x_o,t_o)\, dx_o\, dt_o + 2F(x_1,t) \qquad (2.1)$$

$$u_j^n = \sum_{m=1}^{N} \sum_{i} DG_{ji}^{n-m}\, \tau_i^m + 2F(\underline{r}_j,t_n) \qquad (2.2)$$

The displacement terms are absent from the right-hand sides for this geometry because $\underline{n}(\underline{r}_o) \cdot (\underline{r} - \underline{r}_o) = 0$ for $\underline{r},\underline{r}_o \in \partial B$.

This circumstance permits the investigation of the consequences of particular interpolation schemes for the tractions without the additional complication of interpolating the displacements. The conclusions regarding traction interpolation reached through a study of

(2.1) and (2.2) are expected to apply to any boundary whose local radius of curvature is much greater than the discretization length, if the discretization of the boundary is fairly uniform.

Before proceeding to the construction of the interpolator and the numerical operator DG^n_{ij} it is useful to note some features of the analytic equation (2.1) and previous efforts in treating the problems it represents numerically.

If the dependent variables are not a function of x_1, an analogy with the one-dimensional wave equation can be developed. In this case the integration over x_o may be carried out in (2.1) to give

$$u(t) = \frac{\beta}{\mu} \int_0^t \tau(t_o)\, dt_o + 2F(t) \tag{2.3}$$

In differential form this is

$$\frac{\partial}{\partial t} u = \frac{\beta}{\mu}\, \tau + 2\, \frac{\partial F}{\partial t} \tag{2.4}$$

For comparison, the one-dimensional wave equation in t and x_2 is (see 1.18)

$$\left(\frac{1}{\beta}\frac{\partial}{\partial t} + \frac{\partial}{\partial x_2}\right)\left(\frac{1}{\beta}\frac{\partial}{\partial t} - \frac{\partial}{\partial x_2}\right) u = \frac{1}{\mu}\, f(x_2,t) \tag{2.5}$$

If $f(x_2,t) = 0$ near $x_2 = 0$, the solution of (2.5) may be written as

$$u(x_2,t) = u^+(\beta t - x_2) + u^-(\beta t + x_2)$$

where u^- propagates toward the boundary from the region $x_2 > 0$ and u^+ propagates away from it. Therefore, near $x_2 = 0$

$$(\frac{1}{\beta}\frac{\partial}{\partial t} + \frac{\partial}{\partial x_2})u = \frac{2}{\beta}\frac{\partial}{\partial t}u^-(\beta t + x_2) \tag{2.6}$$

In (2.4) the traction τ may be identified as

$$\tau = -\mu\frac{\partial u}{\partial x_2}$$

(The outward normal is used in the definition of τ.) Thus, (2.4) may be rewritten at $x_2 = 0$ as

$$(\frac{1}{\beta}\frac{\partial}{\partial t} + \frac{\partial}{\partial x_2})u = \frac{2}{\beta}\frac{\partial}{\partial t}F \tag{2.7}$$

Now, the definition of F states that it is the displacement due to sources in B', i.e., the region $x_2 > 0$. Near $x_2 = 0$ F is a function of $t + x_2/\beta$ only so the quantities on the right of equations (2.6) and (2.7) must be the same. The BIE (2.3) may thus be identified as an integrated version of a factor of the wave equation (2.5).

The discrete version of the integrated equation (2.3) is:

$$u^n = \sum_{m=1}^{N} DG^{n-m}\ \tau^m + 2F(t_n) \tag{2.8}$$

where

$$DG^m = \sum_{j=-\infty}^{\infty} DG^m_{ji}$$

is assumed to be independent of j and $\tau^n = \tau^n_j$ does not depend on j, the spatial index.

If the BIE (2.2) is to accurately represent equation (2.1) its summed version (2.8) must accurately reproduce equation (2.3) for any interpolation scheme used. Furthermore, when (2.8) is solved for τ^n the result (2.4) must be accurately reproduced. Since we are interested in solving dynamic problems, this will be regarded as a fundamental requirement of any interpolation scheme.

The analogy with the wave equation may be extended to include two-dimensional waves. If equation (2.1) is Fourier transformed in the x_1 variable, we obtain

$$\hat{u}(k_1,t) = \frac{\beta}{\mu} \int_0^t J_0(k_1\beta(t-t_0))\, \hat{\tau}(k_1,t_0)\, dt_0 \qquad (2.9)$$

where

$$\hat{u}(k_1,t) = \int_{-\infty}^{\infty} e^{ik_1x}\, u(x_1,t)\, dx_1$$

and J_0 is the Bessel function of order zero (Gradshteyn and Ryzhik, p. 953, 8.411.8). The force term has been dropped for the moment. For

$k_1 = 0$ this equation simplifies to give (2.3). Upon carrying out a Fourier transform with respect to time, one obtains the transformed BIE

$$\hat{u}(k_1,\omega) = \frac{1}{[k_1^2 - \omega^2/\beta^2]^{\frac{1}{2}}} \frac{\hat{\tau}(k_1,\omega)}{\mu} \tag{2.10}$$

(Gradshteyn and Ryzhik, p. 730, 6.671.8-9).

For comparison the wave equation (1.8) may be transformed to give

$$-\frac{\omega^2}{\beta^2} \hat{u}(k_1,x_2,\omega) = (-k_1^2 + \frac{\partial^2}{\partial x_2^2}) \hat{u}(k_1,x_2,\omega) \tag{2.11}$$

or, in a factored form,

$$[\frac{\partial}{\partial x_2} - (k_1^2 - \omega^2/\beta^2)^{\frac{1}{2}}][\frac{\partial}{\partial x_2} + (k_1^2 - \omega^2/\beta^2)^{\frac{1}{2}}] \hat{u}(k_1,x_2,\omega) = 0 \tag{2.12}$$

Identifying $\hat{\tau}$ as $-\mu\, \partial/\partial x_2 \hat{u}$ in (2.10), the BIE may again be seen to be an integrated version of a factor of the equation of motion.

The solution of (2.9) for $\hat{\tau}(k_1,t)$ has been found by several authors (see Srivastava and Buschman (1977)). If $\hat{u}(k_1,t)$ has zero initial conditions and is sufficiently smooth the solution is:

$$\hat{\tau}(k_1,t) = \frac{\mu}{\beta} \int_0^t J_0\,(k_1\beta(t - t_o))\{(\frac{\partial^2}{\partial t_o^2} + k_1^2\beta^2)\, \hat{u}(k_1,t)\}\, dt_o \tag{2.13}$$

Inverting the transform over x_1, one obtains

$$\tau(x_1,t) = \frac{\mu}{\beta}\int_{t_o=0}^{t}\int_{x_o=-\infty}^{\infty}\frac{H(t-t_o-|x_1-x_o|/\beta)}{[(t-t_o)^2-(x_1-x_o)^2/\beta^2]^{\frac{1}{2}}}$$

$$\{(\frac{1}{\beta^2}\frac{\partial^2}{\partial t_o^{\,2}}-\frac{\partial^2}{\partial x_o^{\,2}})\,u(x_o,t_o)\}\,dx_o\,dt_o \qquad (2.14)$$

The causality properties of the integral equations are now apparent. The integral operator of (2.1) is nonlocal but it is causal, i.e., $u(x_1,t)$ depends only on the values of $\tau(x_o,t_o)$ in the region $|x_1 - x_o| \le \beta(t-t_o)$. This is the portion of ∂B inside the volume $|\underline{r} - \underline{r}_o| \le \beta(t-t_o)$ which is the spacetime region from which $(x_1,0,t)$ can receive signals propagating at velocity β. These causality properties are preserved in the inverted equation (2.14), which contains the same nonlocal integral operator as (2.1) combined with the local differential operator $(1/\beta^2)(\partial^2/\partial t_o^{\,2}) - (\partial^2/\partial x_o^{\,2})$. Because of these causality properties it seems reasonable to expect that a successful discretization of (2.1) is possible which does not greatly reduce the causal isolation of the node points $\underline{r}_j$.

In terms of interpolators for the tractions, it means that they can be highly localized in space and time. The use of low order interpolation schemes is of some advantage in the BIE approach since it

simplifies the task of calculating the discrete kernels defined in (1.13) and (1.14).

One situation in which equation (2.1) arises and a numerical approach to its solution is required is in the treatment of Mode III fracture propagation problems. In these problems, at each instant of time, the displacement u is specified along some portion of the line $-\infty < x_1 < \infty$ and the traction τ or some relationship between τ and u is specified elsewhere. The portions of the line on which the two boundary conditions apply change with time as the crack grows. Some analytic solutions to special problems of this type have been found (Kostrov (1966), Freund (1976)) but analytic methods to treat the general problem are not available.

Das (1977) treated problems of this type by discretizing (2.1) and time stepping. The approach taken there was somewhat different from the one used here. Rather than employing an interpolation formalism, the analytic kernel was smoothed for numerical use by integrating it twice in space. The line $-\infty < x_1 < \infty$ was divided into equally sized intervals and the displacements and tractions were taken to be constant over these intervals. The kernel was then integrated over the source interval and the receiver interval. The resulting discrete kernel was used to evaluate the traction or displacement on portions of the line on which they were not specified. The intended function of the discrete kernel in this case was exactly the same as the function of DG^n_{ij} in equation (2.2).

Another numerical treatment of Mode III fraction propagation problems has been given by Burridge (1969). In this case a less direct approach to the creation of a discrete kernel was taken. It was noted there that the convolutional inverse of the integral operator of (2.1) should, when convolved with itself, produce the differential operator $(1/\beta^2)(\partial^2/\partial t^2) - (\partial^2/\partial x^2)$. This may be readily verified by examination of the transformed version of equation (2.1) given by equation (2.10). This differential operator was discretized in a standard way and the causal square root of the operator was found algebraically. The resulting discrete operator was intended to serve the same purpose as the convolutional inverse of the discrete kernel DG^n_{ij} of equation (2.2).

The problem of finding discrete representations in the (x_1,x_2,t) domain of the factors of the wave equation (2.12) has received considerable attention in the seismic exploration literature. In this context the equation

$$\frac{\partial}{\partial x_2}\hat{u}(k_1,x_2,\omega) = i(\omega^2/\beta^2 - k_1^2)^{\frac{1}{2}}\,\hat{u}(k_1,x_2,\omega) \qquad (2.15)$$

is regarded as a means of extrapolating a wave field $u(x_1,\cdot,t)$ in one direction of x_2. One procedure for finding discrete representations of this equation is given by Claerbout (1976, chapter 10). In this development the square root of (2.15) is expanded in powers of (k_1/ω) to some finite order and the resulting expression is rearranged to be the transform of a purely differential equation by multiplying both

sides by a power of ω. This equation is then converted to a differential equation in (x_1,x_2,t) domain and discretized using difference operators.

A notable feature of this approach is that expansion of the square root of (2.15) in this manner involves the assumption that $|k_1/\omega| < 1$; that is, the waves are not travelling parallel to the x_1 axis. The various discretizations of (2.15) found by this method are known to be inaccurate for waves travelling parallel to the x_1 axis. In the case of fracture propagation with a straight crack, on the other hand, the wavefronts at the crack plane propagate parallel to the crack. The discretization of (2.15) as used in waveform extrapolation produces numerical operators which are not simple analogs of the discrete kernel DG^n_{ij} because of the use of a moving coordinate system, and the presence of differencing with respect to x_2. Nevertheless, it is possible to find discrete operators by the method of Claerbout which are directly comparable to DG^n_{ij}. Clayton and Engquist (1977) have applied Claerbout's discretization methods to the problem of reducing grid-edge reflections in finite difference calculations. In this case, the difference approximation of (2.15) were applied as boundary conditions for a finite difference grid. Minor modifications of the difference operators used in these calculations produce an operator directly comparable to DG^n_{ij}.

The methods of Burridge and Claerbout for finding numerical operators similar to DG^n_{ij}or its inverse involve the use of a local

differential operator as a starting point. Because of this these methods cannot be generalized in a simple way to produce analogs of DG^n_{ij} for a boundary of arbitrary shape. These numerical operators all have a common intent, however. Their purpose is to provide a relationship based on the equation of motion between $u(x_1,x_2,t)$ and $\partial/\partial x_2\ u(x_1,x_2,t)$ along a line x_2 = constant. Since the numerical operators are produced by different methods it is of considerable interest to see the results of their application to a common problem. This will be done after the development of an interpolator for the BIE method in the next section.

2. A Simple Traction Interpolator

The grid upon which (2.1) will be discretized will be taken to be uniformly spaced in x_1 and t. The node points are at $x_2 = 0$ and $x_1 = jL$. The discrete times are $t_n = n\Delta t$ (see Fig. 2.1). The grid parameter is denoted by the letter Q:

$$Q = \beta\Delta t/L \quad .$$

For this uniform grid the discrete kernels DG^n_{ij} will depend only on $|i-j|$. They will be renumbered as DG^n_{i-j}. The resulting BIE is a two-dimensional convolution equation

$$u^n_j = \sum_m \sum_i DG^{n-m}_{j-i}\ \tau^m_i + 2F(jL,n\Delta t) \qquad (2.16)$$

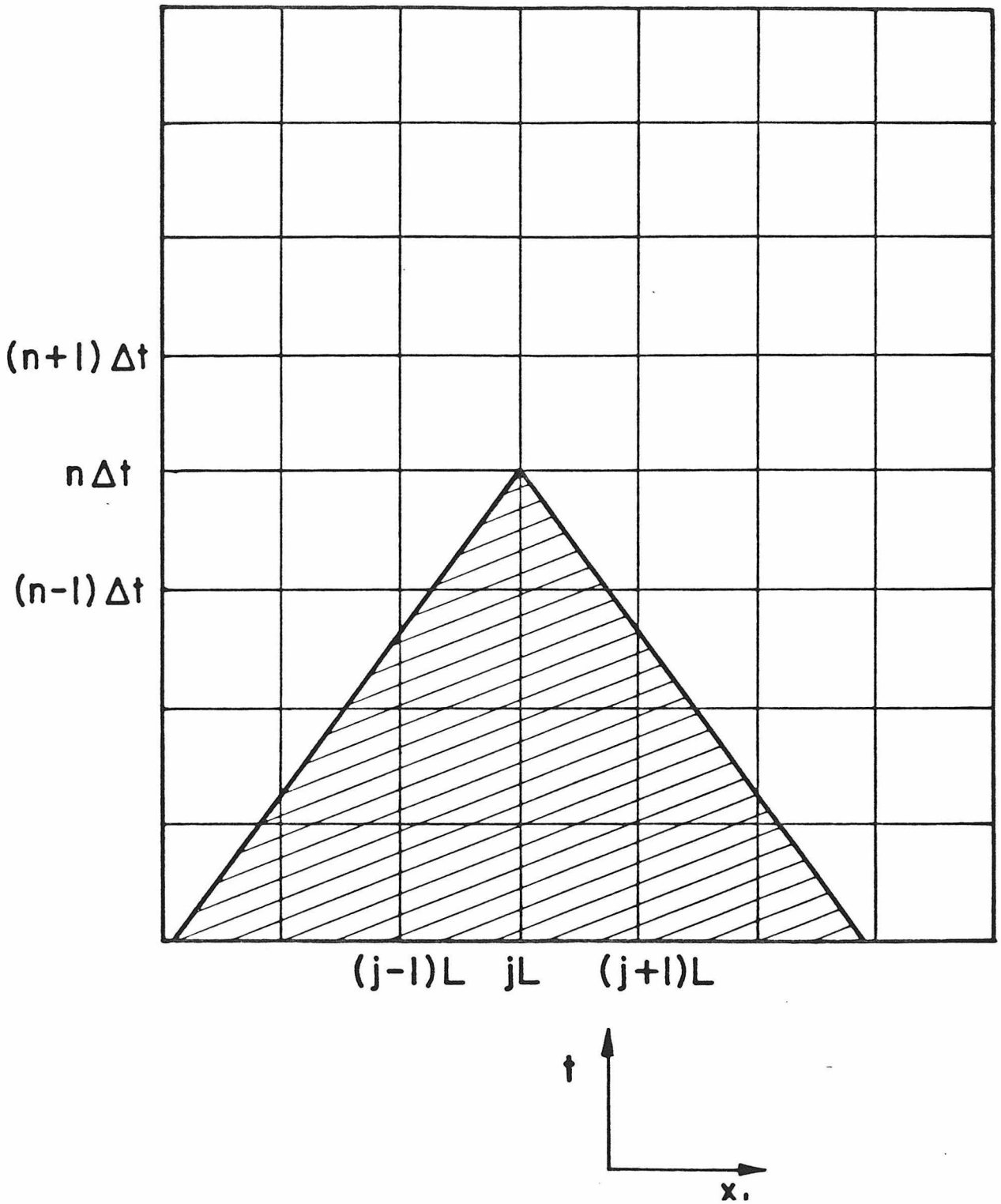

Figure 2.1. Space-time computational grid. The point ($n\Delta t$,jL) receives signals from the shaded area.

In view of the previous comments on localization, the spatial dependence of the interpolator $T_j^n(x_1,t)$ will be taken to be the simplest possible; piecewise constant on intervals $(j-\frac{1}{2})L < x_1 < (j+\frac{1}{2})L$. The interpolator $T_j^n(x_1,t)$ may then be written as

$$T_j^n(x_1,t) = \begin{cases} 0 \quad , & |x_1 - jL| > L/2 \\ T^n(t) \ , & |x_1 - jL| < L/2 \end{cases} \tag{2.17}$$

From (1.13) we have

$$DG_j^{n-m} = \frac{1}{\pi\mu} \int_{t_o=0}^{t_n} \int_{x_o=(j-\frac{1}{2})L}^{(J+\frac{1}{2})L} T^m(t_o) \frac{H(t_n - t_o - |x_o|/\beta)}{[(t_n - t_o) - x_o^2/\beta^2]^{\frac{1}{2}}} \, dx_o \, dt_o \tag{2.18}$$

From this formula it is found that for the piecewise constant spatial interpolator, or any other with the property that $\sum_{j=-\infty}^{\infty} T_j^n(x,t_o)$ is independent of x, the spatial sum of DG_j^n is (see equation 2.8)

$$DG^{n-m} = \frac{\beta}{\mu} \int_o^{t_n} T^m(t_o) \, dt_o \tag{2.19}$$

and so

$$u^n = \frac{\beta}{\mu} \int_o^{t_n} \sum_{m=1}^{N} T^m(t_o) \quad \tau^m \, dt_o + 2F(t_n) \tag{2.20}$$

The coefficient τ^m is intended to represent the traction acting at time t_m. Adherence to the idea of causality in (2.20) would then require that the coefficients τ^{n+1}, τ^{n+2}, $\cdots$ not appear on the right. This is most easily accomplished by requiring that the interpolator be causal, i.e.,

$$T^m(t) = 0 \quad , \qquad t < t_{m-1} \tag{2.21}$$

It is now possible to find a simple time dependence for the interpolator. From (2.21) we have $DG^m = 0$, $m < 0$, so

$$u^n = \sum_{1}^{n} DG^{n-m} \, \tau^n + 2F(t_n) \tag{2.22}$$

If $DG^o = DG^1 = \cdots = \beta\Delta t/\mu$ this equation reproduces (2.3) to order Δt. Differencing it gives the analog of (2.4):

$$\tau^n = (u^n - u^{n-1} - 2(F(t_n) - F(t_{n-1}))) \, \mu/\beta\Delta t \tag{2.22a}$$

which reproduces (2.4) to order Δt when expanded about t_n or to order Δt^2 when expanded about $t_n - \Delta t/2$. The appropriate simple time dependence for $T^n(t)$ is then centered at $t_n - \Delta t/2$:

$$T^n(t) = \begin{cases} 0 \ , & |t - t_n - \Delta t/2| > \Delta t/2 \\ \\ 1 \ , & |t - t_n - \Delta t/2| < \Delta t/2 \end{cases} \tag{2.23}$$

This interpolator will be called D_o in the remainder of this work. A displacement interpolator appropriate to D_o will be selected in Chapter 3.

The discrete kernel may now be calculated explicitly: it is

$$DG_k^m = \frac{QL}{\pi\mu} (E_m^{+1} - 1) (E_k^{+1/2} - E_k^{-1/2}) \, mH(m) \, g(\frac{k}{mQ}) \tag{2.24}$$

where $Q = \beta\Delta t/L$, E_k^b is the translation operator, $E_k^b f(k,m) = f(k+b,m)$, and

$$g(\eta) = \begin{cases} \eta \cosh^{-1} (|\eta|^{-1}) + \sin^{-1} (\eta) \ , & |\eta| \leq 1 \\ \\ \frac{\pi}{2} \operatorname{sgn}(\eta) \ , & |\eta| \geq 1 \end{cases}$$

Note that if $\beta\Delta t/L = Q \leq 1/2$, $DG_o^o = \beta\Delta t/\mu$ and $DG_k^o = 0$, $k \neq 0$. For sufficiently short time steps equation (2.2) then gives an explicit algorithm for calculating the tractions τ_j^n by time stepping. If $3/2 \geq Q > 1/2$ a tridiagonal matrix equation occurs at each time step, if $5/2 \geq Q > 3/2$ a bandwidth 5 system occurs, and so on.

In Appendix C it is shown that the BIE method implemented with this interpolation scheme produces a convergent technique for solving

the two fundamental antiplane strain boundary value problems on a half plane. If $\beta\Delta t/L \leq 1/2$ is held constant and equation (2.2) is solved for either the displacement or traction the numerical solution approaches the exact solution as $L \to 0$, provided that the exact solution is sufficiently differentiable.

In the practical situation, the use of piecewise constant interpolation means that the number of grid points per period or wavelength will have to be fairly large to achieve high accuracy. To give an idea of the grid density requirements the following calculation was made. The displacement due to a traction

$$f_g(x,t) = \mu \begin{cases} 0 & t < 0 \ , \ t > T_g \ , \ x < 0 \ , \ x > L_g \\ \sin(2\pi t/T_g)\ \sin(2\pi x/L_g) & \text{otherwise} \end{cases}$$

was calculated for different values of $T_g/\Delta t$ and L_g/L with $\beta\Delta t/L = 0.5$. The traction coefficients are given by

$$\tau_j^n = f_g(jL,(n-\tfrac{1}{2})\ \Delta t)$$

The displacement coefficients were calculated from (2.16) with $F \equiv 0$ using a multidimensional FFT algorithm and a grid of 128 nodes by 64 time steps. For each value of $T_g/\Delta t$ and L_g/L a second calculation was made with a greatly refined grid. The calculation on the refined

grid was very accurate, with pointwise errors of less than 0.1%. This solution was taken to be exact for purposes of error estimation and will be denoted by u_{ex}. Table 2.1 gives the maximum error

$$\varepsilon = \max_{n,j} |u_j^n - u_{ex}(x_j,t_n)| / \max_{n,j} |u_{ex}(x_j,t_n)|$$

as a function of $T_g/\Delta t$ and L_g/L.

A typical displacement $u(x,t)$ is shown in Figure 2.2. The parameters were $T_g/\Delta t = 8$, $L_g/L = 8$ and every second time step was plotted. As can be seen there, the displacement consists of a fairly sharp two-sided pulse in the region where the traction is applied, with a two-sided wave propagating into the traction-free regions. This wave diminishes approximately as $x_1^{-\frac{1}{2}}$ as it propagates outward due to geometric spreading. The displacement is antisymmetric about $x/L_g = 0.5$. Figure 2.3 is a plot of the error

$$\varepsilon_j^n = (u_j^n - u_{ex}(x_j,t_n)) / \max_{n,j} |u_{ex}(x_j,t_n)| \qquad (2.25a)$$

for the same parameters as in Figure 2.2. The vertical scale in Figure 2.3 is not the same as that in Figure 2.2. The maximum error from (2.25a) is about 5% and occurs in the area where the traction was applied. The error outside that area is smaller and decreases approximately as $x^{-\frac{1}{2}}$. The relative rate at which the error falls off with x is more clearly shown in Figure 2.4. The error in that plot is

Table 2.1. Maximum Error in Calculated Displacement

L_g/L \ $T_g/\Delta t$	24	16	12	8	6	4
24	.01	.01	.02	.04	.08	.14
16	.01	.02	.02	.04	.08	.15
12	.04	.04	.04	.05	.08	.15
8	.06	.07	.07	.08	.10	.15
6	.13	.16	.13	.17	.19	.20
4	.20	.28	.28	.28	.27	.33

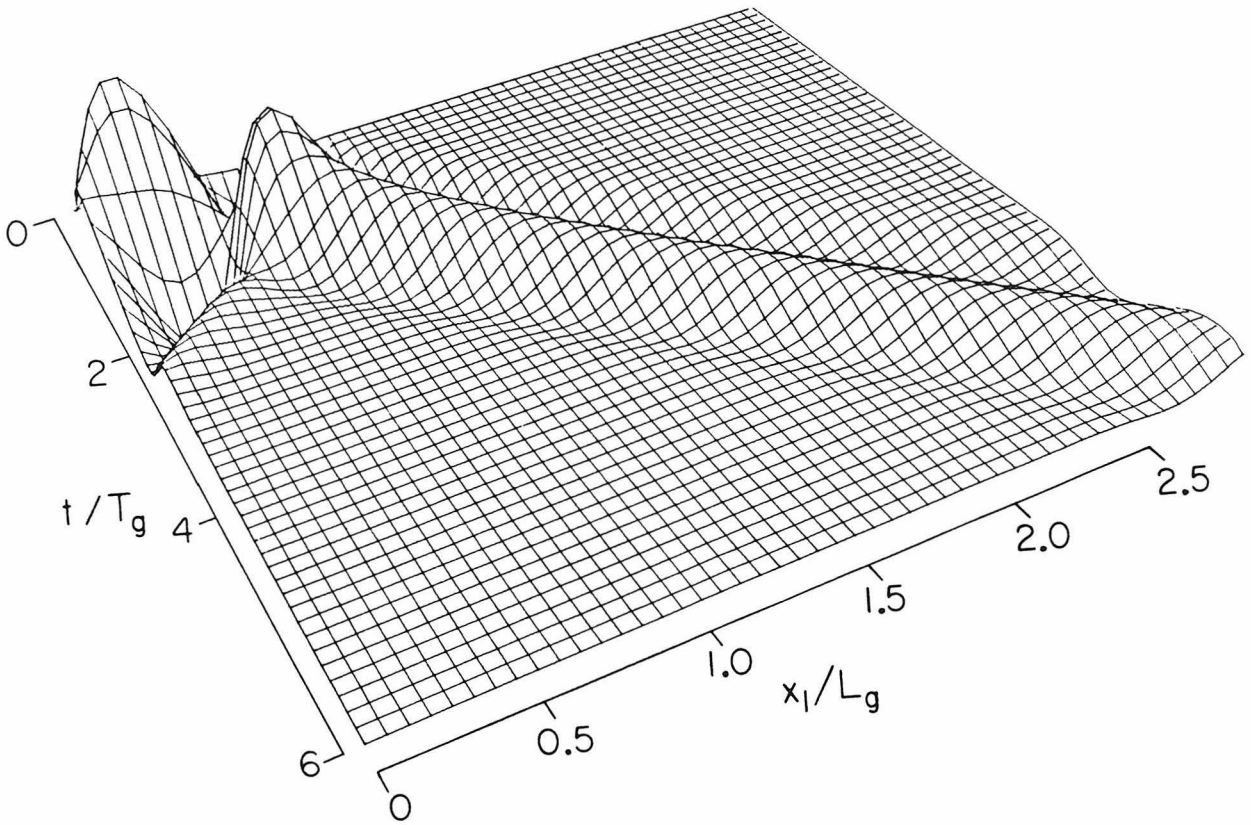

Figure 2.2. Three-dimensional plot of exact SH displacement on a half-plane surface as a function of x and t.

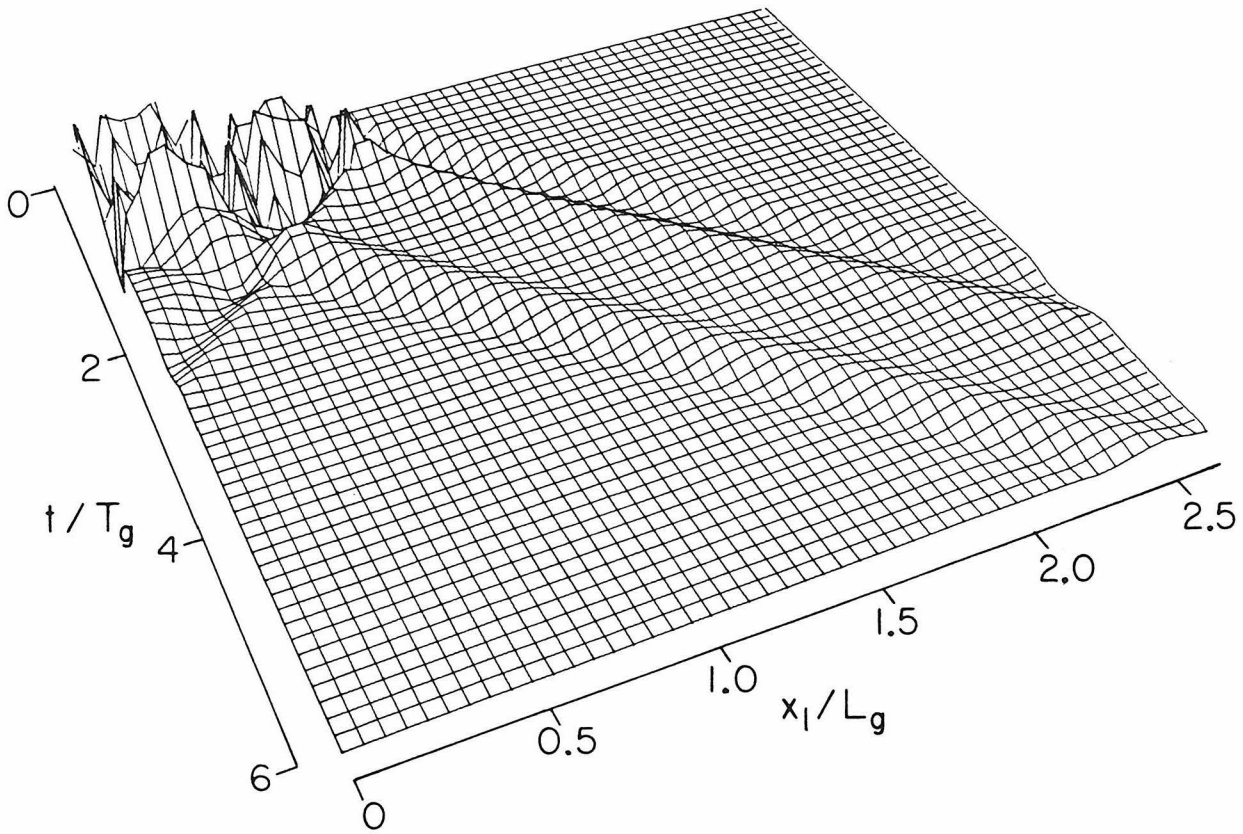

Figure 2.3. A plot of the error defined in equation (2.25a) for the numerically evaluated displacement.

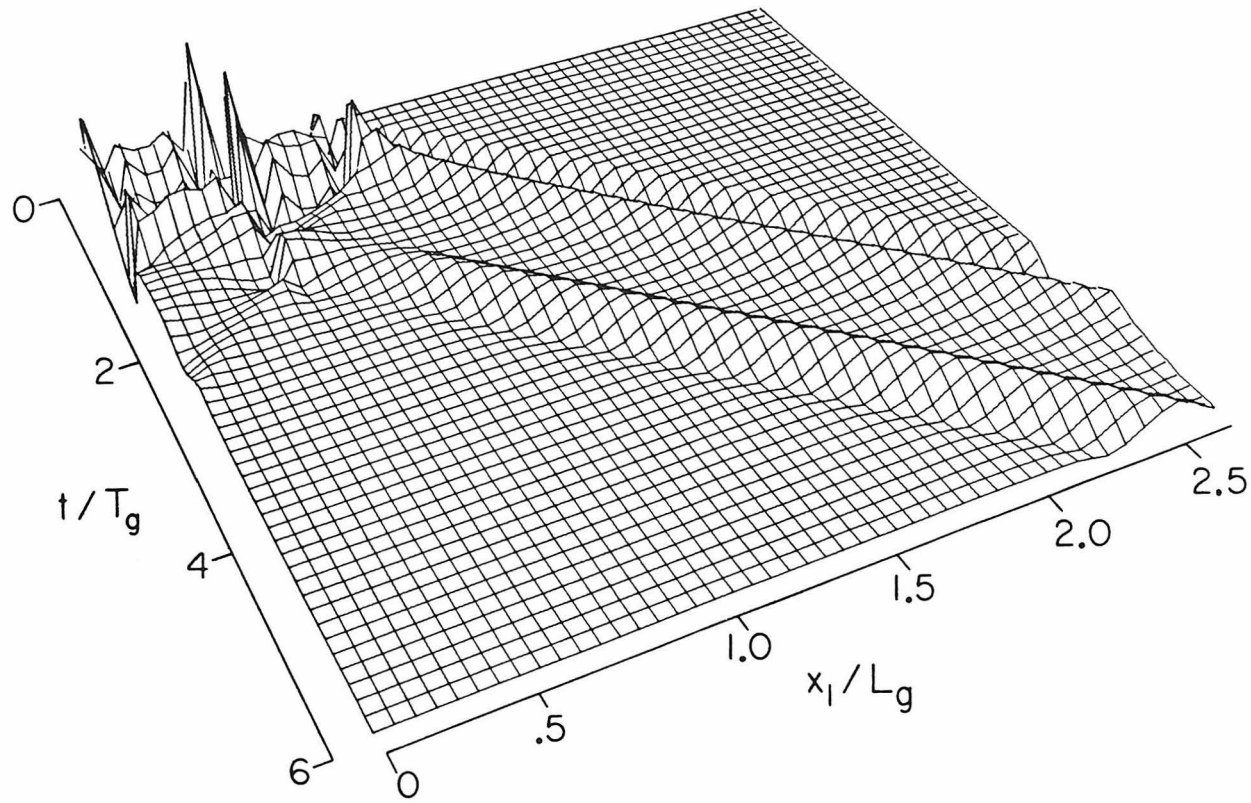

Figure 2.4. A plot of the error in the numerically evaluated displacement, normalized by time series maxima according to equation (2.25b)

normalized by the maximum displacement encountered at each node:

$$\varepsilon_j^n = (u_j^n - u_{ex}(jL,t_n))/\max_n |u_{ex}(jL,t_n)| \qquad (2.25b)$$

The vertical scale in Figure 2.4 is the same as that in Figure 2.3. The maximum value of ε_j^n is about 0.1 and occurs near $x/L_g = 0.5$, where the normalizing displacement is small. The maximum error elsewhere on the grid is about 5% and does not change appreciably with x_1 in this normalization. From these figures and Table 2.1 it is possible to estimate the grid density required in most applications. For many wave propagation problems, 10 points per wavelength or period is a sufficiently dense grid for evaluating displacements.

The performance of the interpolator D_o when used for calculating displacements in equation (2.16) is easily understood in terms of the accuracy of the interpolation method. When equation (2.16) is used to calculate the traction along the half plane boundary the situation is not so simple. Consider the following problem: a line source with time dependence g(t) acts in a half-space at a distance $H > 0$ from the surface $x_2 = 0$. The whole-space displacement due to the source is

$$F(x_1,x_2,t) = g(t) * \frac{H(t - r/\beta)}{[t^2 - r^2/\beta^2]^{\frac{1}{2}}} \qquad (2.26)$$

where $r^2 = x_1^2 + (x_2 - H)^2$ (see Fig. 2.5).

If a boundary condition of zero displacement is applied at $x_2 = 0$ the traction acting there is

$$\tau(x_1,t) = -2\mu \frac{\partial}{\partial x_2} F(x_1,x_2,t)\Big|_{x_2 = 0} \tag{2.27}$$

The numerical BIE solution for the tractions may be written as

$$\tau_j^n = -2 \sum_{m=1}^{n} \sum_{i} DGI_{j-i}^{n-m} \; F(iL,0,m\Delta t) \tag{2.28}$$

Note that the variation of F with x_2 does not appear explicitly in this equation.

The operator represented by the coefficients DGI_j^n is convolutionally inverse to DG_j^n and is causal. It is defined by the relations

$$DGI_j^n = 0 \quad , \quad n < 0$$

$$\sum_{i} DGI_i^o \; DG_{j-i}^o = \delta_{jo} \tag{2.29}$$

$$\sum_{m=0}^{n} \sum_{i} DGI_i^m \; DG_{j-i}^{n-m} = 0 \qquad \text{for } n \geq 1 \tag{2.30}$$

The coefficients DGI_i^m are symmetric in i. The last expression may be combined with the one before to give

$$DGI_j^n = -\sum_{m=1}^{n} \sum_i DGI_i^{n-m} \sum_k DGI_{j-k}^o \; DG_{k-i}^m \qquad (2.31)$$

This equation shows that once the series DGI_j^o , j = 0, 1, 2, ··· is found, the remaining coefficients DGI_j^n may be calculated in a straightforward manner because the coefficients DGI_k^ℓ are absent from the right-hand side for $\ell \geq n$.

If the time step is short enough that $Q \leq 0.5$ the series DGI_j^o is simply

$$DGI_o^o = 1/DG_o^o$$

$$DGI_k^o = 0 \qquad k \neq 0 \quad .$$

If Q is greater than 0.5 the series DGI_k^o may be found by a number of methods; the method used here was to calculate it by inverting the discrete Fourier transform of DG_k^o , k = 0, ±1, ±2, ···. This technique works because, in the language of time series analysis, the series DG_k^o is minimum phase. The series DGI_k^n were calculated using equation (2.31) for successive values of n. The required convolutions over the spatial index were computed using an FFT algorithm. It should be noted that the number of operations involved in evaluting DGI_j^n up to

time level n = N is of order N^2J when this procedure is used. Table 2.2 displays a few of the coefficients DG_j^n and DGI_j^n for values of Q equal to 0.25, 0.5 and 1.

The coefficients DG_j^n in this table vary in a somewhat regular fashion, since they are just average values of the analytic Green's function G over intervals of x_1 and t. The coefficients of the inverse kernel have mixed signs and represent a differential operator. The inverse kernel is more localized than the forward operator and the variation of the coefficients with n and j is only vaguely systematic, with the magnitude of the elements being slightly larger along the line n = j/Q than for n > j/Q.

The problem described previously was solved with a time function

$$g(t) = -\sqrt{2}\ t^*\ \exp(1/2 - t^{*2}) \tag{2.32}$$

where $t^* = 2.72(t/T_h - 1)$. The half power period of this source function is T_h.

The whole-space displacement $F(x_1,x_2,t)$ was evaluated for $x_2 = 0$, $x_1 = jL$ and $t = n\Delta t$ by carrying out the convolution in equation (2.26). The traction at $x_2 = 0$ was then evaluated from the BIE equation (2.28) using a two-dimensional FFT. The traction was also evaluated through an implementation of equation (2.27) in which the only numerical step was a convolution in time. The second

Table 2.2. Coefficients of Discrete Kernels

$\frac{\mu}{L} DG_j^n$ $\frac{\mu}{L} DGI_j^n$

Q = 0.25

		j				j			
		0	1	2	3	0	1	2	3
	0	.250	0	0	0	4.00	0	0	0
	1	.250	0	0	0	-4.00	0	0	0
	2	.155	.048	0	0	1.52	-.76	0	0
n	3	.098	.076	0	0	-.61	.31	0	0
	4	.074	.088	0	0	.34	-.32	.145	0
	5	.059	.095	0	0	-.14	.36	.29	-.03

Q = 0.50

		j				j			
		0	1	2	3	0	1	2	3
	0	.500	0	0	0	2.00	0	0	0
	1	.253	.124	0	0	-1.01	-.49	0	0
	2	.133	.183	0	0	.22	-.23	.12	0
n	3	.093	.123	.080	0	.26	.04	-.14	-.03
	4	.072	.081	.133	0	.10	-.02	-.12	.09
	5	.058	.063	.094	.064	-.04	.07	.05	-.07

Q = 1.0

		j				j			
		0	1	2	3	0	1	2	3
	0	.753	.124	0	0	1.41	0.24	.04	-.01
	1	.226	.307	.080	0	-.08	-.48	.02	.01
	2	.130	.144	.227	.064	.02	.05	-.18	.02
n	3	.092	.096	.115	.188	-.02	.07	.03	-.10
	4	.071	.073	.080	.098	.03	-.01	.03	.02
	5	.058	.059	.063	.070	-.01	.02	-.01	.02

procedure produced a very accurate evaluation of $\tau(x_1,t)$. The results of the two evaluations of τ were compared for different values of $T_h/\Delta t$, H/L and Q. Figure 2.5 displays the free-space displacement $F(x_1,x_2,t)$ for $x_2 = 0$, $T_h/\Delta t = 8$, $H/L = 4$ and $Q = 0.5$. Figure 2.6 is a plot of the traction on the surface $x_2 = 0$ due to this wave. Figure 2.7 is a plot of the error in the tractions calculated using the BIE technique. The error shown there is

$$\varepsilon_j^n = (\tau_j^n - \tau_{ex}(jL,(n-\tfrac{1}{2})\Delta t))/\max_{n,j} |\tau(jL,(n-\tfrac{1}{2})\Delta t)| \qquad (2.33)$$

The maximum error in Figure 2.7 is about 0.06 and occurs near $x_1 = 0$. The traction τ_j^n and error ε_j^n diminish with x_1 approximately as $(x_1^2 + H^2)^{-3/4}$. Figure 2.8 shows the error renormalized by the maximum traction acting at each node;

$$\varepsilon_j^n = (\tau_j^n - \tau_{ex}(jL,(n-\tfrac{1}{2})\Delta t))/\max_{n} |\tau_{ex}(jL,(n-\tfrac{1}{2})\Delta t)| \qquad (2.34)$$

The vertical scale in Figure 2.8 is one-half that in Figure 2.7. The maximum value of ε_j^n in Figure 2.8 is about 0.15 and occurs at $x_1/H = 4$, where the maximum traction is about 0.13 as large as the maximum traction acting on the grid. The wavefronts at $x_1/H = 4$ are oriented at about 75° to the surface normal. The error defined in (2.34) for greater values of x_1 than shown in Figure 2.8 are of about the same magnitude as at $x_1/H = 5$. The error for large values of x_1/H may be

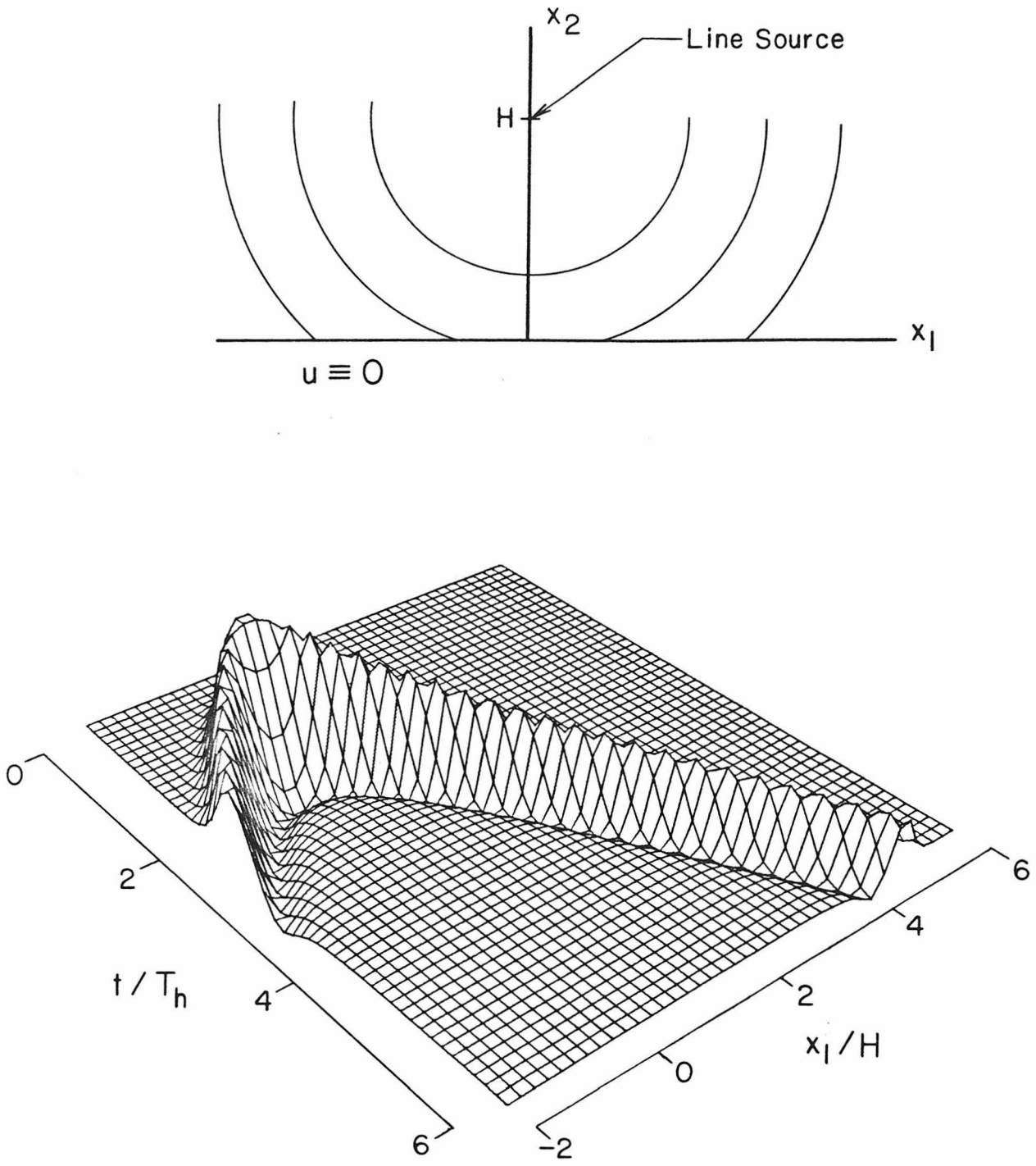

Figure 2.5. The incident displacement wave due to a line source as a function of x_1 and t.

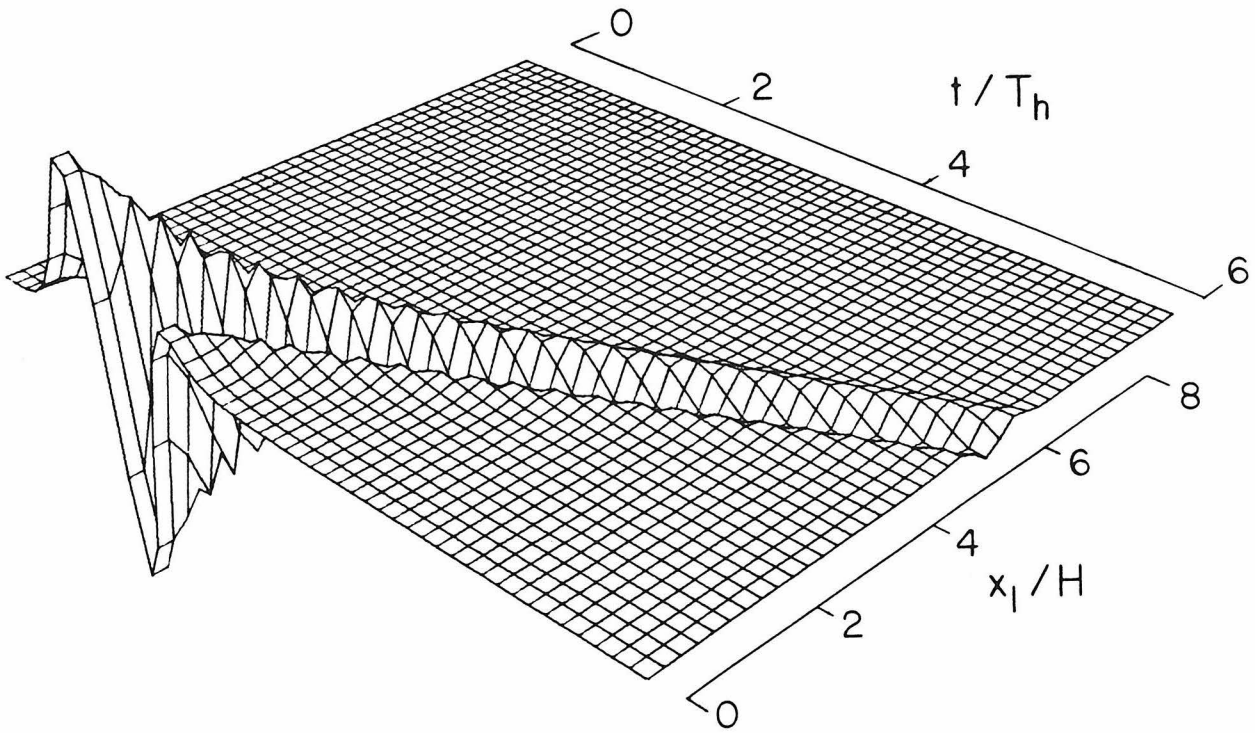

Figure 2.6. The exact traction of $x_2 = 0$ as a function of x_1 and t.

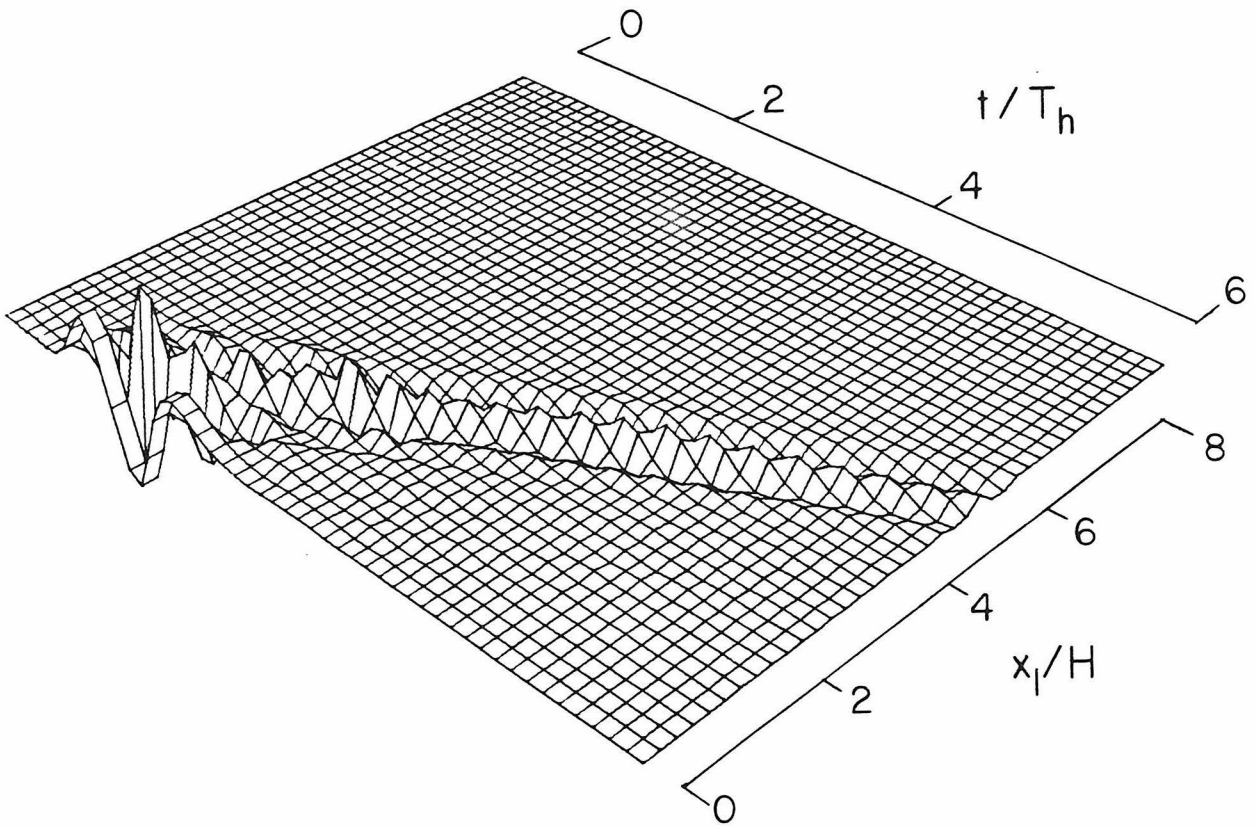

Figure 2.7. The error in the numerically calculated traction defined in equation (2.33).

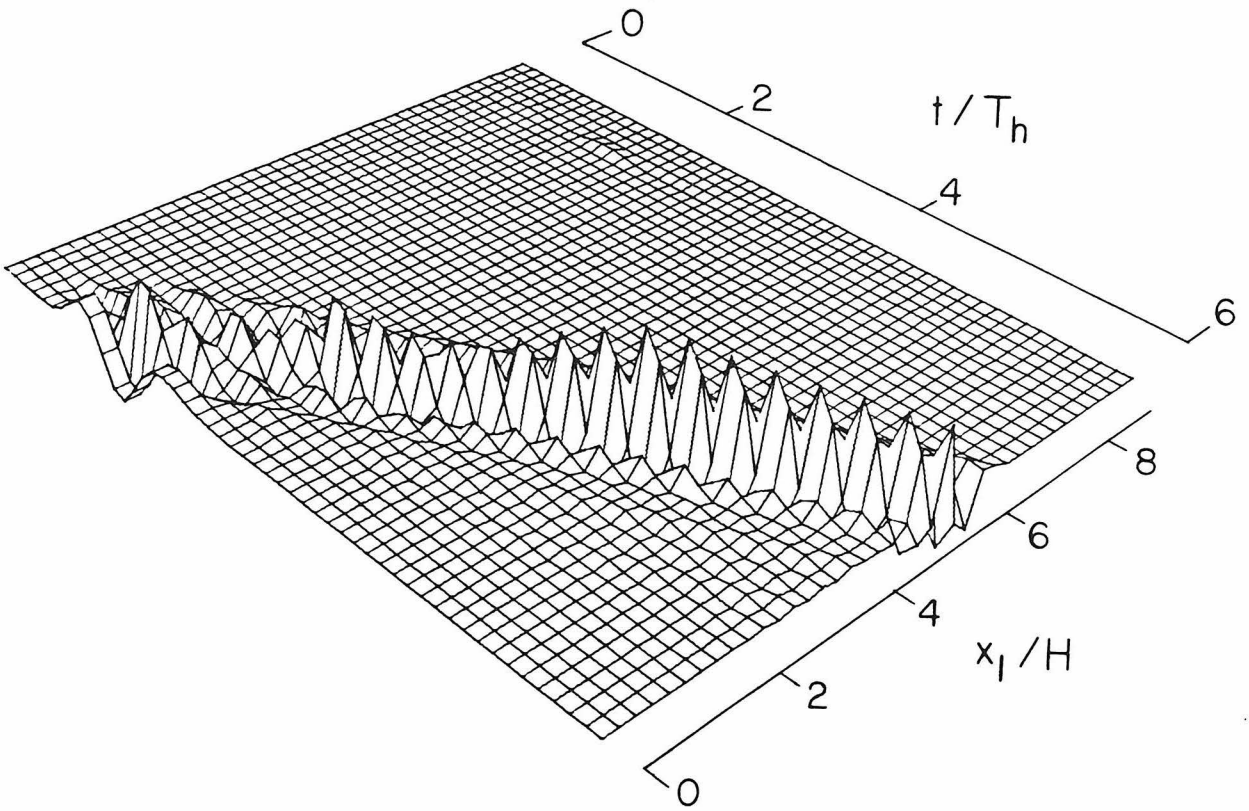

Figure 2.8. The error in the numerically calculated traction defined in equation (2.34).

interpreted as the inherent error involved in calculating tractions for waves traveling nearly parallel to the boundary $x_2 = 0$; it should be remembered that the tractions associated with these waves are much smaller than the tractions due to similar waves which propagate at near normal incidence.

If the tractions evaluated by this method were to be used to reconstruct the reflected wave for a point in the region $x_2 > 0$, it would be necessary to convolve them over x_1 and t with the Green's function

$$G = \frac{1}{2\pi\mu} \frac{H(t - (x_2^2 + x_1^2)/\beta)}{[t^2 - (x_2^2 + x_1^2/\beta^2)]^{\frac{1}{2}}}$$

(see equation (1.4)). This function is nonnegative everywhere and varies smoothly away from the singularity at $t = (x_1^2 + x_2^2)^{\frac{1}{2}}/\beta$. As a result of this operation, high frequency errors in τ_j^n would be smoothed out. The maximum error in τ_j^n would then be much larger than the maximum error in the calculated reflected displacement wave. As can be seen from Figure 2.7, the error in τ consists mainly of high frequency components, particularly as a function of x_1.

The problem of evaluating the tractions due to a line source was solved for several values of the parameters $T_h/\Delta t$, H/L and Q. The maximum of the globally normalized error ε_j^n, defined in equation (2.33), is given in Table 2.3 for each of these calculations. In

Table 2.3. Maximum Error in Calculated Traction for Interpolator D_o.

Q = 0.25

$T_h/\Delta t$ \ H/L	4	6	8	10
8	.11	.11	.11	.11
12	.05	.06	.06	.06
16	.03	.03	.03	.03
20	.02	.02	.03	.02

Q = 0.50

$T_h/\Delta t$ \ H/L	4	6	8	10
8	.06	.06	.06	.05
12	.07	.05	.05	.06
16	.06	.05	.04	.06
20	.05	.04	.04	.05

Q = 1.00

$T_h/\Delta t$ \ H/L	4	6	8	10
8	.12	.13	.16	.19
12	.10	.12	.16	.12
16	.09	.11	.13	.11
20	.08	.09	.10	.10

Q = 2.00

$T_h/\Delta t$ \ H/L	4	6	8	10
8	.27	.29	.29	.25
12	.22	.24	.26	.22
16	.19	.21	.23	.19
20	.16	.19	.20	.17

each case, the maximum of this error occurred near $x_1 = 0$; that is, at a point where the wavefronts were at near normal incidence and the absolute value of the traction was a maximum. As a result of this circumstance the errors displayed in Table 2.3 do not depend strongly on the parameters H/L.

Another measure of the error in each of these calculations is given in Table 2.4. The quantity shown there is an RMS type error defined by

$$\varepsilon_\eta = \left(\sum_n \sum_j \left(\tau_j^n - \tau_{ex}(jL,(n-\tfrac{1}{2})\Delta t)\right)^2\right)^{\frac{1}{2}}/w \qquad (2.35)$$

The points included in the sum are those points at which the absolute value of the analytic traction exceeded $\tau_c = \eta \cdot \max_{n,j} |\tau_{ex}(jL,(n-\tfrac{1}{2})\Delta t)|$. The parameter η was chosen to be 0.2. The value of ε_η did not vary by more than a factor of two in the range $0.1 < \eta < 0.5$. For most choices of Q, H/L and $T_h/\Delta t$ the variation was much less. The normalizing factor w is the product of the number of points in the sum and the maximum traction acting on the grid. This measure of the error did not depend on H/L, so only the values for H/L = 4 are shown.

Table 2.4. RMS error in calculated traction for H/L = 4.

$T_n/\Delta t$	Q = .25	Q = .50	Q = 1.0	Q = 2.0
8	.03	.03	.04	.08
12	.02	.02	.03	.06
16	.01	.02	.03	.05
20	.01	.02	.02	.05

The variation of the locally normalized error with x_1 is shown in Figure 2.9 for H/L = 4, $T_n/\Delta t$ = 8, 12, 16, 20 and different values of Q. The error plotted there is

$$\varepsilon_j = \max_n |\tau_j^n - \tau_{ex}(jL,(n-\tfrac{1}{2})\Delta t)| / \max_n |\tau_{ex}(jL,(n-\tfrac{1}{2})\Delta t)| \quad .$$

The error is plotted against $\tan^{-1}(H/x_1)$, the angle between the normal to the cylindrical free-space wavefront and the x_1 axis when the wavefront passes through a point at x_1 along $x_2 = 0$. Because the inverse kernel DGI is somewhat localized the error associated with a particular angle is probably similar to the error associated with a plane wave incident at that angle, although the cylindrical wave has curved wavefronts and its maximum amplitude diminishes as x_1 increases. The plotted values do not extend to zero angle of incidence

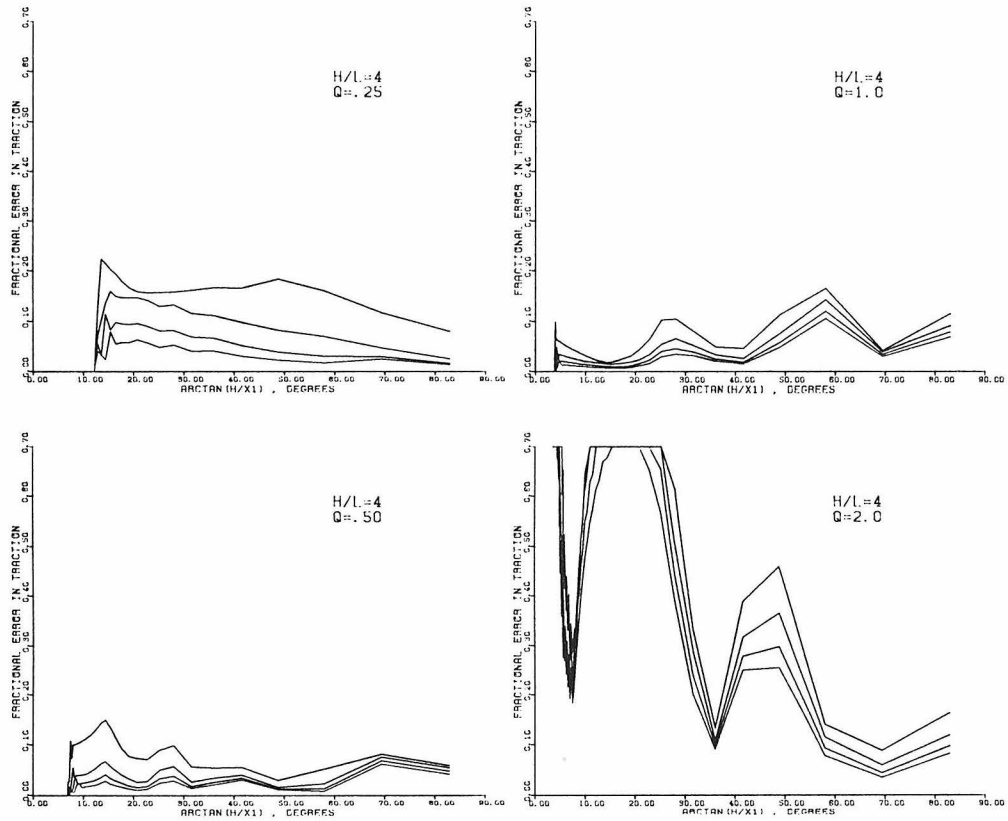

Figure 2.9. The error in calculated tractions as a function of angle of incidence of the cylindrical wavefront at the surface $x_2 = 0$. Normal incidence is at 90°.

because of the finite number of time steps over which the calculation was carried out.

For each value of Q and H/x_1 in these plots the error decreases monotonically as $T_h/\Delta t$ increases. The top trace in each plot corresponds to $T_n/\Delta t = 8$ and the bottom trace corresponds to $T_n/\Delta t = 20$. Because ϵ_j does not vary much with H/x_1 in these plots it appears likely that errors produced by the BIE technique are not sensitive to the angle of incidence of wavefronts for values of Q over a fairly wide range. The large errors shown for the case Q = 2 demonstrate that there is an upper limit to the acceptable ratio of $\beta\Delta t/L$ when the traction must be calculated and the wavefronts are oriented nearly parallel to the boundary.

In summary, the results of this section have shown by practical applications that the BIE method implemented with traction interpolator D_o can be used to evaluate unknown boundary values along the surface of a half-space in antiplane strain for unmixed type problems. Although the errors shown here are problem dependent, the general behavior of the technique for half-plane problems may be conjectured from the numerical information given. The performance of the operators DG and DGI for curved cylindrical surfaces is similar to the results found here, since the forward operator DG is insensitive to small surface curvatures. The performance of the method for curved surfaces will be evaluated in detail in Chapter 3, where interpolation of displacements is considered.

3. Comparison to Other Methods

The accuracy of the BIE method implemented with traction interpolator D_0 will now be compared with results obtained using the discretization methods of Das (1977), Burridge (1969) and Claerbout (1976). The problem employed here will be the one used in the last section to evaluate the performance of the inverse operator DGI_j^n in calculating tractions along a line. This problem is a suitable context for comparison because it includes curved wavefronts that propagate normal and also nearly parallel to the boundary. The problem of evaluating the tractions requires the use of a numerical operator which approximates a differential operator. This is a much more sensitive test of the discretization method than a problem in which the displacement is to be evaluated.

The discrete kernel analogous to DG_j^n for a half-space has been given explicitly by Das (1977). For $n > 0$ it is

$$DG_j^n = \frac{\beta}{\pi\mu L}\, nQ\, (E_j^1 - 2 + E_j^{-1})\, \Gamma\left(\frac{j}{nQ}\right) \tag{2.36}$$

where

$$\Gamma(\eta) = \begin{cases} \eta \sin^{-1}(\eta) + (1-\eta^2)^{\frac{1}{2}} & |\eta| < 1 \\ \\ \frac{\pi}{2}\,|\eta| & |\eta| \geq 1 \end{cases}$$

For n = 0,

$$DG_0^0 = \frac{\beta \Delta t}{\mu}$$

$$DG_k^0 = 0 \quad , \qquad k \neq 0 \quad .$$

The time stepping algorithm for calculating tractions with this method is explicit for all values of Q. As a result of this it is a simple matter to calculate the convolutional inverse of this operator using the methods of section 2.

When Burridge's method is used to calculate the operator analogous to DGI_j^n, the only choice to be made is the selection of the discrete representation of the differential operator

$$\frac{1}{\beta^2} \frac{\partial^2}{\partial t^2} - \frac{\partial^2}{\partial x_1^2} \quad .$$

Using Burridge's choice of difference operators,

$$\frac{L^2}{\beta^2} \frac{\partial^2}{\partial t^2} \rightarrow \frac{1}{Q^2} (E_n^{+1} - 2 + E_n^{-1})$$

$$L^2 \frac{\partial^2}{\partial x_1^2} \rightarrow (E_j^{+1} - 2 + E_j^{-1}) \qquad (2.38)$$

The analog of $\frac{L}{\mu} DGI_j^n$, convolved with itself, is then D_j^n.

The nonzero values of D_j^n are given in Table 2.4

Table 2.4. Nonzero values of D_j^n.

n \ j	0	1	2
0	Q^{-2}	0	0
1	$2(1 - Q^{-2})$	-1	0
2	Q^{-2}	0	0
3	0	0	0

The first three time levels of $\frac{L}{\mu} DGI_j^n$ are given in Table 2.5

Table 2.5. Values of $\frac{L}{\mu} DGI_j^n$ by Burridge's method.

n \ j	0	1	2	3
0	Q^{-1}	0	0	0
1	$Q - Q^{-1}$	$-Q/2$	0	0
2	$Q^{-1}(1 - (1 - Q^2)^2)/2$	$Q(Q^2 - 1)$	$-Q^3/8$	0

The remaining time levels may be calculated numerically from the formula

$$DGI_j^n = -\frac{LQ}{\mu} \sum_i \sum_{m=0}^{n-1} DGI_{j-i}^{n-m} \, DGI_i^m \quad , \qquad n \geq 3 \quad .$$

In adapting Claerbout's method of discretization to this problem, some modification of his technique is required. The "45 degree" paraxial approximation of equation (2.15) in x_1, x_2, t domain is given by Clayton (1978) as

$$\left(\frac{\partial^2}{\partial t^2} - \left(\frac{\beta}{2}\right)^2 \frac{\partial^2}{\partial x_1^2}\right) \frac{\tau}{\mu} = \frac{1}{\beta} \frac{\partial}{\partial t} \left(\frac{\partial^2}{\partial t^2} - \frac{3}{4} \beta^2 \frac{\partial^2}{\partial x_1^2}\right) u \qquad (2.39)$$

where

$$\frac{\tau}{\mu} = \frac{\partial u}{\partial x_2} \quad .$$

In approximating this equation for use as a transparent boundary condition in finite difference calculations the derivative of u with respect to x_2 was included in order to extrapolate u one space-step outside the finite difference grid. In addition, certain averages of u over the two boundary grid lines at $x_2 = 0$ and $x_2 = \Delta x_2$ were employed in the x_1 and t derivatives of u. The effects of these details cannot be reproduced in the current calculation, so the results found here may not reproduce exactly the behavior of the method for reducing grid edge reflections.

In approximating equation (2.39) the second order derivatives, as grouped there, were replaced according to the correspondences in equation (2.38). The remaining derivative $\frac{\partial}{\partial t}$ was approximated by the forward difference operator. The resulting difference equation is

$$\left[\frac{1}{Q^2}\left(E_n^{+1} - 2 + E_n^{-1}\right) - \frac{1}{4}\left(E_j^{+1} - 2 - E_j^{-1}\right)\right] \tau_j^n/\mu =$$

$$\frac{1}{Q}\left(E_n^{+1} - 1\right)\left[\frac{1}{Q^2}\left(E_n^{+1} - 2 + E_n^{-1}\right) - \frac{3}{4}\left(E_j^{+1} - 2 + E_j^{-1}\right)\right] u_j^n/L \tag{2.40}$$

This approximation of equation (2.39) provides an explicit means of estimating τ_j^n and is stable when used for that purpose if $Q \leq 2$. It is accurate to orders Δt^2 and L^2 when considered as an approximation of equation (2.39). If τ_j^n and u_j^n do not depend on j this equation may be rearranged to give

$$\tau^n = \frac{\mu}{\beta \Delta t}\left(u^{n+1} - u^n\right)$$

Thus, τ_j^n is most favorably compared to $\tau_{ex}(jL,(n-\frac{1}{2})\Delta t)$. This is also true of the other methods.

The calculation of tractions was carried out by the procedure described in section 2 for $H/L = 4$ and $T_n/\Delta t = 12$. The exact traction resembles the traction shown in Figure 2.6. Figures 2.10 and 2.11

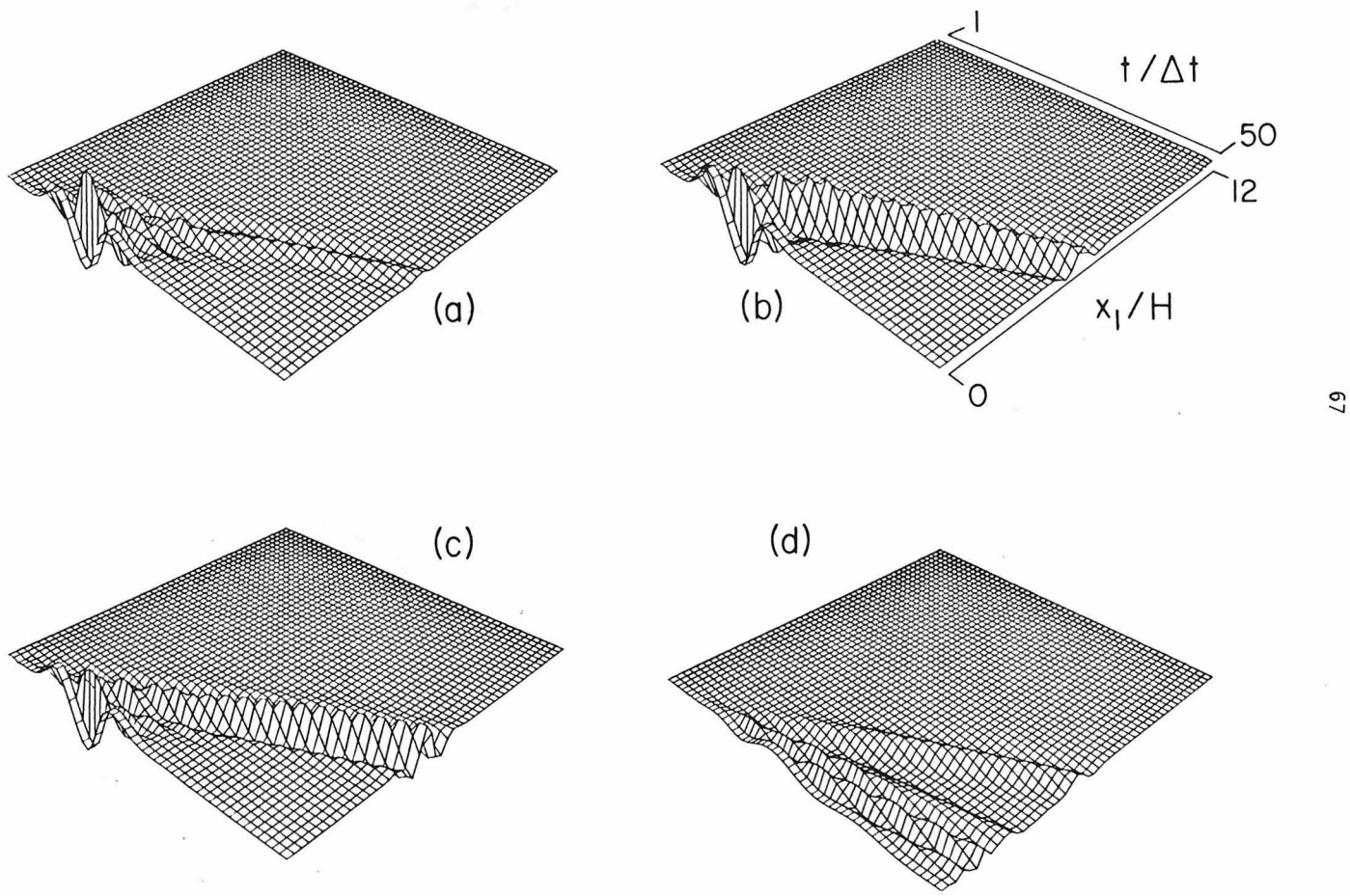

Figure 2.10. The error in the tractions calculated by various methods (a) BIE; (b) DAS; (c) Burridge, and; (d) 45 degree. Q = 0.5. See text.

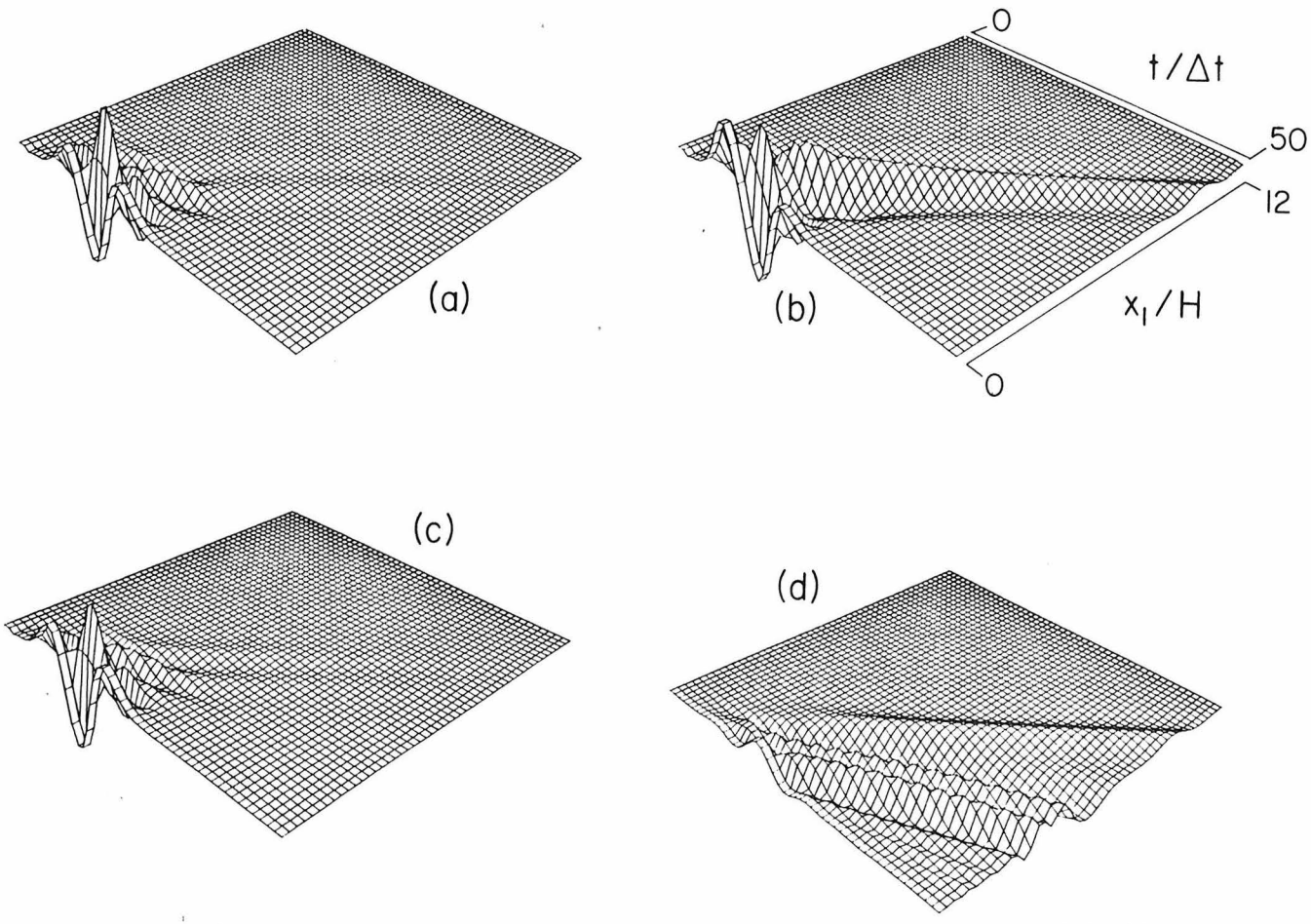

Figure 2.11. The error in the tractions calculated by various methods (a) BIE; (b) DAS; (c) Burridge, and; (d) 45 degree. Q=1.0

display the absolute error in τ_j^n, as defined in equation (2.33), for the four methods considered and values of Q equal to 0.5 and 1.0, respectively. The vertical scales in these figures are all the same except for plots displaying errors from the "45 degree" method, in which the vertical scale has been reduced by a factor of eight relative to the others to improve legibility.

Figure 2.12 displays the locally normalized error

$$\varepsilon_j = \max_n |\tau_j^n - \tau_{ex}(jL,(n-\tfrac{1}{2})\Delta t)| / \max_n |\tau_{ex}(jL,(n-\tfrac{1}{2})\Delta t)|$$

for the different methods and values of Q.

From comparison of the plots of Figure 2.10 it can be seen that the BIE method gives the best overall performance for Q = 0.5. The error for $x_1/H < 1$, or $\tan^{-1}(H/x_1) > 45°$, is of comparable size for all of the methods considered, although the 45 degree method gives somewhat larger errors, which may be because it is more sensitive to wavefront curvature. For larger values of x_1/H ($\tan^{-1}(H/x_1) < 45°$) the 45 degree method and Burridge's method give errors of order 1 in the local normalization (see Figure 2.12a). The error for Das' method is around 0.25 (maximum) as compared with 0.06 with the BIE method.

For Q = 1.0 the BIE and Burridge's methods give nearly identical results, as can be seen in Figures 2.11a and 2.12b. This is a rather surprising result. From Tables 2.2 and 2.5 it is apparent that the two methods give kernel coefficients DGI_j^n that are quite dissimilar

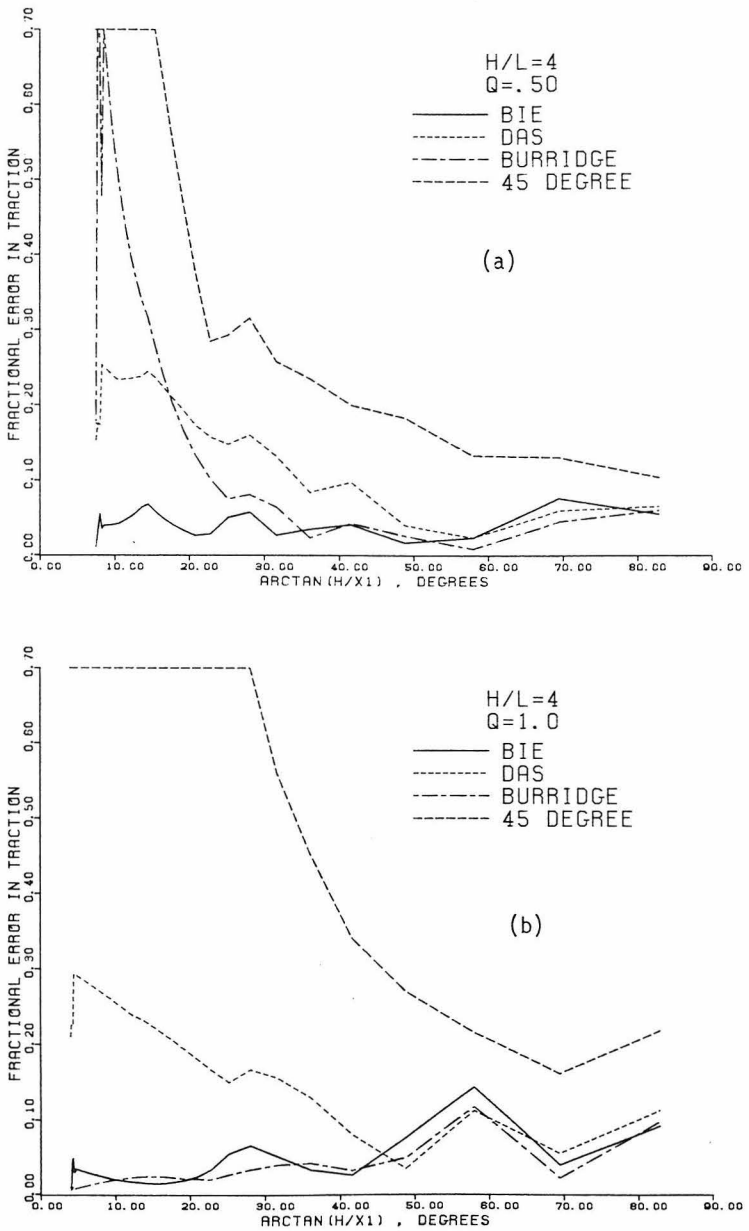

Figure 2.12. The errors in the numerically evaluated traction as a function of angle of incidence of the cylindrical wavefront. (a) Q = 0.5 (b) Q = 1.0.

for small n and j. Since the coefficients die out rapidly with n and j a substantial difference in performance would be expected in a problem involving both normally incident and parallel propagating waves. The method of Das again gives rather large errors for parallel propagating waves. With the 45 degree method the errors are very large for $x_1/H > 1$ and a wave propagating with velocity $\beta/2$ can be seen in Figure 2.11. The analytic tractions are nearly zero where this wave appears. It is also present in Figure 2.10 and is due to the presence of a one-dimensional wave operator with velocity $\beta/2$ which appears in the analytic form of the 45 degree approximation, equation (2.39). The quantity on the right hand side of that equation is largest near $x_1 = 0$ and acts as a source of the nondiminishing spurious wave propagating outward from that area.

From the numerical results of this section it appears that the BIE method is the better of the methods employed here to evaluate tractions because it gives an accurate evaluation of the desired derivative for any direction of wave propagation. The accuracy of the evaluated traction does not depend strongly on the grid parameter Q, as is the case with Burridge's method. This is an important property if heterogeneous media are to be considered, since different values of Q would appear in media with different velocities when Δt and L are the same in both.

Chapter 3

GENERAL BOUNDARY SHAPES IN ANTIPLANE STRAIN

1. Introduction

In this chapter the antiplane strain BIE method is extended to include calculations involving bodies with curved boundaries. In doing this it is necessary to select an interpolation method for displacements along the boundary. The displacement interpolator chosen here will be one which is appropriate for use with the traction interpolator D_o discussed in Chapter 2.

The general antiplane strain integral equation may be written as

$$\Gamma(\underline{r})\, u(\underline{r},t) = v(\underline{r},t) - w(\underline{r},t) + F(\underline{r},t) \tag{3.1}$$

where

$$v(\underline{r},t) = \int_{\partial B} \int_{t_o} G(\underline{r},t;\underline{r}_o,t_o)\, \tau(\underline{r}_o,t_o)\, dt_o\, dS_o \tag{3.1a}$$

$$w(\underline{r},t) = \int_{\partial B} \int_{t_o} u(\underline{r}_o,t_o)\, \mu \frac{\partial}{\partial n_o} G(\underline{r},t;\underline{r}_o,t_o)\, dt_o\, dS_o \tag{3.1b}$$

$F(\underline{r},t)$ is the infinite space solution of the initial value - body force problem.

$$\Gamma(\underline{r}) = \begin{cases} 1/2 & \varepsilon \quad \underline{r} \in \partial B \\ 1 & \varepsilon \quad \underline{r} \in B' \\ 0 & \notin \quad \underline{r} \notin B \end{cases}$$

G is the whole plane Green's function, and $\partial/\partial n_o$ is the derivative along the outward normal of ∂B with respect to the source coordinates. The integrals of (3.1a) and (3.1b) are intended as principal values if $\underline{r} \in \partial B$. The functions $v(\underline{r},t)$ and $w(\underline{r},t)$ may be regarded as the displacement fields due to, respectively, a distributed force $\tau(\underline{r},t)$ and a distributed dislocation $u(\underline{r},t)$ applied along a curve ∂B in a whole plane. The need for displacement interpolation along ∂B arises from the presence of the term $w(\underline{r},t)$ in (3.1).

The general properties of the time harmonic version of displacement fields v and w are discussed by Kupradze (1963, Chapter 2) and they are similar to the properties of the analogous static fields of the potential theory (see Kellogg, (1953)). These properties will be briefly stated here for completeness.

Away from the curve ∂B the fields v and w are solutions of the homogeneous two dimensional wave equation. Their properties at ∂B are dependent on the smoothness of the functions τ and μ on ∂B. If these functions and the boundary ∂B are sufficiently smooth:

i) $v(\underline{r},t)$ is finite and continuous across ∂B

ii) the derivative of $v(\underline{r},t)$ with respect to the outward normal of ∂B has a jump of amplitude $\frac{1}{\mu}\tau(\underline{r},t)$ across ∂B. In general

$$\lim_{\underline{r}_o \to \partial B} \frac{\partial}{\partial n_o} v(\underline{r}_o,t) \neq \frac{1}{\mu}\tau(\underline{r}_o,t)$$

iii) $w(\underline{r},t)$ is finite at ∂B and has a jump of amplitude $u(\underline{r},t)$ across ∂B. In general $\lim_{\underline{r}_o \to \partial B} w(\underline{r}_o,t) \neq u(\underline{r}_o,t)$

iv) the normal derivative of $w(\underline{r},t)$ at ∂B is finite and continuous across ∂B, and

v) the tangential derivatives of v and w are finite and continuous across ∂B.

These results also apply to general elastic deformations, in three dimensions, with normal derivatives of displacement replaced by tractions.

The object of solving equation (3.1) for specified boundary data may thus be viewed as finding a distribution of point forces or dislocations along a curve ∂B in a whole space. The superposed fields due to these sources must produce the required boundary values at ∂B. Equations (3.1), (3.1a) and (3.1b) are simply a statement of the manner in which the displacement at points in the plane is affected by the sources along ∂B. The properties i) - v) quoted above provide assurance that the effects of these sources on the limiting values of displacement and stress at ∂B can be finite.

In order to determine the time dependence of an appropriate displacement interpolator for D_o, consider the situation in which a plane wave deformation is normally incident on a half plane surface. The medium B is the semi-infinite region $x_2 \geq 0$. The boundary ∂B is then the line $x_2 = 0$, $-\infty < x_1 < \infty$. The traction along this line will be interpolated according to equations (2.17) and (2.23). The displacement along the line is interpolated as

$$u(x_1,0,t) = \sum_{j,n} u_j^n U_j^n (x_1,t)$$

where u_j^n is intended to represent $u(jL,0,n\Delta t)$. If F = 0 and u and τ do not depend on x_1, and

$$\sum_{j=-\infty}^{\infty} U_j^n (x_1,t) = U^n(t)$$

is independent of x_1, the integration over x_1 in equations (3.1a) and (3.1b) may be carried out to give

$$\frac{1}{2\mu} \int_{t_o=0}^{\infty} \sum_n \tau^n T^n(t_o) H(t + x_2/\beta - t_o)\, dt_o$$

$$= \frac{1}{2} \int_{t_o=0}^{\infty} \sum_n u^n U^n(t_o) \frac{\partial}{\partial x_2} H(t + \frac{x_2}{\beta} - t_o)\, dt_o \qquad (3.2)$$

The receiver point at $\underline{r} = (\cdot, x_2)$ is now exterior to B; i.e., $x_2 < 0$. Recall that for D_o on a half plane

$$\tau^n = \frac{\mu}{\beta\Delta t} (u^n - u^{n-1}) \qquad \text{(see equation (2.22a) } \underline{\text{et. seq.}}\text{)}$$

Upon substituting this into equation (3.2) it is found that

$$\frac{(t + x_2/\beta - m\Delta t)}{\Delta t}\,(u^{m+1} - u^m) + u^m = \sum_{n=1}^{\infty} u^n\, U^n(t + x_2/\beta) \qquad (3.3)$$

where m is the largest integer in $(t + x_2/\beta)/\Delta t$. If this relation is to hold for all values of u^m and u^{m+1}, all negative values of x_2/β, and $U^m(t)$ is to possess the time translation symmetry of equation (1.15), one finds that

$$U^n(t) = \begin{cases} 0 & , \quad |t - n\Delta t| > \Delta t \\ 1 - \dfrac{|t - n\Delta t|}{\Delta t} & , \quad |t - n\Delta t| \leq \Delta t \end{cases} \qquad (3.4)$$

Another line of reasoning leading to this time dependence for $U^n(t)$ is given in Cole et al. (1978).

The task of calculating the discrete kernels DK^n_{ij} is greatly simplified by taking $U^n_j(x_1,t)$ to be separable, so the time dependence of $U^n(t)$ will be used as the time dependence of $U^n_j(x_1,t)$. The spatial variation of the displacement interpolator will be taken to be the most localized possible and the one most easily used in discrete kernel calculations; piecewise constant. Thus, for a general boundary shape ∂B with node points $\underline{r}_j$ and associated non-overlapping arcs A_j whose union is ∂B,

$$U_j^n(\underline{r},t) = \begin{cases} 1 - \dfrac{|t - n\Delta t|}{\Delta t} & , \ \underline{r} \in A_j \ \text{ and } \ |t - n\Delta t| < \Delta t \\ \\ 0 & , \ \text{otherwise} \end{cases} \tag{3.5}$$

The associated generalization of the traction interpolator is

$$T_j^n(\underline{r},t) = \begin{cases} 1 & , \ \underline{r} \in A_j \ \text{ and } \ t_{n-1} < t \leq t_n \\ \\ 0 & , \ \text{otherwise} \end{cases} \tag{3.6}$$

These equations constitute the most general definition of interpolation scheme D_o.

This displacement interpolator has been chosen partially on the basis of convenience in application rather than for optimal numerical accuracy. The conclusion from equation (3.3) that $U^n(t)$ should be a piecewise linear function of time was reached by requiring consistency of the traction and displacement interpolators for a straight boundary and normally propagating plane waves. If consistency were required in this sense for other types of deformation, the resulting optimal displacement interpolator would in general be nonseparable and the calculation of discrete kernels would become quite cumbersome.

Among the separable interpolators along the line it seems likely that, for use with the traction interpolator D_o, linear interpolation in time is the best. The use of some other time dependence in U_j^n would preclude consistency of the sort demanded by equation (3.3). If equation

(3.3) were not satisfied the numerical representation of the boundary $x_2 = 0$ would not accurately reproduce the reflection of even normally incident plane waves.

The spatial variation of separable interpolators is one point at which some practical improvement might be possible. The use of piecewise constant displacement interpolation as in equation (3.5) has some serious drawbacks. For example, if one were to calculate analytically the tractions on a half plane appropriate to a displacement boundary condition $u(x_1,t) = U_j^n(x_1,t)$ it would be found (see equation (2.14)) that the traction $\tau(x_1,t)$ is not finite at the endpoints of the j^{th} surface element due to the discontinuity of $u(x_1,t)$ there. The traction would, however, be integrable and its average value over x_1 as a function of time would be

$$\frac{\mu}{\beta}\frac{\partial}{\partial t}\int_{-\infty}^{\infty} U_j^n(x_1,t)\,dx_1 \quad .$$

The traction interpolator which is piecewise constant in x_1 is completely incapable of representing this type of singular behavior, but it gives the correct average traction. Thus, the boundary value problem is accurately represented numerically only in the case of smooth variations of the displacement along the boundary. The use of higher order interpolation in space for the displacements could conceivably result in a more accurate numerical method by implying a more smoothly varying traction along the boundary. This more smoothly varying traction is

better represented by the traction interpolator. The principal justification for interpolating the displacement spatially according to equation (3.5) is that the resulting numerical scheme is capable of successfully treating representative problems requiring displacement interpolation.

The remainder of this chapter consists of a series of problems in which the accurate representation of the displacement integrals takes a critical role. These problems are intended to display the dependence of errors on discretization parameters and to give an idea of the grid density that is required for the solution of general types of problems. Section 2 contains the solution of a traction boundary value problem on a circular cavity in a whole plane. In this problem there is a shadow zone along the cavity boundary and accurate evaluation of the displacement there requires accurate treatment of the displacement integral. Section 3 contains the treatment of a displacement boundary value problem on a circular boundary. The analytic solution of the problem is obtained trivially through the selection of a specialized deformation and boundary condition. The numerical solution is nontrivial and requires accurate evaluation of the displacement integral. This problem also displays the accuracy of the numerical representation of the nonlocal normal derivative operator for a curved boundary, analogous to the operator DGI_j^n of Chapter 2. Section 4 contains the solution of a displacement boundary value problem similar to that of Section 3, but with the added complication of a nonsymmetric boundary. This problem illustrates the behavior of errors in a case where the boundary shape is not well represented by the boundary grid.

2. Diffraction by a Circular Cavity

Consider the problem depicted in Figure 3.1a. A localized traction is applied to the wall of a cylindrical circular cavity in a whole space. The waves propagate outward from this source into the medium and around the circumference of the cavity. Most of the boundary is well outside of the region affected by geometric rays and the displacement at those points is due to diffracted waves whose wave fronts propagate parallel to the boundary at the boundary. If the source near $\theta = 0$ is impulsive the waves propagating around the boundary decay rapidly with θ and are dispersive. For a detailed discussion of the wavefront system see Friedlander (1954). An approximate analytic solution to this problem is presented in Appendix E. It is based on a modification of Friedlander's waveform expansion technique given by Peck and Miklowitz (1969). This solution is valid for points on the boundary sufficiently far away from the area where the traction is applied. It will be used to evaluate the errors found in the numerical BIE solution of the problem in the shadow zone.

The analytic BIE formulation of this problem is

$$u(\theta,t) + P\int_{\theta'=0}^{2\pi}\int_{t'=0}^{\infty} 2K(a,\theta-\theta',t-t')\, u(\theta',t')\, dt'\, d\theta'$$

$$= \int_{\theta'=0}^{2\pi}\int_{t'=0}^{\infty} 2G(a,\theta-\theta',t-t')\, \tau(\theta',t')\, d\theta'\, dt' \qquad (3.7)$$

where

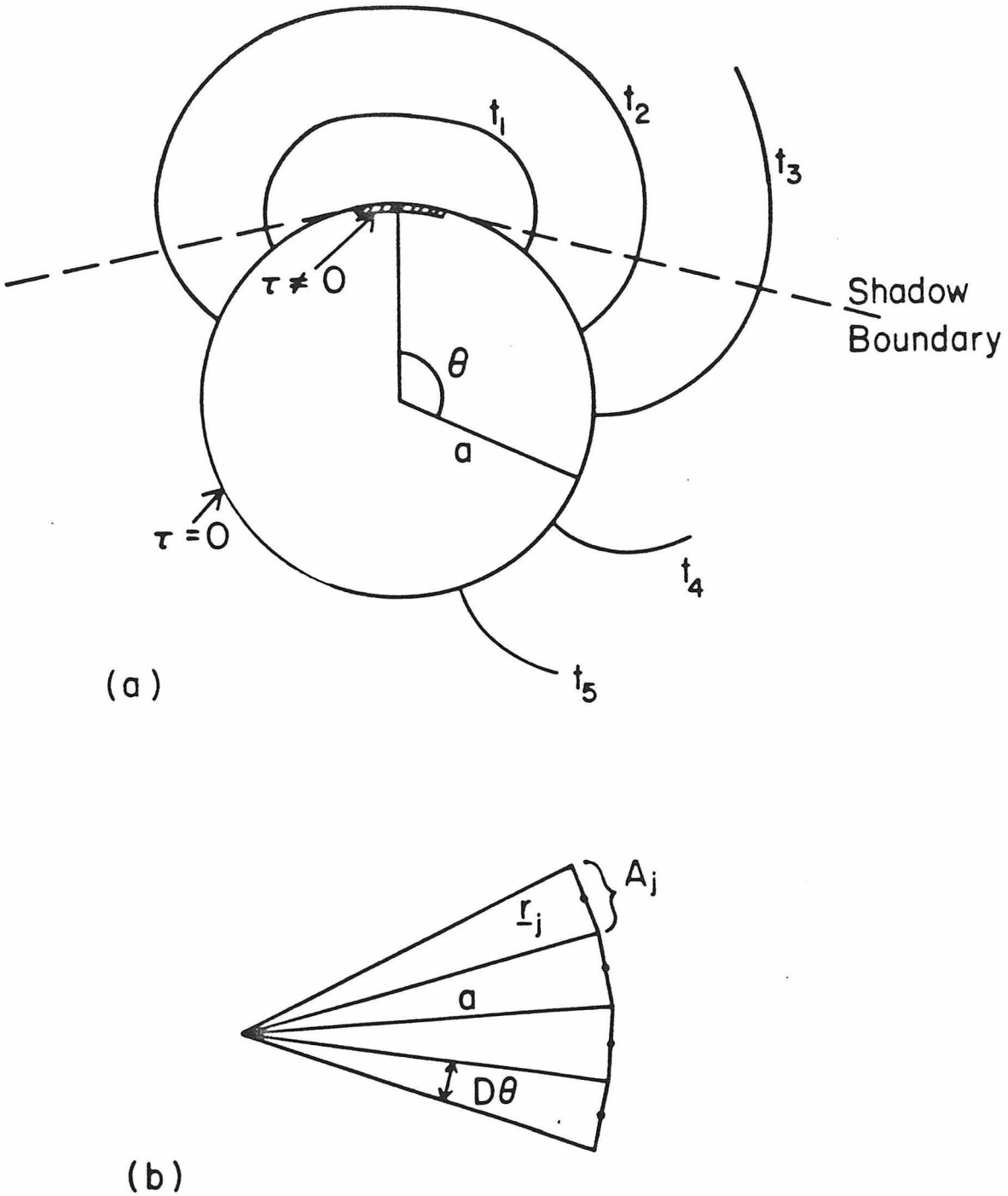

Figure 3.1. (a) The cavity geometry and wavefront system at different times. (b) Approximation of the boundary.

$$G(a,\theta,t) = \frac{1}{2\pi\mu} \frac{H(t - 2a|\sin(\theta/2)|/\beta)}{[t^2 - 4a^2 \sin^2(\theta/2)/\beta^2)]^{1/2}}$$

is the whole space Green's function specialized to points on a circle, and $K(a,\theta,t) = -\frac{\mu}{2} \frac{\partial}{\partial a} G(a,\theta,t)$. $u(\theta,t)$ and $\tau(\theta,t)$ are the displacement and traction on the circumference of the circle of radius a. They are periodic as a function of θ; e.g., $u(\theta,t) = u(\theta + 2m\pi,t)$.

The first step in carrying out the numerical BIE solution of this problem is to select the grid representing the boundary of the medium. The node points were selected to be equally spaced at intervals $D\theta$ along the boundary (see Figure 3.1b). The number of node points, J, was taken to be a power of 2. The surface elements A_j were approximated by straight line segments centered on the node points $\underline{r}_j$ and oriented tangent to the circle at r = a. Their length was

$$L = 2a \tan(D\theta/2).$$

The grid parameter for this problem is

$$Q = \beta\Delta t/L.$$

This grid is invariant under rotation about the center of the circle in steps $D\theta$. Since this symmetry exists in equation (3.7) the discrete kernels DG^n_{ij} and DK^n_{ij} depend on the spatial indices i and j only through the difference (i - j), modulo J. The numerical BIE can thus be written with index notation as

$$u^n_j + \sum_{i=1}^{J} \sum_{m=1}^{n} DK^{n-m}_{j-i} \; u^m_i = \sum_{i=1}^{J} \sum_{m=1}^{n} DG^{n-m}_{j-i} \; \tau^m_i \qquad (3.9)$$

or schematically as

$$(I + DK) \;**\; u_j^n = DG \;**\; \tau_j^n \tag{3.10}$$

The operation ** denotes discrete convolution over time and space indices with $DG_j^n = DG_{j+mJ}^n$ and likewise for DK_j^n, u_j^n and τ_j^n. $I = \delta_{no}\,\delta_{jo}$.

The solution of equation (3.10) for arbitrary τ_j^n may be accomplished by finding the causal convolutional inverse of the numerical operator I + DK, denoted by DS. Thus

$$u_j^n = (DS \;**\; DG) \;**\; \tau_j^n \tag{3.11}$$

The operators I + DK, DG, DS and DS ** DG are shown in Figure 3.2 for J = 32 and Q = 1/2. The inverse operator DS was calculated using the method described in Chapter 2. Algebraic manipulations were carried out using the FFT algorithm. The required periodicity in the spatial index was accomplished by not padding the spatial arrays with zeros in these processes.

As can be seen in Figures 3.2a, 3.2b and 3.2c, the operators DK, DG and DS are acausal. They transmit information between points on the circle with time delays corresponding to travel times across the interior of the circle rather than around the circumference. The composite operator DS ** DG is a numerical approximation of the impulse solution of the problem and should be causal; i.e., $DG_j^n = 0$ for $0 < nQ < j < J/2$. This is achieved in the operator shown in Figure 3.2d only in an approximate sense. Figure 3.3 is a plot of the same operator as in Figure 3.2d, with the near field portion truncated. There is a considerable amount

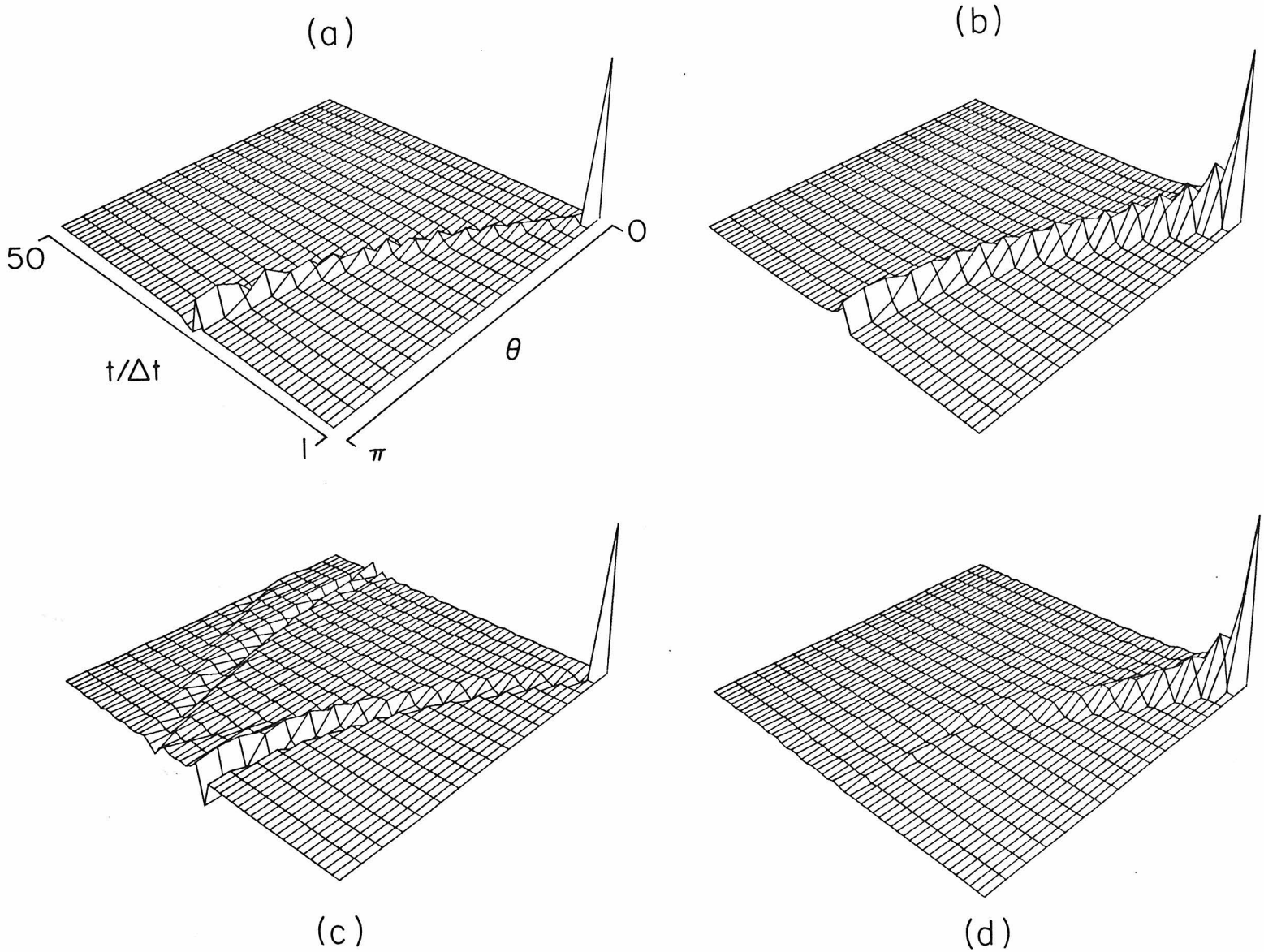

Figure 3.2. Numerical operators on the cavity boundary: (a) I + DK; (b) DG; (c) DS, and; (d) DS ** DG. See text.

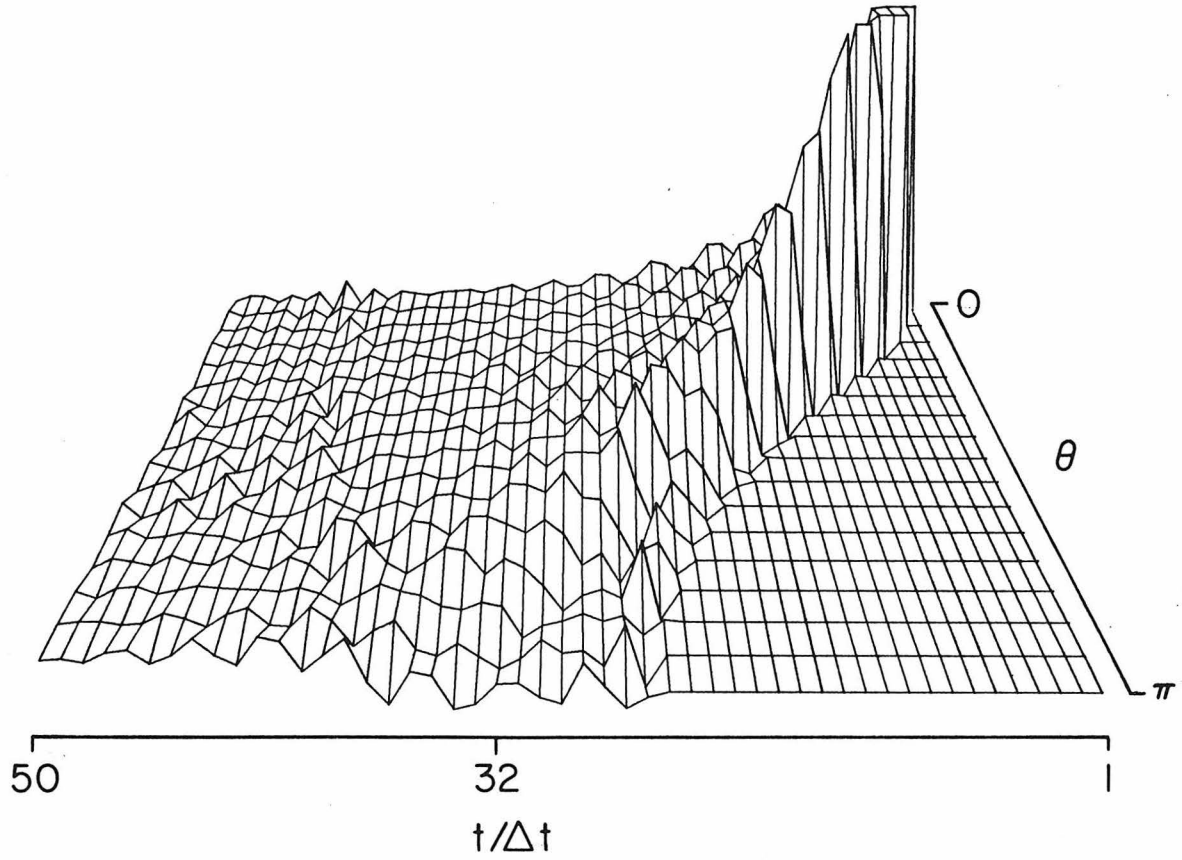

Figure 3.3. Detail of Figure 3.2(d). The arrival time of the diffracted wave is $t/\Delta t = 32$.

of high frequency noise in the operator, of which some is acausal. The acausal portion is of much smaller relative amplitude than the acausal portion of DG. It is the low frequency portion of the composite operator that is of interest here. The accuracy of the low frequency portion can be determined by low pass filtering. This will be accomplished by allowing $\tau(\theta,t)$ to be a smooth function of θ and t;

$$\tau(\theta,t) = e^{-(t_1^2 + \theta_1^2)} \tag{3.12}$$

where

$$t_1 = 5.34\ (t/T_h - 1)$$

$$\theta_1 = 5.34\ \theta/\theta_h$$

The half-power period of this source is T_h. The pulse width is about $T_h/2$.

Figure 3.4a is a plot of the displacement calculated by the analytic method of Appendix E for traction parameters $\theta_h = \pi/2$ and $\frac{\beta}{a} T_h = \pi/3$. This solution is taken to be exact for $|\theta - \pi| < 2\pi/3$. It is known to be inaccurate for values of θ near 0 and 2π. Figure 3.4b is a plot of the numerically evaluated displacement with discretization parameters J = 32 and Q = 1/2. The source parameters and vertical scale are the same as in Figure 3.4a. The maximum displacement at $\theta = \pi$ is about 0.05 of the maximum displacement at $\theta = 0$. The difference of the two solutions is shown in Figure 3.4c. The vertical scale in this figure has been exaggerated by a factor of about 5 relative to the

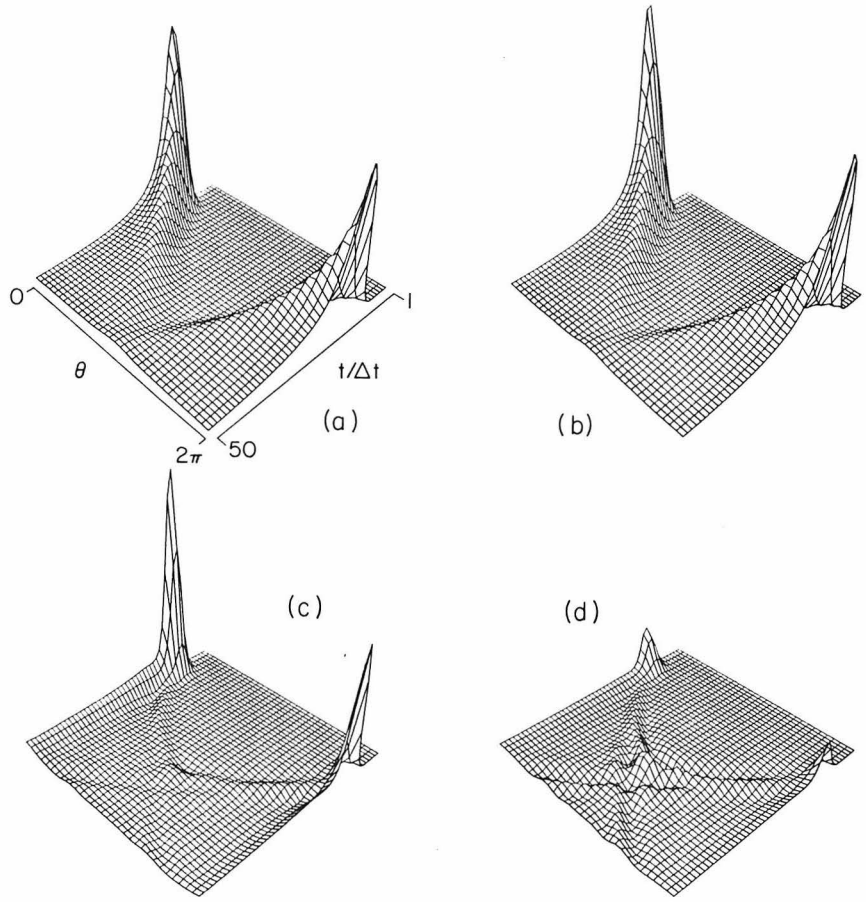

Figure 3.4. Diffracted waves and errors. (a) Analytic evaluation of displacement. (b) Numerical evaluation of displacement. (c) Difference between the two. (d) Difference normalized by the maximum value of the time series at each node.

vertical scale of Figure 3.4a in order to display the error near $\theta = \pi$. The maximum error at $\theta = \pi$ is about 0.01 of the maximum displacement at $\theta = 0$ in Figure 3.4a. Figure 3.4d is a plot of the error in Figure 3.4c renormalized at each value of θ by the maximum value of displacement occurring in Figure 3.4a at that value of θ. This figure displays the error in the time series at each value of θ as a fraction of the maximum exact displacement at that point. The maximum error at $\theta = \pi$ in this normalization is about 0.09. The largest errors near $\theta = \pi$ are acausal and could easily be eliminated using that criterion. The largest causal error in Figure 3.4d at $\theta = \pi$ is about 0.03.

A typical time series at $\theta = \pi$ is shown in Figure 3.5. The grid parameters there are $Q = 1/2$ and $J = 64$. The traction parameters are $\frac{\beta}{a} T_h = \theta_h = \pi/4$.

The errors in the BIE solution of the problem were evaluated for several values of traction parameters and values of J. It was found that the errors in the shadow zone scaled roughly linearly with the maximum error at $\theta = \pi$, normalized by the maximum displacement at that point. This value is given in Table 3.1 for the various problem parameters investigated. The error tabulated there is specifically

$$\varepsilon = \max |u_j^n - u_{ex}(\pi, n\Delta t)| / \max_n u_{ex}(\pi, n\Delta t) \qquad (3.13)$$

where $j = J/2 + 1$. To obtain a rough estimate of the size of the error as a fraction of the maximum displacement occurring on the grid; i.e., at $\theta = 0$, these numbers should be divided by 20.

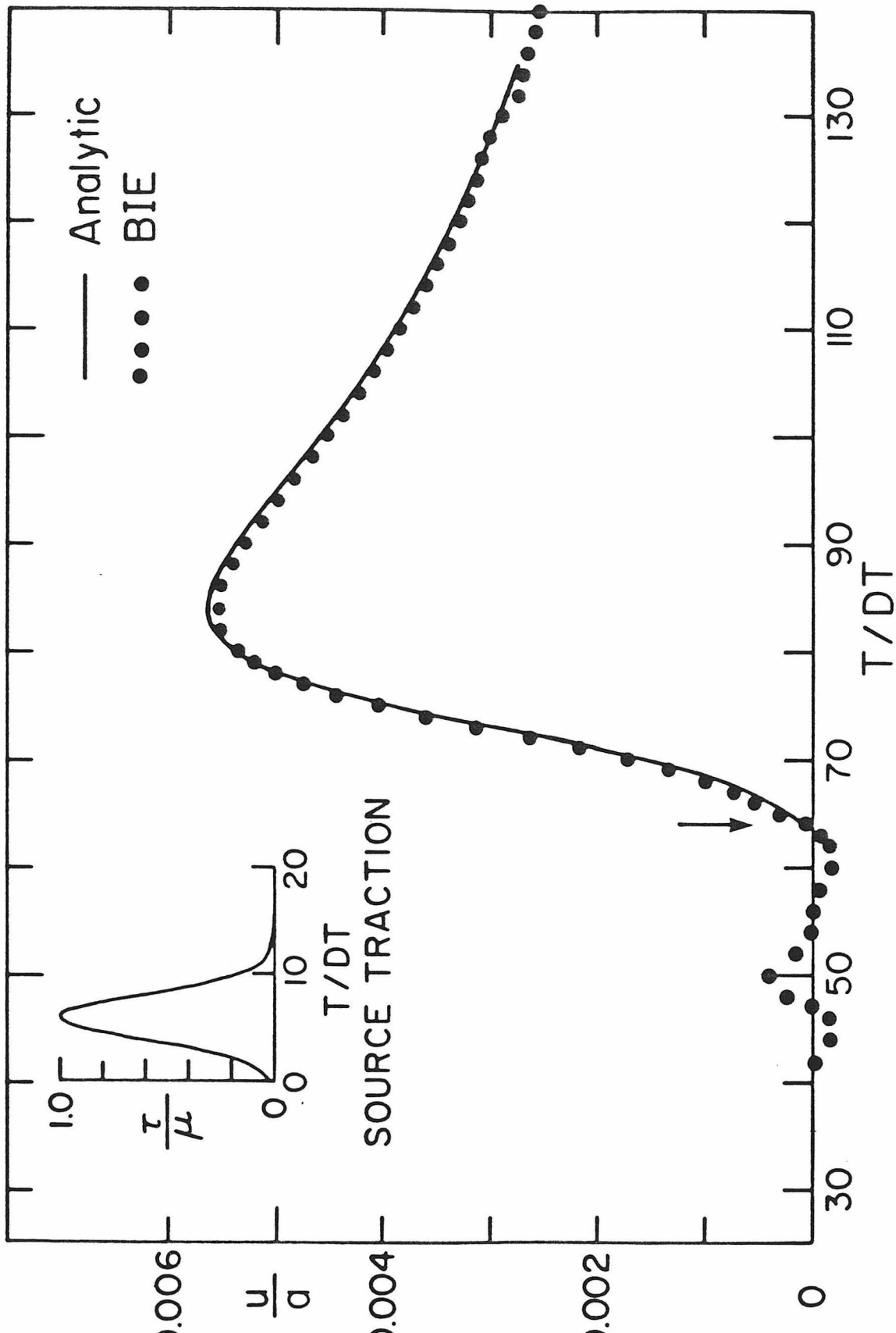

Figure 3.5. The history of displacement at $\theta = \pi$.

As can be seen in Table 3.1 the errors vary in a systematic way, decreasing monotonically as the grid is refined or the specified traction is made smoother. The dependence of these errors on T_h and J is rather interesting. For $J\,T_h > 8\pi\,a/\beta$ a rough estimate of ε is given by

$$\varepsilon \simeq \frac{2\pi}{JT_h} \quad .$$

For Q = 1/2,

$$T_h/\Delta t \simeq J\,T_h/\pi$$

so,

$$\varepsilon \simeq \frac{2}{T_h/\,t} \quad , \qquad T_h/\Delta t > 8 \quad .$$

This suggests that, for a given value of Q, the errors in the shadow zone vary linearly as $\Delta t/T_h$ regardless of the number of node points used, as long as the boundary is well represented.

Table 3.1. Maximum error ε in displacement at $\theta = \pi$ for $\theta_h = T_h$ and $Q = 0.5$, as defined in equation (3.13).

		J			
		16	32	64	128
$\frac{\beta}{a} T_n$	$\pi/6$	1.20	.442	.197	.099
	$\pi/3$	.793	.133	.076	.019
	$\pi/2$	.297	.088	.038	.015
	$2\pi/3$	.202	.054	.025	.013
	$5\pi/6$	.117	.032	.018	.012

3. Evaluation of Tractions on a Circle

The problem considered in this section is one in which the displacements are specified on a circular cavity in a whole space and the traction on the boundary is to be evaluated. As the boundary undergoes the prescribed motion, a plane wave propagating in the region exterior to the cavity will strike the boundary. The displacement boundary condition will be required to be of a special type so that the analytic solution to the problem becomes trivial, while the numerical solution is not. Specifically, if the incident wave is $F(r,\theta,t)$, then the incident wave is introduced in the analytic BIE (3.7) by adding $2F(a,\theta,t)$ to the right-hand side. If the displacement boundary condition requires

$$u(\theta,t) = F(a,\theta,t) \tag{3.14}$$

the effect of the cavity on the incident wave is nullified; i.e., the displacement in the region $r \geq a$ is exactly $F(r,\theta,t)$. It is asserted by the uniqueness theorems of elasticity that the solution of equation (3.7) should then be

$$\tau(\theta,t) = -\mu \frac{\partial}{\partial r} F(r,\theta,t)\Big|_{r=a} \tag{3.15}$$

The numerical BIE representation of this problem may be obtained in the same manner as in the previous section. It takes the schematic form

$$(DK - I) \;**\; F_j^n = DG \;**\; \tau_j^n \tag{3.16}$$

where $F_j^n = F(a,(j-1)D\theta,n\Delta t)$ and τ_j^n is intended to represent $\tau((j-1)D\theta,(n-1/2)\Delta t)$. The solution may be obtained by calculating the causal convolutional inverse of DG, which will again be called DGI. Then

$$\tau_j^n = (DGI \;**\; (DK - I)) \;**\; F_j^n \tag{3.17}$$

The incident wave was taken to be a plane wave Gaussian form,

$$F(r,\theta,t) = \exp(-\xi^2)$$

$$\xi = 5.34(t - T_h + r\cos\theta/\beta)/T_h$$

The half power period of this displacement wave is T_h. The pulse width is about $T_h/2$. The half power period of the traction given by equation (3.15) is about $0.51\ T_h$.

Figure 3.6a displays the analytic traction $\tau(\theta,t)$ as a function of θ and t for $\frac{\beta}{a} T_h \simeq \pi/2$. Figure 3.6b is a plot of the numerically evaluated traction for grid parameters Q = 1/2 and J = 32. Figure 3.6c is a plot of the difference of the analytic and numerical results, with the vertical scale exaggerated by a factor of about 6. The maximum error, occurring at $\theta = \pi$, is about 0.12 as large as the maximum traction occurring there. This is also the maximum traction acting on the grid. As can be seen in this figure, the largest error at each value of θ is coincident in time with the propagating wavefront. At a given value of θ, this error is proportional to the time derivative of the

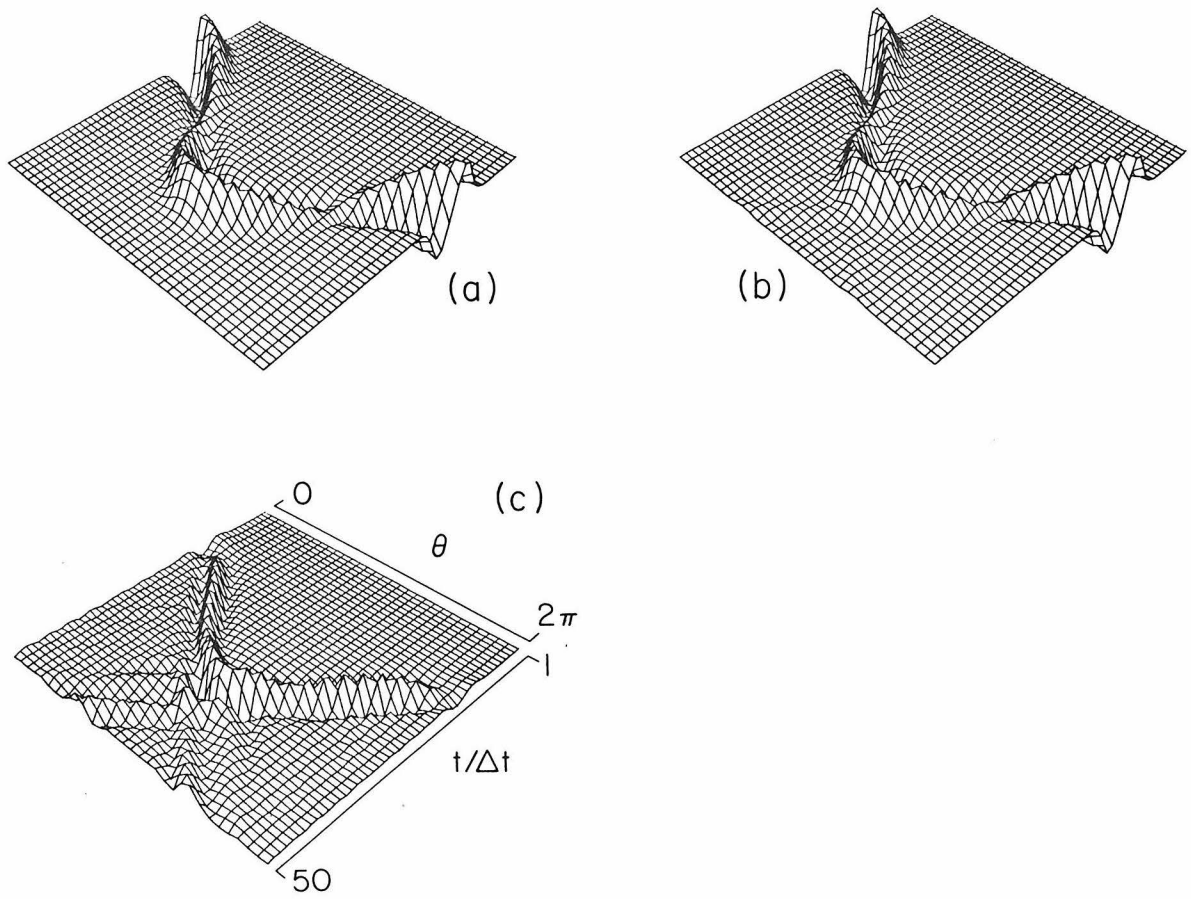

Figure 3.6. The traction evaluated on a circle (a) analytically and (b) numerically. The difference is plotted in (c). The maximum error at $\theta = \pi$ is about 12%.

analytic traction. There is also a smaller error propagating circumferentially after passage of the incident wave.

The calculation described here was repeated for several values of $T/\Delta t$ and J, with Q = 1/2. The maximum error occurring at $\theta = \pi$ is given in Table 3.2, as a fraction of the maximum analytic traction acting there. As can be seen from that table, the size of the error depends primarly on the parameter $T_n/\Delta t$ rather than some combination of $T_n/\Delta t$ and J. This result is consistent with conclusions reached regarding dependence of errors on grid parameters in the last section; i.e., for a well represented boundary errors depend primarily on the ratio of time step (or grid length) to deformation time scale (or length scale).

4. Evaluation of Tractions on a Nonsymmetric Boundary

This section contains the treatment of a displacement boundary value problem on a nonsymmetric boundary. The boundary shape is shown in Figure 3.7a. Figures 3.7b-3.7e show the increasingly finer discretizations of this boundary used in calculations here. They have the common property that at two points on the boundary (see, e.g., nodes 13 and 30 in Figure 3.7d) the shape is poorly represented by straight line segments because of the rapid rotation of the normal along the boundary. By setting up the boundary value problem in the manner described at the beginning of the previous section it is possible to find an analytic solution to the problem; i.e., there is an inhomogeneous term $2F(\underline{r},t)$ in the BIE and the displacement boundary condition requires

Table 3.2. Maximum error in traction at $\theta = \pi$. $Q = 1/2$ and $\beta T_h/a \simeq (T_h/\Delta t)/J$.

		J			
		16	32	64	128
$T_n/\Delta t$	5	.79	.60	.79	.65
	10	.30	.17	.35	.22
	15	.13	.12	.15	.10
	20	.06	.07	.09	.07
	25	.04	.05	.07	.04

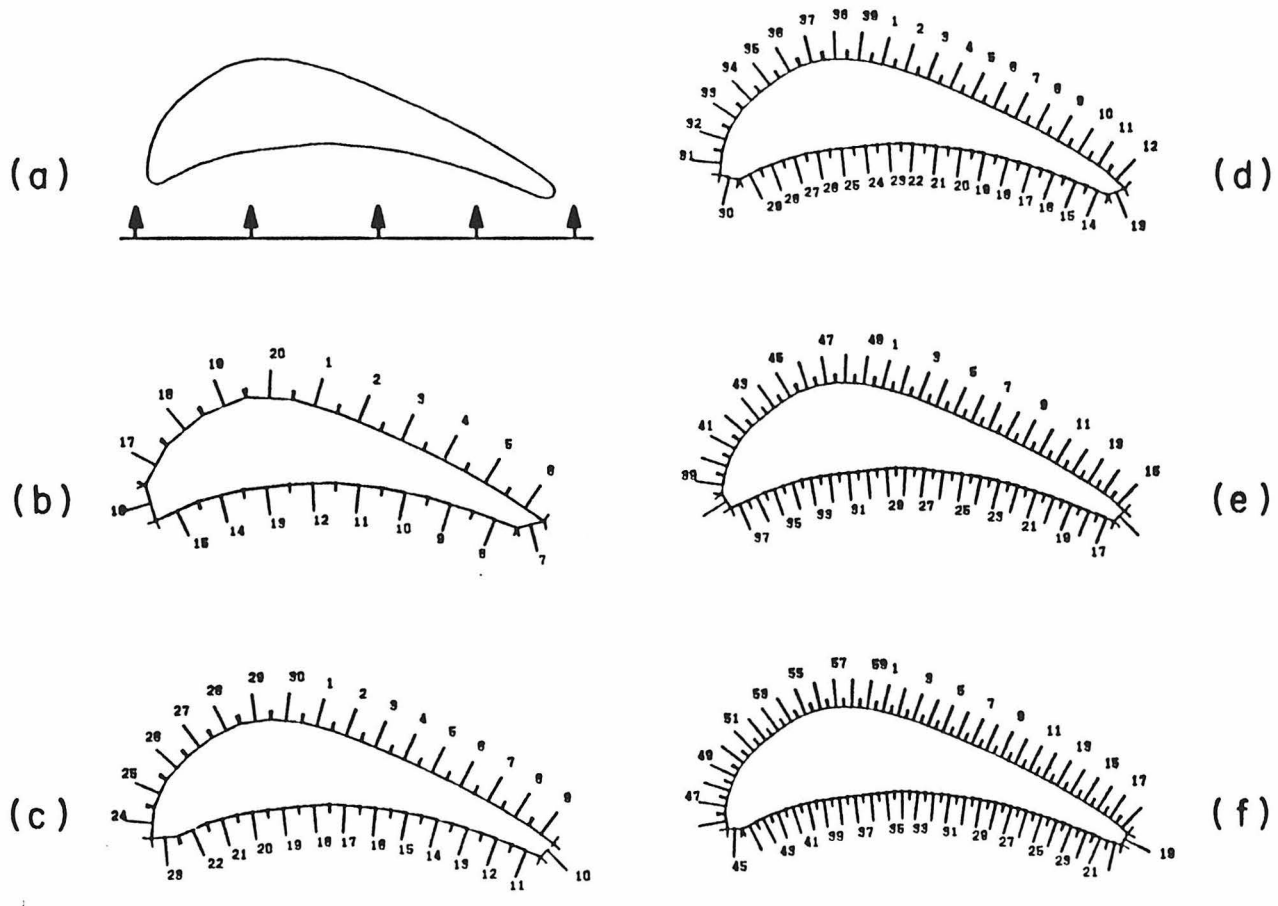

Figure 3.7. Boundary shape and its discretizations. Tic marks indicate the extent of tangential straight line segments. Normal directions are numbered according to nodes. The incident wavefront is indicated in (a).

$$u(\underline{r},t) = F(\underline{r},t) \quad , \quad \underline{r} \in \partial B \quad .$$

Then

$$\tau(\underline{r},t) = \mu \frac{\partial}{\partial n} F(\underline{r},t) \quad , \quad \underline{r} \in \partial B \quad .$$

The incident wave will again be taken to be a Gaussian plane wave with half power period T_h. The wave will propagate so as to encounter the concave portion of the boundary first. The direction of propagation is indicated in Figure 3.7a.

The numerical BIE describing this problem may be written as

$$\sum_{m=1}^{n} \sum_{j=1}^{J} DK_{ij}^{n-m} F_j^m - F_j^n = \sum_{m=1}^{n} \sum_{j=1}^{J} DG_{ij}^{n-m} \tau_j^m \qquad (3.18)$$

where $F_j^n = F(\underline{r}_j, n\Delta t)$. The coefficients DG_{ij}^n have indices ij corresponding to $\underline{r}_i$, the receiver coordinate, and $\underline{r}_j$, the source coordinate. Because of the surface orientation involved in the definition of DG_{ij}^n (see Appendix D) these coefficients do not possess the symmetry in receiver and source coordinates present in the analytic Green's function; i.e., $DG_{ij}^n \neq DG_{ji}^n$. The dependence of these discrete kernels on surface element orientation is much weaker than that of the kernels DK_{ij}^n. These contain a factor of form $(\underline{r}_j - \underline{r}_i) \cdot \hat{n}_j$, where $\hat{n}_j$ is the outward normal of the j^{th} surface element. Because of this the kernels DK_{ij}^n play an important role in representing the boundary shape when surface normals change orientation substantially over a length of the order of a surface element length. The other important role of the coefficients DK_{ij}^n, the casting

of shadows, has been examined in the previous sections of this chapter. It is the purpose of this section to examine the dependence of errors in numerically evaluated tractions on discretization parameters when the boundary shape is poorly represented by the surface grid and when the interpolation scheme poorly represents the actual behavior of the tractions.

In carrying out the solution of equation (3.18) for τ_j^n it was first necessary to evaluate the quantities

$$V_j^n = \sum_{m=1}^{n} \sum_{j=1}^{J} DK_{ij}^{n-m} F_j^m - F_j^n \tag{3.19}$$

This was done by first tabulating the values of the incident displacement wave F_j^m. The time series F_j^m, m=1, ···, M were then transformed using the FFT and stored. For a fixed value of receiver index i the time series DK_{ij}^n were calculated and stored for j=1, ···, J. These were then transformed, multiplied by the discrete Fourier transform of F_j^m, and summed over source index j. Inversion of the transform and subtraction of F_i^n gave V_i^n. This procedure accomplished the calculation of V_i^n without requiring storage of all MJ^2 of the coefficients DK_{ij}^n at one time.

To complete the solution it was required to solve the algebraic system

$$\sum_{j=1}^{J} \sum_{m=1}^{n} DG_{ij}^{n-m} \tau_j^m = V_i^n \tag{3.20}$$

As discussed previously, this algebraic system may be solved trivially by time stepping if the time step is selected to be small enough. Let

$$Q = \max_{j=1,\cdots,J} \left(\frac{\beta \Delta t}{L_j}\right)$$

where L_j is the length of the j^{th} surface element. In this problem the node points were taken to be centered on the surface elements. It was desired that the element lengths L_j be as uniform as possible in order to obtain the maximum time step for a given value of Q. If $Q \leq 1/2$ the causality properties of the Green's function cause the algebraic system to be diagonal; i.e.,

$$DG^0_{ij} = 0 \qquad \text{for } i \neq j \ .$$

Equation (3.20) may then be rearranged as

$$\tau^n_j = \frac{1}{DG^0_{ii}} \left\{V^n_i - \sum_{m=1}^{n-1} \sum_{j=1}^{J} DG^{n-m}_{ij} \, \tau^m_j\right\} \tag{3.21}$$

At time step n, the tractions τ^m_j for m = n-1, n-2, $\cdots$, 1 are already known, so it is a simple matter to evaluate τ^n_i.

In calculating the quadratures in this formula, there are some practical problems stemming from the fact that there are MJ^2 coefficients DG^n_{ij}. This can be a very large number and it is worth the effort to use computer storage in an efficient manner. The arrangement of storage used here was motivated by the circumstance that the kernels

DG^n_{ij} preserve the time translation invariance of the analytic Green's function and by characteristics of the computer used. The machine used here had a large virtual memory on disk and semiconductor memory sufficient to simultaneously hold arrays containing τ^n_j and V^n_j for all values of n and j, and DG^n_{ij} for all ij and a fixed value of n. When a variable was referenced which was not available in semiconductor memory, blocks of size one kiloword were automatically written to and from disk to make them available. In order to reduce the amount of disk I/O involved in the calculation it was desired that when a portion of the array containing DG^n_{ij} was in semiconductor memory, that portion should be used in all possible calculations before another portion was referenced. To this end, the array containing DG^n_{ij} was ordered in the FORTRAN program such that the time index n corresponded to the most slowly varying address of the array; i.e., DG^n_{ij+1} occupied the register next in address to the register containing DG^n_{ij}, $DG^n_{i+1\,1}$ was next to DG^n_{iJ}, and $DG^{n+1}_{1\,1}$ was next to DG^n_{JJ}. Thus, one could place DG^n_{ij}, i=1, ···, J; j=1, ···,J in a small temporary array in fast memory with a minimum amount of disk I/O.

Equation (3.21) may be rewritten in the form

$$\tau^n_i = \frac{1}{DG^o_{ii}} \left\{ V^n_j - \sum_{m=1}^{n-1} b^{nm}_i \right\} \tag{3.22}$$

$$b^{nm}_i = \sum_{j=1}^{J} DG^{n-m}_{ij}\, \tau^m_j \tag{3.23}$$

In order to evaluate b_i^{nm} for i=1, ···, J it is necessary to have DG_{ij}^{n-m} for all i,j in fast memory. At time step n, τ_i^{n-1}, τ_i^{n-2}, ···, τ_i^1 for i=1, ···, J have already been evaluated and may be referenced in the program without causing a great deal of I/O activity, if any. It is thus efficient to evaluate $b_i^{n+p,m+p}$ for any p, $n-m \leq p < 2n$, at the same time as b_i^{nm}. After some thought one arrives at the following scheme:

1) at time step n determine all numbers ℓ_1, ℓ_2, ···, ℓ_q which are integer factors of (n - 1); i.e., $(n - 1)/\ell_p$ is an integer;

2) place in a small temporary storage array the values of $DG_{ij}^{\ell_1}$ for all i,j;

3) calculate $b_i^{n(n-\ell_1)}$, $b_i^{(n+1)(n-\ell_1+1)}$, ···, $b_i^{(n+\ell_1-1)(n-1)}$ for i=1, ···, J and accumulate them according to equation (3.23). This could be the same array as that used to store the tractions τ_j^n;

4) repeat the process for ℓ_2, ℓ_3, ···;

5) at this point the sums

$$\sum_{m=1}^{n-1} b_i^{nm}$$

i=1, ···, J have been accumulated, during the current time step and previous time steps. It is now possible to evaluate τ_i^n, i=1, ···, J; and,

6) proceed to the next time step.

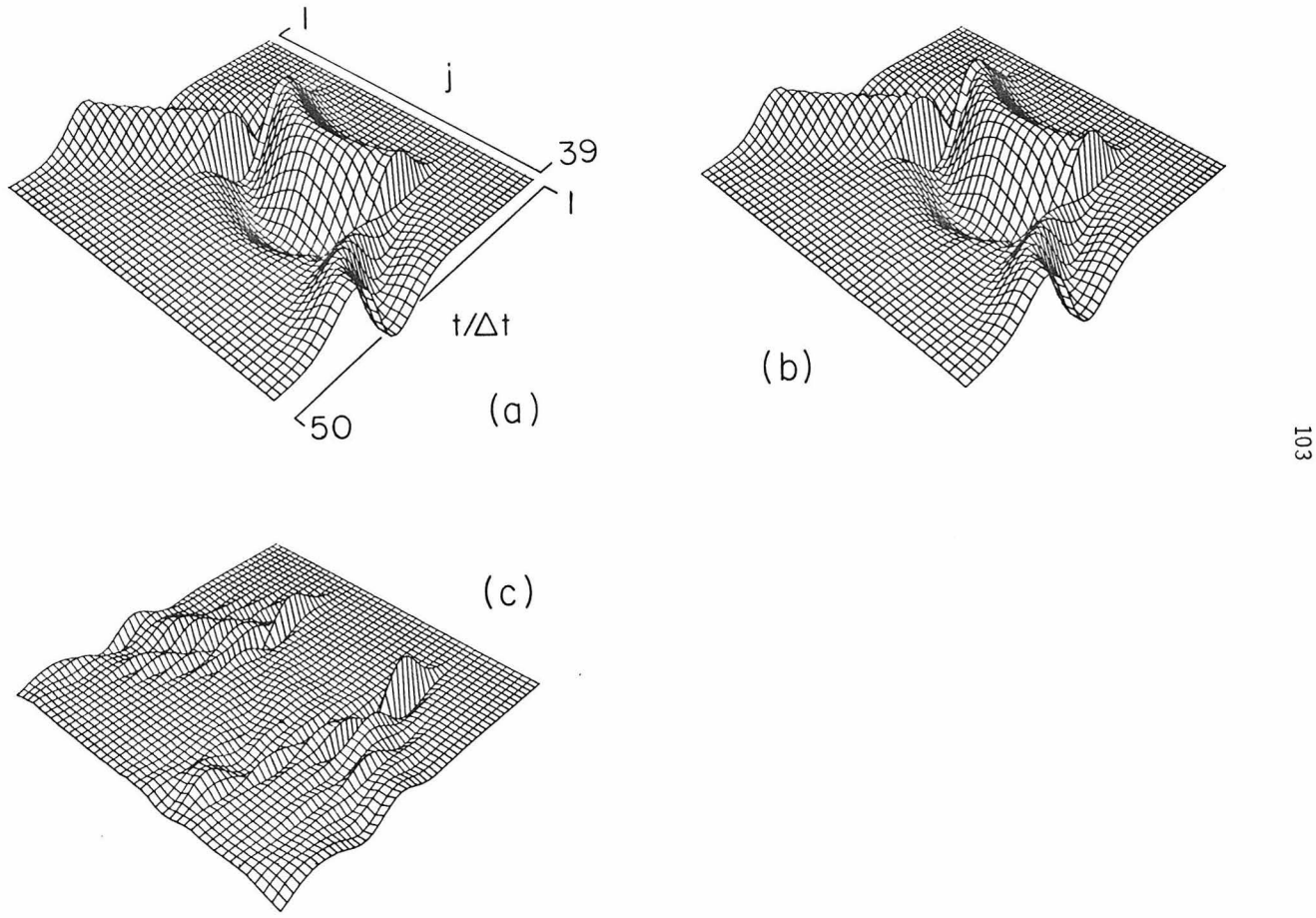

Figure 3.8. Analytically and numerically evaluated tractions are shown in (b) and (a), respectively. The difference between them is shown in (c). The maximum error at j = 30 is about 12%.

Using this technique the amount of disk I/O used in bringing the discrete kernels into fast memory is minimized. The process may be adapted to calculations for any type of elastic deformation. One consequence of this procedure is that DG_{ij}^{n} for $n > M/2$ need only be brought into fast memory once, where M is the total number of time steps. For $n = M/3$, DG_{ij}^{n} need only be fetched three times, etc. As a result of this, it may be convenient to recalculate some of the kernels DG_{ij}^{n} for "large" n as they are needed, rather than calculating them all at once and storing them.

The calculation just described was carried out for various values of $T_h/\Delta t$ and J. Figure 3.8b displays the traction for J = 39 and $T_h/\Delta t = 25$. Figure 3.8a is a plot of the analytically calculated traction, and Figure 3.8c is a plot of the difference of the two. The maximum errors appearing there, as a fraction of the maximum analytic traction, are at nodes 13 and 30 with errors, respectively, of 0.08 and 0.12. The errors elsewhere on the grid are smaller than 0.04. It is important to note that the largest errors are confined to small regions near nodes 13 and 30; i.e., the effects of the badly represented boundary shape are confined to the sharp corners and do not greatly affect errors elsewhere.

Table 3.3 gives the maximum value of the error occurring near one point on the boundary for various values of J and $T_h/\Delta t$ for Q = 1/2. The half power period of the traction is about T /2; there are about $T_h/4\Delta t$ grid points per traction half power wavelength. The specific node selected for each value of J was the one which had the maximum

Table 3.3. Maximum error in traction.

$T_h/\Delta t$	J = 20	30	39	49	59
5	.26	.51	.32	.57	.47
10	.16	.17	.12	.21	.32
15	.11	.15	.08	.11	.16
20	.08	.15	.08	.09	.11
25	.07	.15	.08	.09	.09
j =	7	10	13	15	18

error for the largest value of $T_n/\Delta t$. As can be seen from this table, the maximum error does not vary in a systematic way with increasing fineness of the grid, but for fixed J it does decrease for larger values of $T_n/\Delta t$. Considering the low quality of the representation of the boundary shape, it is rather surprising that errors of order 10% may be achieved at all. It should also be noted that there are two distinct bad approximations affecting the errors produced in this calculation. The surface elements approximate the shape of boundary poorly and, in addition, the tractions have been taken to be constant across these elements. If it were desired to improve the accuracy of the technique for sharp corners it would be necessary to use curved surface elements as well as an improved method of interpolation along the boundary. The use of curved boundary elements alone leads to no significant improvement in performance. This has been verified by numerical experiment. A method for producing discrete kernels for curved surface elements is outlined in Appendix D.

5. Conclusions

The numerical results of this chapter and Chapter 2 and the specialized theoretical results of Appendix C suggest that the time stepping elastodynamic BIE techniques produce errors which vary in a systematic way for arbitrary boundary shapes. It is then possible to control them by proper selection of discretization parameters. For a well represented boundary shape the error evaluations given in this chapter and the previous one for the fundamental boundary value problems

are likely to be typical. In general, for a well represented boundary, the maximum error is primarily a function of the ratio of time step to deformation period. For a specific application, examination of the results of these two chapters should indicate what this ratio should be for a given acceptable largest error. For many seismological problems, in which displacement is to be evaluated, 10 to 15 time steps per period are adequate. This ratio is usually quoted as a ratio of grid length to deformation wavelength. For Q = 1/2, 5-10 grid lengths per wavelength will yield equivalent results to those typically obtained using other numerical methods. In general, the BIE technique is found to be competitive with these other methods.

If the boundary shape is not represented well by the set of surface elements, the maximum value of the error is not easily predictable at a given node point. The error is systematic as a function of the ratio of time scales and tends to be localized near the poorly represented part of the boundary when the ratio of time step to deformation period is small. Because of this it is possible to carry out calculations that are accurate along most of the boundary, while errors at isolated poorly represented points along the boundary may be rather large. This is an important feature since it allows one to discretize a boundary without using a strict requirement regarding the maximum value of the ratio of grid length to local radius of curvature. In order to properly estimate tractions near a sharply curved boundary point it is still necessary to represent the boundary with a large number of node points.

Chapter 4

LOVE WAVE WITH TOPOGRAPHY

1. Introduction

This chapter describes a calculation in which an effect of surface topography on Love waves is evaluated. The propagating medium consists of a homogeneous layer over a homogeneous half-space, and the contacting surface is perfectly flat. The thickness of the layer is allowed to increase over a restricted area (see Figure 4.1 for a description of the medium). The deformation is assumed to be purely two dimensional, i.e., the Love waves are normally incident on an infinitely long mountain range of constant cross section. The particular aspect of the problem considered in detail here is the effect that such surface topography can have on observationally determined dispersion relations in the vicinity of the mountain range.

There have been several previous studies of Love wave propagation through regions of laterally varying structure. Hudson and Knopoff (1964) consider a problem in which Love waves propagate in a layered wedge with traction-free surfaces. The motion is assumed to be composed of Love modes only, and reflection coefficients are evaluated by means of an analytic integral equation method. Knopoff and Hudson (1964) extend this method to the problem of transmission of Love nodes at the contact of abutting layered quarter spaces. The absence of reflected waves is assumed. Alsop (1966) treats a similar problem in which the motion is again assumed to be composed of Love modes only.

Reflection and transmission coefficients are evaluated by satisfying the displacement continuity conditions at the quarter spaces' contact in a least squares sense, while equating the tractions.

Slavin and Wolf (1970) consider problems in which a Love wave propagates in a layer of varying thickness overlying a perfectly rigid half-space. In this study, boundary conditions at the free surface are satisfied in a least squares sense. The analysis involved is rather elaborate and the restriction to rigid boundary conditions at the bottom of the layer makes this approach unappealing for geophysical applications. Lysmer and Drake (1971) treat a large number of problems using a time harmonic finite element method. The problems are appropriate to ocean-continent transition zones and one is quite complex, including a dipping slab and details of crust and upper mantle structure. The study is restricted in the sense that all waves reflected and transmitted from the finite width transition zone are assumed to be Love modes. Transmission and reflection coefficients are calculated.

Boore (1970) treats ocean-continent type transition Love wave problems using a time-stepping finite difference method. The method employed is sufficiently accurate to determine the effect of such regions on dispersion relations. The incident wave is introduced using an initial value technique.

Gregerson and Alsop (1974) model the horizontal refraction of Love waves. Hudson (1979) gives a perturbation scheme for similar calculations which is based on a parabolic approximation of the equations of motion. It assumes short horizontal wavelengths and no backscattering.

Minor modifications of this theory are necessary for applications to Love waves.

This problem serves as an expository example for several useful procedures which may be employed with the BIE technique. These procedures are methods of rearranging and partially solving systems of discrete BIEs to obtain particularly useful numerical representations of the dynamic behavior of the medium. These rearrangements are feasible because of the causal nature of the kernels used in the time domain BIE technique. As will be shown, this flexibility allows one to combine the BIE technique with available analytic methods of treating wave propagation problems. The resulting hybrid approach to problem solutions permits the economical treatment of problems not normally considered to be entirely within the scope of the either analytic or numerical methods.

In the present problem there are two length scales of greatly differing magnitude: the distance of the source from the mountain range and the width of the mountain range. In order to examine the details of wave propagation in the vicinity of the mountain range, the discretization length scale must be considerably smaller than the mountain range width. The numerical problem of propagating the incident Love waves over a distance large compared to the mountain range width, with resolution at the desired discretization length, is then rather extreme in terms of the required storage and computation time. On the other hand, analytic methods are not available for treating the propagation problem in the vicinity of topographic relief in other than a perturbative sense.

The approach taken to the problem here uses an analytic method to evaluate the incident wave field in the vicinity of the mountain range. A BIE technique is then used to evaluate the effect of the topography on the propagation of the wave in the vicinity of the mountain range. This can be done in a straightforward manner by casting the numerical representation of the problem in such a form that the incident wave is identified as a separate inhomogeneous term of the discrete equations. The analytically evaluated wave field can then be substituted for this term. The effects of the topography on the waves far from the mountain range may be evaluated by analytic methods employing results from the numerical calculation.

The medium in this problem will be considered to be composed of three homogeneous bodies: the half-space (B_3 in Fig. 4.1), a layer of uniform thickness (B_2) and a third body (B_1) representing the topographic relief. The tractions and displacements are continuous across the contacting surfaces of these bodies. There are traction-free surfaces as indicated in the figure. Consider the mechanical system consisting of the half-space and layer of uniform thickness. This medium has translational symmetry in the horizontal direction. If the surfaces S_1 and S_2 are uniformly discretized the system of discretized BIEs representing this medium will retain this symmetry. The symmetry will be manifested in identity relations among the discrete kernels involving the spatial indices, causing the numerical equations to take the form of discrete convolution equations. By applying the boundary conditions along the layer-half space interface (S_2 in Fig.

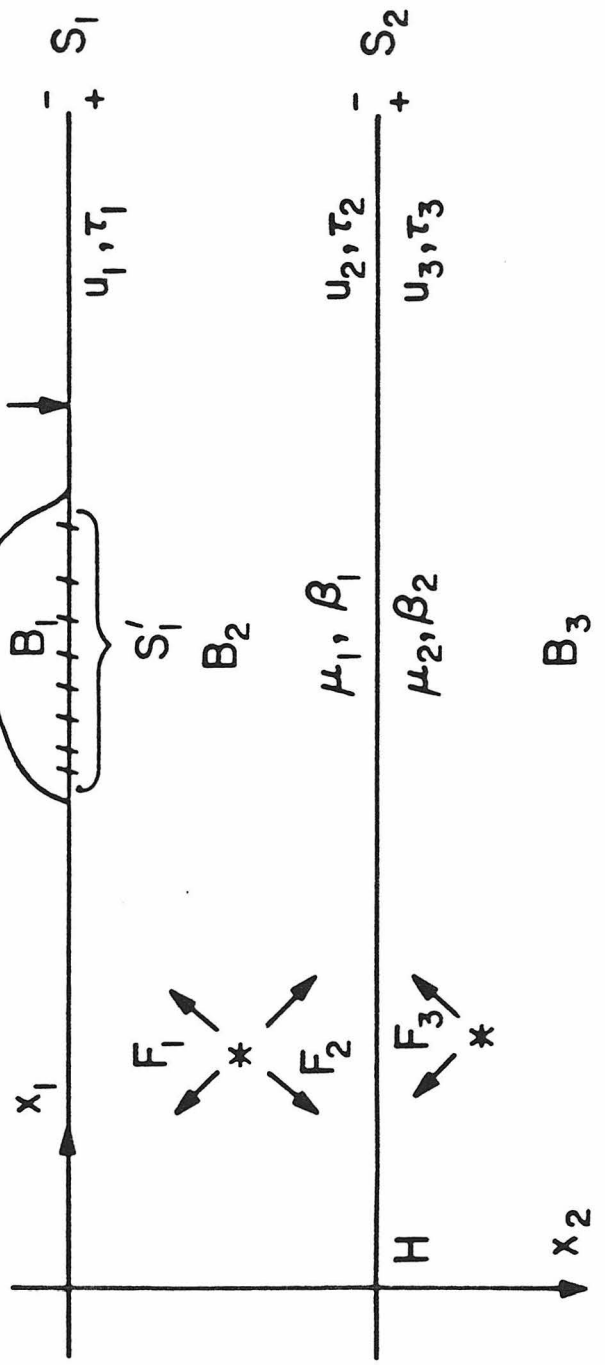

Figure 4.1. Problem geometry and definition of variables.

4.1) these equations may be efficiently rearranged, through numerical operations carried out on the discrete kernels, to yield a composite discrete BIE along S_1, the layer's upper surface. This composite BIE is a discrete relation between the tractions and displacements along S_1 and it represents the dynamic behavior of the layer and half-space system. It is a direct formulation of the boundary value problem for a heterogeneous medium and is arrived at by a process of eliminating unknown variables appearing in the discrete BIE representation of the boundary value problems for the homogeneous subregions. In this respect, the discrete equations are manipulated in a manner somewhat similar to the way that analytic equations are treated.

If this composite BIE is cast in an appropriate form, the inhomogeneous term in it may be identified as the wave which would be propagating in the medium if tractions along S_1 were everywhere zero. In Sections 2 and 3 of this chapter the correspondence between conventional analytic and BIE treatments of the propagation problem in the uniform layer and half space is examined. In Section 2 the analytic BIEs representing this medium are arranged to form an analytic analog of the discrete composite BIE. Identification of the various quantities in this equation yields considerable insight into the meaning of the discrete, numerically evaluated operators of the composite BIE. The numerical operators are shown to be discrete versions of reflection coefficients, phase delays and so forth. The method used to produce the composite numerical operators is discussed in Section 3. Section 4 discusses the manner in which the topographic body is introduced

into the calcuation. This is done by producing a discrete BIE representation of its dynamic behavior in which the traction-free boundary condition on its upper surface is explicitly included. Section 5 contains a solution to a particular wave propagation problem in which the incident wave is a fundamental mode Love wave. The dispersion curve resulting from a standard observational procedure is displayed there.

2. Analytic Composite BIE

This section contains a discussion of an analytic analog of the composite discrete BIE which plays a central role in the solution of the problem. This discussion is present primarily to make clear the physical meaning of discrete quantities which will appear later in the chapter. The analytic system of BIEs representing the motion of the uniform layer and half-space can be written as three equations. The analytic BIE representing the boundary value problem for the homogeneous half-space is

$$u_3(x_1,t) = 2G_2(x_1,0,t) ** \tau_3(x_1,t) + 2F_3(x_1,t) \qquad (4.1)$$

where u_3 is the displacement at the top of the half-space and τ_3 is the traction acting there. F_3 is the displacement field incident on the top of the half-space due to sources in the half-space. The operation ** denotes convolutions over x_1 and t. The BIE representing

the boundary value problem for the uniform layer may be written as two equations

$$u_2(x_1,t) = 2G_1(x_1,0,t) ** \tau_2(x_1,t) + 2G_1(x_1,H,t) ** \tau_1(x_1,t)$$
$$- 2K_1(x_1,H,t) ** u_1(x_1,t) + 2F_2(x_1,t) \qquad (4.2)$$

$$u_1(x_1,t) = 2G_1(x_1,0,t) ** \tau_1(x_1,t) + 2G_1(x_1,H,t) ** \tau_2(x_1,t)$$
$$- 2K_1(x_1,H,t) ** u_2(x_1,t) + 2F_1(x_1,t) \qquad (4.3)$$

where u_2,τ_2 and u_1,τ_1 are the displacement and traction at the bottom of the layer and the top of the layer, respectively. The outward normal is used to define traction. The source terms F_2 and F_1 are the whole-space displacements at S_2 and S_1 due to sources within the layer. The kernels G and K are the usual singular whole-space influence functions

$$G_i(x_1,x_2,t) = \frac{1}{2\pi\mu_i} \frac{H(t - (x_1^2+x_2^2)^{1/2}/\beta_i^2)}{[t^2 - (x_1^2+x_2^2)/\beta_i^2]^{1/2}}$$

$$K_1(x_1,x_2,t) = \mu_1 \frac{\partial}{\partial x_2} G_1(x_1,x_2,t)$$

Note that the index i of G_i pertains to material properties. Equation (4.1) is coupled to equations (4.2) and (4.3) by the boundary condition along S_2

$$\begin{aligned} \tau_2(x_1,t) &= -\tau_3(x_1,t) \\ u_2(x_1,t) &= u_3(x_1,t) \end{aligned} \tag{4.4}$$

Equations (4.1) - (4.3) may be converted to algebraic relations by use of the Fourier transform in x_1 and t. Let

$$\tilde{u}_i(k,\omega) = \int_{-\infty}^{\infty} e^{ikx_1} \int_{-\infty}^{\infty} e^{-i\omega t} \; u_i(x_1,t)\, dt\, dx_1$$

and likewise for $\tilde{\tau}_i$, $\tilde{G}_i$ and $\tilde{F}_i$. We then obtain

$$\begin{aligned} \tilde{G}_j(k,H,\omega) &= \frac{-i}{2\mu_j\gamma_j} \; e^{-i\gamma_j H} \\ \tilde{K}_1(k,H,\omega) &= \frac{-1}{2} \; e^{-i\gamma_1 H} \end{aligned} \tag{4.5}$$

$$\gamma_j = (\omega^2/\beta_j^2 - k^2)^{1/2}$$

$$\text{Im}\,(\gamma_j) \leq 0$$

The transforms of equations (4.1) - (4.4) constitute five algebraic relations among the six unknown quantities: $\tilde{u}_1$, $\tilde{\tau}_1$, $\tilde{u}_2$, $\tilde{\tau}_2$, $\tilde{u}_3$ and $\tilde{\tau}_3$. They may be rearranged to give a relation involving only

$\tilde{u}_1$ and $\tilde{\tau}_1$. It is

$$\frac{1}{2}\left[1 - 2\tilde{K}_1(k,H,\omega)\,\tilde{A}(k,H,\omega)\right]\tilde{u}_1$$

$$= \left[\tilde{G}_1(k,0,\omega) - \tilde{G}_1(k,H,\omega)\,\tilde{A}(k,H,\omega)\right]\tilde{\tau}_1(k,\omega)$$

$$+ \tilde{F}_1 - \tilde{A}(k,H,\omega)\,\tilde{F}_2 + \left[\tilde{A}(k,H,\omega) - 2\tilde{K}_1(k,H,\omega)\right]F_3 \qquad (4.6)$$

where

$$A(k,H,\omega) = \frac{\tilde{G}_1(k,H,\omega) + 2\tilde{K}_1(k,H,\omega)\,\tilde{G}_1(k,0,\omega)}{\tilde{G}_1(k,0,\omega) + \tilde{G}_2(k,0,\omega)} \qquad (4.7)$$

Let

$$R_{12}(k,\omega) = \frac{\gamma_1\mu_1 - \gamma_2\mu_2}{\gamma_1\mu_1 + \gamma_2\mu_2} \qquad (4.8)$$

$$D_1 = e^{-i\gamma_1 H}$$

R_{12} is the complex reflection coefficient for a plane SH wave incident from side 1 on an interface between two half-planes with material contrasts as at S_2, at an angle

$$\theta = \cos^{-1}(k\beta_1/\omega).$$

D_1 is the phase delay factor corresponding to a vertical movement of distance H through the plane wave field. In terms of these quantities

$$\tilde{A}(k,H,\omega) = -D_1 R_{12}(k,\omega)$$

$$\tilde{K}_1(k,H,\omega) = -\frac{1}{2} D_1 \tag{4.9}$$

Also, from equation (4.5)

$$\tilde{G}_1(k,H,\omega) = -2\tilde{K}_1(k,H,\omega)\, \tilde{G}_1(k,0,\omega) \tag{4.10}$$

Using these relations, equation (4.6) may be rewritten as

$$\frac{1}{2} [1 - D_1^2 R_{12}(k,\omega)]\, \tilde{u}_1$$

$$= [1 + D_1^2 R_{12}(k,\omega)]\, \tilde{G}_1(k,0,\omega)\, \tilde{\tau}_1 + \tilde{F}_1 + D_1 R_{12}(k,\omega)\, \tilde{F}_2$$

$$+ D_1 [1 - R_{12}(k,\omega)]\, \tilde{F}_3 \tag{4.11}$$

In order to give a simple physical interpretation of the inhomogeneous terms of this equation, suppose for a moment that the surface S_1 were bonded to a half-plane occupying the region $x_2 < 0$ and having material properties the same as those of the layer. The BIE for this half-plane would take the form

$$\tilde{u}_1 = -2\tilde{G}_1(k,0,\omega)\, \tau_1$$

hence, from equation (4.11), we would obtain

$$\tilde{u}_1 = \tilde{F}_1 + D_1 R_{12} \tilde{F}_2 + D_1 [1 - R_{12}] \tilde{F}_3$$

The physical situation is now very simple. The surface S_1 is a fictitious surface within a half-plane of material properties μ_1,β_1. S_1 lies a distance H from S_2, the contact of this half-plane with another half-plane with material properties μ_2,β_2. The inhomogeneous term $\tilde{F}_1$ is simply the direct SH displacement received at S_1 due to sources between S_1 and S_2. $\tilde{F}_2$ is the direct wave due to sources in that region received at S_2, and $D_1 R_{12} \tilde{F}_2$ is the reflected wave received at S_1. $\tilde{F}_3$ is the direct wave received at S_2 due to sources in the lower half-plane and $D_1(1 - R_{12})\tilde{F}_3$ is the transmitted wave received at S_1, the transmission coefficient being $(1 - R_{12})$.

In a similar manner one might regard the quantity $\tilde{u}_1$ as a wave detected at S_1 and traveling toward S_2, and the quantity $D_1^2 R_{12} \tilde{u}_1$ is the resulting displacement at S_1 after the wave has traversed the distance to S_2 and been reflected to S_1 again. This leads to the familiar interpretation of Love waves in terms of interference phenomena. Regarding equation (4.11) as a BIE, suppose that

$$\tilde{F}_1 = \tilde{F}_2 = \tilde{F}_3 = 0$$

Also, let the boundary condition

$$\tilde{\tau}_1 = 0$$

be satisfied. One obtains from equation (4.11)

$$\tilde{u}_1(k,\omega) = D_1^2 R_{12}(k,\omega) \tilde{u}_1(k,\omega) \tag{4.12}$$

This relation demands either that

$$\tilde{u}_1(k,\omega) = 0$$

or

$$D_1^2 R_{12}(k,\omega) = 1 \tag{4.13}$$

The latter of these is the condition under which plane waves reflected between S_1 (with reflection coefficient +1) and S_2 superpose at S_1 with equal amplitude and a phase shift of $2n\pi$. Since one propagates toward S_1 and the other propagates away from S_1, the condition of zero traction is satisfied at S_1. Substitution from equations (4.5) and (4.8) into equation (4.13) yields the period equation for Love waves in this medium. A similar interpretation applies to the relation obtained for the boundary condition of vanishing displacement

$$[1 + D_1^2 R_{12}(k,\omega)] G_1(k,0,\omega) \tilde{\tau}_1(k,\omega) = 0 \tag{4.14}$$

In this case displacement waves superpose at S_1 with equal amplitude and a phase shift of $(2n+1)\pi$, i.e.,

$$D_1^2 R_{12}(k,\omega) = -1$$

Equation (4.11) can be cast in a form similar to equation (4.1)

$$\tilde{u}_1(k,\omega) = 2\tilde{\tilde{GC}}(k,H,\omega)\,\tilde{\tau}_1(k,\omega) + \tilde{u}_o(k,\omega) \tag{4.15}$$

or

$$u_1(x_1,t) = 2GC(x_1,H,t) ** \tau_1(x_1,t) + u_o(x_1,t) \tag{4.15a}$$

where

$$\tilde{\tilde{GC}}(k,H,\omega) = \tilde{G}_1(k,0,\omega)\,\frac{1 + D_1^2\,R_{12}(k,\omega)}{1 - D_1^2\,R_{12}(k,\omega)} \tag{4.16}$$

and

$$\tilde{u}_o = 2(\tilde{F}_1 + D_1\,R_{12}\,\tilde{F}_2 + D_1(1 - R_{12})\tilde{F}_3)\,\frac{1}{1 - D_1^2\,R_{12}}$$

When written in this form, the transformed analytic composite BIE corresponds most closely to the discrete composite BIE which will be employed in the problem solution. The composite source term $u_o(x_1,t)$ can be recognized as the solution of the propagation problem in the case that τ_1 is zero. There are several methods in common use which approximately invert the transforms to obtain $u_o(x_1,t)$ for single values of x_1 and specific sources in B_2 and B_3. Among these methods the generalized ray method and the Love mode (residue) method are also particularly appropriate to obtain the values of $GC(x_1,H,t)$ for X_1 of the order of H or greater. Since $GC(x_1,H,t)$ is the surface response to the layer half-space composite to a concentrated surface load it will be singular when x_1 is zero. One role of the BIE technique in this problem is to obtain a smoothed discrete version of GC for small

x_1 to use in the time stepping process to evaluate $\tau_1(x_1,t)$. Once $\tau_1(x_1,t)$ has been evaluated numerically the approximate, analytic forms of $GC(x_1,H,t)$ may be used to calculate the remote scattered wave by carrying out the integration implied in equation (4.15a) numerically.

An important consequence of casting the composite BIE in the form of equation (4.15a) is that only limited knowledge of $u_o(x_1,t)$ is required to evaluate $\tau_1(x_1,t)$. It is necessary to know the value of $u_o(x_1,t)$ only at points $(x_1,0)$ lying on S_1', the subset of S_1 which is the contact between B_1 and B_2 (see Fig. 4.1). This, combined with the BIE for B_1, the topographic body, and the values of $\tau_1(x_1,t)$ at points $(x_1,0)$ not on S_1', is sufficient information to evaluate $\tau_1(x_1,t)$ on S_1'. Because of this it is feasible to use standard waveform modeling techniques to evaluate u_o for use in the numerical problem. This circumstance also raises the possibility of addressing questions which arise primarily in the context of a particular waveform modeling technique. For example, one might wish to determine the effect of the topography on a particular generalized ray which encounters the surface S_1'. For this purpose it would suffice to include only the contribution of that specific generalized ray in u_o. In a similar manner one might consider u_o to be composed of particular Love modes. In the problem treated here, the incident wave will be taken to consist of waves propagating in the fundamental Love mode only. The incident wave may in general be taken to be the evaluation at S_1 of any superposition of waves satisfying the equations of motion in B_2 and B_3,

the continuity conditions at S_2 and the boundary condition of vanishing traction for every point $(x_1,0)$ in S_1.

3. Numerical Composite BIE

This section is a description of the process used to construct the discrete version of the kernel $GC(x_1,H,t)$ of Section 2, equations (4.15) and (4.16). The discrete kernel will be represented by the numbers $DGC(j,n)$ where n is the time index and j is the spatial index. The composite discrete kernel will be constructed by concatenating the discrete kernels analogous to the analytic ones appearing in equations (4.1) - (4.3). The discretization of those equations can be carried out using interpolation scheme D_0 once the surface grids on S_1 and S_2 have been selected. The grid used in the calculations shown here is depicted in Figure 4.2. The node points on S_1 and S_2 are equally spaced at a distance L apart. They are considered to be centered on surface elements of length L. In the resulting discrete equations the summation over time indices appears as a discrete convolution because of the time translation property of the interpolators. Because the node spacing is uniform and the same on S_1 as on S_2 the sums over spatial indices also appear as discrete convolutions. This permits the use of the FFT algorithm in carrying out manipulations of the discrete kernels.

The basic discrete kernels which must be calculated are the numerical analogs of $2G_1(x_1,0,t)$, $2G_2(x_1,0,t)$, $2K_1(x_1,H,t)$ and $2G_1(x_1,H,t)$. These will be denoted, respectively, by $DG_1(j,0,n)$,

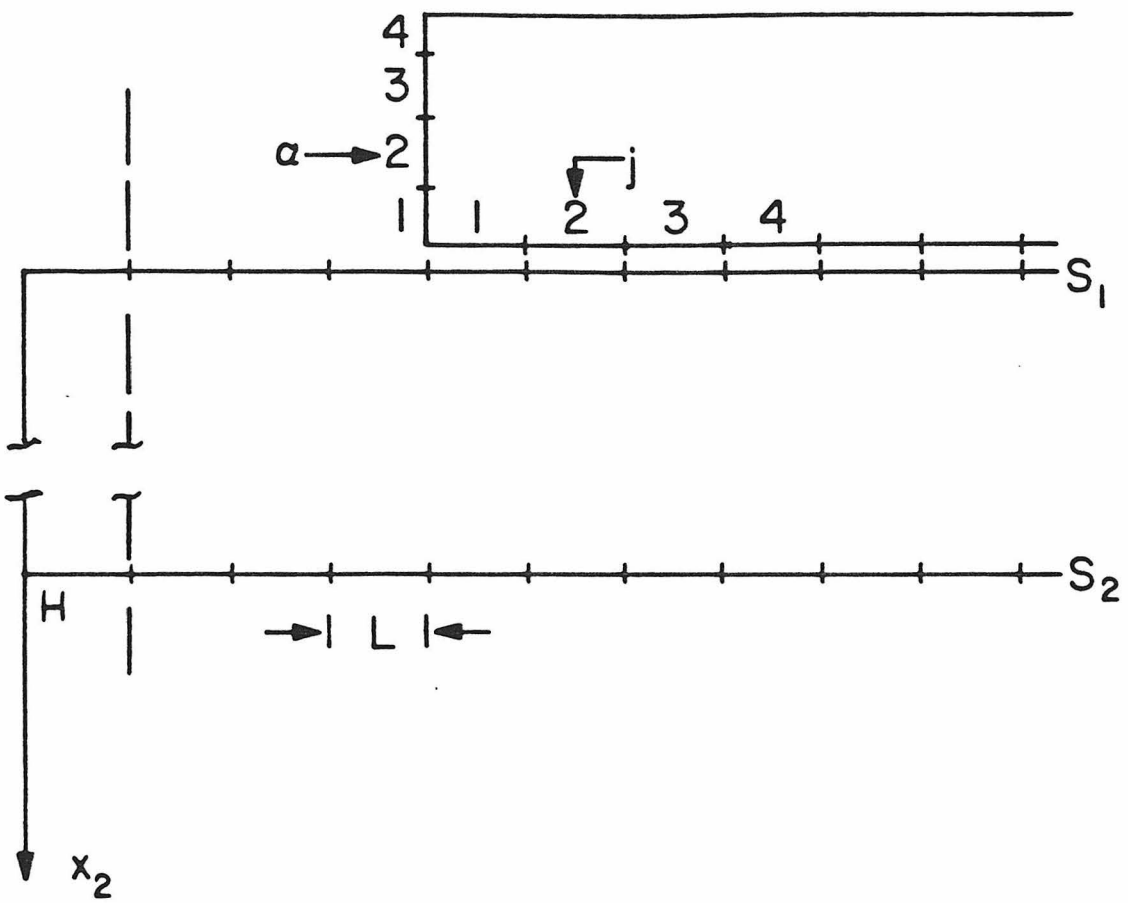

Figure 4.2. Grid for numerical calculation. Note the alignment of the grids on S_1 and S_2.

$DG_2(j,0,n)$, $DK_1(j,H,n)$ and $DG_1(j,H,n)$ for $j = 0, \pm1, \cdots \pm J$ and $n = 0, \cdots, N$. Notation such as $DG_1(j,0,n)$ will be used to refer to individual numbers and also to represent an assemblage of numbers considered as a numerical operator. The action of the operator on another discrete quantity will be understood to be discrete convolution over j and n, denoted by **. The arrays $DG_1(j,0,n)$ and $DG_2(j,0,n)$ are symmetric in the index j because of the uniform node spacing used. The arrays $DK_1(j,H,n)$ and $DG_1(j,H,n)$ are also symmetric because of the alignment of the grid on S_1 with respect to the grid on S_2 (see Fig. 4.2).

The discrete operator analogous to the operator $A(x_1,H,t)$ will be denoted by DA(j,n). The (ω,k) transform of A is defined in equation (4.7). The operator DA can be constructed as the convolution over j and n of the operator represented by

$$DG_1(j,H,n) + DK_1(j,H,n) ** DG_2(j,0,n)$$

with the operator which is inverse to

$$DP(j,n) = DG_1(j,0,n) + DG_2(j,0,n)$$

The causal convolutional inverse of the operator DP(j,n) will be denoted as DPI(j,n). The inverse operator can be evaluated by the method described in Chapter 2, Section 2. The procedure for doing this, as described there, requires on the order of N^2J arithmetic

operations to evaluate DPI(j,n) for j = 0, ±1, ···, ±J and n = 0, ···, N. If the number of time steps N is large the calculation of DPI(j,n) can become prohibitively expensive. It is therefore worthwhile to examine the possibility of economizing this calculation.

The general features of the numerical operator DPI(j,n) are similar to those of the operator DGI of Chapter 2. That is, the individual numbers DPI(j,n) have mixed signs and decrease in absolute value with increasing |j| and n. For a particular large value of n, the maximum absolute values of DPI(j,n) occur for j in the vicinity of $\pm Q_1 n$ and $\pm Q_2 n$, where

$$Q_1 = \beta_1 \Delta t/L$$

$$Q_2 = \beta_2 \Delta t/L > Q_1$$

The analytic analog of DPI, as a Fourier transform, is

$$\tilde{\tilde{PI}}(k,\omega) = \frac{\mu_1\gamma_1\mu_2\gamma_2}{\mu_1\gamma_1 + \mu_2\gamma_2}$$

where $\gamma_i = (\omega^2/\beta_i^2 - k^2)^{1/2}$.

The inverse transform of $\tilde{\tilde{PI}}(k,\omega)$ can be shown to be approximated by

$$PI(x_1,t) \sim \frac{1}{x_1^{3/2}} \left(\frac{C_1}{(t - x_1/\beta_1)^{3/2}} + \frac{C_2}{(t - x_1/\beta_2)^{3/2}}\right) \qquad (4.17)$$

for sufficiently large positive x_1, $t - x_1/\beta_1$ and $t - x_1/\beta_2$. The

constants C_1 and C_2 depend on the material properties. The important feature of this analog is that for fixed x_1, $PI(x_1,t)$ diminishes as $t^{-3/2}$ and for fixed $\beta t - x$, the terms of $PI(x_1,t)$ decreases as $x_1^{-3/2}$. This behavior has been found to be approximately duplicated by the dependence of DPI(j,n) on j and n.

These observations suggest that for a fixed value of j it should be acceptable to substitute zero for DPI(j,n) for sufficiently large n. This large value of n will be proportional to j. Since DGC(j,n) will be needed for only small values of |j| in this application, the values of DPI(j,n) for all j and sufficiently large n may be set equal to zero. This permits one to truncate the inversion process at some time step N' and maximum number of operations required to evaluate DPI(j,n) will be of order N'^2J. The accuracy of this procedure has been verified by numerical experiment.

In the case that it is required to evaluate DPI(j,n) for large values of j and n this procedure is not effective. In that case one may employ FFT-based methods to evaluate the deconvolution operator for the real time series $\tilde{\tilde{DP}}(k,n)$, $n = 0, \cdots, N$. Here $\tilde{\tilde{DP}}(k,n)$ is the discrete Fourier transform over the spatial index j, of DP(j,n). Initial numerical experiments indicate that these procedures can be very accurate for $j \neq 0$. The deconvolution operator for $\tilde{\tilde{\tilde{\tilde{DPI}}}}(0,n)$ may be obtained trivially since these numbers are constant as a function of $n > 0$. Using the FFT deconvolution procedures, on the order of $NJ(\log_2 N + \log_2 J)$ arithmetic operations are required to evaluate DPI(j,n).

Once the operator DPI(j,n) has been evaluated, the operator DA(j,n) may be obtained using the FFT to carry out the required discrete convolution. The operator DA(j,n) is displayed in Figure 4.3 for the parameters

$$\begin{aligned} Q_1 &= Q_2/2 = 1/4 \\ H/L &= 8 \\ \mu_2/\mu_2 &= 4 \\ \beta_2/\beta_1 &= 2 \\ J &= 63 \\ N &= 127 \quad . \end{aligned} \tag{4.18}$$

These values were selected to make various features of the operator clearly visible. Figure 4.4 is a plot of the operator DA after smoothing in j and n with a three point filter; the quantity plotted is

$$(E_j^{+1} + 2 + E_j^{-1})(E_n^{+1} + 2 + E_n^{-1})\ DA(j,n)/16 \quad .$$

E_j^m is the translation operator on index j.

The operator of DA(j,n) on a displacement wave incident on the interface S_2 from side 1 yields the reflected displacement wave at a distance H from the interface. The most notable feature of DA(j,n) are a large negative pulse at small values of j and disturbances traveling at velocities β_2 and β_1 for large values of j. These features give rise, respectively, to the head wave and reflected wave. Note that the

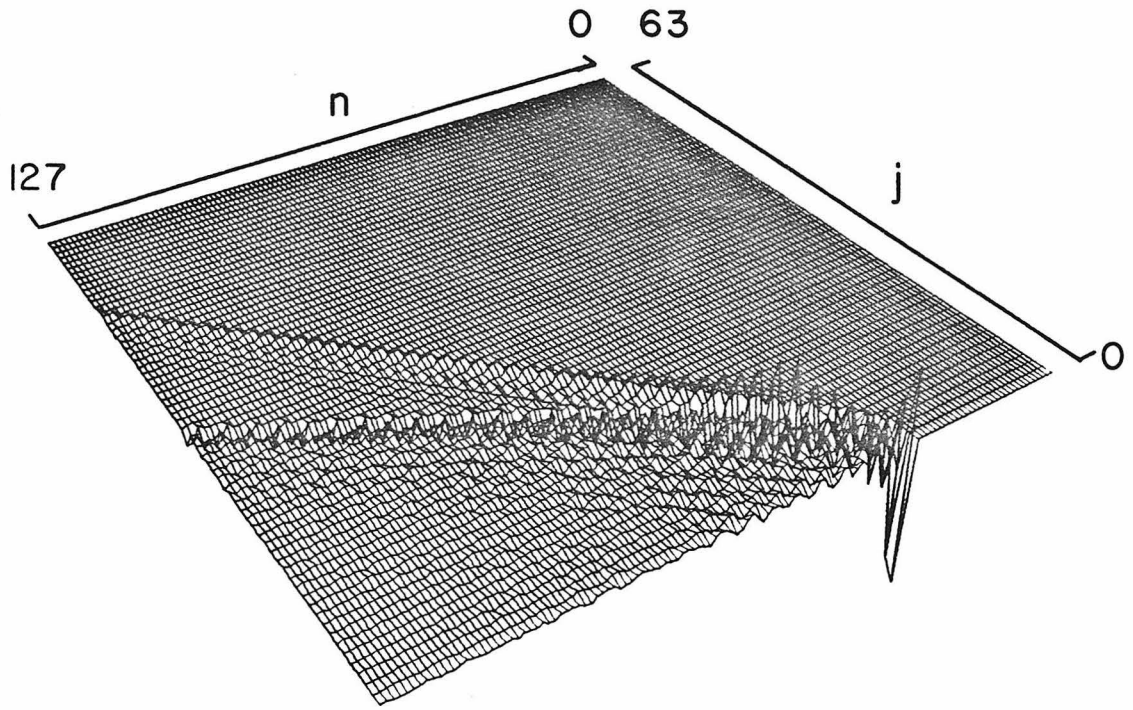

Figure 4.3. The numerical operator DA_j^n. There are two disturbances propogating with velocities β_1 and β_2.

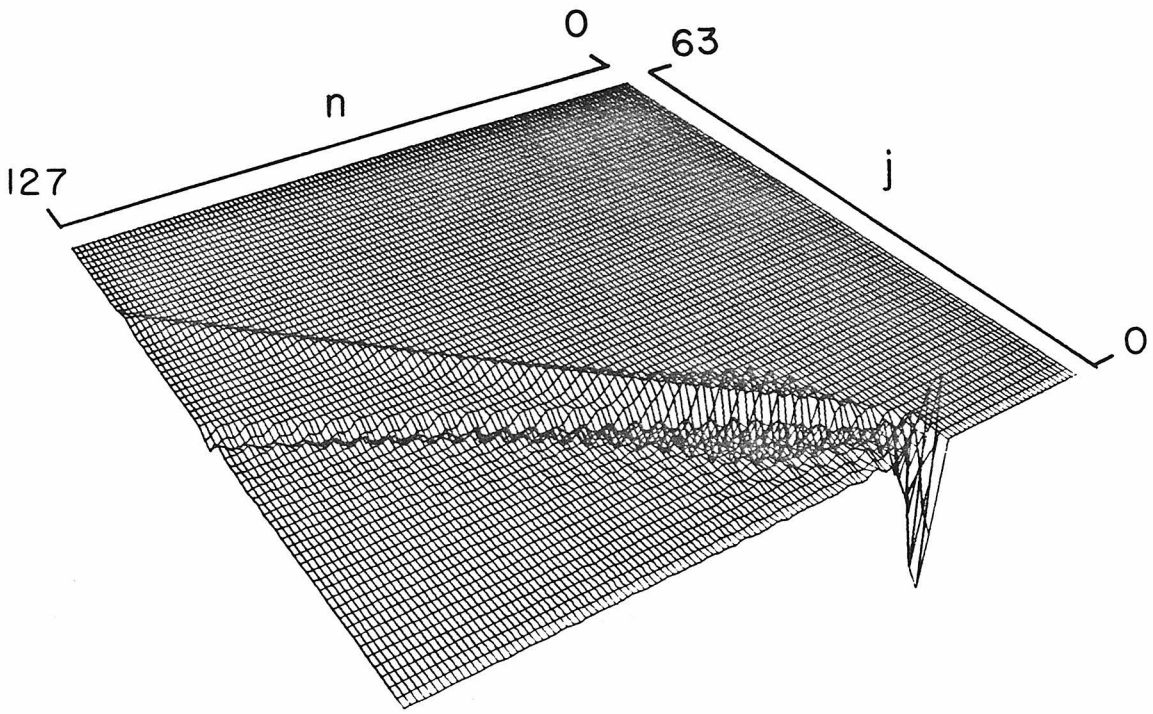

Figure 4.4. Smoothed version of DA_j^n.

"reflection coefficient" for normally incident plane waves and tangentially incident plane waves will be negative. For intermediate angles of incidence a positive plane wave can be reflected as a wave having positive or negative values, or both, corresponding to positive, negative or complex values of reflection coefficient.

Once the operator DA(j,n) is evaluated and

$$DR(j,H,n) = DK(j,H,n) \;**\; DA(j,n)$$

is evaluated, the operator DGC(j,H,n) analogous to $2GC(x_1,H,t)$ of equation (4.15a) can be constructed as the convolution of

$$(I + DR(j,H,n)) \;**\; DG_1(j,n)$$

with the operator inverse to

$$I - DR(j,H,n)$$

This operator will be termed DRI(j,H,n) and can be constructed from DR(j,H,n) by the methods discussed above. The method used here was that described in Chapter 2, Section 2. A rather interesting observation on this operator can be obtained by noting that

$$DR(j,H,n) = 0$$

for $Q_1 n < 2H/L$.

An examination of the inverse construction process of Chapter 2 then shows that process to be exactly equivalent to constructing DRI(j,H,n) as

$$DRI(j,H,n) = \sum_{n=0}^{P} DR^{n}(j,H,n) \qquad (4.19)$$

where $DR^{o} = \delta_{nO}\ \delta_{jO}$

$$DR^{m+1}(j,H,n) = DR(j,H,n) \ ** \ DR^{m}(j,H,n)$$

and

$$P > N\ LQ_1/2H$$

so that

$$DR^{P}(j,H,n) = 0 \quad , \quad n < N \ .$$

This method of obtaining DRI(j,H,n) can be recognized as a close numerical analog of the power series expansion leading to the analytic generalized ray approximation. Figure 4.5 displays the operator DRI(j,H,n) for the parameters of equation (4.18) and Figure 4.6 is a plot of the operator DGC(j,n).

4. Numerical Representation of Topography

In preparing a numerical representation of the topographic relief it is advantageous to carry out some rearrangements of the numerical BIE prior to the time stepping procedure. In the following the surface elements composing the boundary of the topographic body will be separated into two sets. The first set, consisting of those elements for which a zero traction boundary condition is posed, will be numbered with Greek letter indices. The second set consists of the base of the body, which is welded to the top of the uniform layer

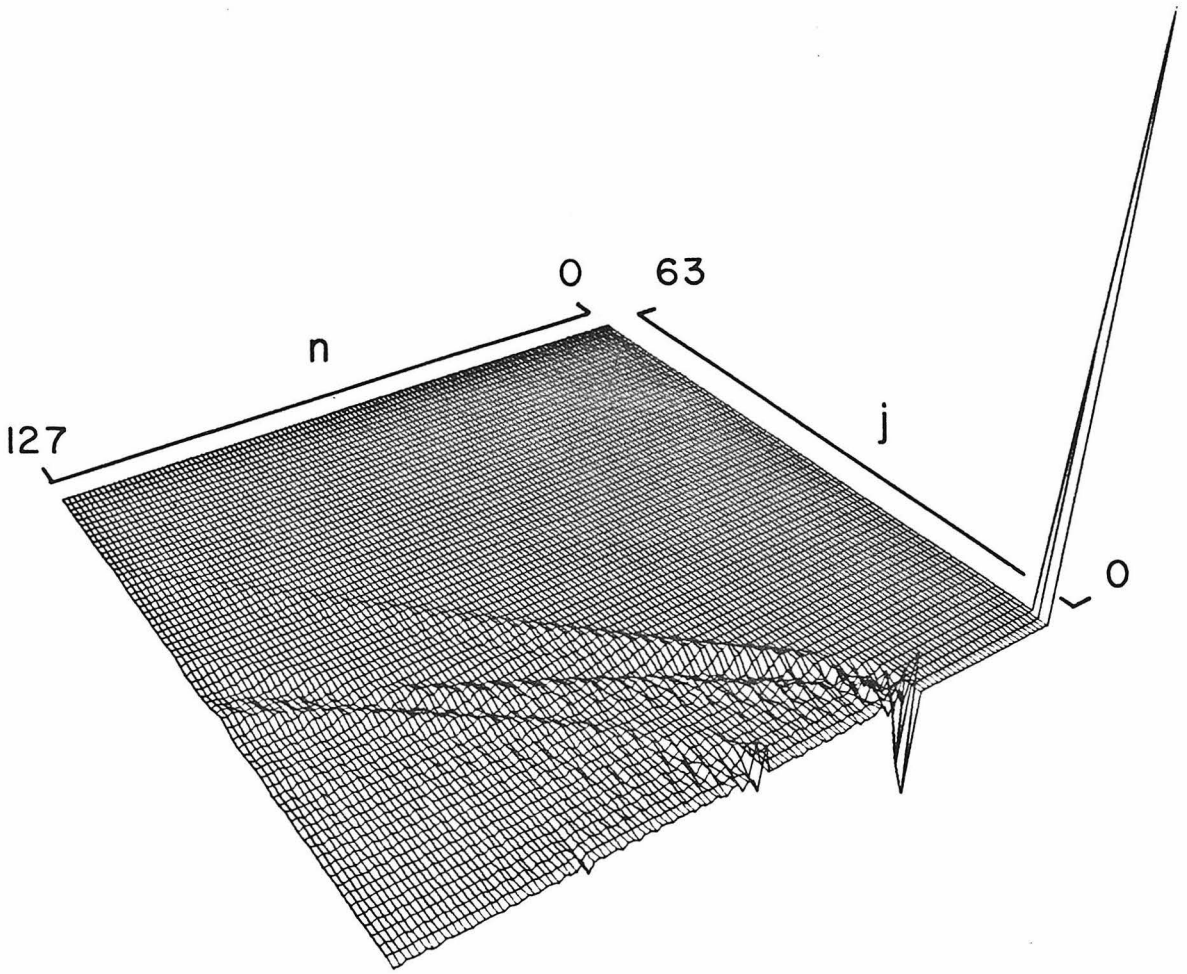

Figure 4.5. The reflection operator DRI (n, H, j). Three reflections are visible near j = 0.

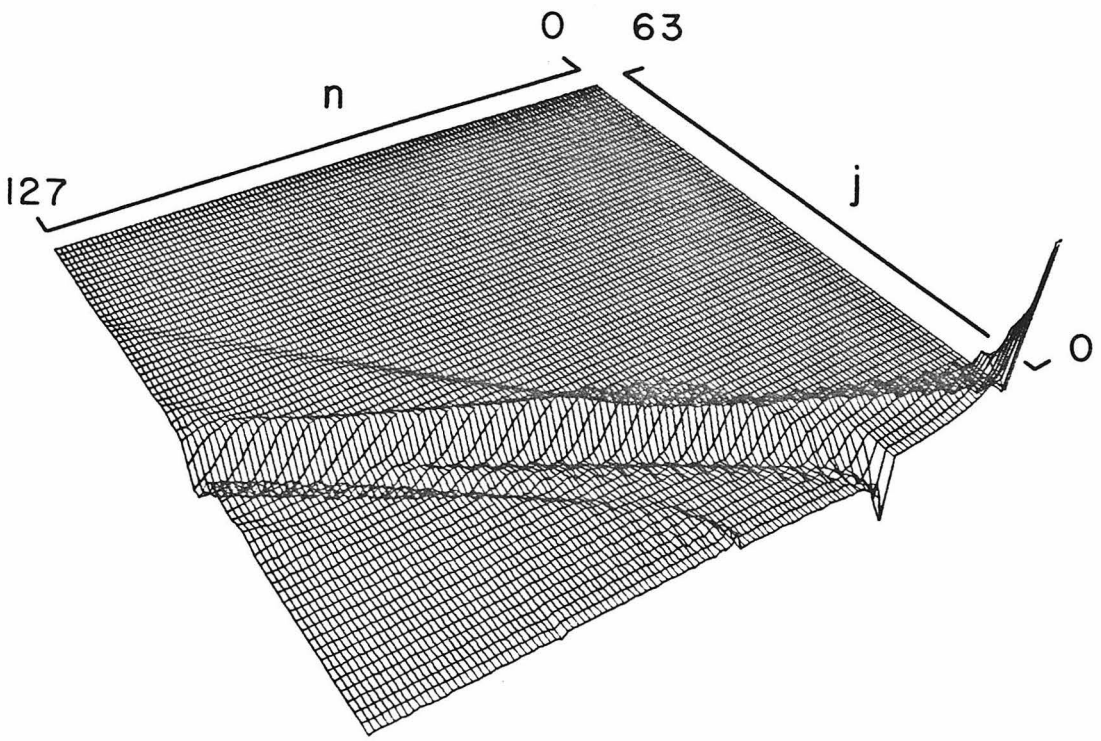

Figure 4.6. The operator DGC_j^n. It is the displacement at the top of the layer due to a point force applied there. Three reflections are visible near j = o. They generate multiple head waves, which propogate with velocity $\beta_2 = 2\ \beta_1$ and have alternating signs. The direct wave and first reflection are dominant at the longer times shown here. At greater distances the multiple reflections will coalesce into a Love wave.

(see Fig. 4.2). The indices will run from $\alpha = 1$ to A for the free surface and $j = 1$ to J for the base. The length of the surface elements on the base will be L, the same as the length of the elements representing the top of the layer. The length of surface elements on the top of the topography will be selected to be approximately L. They need not be of uniform length, i.e., $L_\alpha \neq L_\beta$.

The numerical equations representing the topographic body may be written as

$$u_i^n = \sum_{m=1}^{n} \sum_{j=1}^{J} DG_{ij}^{n-m} \tau_j^m + \sum_{\alpha=1}^{A} (DG_{i\alpha}^{n-m} \tau_\alpha^m + DK_{i\alpha}^{n-m} u_\alpha^m)$$

$$u^n = \sum_{m=1}^{n} \sum_{\beta=1}^{A} (DG_{\alpha\beta}^{n-m} \tau_\beta^m + DK_{\alpha\beta}^{n-m} u_\beta^m) + \sum_{j=1}^{J} (DG_{\alpha i}^{n-m} \tau_i^m + DK_{\alpha i}^{n-m} u_i^m) \qquad (4.17)$$

The fact that the kernels DK_{ij}^n vanish has been employed here. Since the boundary condition at the top of the body is

$$\tau_\alpha^m = 0$$

it is possible to rearrange these two relations into a form

$$u_\alpha^n = \sum_{m=1}^{n} \sum_{j=1}^{J} DGT_{\alpha j}^{n-m} \tau_j^m \qquad (4.18)$$

$$u_i^n = \sum_{m=1}^{n} \sum_{j=1}^{J} DGB_{ij}^{n-m} \tau_j^m \tag{4.19}$$

The first of these equations gives the response at a point on the top of the topographic body due to a distribution of tractions on the base. The second gives the displacement at the base of the body due to tractions acting there. The second relation is particularly convenient for use in a time stepping procedure to evaluate tractions and displacements along the base since it is not necessary to evaluate displacements along the top at the same time. Once the tractions acting on the base have been evaluated, displacements along the top may be calculated in a straightforward manner using the FFT to carry out convolutions over the time indices.

The process of calculating the discrete kernels DGB_{ij}^n and $DGT_{\alpha j}^n$ in equations (4.19) and (4.18) is rather tedious and will not be discussed in detail here. The procedures for efficiently carrying out most of this operation have been described in previous chapters and only one additional process need be used. It will be discribed here. It involves rearrangement of an equation of the form

$$u_\alpha^n - \sum_{m=1}^{n} \sum_{\beta=1}^{A} DK_{\alpha\beta}^{n-m} u_\beta^m = b_\alpha^n \tag{4.20}$$

into a relation of the form

$$u_\alpha^n = \sum_{m=1}^{n} \sum_{\beta=1}^{A} E_{\alpha\beta}^{n-m} b_\beta^m \tag{4.21}$$

Upon substitution of equation (4.21) into equation (4.20) one obtains

$$E^{o}_{\alpha\beta} - \sum_{\gamma=1}^{A} DK^{o}_{\alpha\gamma} E^{o}_{\gamma\beta} = \delta_{\alpha\beta}$$

$$E^{n}_{\alpha\beta} - \sum_{\gamma=1}^{A} DK^{o}_{\alpha\gamma} E^{n}_{\gamma\beta} = \sum_{m=0}^{n-1} \sum_{\gamma=1}^{A} DK^{n-m}_{\alpha\gamma} E^{m}_{\gamma\beta} \quad , n \geq 1 \tag{4.22}$$

If the time step has been selected to be small enough that

$$2\beta\Delta t \leq \min_{\alpha} L_{\alpha} \tag{4.23}$$

and the node points $\underline{r}_{\alpha}$ are centered on their respective surface elements, one finds

$$DK^{o}_{\alpha\beta} = 0 \quad .$$

Since $E^{p}_{\alpha\beta}$, $p \geq n$, does not appear on the right-hand side it is possible to evaluate $E^{n}_{\alpha\beta}$ recursively using equation (4.22). If the time step is larger than this it is still possible to evaluate $E^{n}_{\alpha\beta}$, but it is necessary to evaluate a square matrix inverse to $\delta_{\alpha\beta}$-$DK^{o}_{\alpha\beta}$. For reasonable sized time steps and well-represented boundaries this matrix is diagonally dominant and its inverse is easily approximated. For the calculations shown here condition (4.23) was satisfied. In carrying out the recursive process implied by equation (4.22), a time stepping procedure similar to that described in Chapter 3, Section 4 was used to reduce computer I/O time.

An interesting point regarding the discrete kernels DGB^n_{ij} arises from consideration of the reciprocity theorems of elastodynamics (see Fung (1965), p. 433). Because the surface elements i and j both lie on a straight line and are therefore oriented parallel to each other, one may deduce that, if DGB^n_{ij} were calculated by discretizing an exact Green's function for the topographic body with appropriate boundary conditions, then

$$DGB^n_{ij} = DGB^n_{ji} \tag{4.24}$$

This relation does not actually hold for the kernels produced by the methods used here because $DK^n_{i\alpha} \neq DK^n_{\alpha i}$, $DG^n_{i\alpha} \neq DG^n_{\alpha i}$, and $DK^n_{\alpha\beta} \neq DK^n_{\beta\alpha}$. This relation is approximately satisfied for well-represented boundaries and can be used to detect large errors in the values DGB^n_{ij} or to reduce the number of computations required to evaluate DGB^n_{ij}. In the numerical example to be shown here the topographic body was taken to be a right rectangle. The accuracy of this procedure for evaluating DGB^n_{ij} was independently verified by calculating these numbers using an image source series. The errors were small at nodes not lying near the corners of the base. The errors at the corners were about 10%. Since the base had a large number of nodes the effect of these isolated errors were small.

Alternative methods could easily be used to represent the topographic body. Any procedure which produces a dependable relationship between tractions and displacements along the base of the topographic body could be employed as well as the one here. Numerical

relations which can be explicitly time stepped are the ones most easily combined with the layered half-space BIE.

5. Solution Processes

With application of the continuity conditions on S_1', the numerical equations are

$$u_j^n = -\sum_m \sum_i DGB_{ji}^{n-m} \tau_i^m \tag{4.25}$$

$$u_j^n = \sum_m \sum_i DGC_{j-i}^{n-m} \tau_i^m + u_o(jL, n\Delta t) \tag{4.26}$$

$$u_\alpha^n = -\sum_m \sum_i DGT_{\alpha i}^{n-m} \tau_i^m \tag{4.27}$$

where τ_i^m is the traction acting on S_1' at the top of the layer. The numbers $DGT_{\alpha i}^n$ are the responses at points on the traction-free portion of B_1, with node index α, due to a traction on the base, with node index i. If the number of nodes of the base of B_1 is J, the indices j and i in equations (4.25) and (4.26) range from 1 to J. The

first of these equations represents the motion at the base of B_1 due to tractions acting there. The second gives the motion at the top of the layer. Elimination of u_j^n between these equations yields

$$\sum_m \sum_i DX_{ij}^{n-m} \tau_j^m = -u_o(jL, n\Delta t) \tag{4.28}$$

where

$$DX_{ij}^n = DGB_{ij}^n + DGC_{i-j}^n .$$

This equation can be solved for τ_j^m by several methods. Since

$$DX_{ij}^o = 2LQ_1\delta_{ij}/\mu$$

it can be solved by an explicit time stepping method. One can also evaluate the inverse operator DXI_{ij}^n by methods similar to those used to evaluate the operator DGI in Chapter 2. There is an additional complication in that equation (4.28) is not a convolution in the spatial indices. This is the process employed here. Another approach which is appropriate for questions regarding periodic motions may be pursued by applying a discrete Fourier transform to equation (4.28). This yields the equation

$$\sum_j \tilde{\tilde{DX}}_{ij}^m \tilde{\tau}_j^m = -\tilde{u}_o(jL, \omega_m) \tag{4.29}$$

Successful discretizations will yield operators DX_{ij}^n which are symmetric, or approximately symmetric, in i and j. The matrices $\tilde{\tilde{DX}}_{ij}^m$ are thus complex and approximately symmetric. There is a possibility that

$$\mathrm{Det}(\tilde{\tilde{DX}}^{m}_{ij}) = 0$$

corresponding to the existence of eigenmodes of the mechanical system at frequency ω_m for which the displacement on S_1' vanishes. This does not appear to be a likely occurrence in the problem considered here.

6. Solution for a Rectangle

The operators $DGT^{n}_{\alpha j}$, DGC^{n}_{i} and DXI^{n}_{ij} were calculated for the physical parameters

$\beta_1 = 3.85$ km/sec

$\rho_1 = 3.00$ gm/cm^3

$\beta_2 = 4.75$ km/sec

$\rho_2 = 3.65$ gm/cm^3

$H = 11$ km .

The topographic body was a right rectangle of thickness 4 km and length 32 km. The velocity and density there were the same as for the layer. These parameters are appropriate for a thick oceanic crust. The cutoff period for mode 1 is 3.4 sec., with a horizontal wavelength of 16.2 km.
The discretization parameters are

$L = 1$ km

$\Delta t = 0.130$ sec

$Q_1 = 0.50$

$Q_2 = 0.62$

The operator DGC was truncated at 256 time steps and 128 node points. This included approximately five reflections from the surface S_2 to the surface S_1. The reflection coefficient at normal incidence is -0.20. The critical angle is 54° so, in plane wave terms, there are reflections between points on S_1' which are near the critical angle, where the reflection coefficient is +1.0. The operators DGB_{ij}^n and $DGT_{\alpha i}^n$ were truncated after 512 time steps. The operator DXI_{ij}^n was calculated for 512 time steps, enough time for six reflections between endpoints of the topographic body along a ray path reflecting from S_2. The traction on S_1' is given by

$$\tau_i^n = -\sum_m \sum_j DXI_{ij}^{n-m} u_o(jL, m\Delta t) \tag{4.30}$$

Some characteristics of the operator DXI_{ij}^n can be deduced from the properties of DGB_{ij}^n and DGC_j^n. One can easily show that for $n > 0$

$$\sum_{j=1}^{J} DGB_{ij}^n = (2\ \mathrm{Int}(n/K) + 1)\ LQ/\mu \tag{4.31}$$

where Int(p) is the largest integer in p and K is the number of time steps required for a vertically traveling pulse to travel twice the thickness of the topographic rectangle. Also

$$\sum_{j=1}^{J} DGC_{i-j}^n = LQ/\mu \tag{4.32}$$

for $0 < n \leq \min((i - 1/2),(J + 1/2 - i))/Q$

For larger values of n the sum in equation (4.32) has pulses corresponding to reflections from S_2 and decays to zero as $n \to \infty$. Some arithmetic reveals that the spatial sum of the inverse operator

$$SX_j^n = \sum_{j=1}^{J} DXI_{ij}^n$$

will be dominated at long times by a series of terms resembling numerical time derivative operators which decay rapidly. Specifically

$$|SX_j^n| < C|R|^{\mathrm{Int}(n/K')} \tag{4.33}$$

where C is some constant of order μ/LQ, R is the reflection coefficient at normal incidence, and $K' = K + H/\beta_1 \Delta t$.

This decay may be interpreted as the result of waves in the topographic body propagating into the half-space and leaving the vicinity of S_1'. Since very long period Love waves will have small horizontal wave numbers, this behavior of SX_j^n suggests that only a finite number of time levels of the inverse operator are needed to model arbitrarily long period Love waves. Since K' in the present problem has the value sixty, 512 time levels of the operator DXI_{ij}^n are probably sufficient to evaluate the tractions for any period of incident Love wave. Thus, equation (4.30) will be assumed to hold for any incident wave if zeroes are substituted for DXI_{ij}^n for n greater than 512.

Once the tractions on S_1 have been evaluated from equation (4.30) the displacements on the traction free surfaces may be obtained from equations (4.25) and (4.26). The incident wave used here was not of a

form encountered in seismic studies. It was a Gaussian pulse of large bandwidth at station A in Figure 4.7 and evolved according to the uniform layer and half space dispersion relation as it propagated toward station D. In this manner it was possible to obtain long period information without the use of very long time series in the calculations. Phase velocities calculated from the incident wave for 512 time steps and station spacing as in Figure 4.7 reproduced the theoretical phase velocities used in its construction to an accuracy greater than 0.1%.

The incident wave traversed the length of the topographic body in about 120 time steps and tractions evaluated from (4.30) were about 1% of their peak value near time step 512, the end of the calculated time series. For long times the tractions were dominated by a disturbance with a period of about 8 seconds, or sixty time steps, corresponding to the travel time for a wave propagating between the surface S_2 and the top of the rectangle. At times when the incident wave was propagating past the rectangle the tractions displayed large values near the corners of the rectangle's base. The values there were five to eight times as large as the values found at the center of the base and the value of the tractions varied smoothly across the base. The strong stress concentrations had primarily short period components.

Information concerning the displacements calculated at stations A to D are given in Figures 4.8a to 4.8d, respectively. The phase and amplitude plotted there are those of $u(x,\omega)/u_0(x,\omega)$, where $u(x,\omega)$ is the displacement calculated in the presence of topography and $u_0(x,\omega)$ is the incident displacement at the same horizontal position. The most

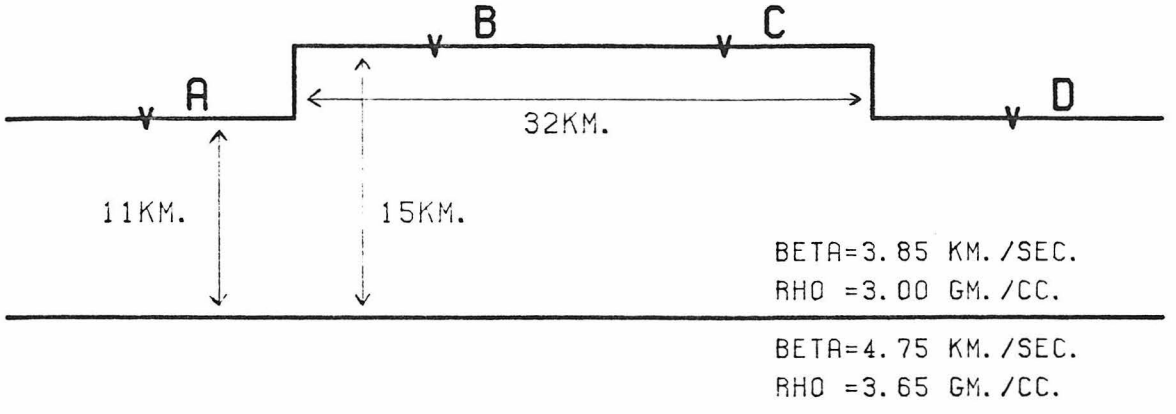

Figure 4.7 The positions of hypothetical seismometers are indicated by the symbol V. They are 16 km. apart. The incident wave travels from left to right.

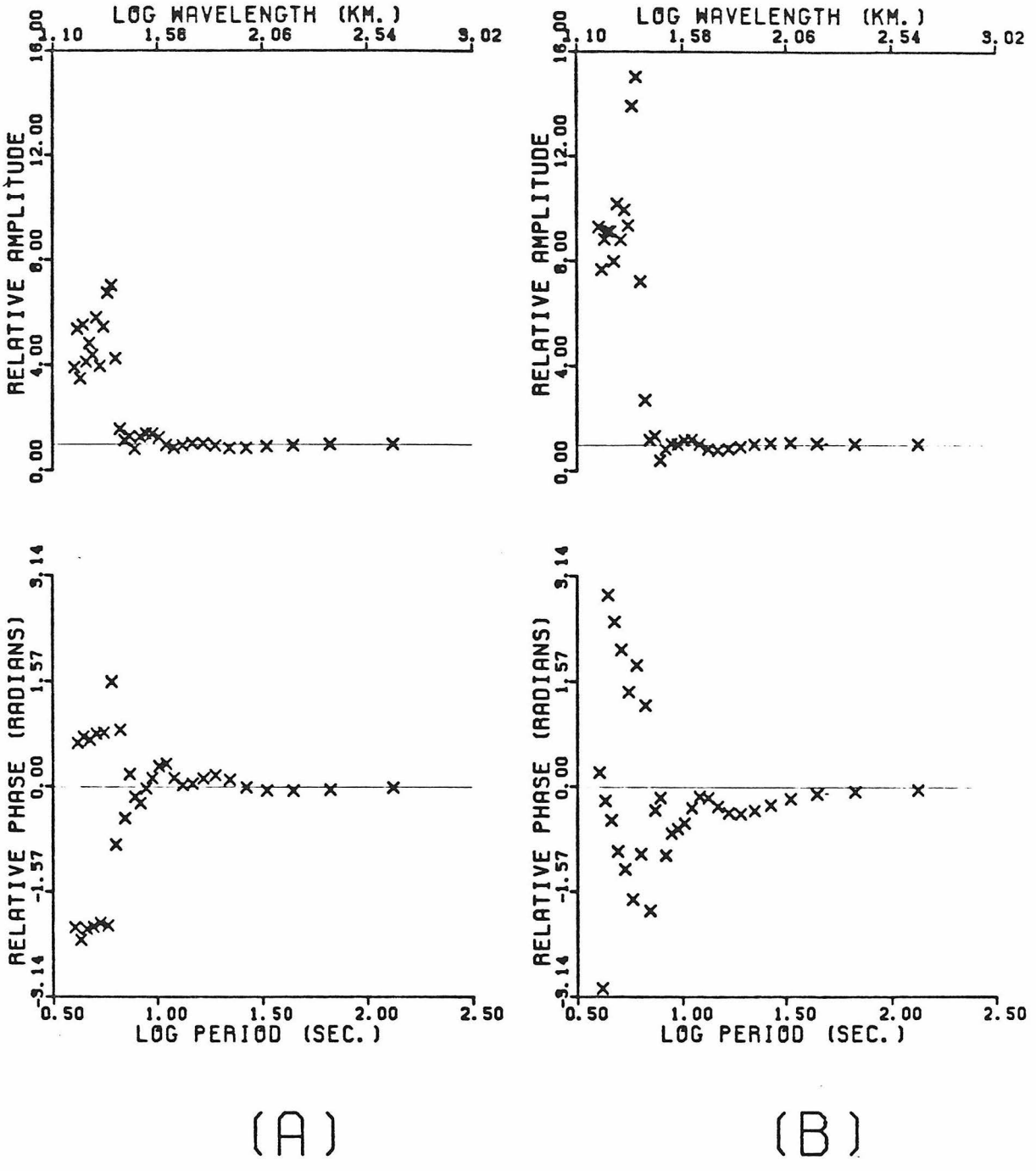

Figures 4.8a and 4.8b. Relative phase and amplitude of the calculated displacements at stations A and B.

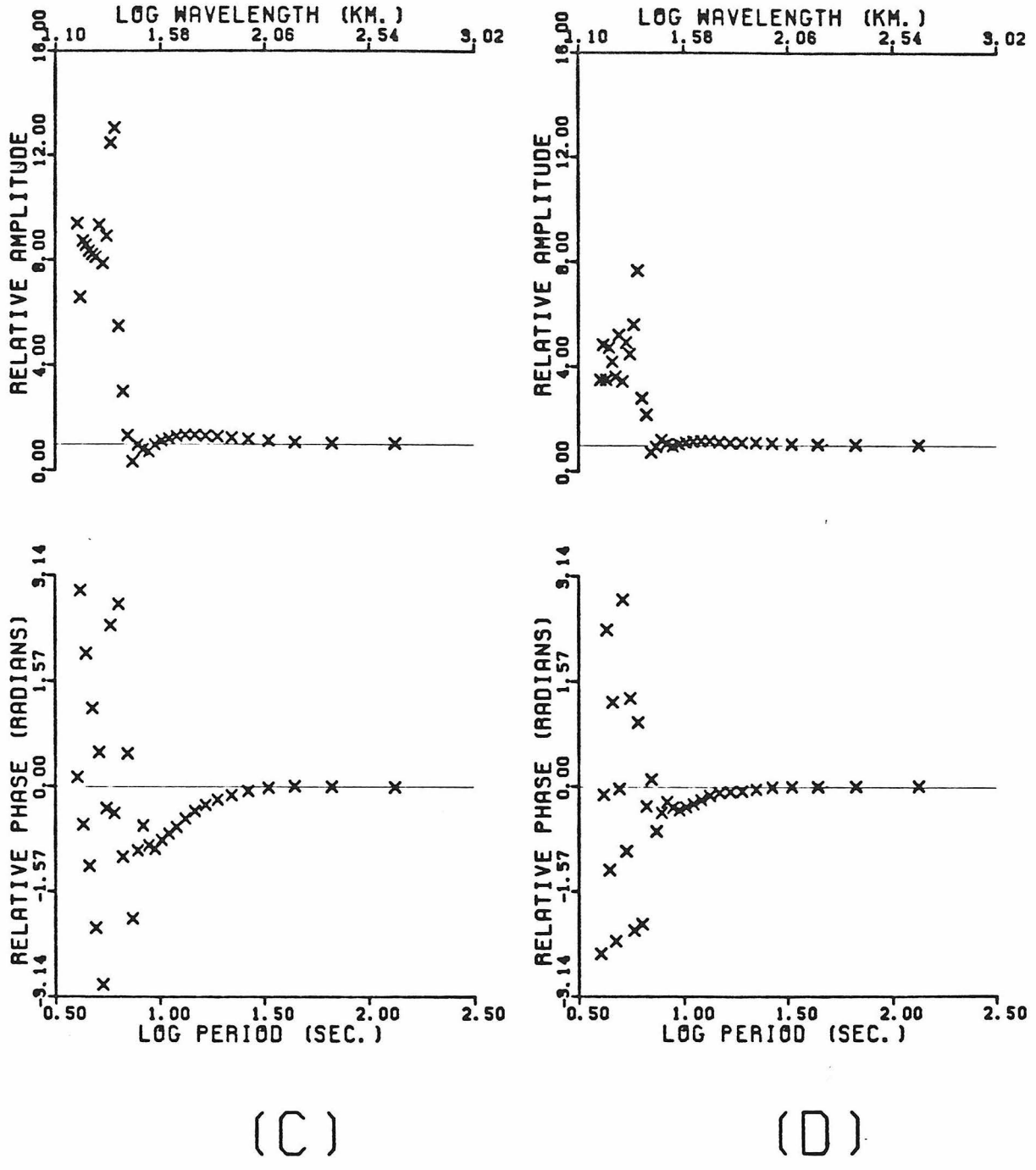

Figures 4.8c and 4.8d. Relative phase and amplitude of the calculated displacements at stations C and D.

prominent feature of the amplitude information is the absence of significant amplification for periods more than about 10 seconds. The actual values of the spectral amplitudes for these periods may be inaccurate due to the short length of the time series used, but it appears certain that large amplifications actually occur.

Significant alterations to the phase of the wave occurred for all periods considered here. These alterations were sufficiently large to make the phase velocities, determined from the calculated displacements using a two station method, inaccurate for determining the dispersion relation for the uniform layer - half space waveguide. At a period of 100 seconds the calculated phase velocity for station pair A-D was 4.2 km/sec, giving an error of about 9%. It is estimated that another station at least 300 km away from the topographic body would be required to give accurate information regarding the nature of the half space at periods greater than 20 sec.

The incident waves for stations A to D are given in Figure 4.9, along with the displacements calculated in the presence of the topographic body. The maximum change in the amplitude of the main pulse occurred at station C, with an increase of 7%. The pulse has been shifted to slightly later times at stations B and C. The magnitude of the time shift is nearly the same as the vertical travel time through the topographic rectangle. There is a small coda following each pulse, which is responsible for the greatly altered spectral amplitudes in Figure 4.8.

The hybrid analytic-BIE method employed here may be adapted to other problems involving lateral heterogeneities. For problems involving

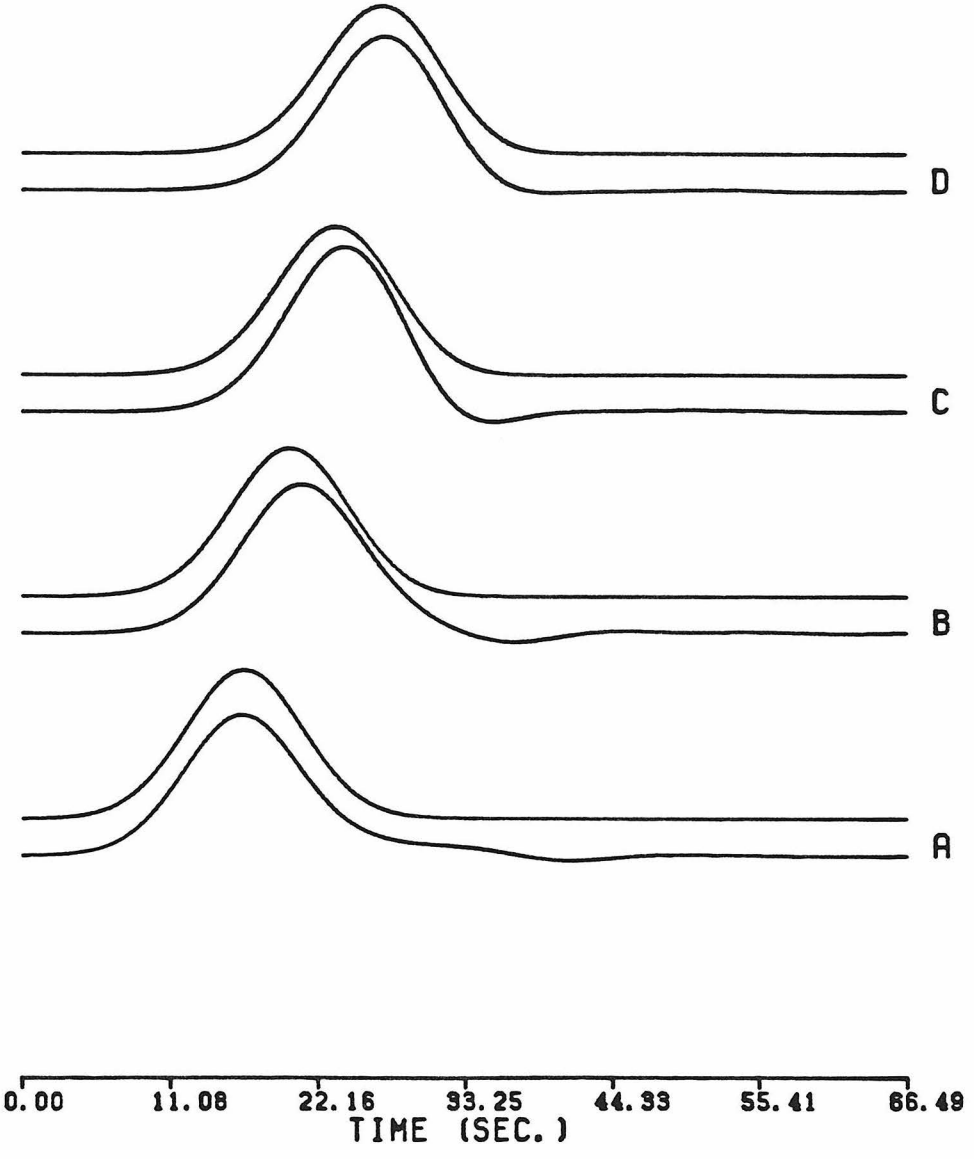

Figure 4.9. Incident waveform and wave with topography for stations A to D in Figure 4.7. The top trace in each pair is the incident wave. This figure indicates the effect of topography on the long period components of the incident wave.

abutting layered quarter spaces one could numerically evaluate surface Green's functions for the two surfaces of the quarter spaces using adaptations of the techniques shown here. These Green's functions would give the displacement at the surface of the quarter space due to a traction applied at some point which would be in contact with the other quarter space. The incident wave would be introduced analytically through the displacement and stress it would produce at the interface in the absence of lateral heterogeneities. By matching boundary conditions of stress and displacement at the interface the true traction and displacement is obtained. The reflected and transmitted waves may be evaluated by integration of the true boundary values with appropriate Green's functions. The treatment of complicated transition zones could be carried out by introducing a finite transition zone between the layered quarter spaces. A complicated model of a transition zone would probably be easiest to obtain using a volume girdding method.

GENERAL SUMMARY

This thesis contains some of the basic steps which are required in the development of the time domain BIE technique for applications to geophysical problems. Previous works on BIE methods have dealt with static or time harmonic deformations and are not easily applied to the propagation of broad band transient waves as found in the earth. The method has been shown to be accurate for waves with periods which are fairly long compared to the time step size. The range of applicability includes all but the high frequency end of the seismic band, where ray methods are more appropriate. The method is versatile and may be readily combined with several propagation modeling techniques which are in common use today.

This study of the BIE technique for transient two-dimensional SH waves has amassed sufficient information to allow a prediction of the performance of the method for a large class of applications. For the simple scattering problems of Chapter 2 and 3, when the traction boundary value is specified and the incident waves are known exactly, the displacement boundary value may be evaluated to a pointwise accuracy of about 5% when the ratio of period to time step is about 10. When the traction is evaluated, pointwise errors of 10% may be obtained for a period to time step ratio of 15. These numbers vary considerably, depending on the boundary shape and nature of the incident wave. For application to a particular scattering problem, it would be best to examine the relevant test solutions and the accompanying discussions of errors.

The errors quoted here are fundamentally different from the usual numerical error estimates in that they are errors in boundary values. The performance of a numerical method is usually discussed in terms of errors evaluated at points in the interior of a body. The errors quoted here are thus not strictly quantitatively comparable to generally used error definitions. The general behavior of errors as a function of discretization parameters is quite similar to that found in volume gridding methods. More finely sampled deformations and better represented boundary shapes will always produce smaller solution errors. The errors are generally proportional to the ratio of time step and period. Some details of this behavior are discussed in Appendix C.

In addition to accuracy of the method, the order of operations counts plays an important role in the selection of numerical methods. The most expensive type of calculation with the method described here is one in which it is desired to evaluate the traction on a completely unsymmetric boundary by time stepping for a long time interval. If N is the number of time steps and J is the number of node points, a calculation of this type requires on the order of N^2J^2 arithmetic operations in the time stepping process. If the problem is solved in the Fourier time transform domain on the order of NJ^3 operations are required, assuming that a Gaussian elimination method is used. If the boundary is a line or a circle N^2J operations may be needed for a time stepping solution, or as little as NJ operations may be needed for a frequency domain solution. For comparison to volume gridding methods, note that wave sampling with J boundary node points is roughly equivalent to the use of J^2 volume node points.

For problems involving material heterogeneities other than cavities, where both traction and displacement boundary values must be evaluated, the error estimates for similarly shaped cavity boundary problems are probably applicable. Error estimates for the boundary values of contacting half-planes may be found in Cole, Kosloff and Minster (1978). Investigations involving curved contacts between different materials have not been carried out in sufficient detail to make a general quantitative statement. For cases of contact between materials with greatly differing properties, the cavity problems give valid error estimates.

Considerable emphasis has been placed here on methods of manipulating and solving discrete BIEs. It is through these techniques that one obtains the ability to create hybrid methods of solving problems, such as the Love mode-BIE method in Chapter 4. The material presented here is by no means the last word on the topic. For example, the use of the numerical analogs of equations (4.9) and (4.10) in Chapter 4 could significantly decrease the computation time involved in that problem. If an FFT based method is used to calculate inverse operators there, this eliminates the most expensive operators involved in that computation. Undoubtedly, there are a great many things that can be done to make the technique more generally useful.

There are other analytic, numerical and seminumerical methods with which the BIE technique may be combined. It appears that combinations with volume gridding methods are possible where the BIE method provides a "boundary formula" (Zienkiewicz (1977)) for the other

numerical methods. This boundary condition would in actuality be an equation of motion for the region exterior to the volume treated by finite difference or finite element methods. This region could be, for example, a layered medium or a whole-space. The Kirchhoff integral method (Berryhill (1979)) may be regarded as a hybrid between the analytic BIE method and geometric ray theory. Similarly, there may be useful methods in which the BIE technique is approximated to give boundary values from formulae which do not deal with the entire surface of a homogeneous body, but only small and connected portions of it. Such a method would be appropriate for the higher frequency waves which could be described by time stepping methods. The combination of the BIE method with generalized ray theory was discussed in Chapter 4. Even more complicated combinations are feasible. For example, problems involving localized but very complicated regions in a regular structure could be treated using BIE methods to create surface Green's functions for regular portions of the medium. The correspondence between BIE and analytic methods could be employed to introduce a highly evolved, analytically evaluated, incident wave, and propagation through the irregular region could be treated with a hybrid finite difference-BIE method. The scattered wave could be evaluated by the BIE method near the irregularity or by semi-analytic methods if a remote scattered wave were desired.

The versatility of the BIE approach is a result of the preservation of important symmetry properties of the analytic Green's functions during the discretization process and the use of a time domain formulation. The accuracy of the method is due to the careful selection of

interpolation methods. Upon extension to plane strain and three-dimensional elastic motions the versatility will be retained. This provides a powerful incentive for the further development of the method. The principal question arising in these extensions is one of accuracy. It appears that the piecewise constant traction interpolation used here is appropriate for use in all types of deformations. The utility of the displacement interpolation method which is linear in time and piecewise constant in space is more uncertain. The interpolation of displacements in time should, by the line of reasoning given in Chapter 3, be linear in time. It may also be necessary to use linear interpolation in space.

The generalization of the method given here to the other deformation types is straightforward. The analytic evaluation of discrete kernels for the general elastic case is a formidable barrier, however. For the general elastic case there are, for each source-receiver pair, nine kernels of the type DG (see equations (1.13) and (1.14)) and twenty-seven of the type DK. Symmetry properties of the Green's tensors can decrease these numbers to six and eighteen, respectively, but these numbers are still large and the Green's tensor contains several non-equivalent terms.

An alternative to the straightforward generalization is possible. Instead of dealing with integral equations for displacements, one could use displacement potential integral equations. In Cartesian coordinates the displacement potentials obey scalar wave equations and they are coupled only a boundaries. This greatly reduces the number of discrete

kernels to be evaluated and simplifies their analytic evaluation enormously. The drawback to this approach is that tractions will involve the second normal derivatives of potentials at a boundary. These derivatives do not appear in the integral equations. They may be evaluated from the scalar equations of motion in terms of tangential and time derivatives of potentials. Numerical differentiation of the boundary values can thus permit one to treat problems involving the boundary values of traction. The consequences of particular interpolation schemes for this approach are unknown, and requirements on the accuracy of boundary representation will probably be more severe.

REFERENCES

Archambeau, C.B. and J.B. Minster (1977). Dynamics in prestressed media with moving phase boundaries; a continuum theory of failure in solids, Geophys. J. R. Astr. Soc. 52, 65-96.

Archambeau, C.B. (1972). The theory of stress wave radiation from explosions in prestressed media, Geophys. J. R. Astr. Soc. 29, 329-366 and 31, 361-363.

Alsop, L.E. (1966). Transmission and reflection of Love waves at a vertical discontinuity, J. Geophys. Res. 71, no. 16, 3969-3984.

Banaugh, Robert P. (1962). Scattering of acoustic and elastic waves by surfaces of arbitrary shape. Ph.D. thesis, University of California, Lawrence Radiation Laboratory, Livermore, CA.

Berryhill, John R. (1979). Wave equation datuming, Geophysics 44, no. 8, 1329-1344.

Biot, M.A. (1957). General theorems on the equivalence of group velocity and energy transport, Phys. Rev. 105, no. 4, 1129-1137.

Boore, D.M. (1970). Love waves in nonuniform wave guides: finite difference calculations, J. Geophys. Res. 75, no. 8, 1512-1527.

Burridge, R. (1969). The numerical solution of certain integral equations with non-integrable kernels arising in the theory of crack propagation and elastic wave diffraction, Proc. Roy. Soc. London A 265, 353-381.

Claerbout, J.F. (1976). Fundamentals of Geophysical Data Processing, McGraw-Hill, NY.

Clayton, R. and B. Engquist (1977). Absorbing boundary conditions, B.S.S.A. 67, no. 6, 1529-1540.

Cole, D.M., D. Koshoff and J.B. Minster (1978). A numerical boundary integral equation method for elastodynamics, I, B.S.S.A. 68, no. 5, 1331-1357.

Courant, R. and D. Hilbert (1966). Methods of Mathematical Physics, Vol. II, Interscience Publishers, NY.

Cruse, T.A. (1968). A direct formulation and numerical solution of the general transient elastodynamic problem I, J. Math. Anal. Appl. 22, 341-355.

Cruse, T.A. and F.J. Rizzo (1975). Boundary-integral equation method: Computational applications in applied mechanics, ASME, AMD-Vol. 11, NY.

Das, S. (1976). A numerical study of rupture propagation and earthquake source mechanism, Ph.D. thesis, Massachusetts Institute of Technology.

Das, S. and K. Aki (1977). Numerical study of two-dimensional spontaneous rupture propagation, Geophys. J. 50, 643-668.

de Hoop, A.T. (1958). Representation theorems for the displacement in an elastic solid and their application to elastodynamic diffraction theory, Thesis, Technische Hogeschool Delft, Delft, The Netherlands.

Ewing, W.M., W.S. Jardetzky and F. Press (1957). Elastic Waves in Layered Media, McGraw-Hill, NY.

Freund, L.B. (1976). The analysis of elastodynamic crack tip stress fields, Mechanics Today 3, 55-91.

Friedlander, F.G. (1954). Diffraction of pulses by a circular cylinder, Comm. Pure Appl. Math. vol. VII, 705-732.

Friedlander, F.G. (1958). Sound Pulses, Cambridge University Press.

Friedman, M.B. and R. Shaw (1962). Diffraction of pulses by cylindrical obstacles of arbitrary cross section, Trans. A.S.M.E., J. Appl. Mech. 29, series E., no. 1, 40-46.

Fung, Y.C. (1965). Foundations of Solid Mechanics, Prentice-Hall, NY.

Goldstein, M. and R.M. Thaler (1959). Math. Tables and Aids Comp. no. 66, April 1959.

Gregerson, S. and L.E. Alsop (1974). Amplitudes of horizontally refracted Love waves, B.S.S.A. 64, no. 3, 535-553.

Gradshteyn, I.S. and I.M. Ryzhik (1965). Table of Integrals, Series, and Products, Academic Press, NY.

Hong, T.L. (1978). Elastic waves propagation in irregular structures, Thesis, California Institute of Technology.

Hudson, J.A. and L. Knopoff (1964). Transmission and reflection of surface waves at a corner. 1. Love waves, J. Geophys. Res. 69, no. 2, 275-280.

Hudson, J.A. (1979). The parabolic approximation for wave propagation as guided models, J. Phys. D: Appl. Phys. 13(1980), 145-152.

Keller, J.B., S.I. Rubinow and M. Goldstein (1963). Zeros of Hankel functions and poles of scattering amplitudes, J. Math. Phys. 4, no. 6, 829-832.

Kellogg, O.D. (1953). Foundations of Potential Theory, Chapter VI, Dover Publications, NY. Reprinted 1953.

Knopoff, L. and J.A. Hudson (1964). Transmission of Love waves past a continental margin, J. Geophys. Res. 69, no. 8, 1649-1653.

Kostrov, B.V. (1966). Unsteady propagation of longitudinal shear cracks, P.M.M. 30, no. 6, 1042-1049.

Kupradze, V.D. (1963). Dynamical Problems in Elasticity, North-Holland Publishing Co., Amsterdam.

Landers, T. and J.F. Claerbout (1972). Numerical calculations of elastic waves in laterally heterogeneous media, J. Geophys. Res. 77, no. 8, 1476-1482.

Love, A.E.H. (1944). A Treatise on the Mathematical Theory of Elasticity, Fourth Edition, Dover Publications, NY.

Lysmer, J. and L.A. Drake (1971). The propagation of Love waves across nonhorizontally layered structures, B.S.S.A. 61, no. 5, 1233-1251.

Miklowitz, J. (1978). The theory of elastic waves and waveguides, vol. 22 of North-Holland Series in Applied Mathematics and Mechanics, North-Holland Publishing Co., NY.

Mitzner, K.M. (1967). Numerical solution for transient scattering from a hard surface of arbitrary shape-retarded potential technique, J. Acoust. Soc. Am. 42, no. 2, 391-397.

Mow, C.-C. and Y.-H. Pao (1971). The diffraction of elastic waves and dynamic stress concentrations, Rand Corporation, Santa Monica, CA.

Peck, J.C. and J. Miklowitz (1969). Shadow zone response in diffraction of a plane compressional pulse by a circular cavity, Int. J. Solids Structures 5, 437-454.

Scott, P. and D.V. Helmberger (1980). Propagational distortions caused by irregular boundary conditions. Abstract in Earthquake Notes 50, no. 4, 23. Published by the Seismological Society of America.

Slavin, L.M. and B. Wolf (1970). Scattering of Love waves in a surface layer with an irregular boundary for the case of a rigid underlying half space, B.S.S.A. 60, no. 3, 859-877.

Srivastava, H.M. and R.G. Buschman (1977). Convolution Integral Equations, with Special Function Kernels, Halsted Press, a division of John Wiley & Sons, NY.

Stevens, J. L. (1979). Seismic radiation from the sudden creation of a spherical cavity in an arbitrarily prestressed medium, submitted to Geophys. J. R. Astr. Soc.

Watson, G.N. (1958). A Treatise on the Theory of Bessel Functions, 2nd Edition, Third printing, Cambridge University Press, MA.

Wheeler, L.T. and E. Sternberg (1968). Some theorems in classical elastodynamics, Arch. Rat. Mech. Anal. 31, 51-90.

Zienkiewicz, O.C. (1977). The Finite Element Method, Third Edition, McGraw-Hill, NY.

APPENDIX A

EVALUATION OF SINGULAR INTEGRALS

We wish to evaluate the limits

$$S\underline{\tau}(\underline{r}_1,t) = \lim_{\varepsilon\to 0}\lim_{\underline{r}\to\underline{r}_1}\int_{t_o=o}^{\infty}\int_{S(\underline{r}_1,\varepsilon)} \underline{\underline{G}}(\underline{r},t;\underline{r}_o,t_o)\cdot\underline{\tau}(\underline{r}_o,t_o)dS_o dt_o \tag{A.1}$$

$$S\underline{u}(\underline{r}_1,t) = \lim_{\varepsilon\to 0}\lim_{\underline{r}\to\underline{r}_1}\int_{t_o=o}^{\infty}\int_{S(\underline{r}_1,\varepsilon)} \underline{u}(\underline{r}_o,t_o)\cdot\underline{\underline{K}}(\underline{r},t;\underline{r}_o,t_o)$$

$$\cdot\,\underline{n}(\underline{r}_o)dS_o dt_o \tag{A.2}$$

If $\underline{r}_1$ is located on a portion of ∂B which satisfies the Liapunov smoothness conditions locally there is a continuously differentiable function $h(R,\theta)$ and constants A and δ such that

$$z = h(R,\theta) \;;\; |h(R,\theta)| < A\,R^{1+\delta},\ 0 < \delta \le 1 \tag{A.3}$$

is a description of ∂B about $\underline{r}_1$. The coordinates (z,R,θ) refer to a cylindrical coordinate system centered on $\underline{r}_1$ with the z-axis parallel to $\underline{n}(\underline{r}_1)$ (see Figure 1.1b).

It will be assumed that $\underline{u}(\underline{r},t)$ and $\underline{\tau}(\underline{r},t)$ satisfy Hölder conditions as a function of space about $(\underline{r},t)$ i.e.,

$$|\tau_i(\underline{r}_1,t) - \tau_i(\underline{r},t)| < C\,|\underline{r}-\underline{r}_1|^{\gamma},\ 0 < \gamma \le 1 \tag{A.4}$$

and likewise for $\underline{u}(\underline{r}_1,t)$. C is a constant. It will also be assumed that $\underline{\tau}$ and $\frac{\partial}{\partial t}\underline{u}$ satisfy Hölder conditions near $(\underline{r}_1,t)$ as a function of time.

To show that $S\underline{\tau} = 0$ it is only necessary to demonstrate that a representative term of $S\underline{\tau}$ is zero, e.g., $S\tau_i^* = 0$ where

$$S\tau_i^* = \lim_{\varepsilon\to 0}\lim_{\underline{r}\to\underline{r}_1}\int_{t_o=o}^{\infty}\int_{S(\underline{r}_1,\varepsilon)}\tau\,\frac{\delta(t-t_o-y/\alpha)}{y}\,dS_o dt_o \qquad (A.5)$$

The other type of term of $\underline{\underline{G}}$ has the same order of singularity, since $|y_i y_j/y^2| \le 1$, and its integral in the limit must also be zero.

If the order of integration of (A.5) is reversed and the integration over time is carried out one obtains

$$s\tau_i^*(\underline{r}_1,t) = \lim_{\varepsilon\to 0}\lim_{\underline{r}\to\underline{r}_1}\int_{S(\underline{r}_1,\varepsilon)}\frac{\tau_i(\underline{r}_o,t-y/\alpha)}{y}\,dS_o \qquad (A.6)$$

Since $\underline{\tau}$ satisfies a Hölder condition as a function of time an expression similar to (A.4) holds;

$$\tau_i(\underline{r}_o,t-y/\alpha) = \tau_i(\underline{r}_o,t) + \mathbf{O}(y^{\eta})$$

where

$$0 < \eta \le 1 \quad .$$

Thus an expansion of τ_i about $(\underline{r}_1,t)$ is possible which is of the form

$$\tau_i(\underline{r}_o,t-y/\alpha) = \tau_i(\underline{r}_1,t) + \mathbf{O}(y^{\eta}) + \mathbf{O}(y^{\gamma})$$

as $\underline{r} \to \underline{r}_1$. Since $y^{\gamma-1} < y^{-1}$ as $y \to 0$ it is sufficient to show that

$$\lim_{\varepsilon\to 0} \lim_{\underline{r}\to\underline{r}_1} \int_{s(\underline{r}_1,\varepsilon)} \frac{1}{y}\, dS_o = 0 \qquad (A.7)$$

The vanishing of less singular contributions then follows.

In the local coordinate system, if $\underline{r} \to \underline{r}_1$ along the z-axis

$$y^2 = R_o^2 + (|\underline{r}-\underline{r}_1| - h(R_o,\theta))^2$$

using (A.3) for small R_o

$$\frac{1}{y} = \frac{1}{[R_o^2 + z'^2]^{1/2}} \left[1 + \mathbf{O}\left(\frac{Az' R_o^{1+\delta}}{R_o^2 + z'^2}\right)\right]$$

where $z' = |\underline{r} - \underline{r}_1|$. Also,

$$dS_o = [1 + \mathbf{O}(R_o^{\delta})]R_o dR_o d\theta$$

Neglecting the higher order, less singular terms, the integral in (A.7) becomes

$$\lim_{\varepsilon\to 0}\lim_{z'\to 0} 2\pi\int_{R_o=0}^{\varepsilon} \frac{R_o dR_o}{[R_o^2 + z'^2]^{1/2}} = 2\pi \lim_{\varepsilon\to 0}\lim_{z'\to 0}\left[[\varepsilon^2 + z'^2]^{1/2} - z'\right] = 0$$

This proves (A.7) and therefore $S\underline{\tau}^*(\underline{r}_1,t) = 0$ and $S\underline{\tau}(\underline{r}_1,t) = 0$. The proof of (A.7) is easily extended to show that

$$\lim_{\varepsilon\to 0}\lim_{\underline{r}\to\underline{r}_1} \int_{S(\underline{r}_1,\varepsilon)} \frac{1}{y^{2-\xi}}\, dS_o = 0 \qquad \text{for } \xi > 0$$

In evaluating $S\underline{u}(\underline{r}_1,t)$ we note that the only possible nonzero contributions will come from terms of $\underline{\underline{K}}$ of the form

$$\delta(t-t_o-y/\alpha)\,\frac{y_i y_j y_k}{y^5} \quad \text{and} \quad \delta(t-t_o-y/\alpha)\,\frac{y_i \delta_{jk}}{y^3}$$

since all other terms are of order $1/y$ as $y \to 0$ and $\partial\underline{u}/\partial t$ satisfies a Hölder condition. The dot product of $\underline{n}(\underline{r}_o)$ with terms of this form gives three types of singular terms;

$$\frac{y_i y_j y_k n_k}{y^5}\ , \quad \frac{\delta_{ij} y_k n_k}{y^3} \quad \text{and} \quad \frac{y_i n_k}{y^3} \tag{A.8}$$

A property of the Liapunov surface is that for $\underline{r}_1, \underline{r}_o \in \partial B$

$$|\underline{n}(\underline{r}_1) \cdot (\underline{r}_1 - \underline{r}_o)| < A\,|\underline{r}_1 - \underline{r}_o|^{1+\delta}$$

so the first two terms of (A.8) are of the order $1/y^{2-\delta}$ as $\underline{r} \to \underline{r}_1$ and by the previous arguments give no contribution to the integral of (A.2) in the limit. The only remaining singular integrals are then of the form

$$\lim_{\varepsilon\to 0} \lim_{\underline{r}\to\underline{r}_1} \int_{S(\underline{r}_1,\varepsilon)} \frac{u_i(\underline{r}_o,t-y/\alpha)}{y^3}\, y_i n_k \, d\delta_o \tag{A.9}$$

First, the function $\underline{u}(\underline{r}_o,t-y/\alpha)$ may be expanded about $(\underline{r}_1,t)$ and the higher order terms discarded as before. The normal $\underline{n}(\underline{r}_o)$ also varies smoothly about $\underline{r}_1$;

$$\underline{n}(\underline{r}_o) = \underline{n}(\underline{r}_1) + \mathbf{O}(|\underline{r}_1-r_o|^{\delta})$$

Thus (A.9) is equivalent to

$$u_i(\underline{r}_1,t) \lim_{\varepsilon\to 0} \lim_{\underline{r}\to\underline{r}_1} \int_{S(\underline{r}_1,\varepsilon)} \frac{y_i n_k(\underline{r}_1)}{y^3}\, dS_o \tag{A.10}$$

It is easily seen from symmetry arguments that the tangential components of $\underline{y}$, when integrated on a circle about $\underline{r}_1$ in (A.10), will given no contribution to the integral, so (A.10) is equivalent to

$$u_k(\underline{r}_1,t) \lim_{\varepsilon\to 0} \lim_{\underline{r}\to\underline{r}_1} \int_{S(\underline{r}_1,\varepsilon)} \frac{z_o-z}{y^3}\, dS_o \tag{A.11}$$

By use of the expressions for y and dS_o in the local coordinate system one obtains from (A.11) the equivalent integral

$$u_k(\underline{r}_1,t) \lim_{\varepsilon\to 0} \lim_{z'\to 0} \int \frac{-2\pi z'}{[R_o^2 + z'^2]^{3/2}} R_o dR_o \qquad (A.12)$$

where higher order terms have been discarded. This is easily shown to equal $-2\pi u_k(\underline{r}_1,t)$. If the various terms of the form (A.9) are summed one obtains the result

$$S\underline{u}(\underline{r}_1,t) = -\frac{1}{2}\underline{u}(\underline{r}_1,t) \quad .$$

In the case that the boundary does not satisfy the Liapunov smoothness conditions at the receiver point $\underline{r}_1$, these results may be modified. It can be shown, by methods similar to those used above, that $S\underline{\tau}$ is zero at corners formed by the nontangential intersection of regular surfaces. $S\underline{u}$ is altered at such a corner, and its value appears to depend in a complex way upon the geometric parameters. In the numerical calculations it is not necessary to place receiver points at corners. See Banaugh (1962) for a limited discussion of such corners.

APPENDIX B

TREATMENT OF INITIAL VALUES

In this appendix the problem of simplifying the introduction of nonzero initial values into the analytic BIE (1.7) is considered. The initial value portion of $\underline{F}(\underline{r},t)$ will be called $\underline{I}(\underline{r},t)$. From (1.4)

$$\underline{I}(\underline{r},t) = \int_B \rho \left\{ \underline{\underline{G}}(\underline{r},t;\underline{r}_o,t_o) \cdot \frac{\partial}{\partial t_o} \underline{u}(\underline{r}_o,t_o) \right\} \Big|_{t_o=0} dV_o$$

$$- \int_B \rho \left\{ \underline{u}(\underline{r}_o,t_o) \cdot \frac{\partial}{\partial t_o} \underline{\underline{G}}(\underline{r},t;\underline{r}_o,t_o) \right\} \Big|_{t_o=0} dV_o \qquad \text{(B.1)}$$

for $\underline{r} \in B'$. B does not change with time.

The Green's function considered here will be the free-space solution of (1.3) which is given in (1.4a). The first term of (B.1) is due to nonzero initial velocities and will not be considered here. The second term will be identified as $\underline{IS}(\underline{r},t)$ and is due to nonzero initial displacements. Differentiating $\underline{IS}$ once with respect to time and noting that $\underline{\underline{G}}$ is a function of $(t - t_o)$ only, one obtains upon assuming that the differentiation may be taken under the integral;

$$\frac{\partial}{\partial t} \underline{IS}(\underline{r},t) = \int_B \rho \, \underline{u}(\underline{r}_o,t_o) \cdot \frac{\partial^2}{\partial t_o^2} \underline{\underline{G}}(\underline{r},t;\underline{r}_o,t_o) \Big|_{t_o=0} dV_o \qquad \text{(B.2)}$$

Substituting from (1.3) for $\rho \frac{\partial^2}{\partial t_o^2} \underline{\underline{G}}$ in this equation gives

$$\dot{I}S_j = \int_B \left\{ C_{ipqs}\, G_{qj,s_o p_o} + \delta_{ij}\ \delta(t - t_o)\ \delta(\underline{r} - \underline{r}_o) \right\} u_i(\underline{r}_o, t_o) \Big|_{t_o=0} dV_o \tag{B.3}$$

Proceeding toward application of the divergence theorem in the usual manner, we find

$$C_{ipqs}\, G_{qj,s_o p_o}\, u_i = \left\{ C_{ipqs} \frac{\partial}{\partial x_{p_o}} [G_{qj,s_o}\, u_i] - G_{qj,s_o}\, u_{i,p_o} \right\}$$

$$= C_{ipqs} \left\{ \frac{\partial}{\partial x_{p_o}} [G_{qj,s_o}\, u_i] - \frac{\partial}{\partial x_{s_o}} [G_{qj}\, u_{i,p_o}] \right.$$

$$\left. + G_{qj}\, u_{i,p_o s_o} \right\} \tag{B.4}$$

Each of the terms of this quantity is to be evaluated at $t_o = 0$; let

$$u^o(\underline{r}) = u(\underline{r}, t_o)\Big|_{t_o=0}$$

Then (see (1.4b))

$$C_{ipqs}\, G_{qj,s_o p_o}\, u_i \Big|_{t_o=0} =$$

$$\frac{\partial}{\partial x_{p_o}} \left\{ K_{ipj} \Big|^{u_i}_{t_o=0} \right\} - \frac{\partial}{\partial x_{s_o}} \left\{ G_{qj} \Big|^{\sigma^o_{qs}}_{t_o=0} \right\} + G_{qj} \Big|^{\sigma^o_{qs,s_o}}_{t_o=0} \tag{B.5}$$

Upon substituting this into (B.3) and applying the divergence theorem,

$$\dot{I}S_j(\underline{r},t) = \oint_{\partial B} \Big\{ K_{ipj}(\underline{r},t;\underline{r}_o,0)\, u^o_i(\underline{r}_o)\, n_p(\underline{r}_o) - G_{qj}(\underline{r},t;\underline{r}_o,0)\sigma^o_{qp}(\underline{r}_o)\, n_p(\underline{r}_o) \Big\}\, dS_o + \int_B \Big(G_{qj} \Big|^{\sigma^o_{qs,s_o}}_{t_o=0} + u^o_j\, \delta(t)\, \delta(\underline{r} - \underline{r}_o) \Big) dV_o \tag{B.6}$$

for $\underline{r} \in B$.

Integrating in time from $0 - \varepsilon$ to $t + \varepsilon$, and using the time translation property of $\underline{\underline{G}}$, one obtains

$$\underline{IS}(\underline{r},t) = \oint_{\partial B} \int_{t_o=0}^{t+} \left\{ \underline{u}^o(\underline{r}_o) \cdot \underline{\underline{K}}(\underline{r},t,\underline{r}_o,t_o) \cdot \hat{n}(r_o) \right.$$

$$\left. - \underline{\underline{G}}(\underline{r},t;\underline{r}_o,t_o) \cdot \underline{\tau}^o(r_o) \right\} dS_o \, dt_o$$

$$\int_B \int_{t_o=0}^{t+} \underline{\underline{G}}(\underline{r},t;\underline{r}_o,t_o) \cdot (\underline{\nabla}_o \cdot \underline{\underline{\sigma}}^o(\underline{r}_o)) \, dV_o \, dt_o$$

$$+ \int_B \underline{u}^o(\underline{r}_o) \, \delta(\underline{r} - \underline{r}_o) \, dV_o \qquad (B.7)$$

$\underline{r} \in B$

The first integral of this expression is of the same form as the first term of (1.4). Upon taking the limit as $\underline{r} \to \partial B$ the treatment of the singularity may be carried out in the same manner (see Appendix A). In the limit as $\underline{r} \to \partial B$ one obtains the principle value of the integral minus $\frac{1}{2}u^o(r)$. The third term can be evaluated without considering the limit in detail to be $u^o(r)$. The second term is the displacement field due to the disequilibrium of the initial values, represented by the body force equivalent $H(t)\ \underline{\nabla} \cdot \underline{\underline{\sigma}}^o$. This term is zero if the body is initially in a state of static equilibrium. The BIE with these terms included and zero initial velocities takes the simpler form

$$1/2(u(r,t) - u^{o}(r)) =$$

$$\int_{t_o=0}^{t+} \int_{\partial B}^{P} \left\{ \underline{\underline{G}} \cdot (\underline{\tau} - \underline{\tau}^{o}) - (\underline{u} - \underline{u}^{o}) \cdot \underline{\underline{K}} \cdot \hat{n} \right\} dS_o \, dt_o$$

$$+ \int_{t_o=0}^{t+} \int_{B} \left\{ \underline{\underline{G}} \cdot (\underline{f}(\underline{r}_o, t_o) + H(t_o) \, \underline{\nabla}_o \cdot \underline{\underline{\sigma}}^{o}) \right\} dV_o \, dt_o \qquad (B.8)$$

From (B.8) it can be seen that if the elastic body is initially in a state of static equilibrium a redefinition of reference for the displacement and stress relative to the initial state permits treatment of initial value problems in a straightforward way. If the initial velocities are zero but $\underline{\nabla} \cdot \underline{\underline{\sigma}}^{o}$ is not zero the equivalent body force term should be included. If $\underline{\tau}$ and $\underline{u}$ are known on ∂B the displacement at a point $\underline{r} \in B'$ may be evaluated by calculating the integrals in this equation and dropping the factor of 1/2 on the left-hand side.

APPENDIX C

CONVERGENCE FOR D_o FOR THE FUNDAMENTAL BOUNDARY VALUE PROBLEMS FOR THE HALF PLANE

The a priori estimation of errors involved in the numerical technique presented here is of considerable practical interest. The method is different from the familiar volume gridding methods in that the iterative operator is nonlocal, its elements do not depend on the discretization parameters in a simple way and the process of numerical differentiation is substantially absent. Lacking clear analogies to other well-studied methods, it is important to see what effects the various approximations have in general. Since the general error estimates will involve some unknown coefficients it is equally important to compare numerical and exact solutions to a number of representative problems.

The analytic antiplane strain BIE, equation (1.9) may be written in the operational form

$$u(\underline{r},t) = LG(\partial B;\underline{r},t) \cdot \tau - LK(\partial B;\underline{r},t) \cdot u + 2F(\underline{r},t) \qquad (C.1)$$

The linear functionals LG and LK are defined in equation (1.9) and depend on ∂B and the particular Green's function in use. When this equation is discretized the displacement u and traction τ are replaced by their approximations u^* and τ^*. Also, since the inhomogeneous term

F must be represented discretely in any numerical calculations it is approximated in some manner by F*. The boundary ∂B may be approximated to any desired accuracy by DB while the number of node points is held constant. (A simple redefinition of the interpolators is required.) The discrete kernels may be calculated to an accuracy limited only by the word size and the accuracy of any library functions in use. Since the relevant calculations need only be carried out once for a given elastic body and interpolation scheme, it is useful to assume that the discrete kernels are calculated exactly. In any case, near the singularity they must be calculated from analytic formulae, which will presumably be of very high accuracy. Under these circumstances the discretized BIE is the algebraic version of

$$u^*(\underline{r}_j,t_n) = LG(\partial B;\underline{r}_j,t_n) \cdot \tau^* - LK(\partial B;\underline{r}_j,t_n) \cdot u^* + 2F^*(\underline{r}_j,t_n) \tag{C.2}$$

$$j = 1, \cdots, J$$

$$n = 1, \cdots, N$$

The order of accuracy of this equation is then the order of quantity

$$\varepsilon_j^n = LG(\partial B;\underline{r}_j,t_n) \cdot (\tau-\tau^*) - LK \cdot (u-u^*) + 2(F-F^*) \tag{C.3}$$

where u, τ and F satisfy (C.1) exactly and

$$u_j^n = u^*(\underline{r}_j, t_n) = u(\underline{r}_j, t_n)$$

$$\tau_j^n = \tau^*(\underline{r}_j, t_n - \Delta t/2) = \tau(\underline{r}_j, t_n - \Delta t/2)$$

The order of ε_j^n is easily found as follows: the effect of the error F-F* is apparent. If F* is evaluated numerically from its initial value-body force definition one should be careful to maintain errors smaller than those due to the interpolation scheme. Since the Green's function has strong variation near the backward characteristic surface of the receiver point, the errors from this portion of the integral are dominant. The order of ε_j^n is then determined by the local order of accuracy, the order of accuracy of the interpolation scheme. For interpolation scheme D_o, defined in equations (3.5) and (3.6)

$$u - u^* = \mathcal{O}(L \frac{\partial u}{\partial s}) + \mathcal{O}(\Delta t^2 \frac{\partial^2}{\partial t^2} u)$$

$$\tau - \tau^* = \mathcal{O}(L \frac{\partial \tau}{\partial s}) + \mathcal{O}(\Delta t \frac{\partial \tau}{\partial t})$$

where s is an arc length along ∂B and L is the spatial discretization length. Therefore

$$\varepsilon_j^n = \mathcal{O}(L) + \mathcal{O}(\Delta t) \qquad \text{(C.3a)}$$

for D_o.

The relation (C.3) shows that the discretization method is consistent in a conventional sense for any reasonable interpolators. To carry the analysis further some specializations are necessary. If the elastic body is the half plane $y > y_1$ equation (C.1) has the form

$$u(x,t) = \frac{1}{\pi\mu}\int_{t_o=o}^{\infty}\int_{x_o=-\infty}^{\infty}\frac{H(t-t_o - |x-x_o|/\beta)}{[(t-t_o)^2 - (x-x_o)^2/\beta^2]^{1/2}}\tau(x_o,t_o)dx_o dt_o$$

$$+ 2F(x,t) \qquad (C.4)$$

(The argument y_1 has been dropped.) The Fourier transform with respect to x of this equation is;

$$\hat{u}(k,t) = \frac{\beta}{\mu}\int_o^t J_o(k\beta(t-t_o))\,\hat{\tau}(k,t_o)dt_o + 2\hat{F}(k,t) \qquad (C.5)$$

J_o is the Bessel function of zeroth order (Gradshteyn, P. 953, 8.411.8). The discretized version is the same with $\hat{u}$, $\hat{\tau}$ and $\hat{F}$ replaced by their approximations $\hat{u}^*$, $\hat{\tau}^*$ and $\hat{F}^*$. A notable feature of this equation is that since

$$J_o(k\beta t_o) \to \left(\frac{2}{\pi k\beta t_o}\right)^{1/2}\cos(k\beta t_o - \pi/4),\ k\beta t_o >> 1$$

The integral is insensitive to wave number components of $\hat{\tau}(k,t_o)$ for

$k\beta(t-t_o) >> 1$, whenever $\hat{\tau}(k,t)$ is well behaved as $|k| \to \infty$. As a result the large wave number errors in $\hat{\tau}^*$ do not affect the accuracy of the integral after a sufficiently large number of time steps. This result is, of course, just a restatement of the properties of the medium and mode of propagation and it is expected to hold for most boundaries. Similar results are found when the high frequency effects in displacement integrals are examined.

Equation (C.5) is in a form suitable for stability analysis. If $\hat{\tau}^*$ and $\hat{F}^*$ are specified and $\hat{u}^*$ is to be calculated, it is clearly true that the iterative process is stable for a flat boundary. If $\hat{u}^*$ is specified and $\hat{\tau}^*$ is to be evaluated, there is a possibility of instability. Consider the equation for k = o. Let

$$\overline{u}\,(t) = \int_{-\infty}^{\infty} u(x,t)dx$$

From (C.5) we obtain

$$\overline{u}\,(t) = \frac{\beta}{\mu}\int_{o}^{t} \overline{\tau}\,(t_o)dt_o + 2\overline{F}(t) \qquad (C.6)$$

the solution for $\overline{\tau}$ is

$$\overline{\tau}(t) = \frac{\mu}{\beta}\frac{\partial}{\partial t}\left(\overline{u}(t) - 2\overline{F}(t)\right) \qquad (C.6a)$$

The discretized version of (C.6) for interpolators D_o is

$$\bar{u}^n = \frac{\beta\Delta t}{\mu} \sum_{1}^{n} \bar{\tau}^m + 2\bar{F}^n \tag{C.7}$$

where

$$\bar{u}^n = L \sum_{j=-\infty}^{\infty} u_j{}^n$$

(This relation can be deduced by summation of the discrete equation (2.16) over i.) The analog of (C.6a) is readily found from (C.7) to be accurate to order Δt;

$$\bar{\tau}^n = \frac{\mu}{\beta} \left(\frac{\bar{u}^n - \bar{u}^{n-1}}{\Delta t} - 2\,\frac{\bar{F}^n - \bar{F}^{n-1}}{\Delta t}\right) \tag{C.7a}$$

$\bar{\tau}^n$ is dependent only on the data at time levels n and n-1, so this particular scheme is stable for sufficiently small wave numbers. If one were to use a different interpolation method for τ^* the result would not necessarily be the same. For example, if $T^n(t)$ were linearly varying in time, as U^n is in equation (3.5) we would have

$$DG_{ij}^m = \frac{\beta\Delta t}{\pi\mu} (E_m^{+1} + E_m^{-1} - 2)(E_k^{+1/2} - E_k^{-1/2})m^2 H(m) g_1\left(\frac{k}{Qm}\right)$$

where

$$E_m^b f(m) = f(m + b)$$

and where

$$g_1(\eta) = \begin{cases} \eta \, \ell n\left[|\eta|^{-1} + [\eta^{-2}-1]^{1/2}\right] + \frac{1}{2}\sin^{-1}(\eta) \\ \qquad - \eta|\eta| \, \frac{1}{2}\,[\eta^{-2}-1]^{1/2} \quad , \; |\eta| \le 1 \\ \frac{\pi}{4} \quad , \quad |\eta| \ge 1 \end{cases}$$

and $k = |i-j|$.

For this interpolator

$$\bar{u}^n = \frac{\beta\Delta t}{2\mu}\left(\bar{\tau}^n + 2\sum_{1}^{n-1}\bar{\tau}^m\right) + 2\bar{F}^n \tag{C.8}$$

The solution for $\bar{\tau}^n$ is

$$\bar{\tau}^n = -\bar{\tau}^{n-1} + \frac{2\mu}{\beta}\left\{\frac{\bar{u}^n - \bar{u}^{n-1}}{\Delta t} - 2\,\frac{\bar{F}^n - \bar{F}^{n-1}}{\Delta t}\right\} \tag{C.9}$$

or

$$\bar{\tau}^n = \frac{2\mu}{\beta\Delta t}\left\{\bar{u}^n - 2\,\bar{F}^n + (-1)^n\, 2\sum_{m=1}^{n-1}(-1)^m\,(\bar{u}^m - 2\,\bar{F}^m)\right\} \tag{C.10}$$

This solution for $\bar{\tau}^m$ is clearly unacceptable; from (C.10) it is readily seen that arbitrarily large errors of $\bar{\tau}^n$ may be made to persist for all time, for example by setting

$$\bar{u}^1 - 2\,\bar{F}^1 = A,\ \bar{u}^m - 2\,\bar{F}^m = 0 \quad , \quad m > 1$$

$$\text{then } \bar{\tau}^n = (-1)^{n-1}\,\frac{4\mu}{\beta\Delta t}\,A \quad , \quad n > 1$$

Equation (C.9) more closely represents the actual numerical iteration, so in terms of machine manipulations the solution would be

$$\bar{\tau}^n = (-1)^{n-1}\ \bar{\tau}^1 \quad , \quad n > 1$$

This process is marginally stable in theory and has been found to be unstable in practice. The type of divergence arising is global; one finds that after many time steps

$$\tau_j^n = C_j\,(-1)^n\,(1 + a)^n \quad , \quad a > 0$$

where the constants C_j are all of the same sign. For a bonded interface the two interpolation schemes give identical results when solved for $\bar{u}^n$ but the linear traction interpolators again produce divergent tractions.

A complete stability analysis of the approximated version of (C.5) should include all wave numbers k. This cannot be carried out analytically due to the appearance of the special function J_0. It is possible, however, to argue that the type of divergence shown above may be typical and detectable by the zero wave number analysis. First

note that

$$G\ (\underline{r},t;\ \underline{r}_o,t_o)\ \geq\ 0$$

and

$$\sum_i DG^o_{j-i}\ \tau^n_j\ =\ u^n_j - 2F^n_j - \sum_{m=1}^{n-1}\ \sum_i\ DG^{n-m}_{j-i}\ \tau^n_i$$

A realistic discrete kernel DG should have $DG^n_{ij} \geq 0$ for small n. In the iterative solution for τ^*, then τ^n_j will depend on an average over i of τ^{n-1}_i, τ^{n-2}_i, $i = j,\ j \pm 1,\ j \pm 2$. That is, there is only "weak" numerical differentiation along the boundary. If $u^n_j - 2\ F^n_j$ is smoothly varying with respect to j, any large wave number oscillations of the tractions will be smoothed out in the iterative process. Thus, it seems unlikely that divergence of the form $\tau^n_j = C_j(-1)^{j+n}(1+a)^n$ could occur, and any instability would be caused by badly approximating the derivative with respect to time in (C.6a).

It is possible to demonstrate that D_o produces a convergent algorithm for the two fundamental boundary value problems of the half plane. For the first problem, in which the traction is specified, it is sufficient to note that the error estimates (C.3) and (C.3a) give a bound for $u^* - u$ proportional to Δt and L. Therefore, if $\tau(x,t)$ is sufficiently differentiable $u^*(x,t) \to u(x,t)$ as $L \to 0$ with $\beta\Delta t/L$ held constant.

The other fundamental problem is one in which u(x,t) is specified. Due to the singularities of the Green's function, manipulation

of (C.4) presents serious difficulties. Instead, the wave number domain expression (C.5) will be used. The transform of $\tau^*(x,t)$ is given by

$$\hat{\tau}^*(k,t) = \frac{\sin(kL/2)}{(kL/2)} \sum_j L\, e^{ikx_j}\, \tau_j^n \quad , \quad t_n > t > t_{n-1}$$

The discussion here will assume $\frac{kL}{2} < 1$ to permit an interpretation of $\hat{\tau}^*$ and $\hat{u}^*$, which is given by a similar formula with time interpolation the same as in D_o. For explicit time stepping the time step size is restricted to $\beta\Delta t \leq L/2$ and hence $k\beta\Delta t < 1$.

By differentiation (C.5) one obtains for the exact solution,

$$\frac{\mu}{\beta} \frac{\partial}{\partial t} \hat{u}(k,t) = \hat{\tau}(k,t) + \int_{q=0}^{t} \hat{\tau}(k,q) \frac{\partial}{\partial t} J_o\,(k\beta(t-q))\, dq \qquad (C.11)$$

The source term has been dropped here. The time stepping version of (C.5) is

$$\frac{\mu}{\beta} \hat{u}^n = \sum_{m=1}^{n} J_o^{n-m}\, \hat{\tau}^m \qquad (C.12)$$

where

$$\hat{u}^n = \hat{u}^*(k,t_n) = \hat{u}(k,t_n)$$

$$\hat{\tau}^m = \hat{\tau}^*(k,t_m - \Delta t/2)$$

and

$$J_o^{n-m} = \int_{t_{m-1}}^{t_m} J_o\,(k\beta(t_n - q))\, dq$$

Differencing (C.12) gives

$$\frac{\mu}{\beta}\frac{1}{J_o^{\,o}}\left(\hat{u}^n - \hat{u}^{n-1}\right) = \hat{\tau}^n + \sum_{m=1}^{n-1}\frac{1}{J_o^{\,o}}\left(J_o^{n-m} - J_o^{n-1-m}\right)\hat{\tau}^m \qquad (C.13)$$

Subtracting this from (C.11) gives an expression for the error as it would be produced in the time stepping procedure;

$$\hat{\tau}(k,t_n - \Delta t/2) - \hat{\tau}^n = \frac{\mu}{\beta}\left\{\frac{\partial}{\partial t}\hat{u}(k,t)\Big|_{t_n - \Delta t/2} - \frac{1}{J_o^{\,o}}\left(\hat{u}^n - \hat{u}^{n-1}\right)\right\}$$

$$+ k\beta\int_{q=0}^{t_n - \Delta t/2}\hat{\tau}(k,q)\,J_1(k\beta(t_n - \Delta t/2 - q))\,dq$$

$$+ \sum_{m=1}^{n-1}\hat{\tau}^m\frac{1}{J_o^{\,o}}\left(J_o^{n-m} - J_o^{n-m-1}\right)$$

Since $J_o^{\,o} = \Delta t\left\{1 - \left(\frac{k\beta\Delta t}{2}\right)^2\frac{1}{3} + \cdots + \mathcal{O}(h\beta\Delta t)^{2n}\right\}$

and

$$J_o^{n-m} - J_o^{n-1-m} = -k\beta\Delta t\int_{t_{m-1}}^{t_m} J_1(k\beta(t_n - q))dq + \mathcal{O}(k\beta\Delta t)^2$$

This can be reduced to:

$$\hat{\tau}(k,t_n - \Delta t/2) - \hat{\tau}^n = \frac{\mu}{\beta}\left\{(1 - \frac{\Delta t}{J_o^0})\frac{\partial}{\partial t} u(k,t)\Big|_{t_n - \Delta t/2} - \mathcal{O}\frac{\Delta t^3}{J_o^0}\frac{\partial^3}{\partial t^3}\hat{u}\right\}$$

$$+ k\beta\int_0^{t_{n-1}}\left\{(\hat{\tau}(k,q) - \hat{\tau}^*(k,q))\, J_1(k\beta(t_n - q)) + \mathcal{O}(\hat{\tau}^* k\beta\Delta t)\right\} dq$$

For any fixed value of k, as $L \to 0$ with $\frac{\beta\Delta t}{L}$ held constant, the error inside the integral arising from the approximation of J_1 is dominant and of order Δt. Therefore, by induction over time step n

$$\hat{\tau}(k,t_n - \Delta t/2) - \hat{\tau}^n = \theta(k^2\beta^2\Delta t)$$

for all time steps; as $\Delta t \to 0$, $\hat{\tau}^*(k,t) \to \hat{\tau}(k,t)$. The general behavior of the error for fixed Δt and L can also be seen to be proportional to the wave number, i.e., errors at wavelength λ will be proportional to L/λ.

It should be noted that, as in any numerical calculation, convergence depends on the differentiability of the boundary values and source terms. This has important consequences when one is approximating a mixed-type boundary value problem because stress discontinuities commonly arise at points where the type of boundary condition changes. It is possible to demonstrate that many BIE methods will not converge for these problems.

APPENDIX D

ALGEBRAIC RELATIONS FOR CALCULATING DISCRETE KERNELS

This appendix contains algebraic relations for calculating the discrete kernels DG^n_{ij} and DK^n_{ij} defined in (1.13) and (1.14) for the interpolator D_0 which is defined in Chapter 2 (2.24) and Chapter 3 (3.5). At the end of the appendix is a listing of the Fortran subroutine used to calculate these kernels for examples in the text. For times $t_n >> |\underline{r}_i - \underline{r}_j|/\beta$ the subroutine calculates the kernels as the difference of relatively large numbers and, depending on the accuracy of library routines in use, substantial errors may occur for DK^n_{ij} where $|\hat{n} \cdot (\underline{r}_i - \underline{r}_j)| > 0.95\ |\underline{r}_i - \underline{r}_j|$. Under these circumstances the analytic formulae have no advantages over single point evaluations of the required integrals and the latter are by far the more efficient. The analytic formulae assume the surface to be flat over the integration interval, so that $\hat{n} \cdot (\underline{r}_i - \underline{r}_j)$ is constant over the interval (see Figure D.1). This approximation may be avoided by defining the kernels to be a sum over the kernels for a more finely subdivided surface. The subroutine may thus be used to evaluate kernels for approximately curved surface elements. This was not found to be an improvement in the problems on symmetric and unsymmetric boundaries in Chapter 3.

The integrals to be evaluated are:

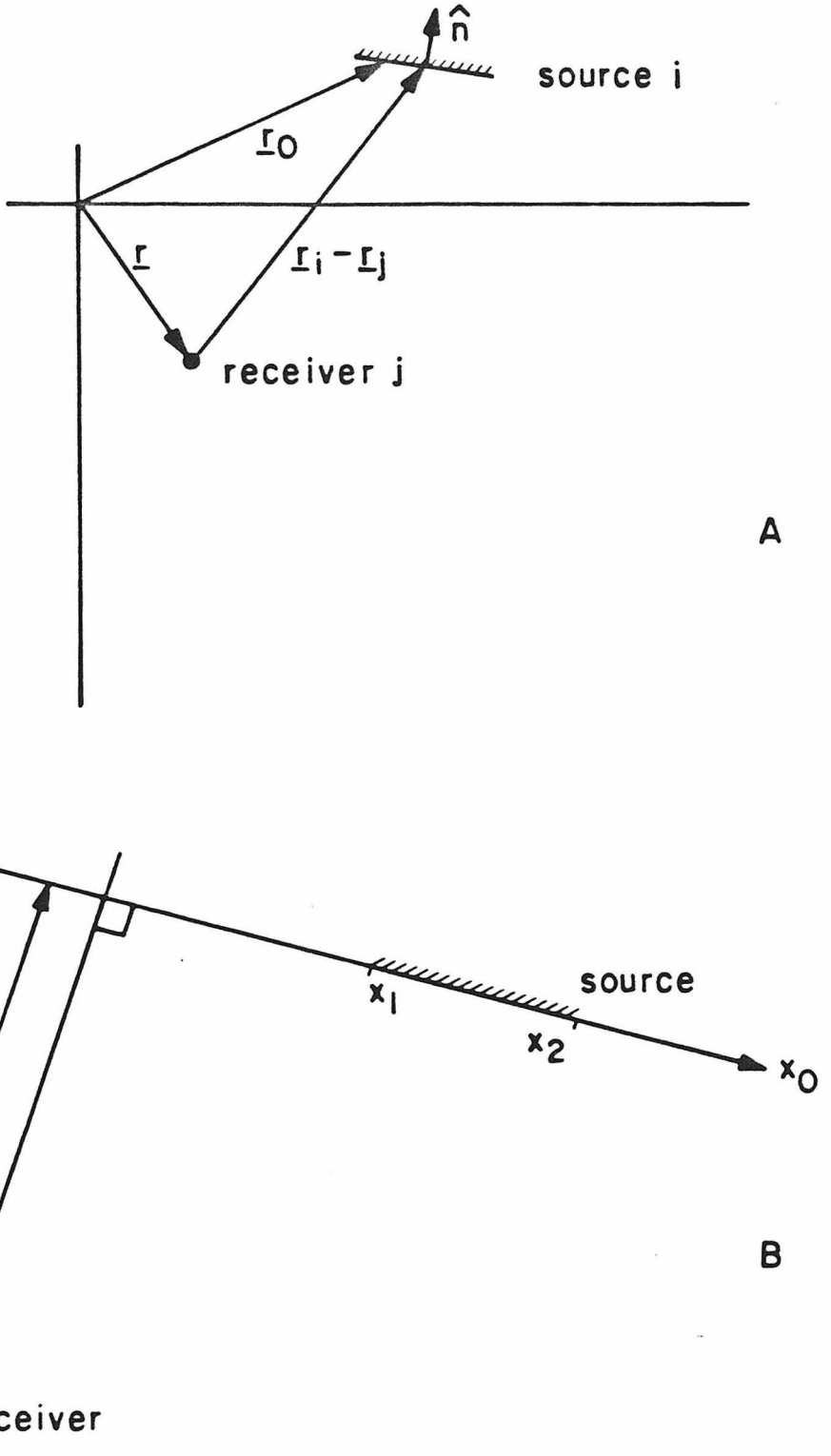

Figure D.1. Source-receiver geometry and coordinate definition.

$$DG_{ij}^{n-m} = \frac{1}{\mu\pi}\int_{\chi_o=\chi_1}^{\chi_2}\int_{t_o=t_m-\Delta t}^{t_m}\frac{H(t_n - t_o - |\underline{r}-\underline{r}_o|/\beta)}{[(t_n-t_o)^2 - (y^2+\chi_o^2)/\ ^2]^{1/2}}\,dt_o\,d\chi_o \tag{D.1}$$

$$DK_{ij}^{n-m} = \frac{1}{\pi}\int_{\chi_o=\chi_1}^{\chi_2}\hat{n}\cdot\underline{\nabla}_r\int_{t_m-\Delta t}^{t_m+\Delta t}\frac{(1-|t_o-t_m|/\Delta t)H(t_n-t_o-|\underline{r}-\underline{r}_o|/\beta)}{[(t_n-t_o)^2-(y^2+\chi_o^2)/\beta^2]^{1/2}}\,dt_o d\chi_o \tag{D.2}$$

The variables y, x_1 and x_2 are depicted in Figure D.1, with

$$y = \hat{n}\cdot(\underline{r}_o-\underline{r})$$

The x_o-t_o integration regions are shown in Figure D.2. These integrals may be written as differences of functions FG and FK

$$DG_{ij}^{n} = (E_n^{+1} - 1)(FG(x_1,n\Delta t) - FG(x_2,n\Delta t))$$

$$DK_{ij}^{n} = \frac{1}{\Delta t}(E_n^{+1} - 2 + E_n^{-1})(FK(x_1,n\Delta t) - FK(x_2,n\Delta t))$$

where

$$FG(x,t) = \frac{1}{\pi\mu}\int_{x_o=x}^{[\beta^2t^2-y^2]^{\frac{1}{2}}}\int_{t_o=(x_o^2+y^2)^{\frac{1}{2}}/\beta}^{t}\frac{dt_o\,dx_o}{[t_o^2-(x_o^2+y^2)/\beta^2]^{\frac{1}{2}}} \tag{D.3}$$

for $\beta t > (x^2+y^2)^{\frac{1}{2}}$ and $FG(x,t) = 0$ if $\beta t \leq (x^2+y^2)^{\frac{1}{2}}$.

$$FK(x,t) = \frac{sgn(y)}{\pi} \int_{x_o=0}^{[\beta^2 t^2 - y^2]^{\frac{1}{2}}} \frac{\partial}{\partial |y|} \int_{t_o=(x_o^2+y^2)^{\frac{1}{2}}/\beta}^{t} \frac{(t - t_o)\, dt_o\, dx_o}{[t_o^2 - (x_o^2+y^2)/\beta^2]^{\frac{1}{2}}} \tag{D.4}$$

for $\beta t > (x^2 + y^2)^{\frac{1}{2}}$ and $y \neq 0$. $FK(x,t) = 0$ if $\beta t \leq (x^2 + y^2)^{\frac{1}{2}}$ or $y = 0$. After some algebra one finds for $\beta t > (x^2 + y^2)^{\frac{1}{2}}$

$$FG(x,t) = \beta t \sin^{-1}(\nu/q) - x \ln \frac{\beta t + \nu}{(x^2 + y^2)^{\frac{1}{2}}} + |y| \left[\tan^{-1}(x/|y|) - \sin^{-1} \frac{\beta t \nu + q^2}{q(\beta t + \nu)}\right] \tag{D.5}$$

$$FK(x,t) = \frac{|y|}{\beta\pi} \left[\sin^{-1}\left(\frac{x}{q}\right) - \frac{\pi}{2}\right] + \frac{t}{\pi} \left[\sin^{-1} \frac{\beta t \nu + q^2}{q(\beta t + \nu)} - \tan^{-1}(x/|y|)\right] \tag{D.6}$$

where $q = (\beta^2 t^2 - y^2)^{\frac{1}{2}}$

$\nu = (q^2 - x^2)^{\frac{1}{2}}$

The following pages contain a listing of the FORTRAN subroutines used to calculate discrete kernels. Subroutine ARBIT is a time series-oriented procedure which calculates the series DG_{ij}^n and DK_{ij}^n for $n = 0, \cdots, N$. These values are returned in the single precision arrays SDG and SDK, respectively, in reversed time order. The information that

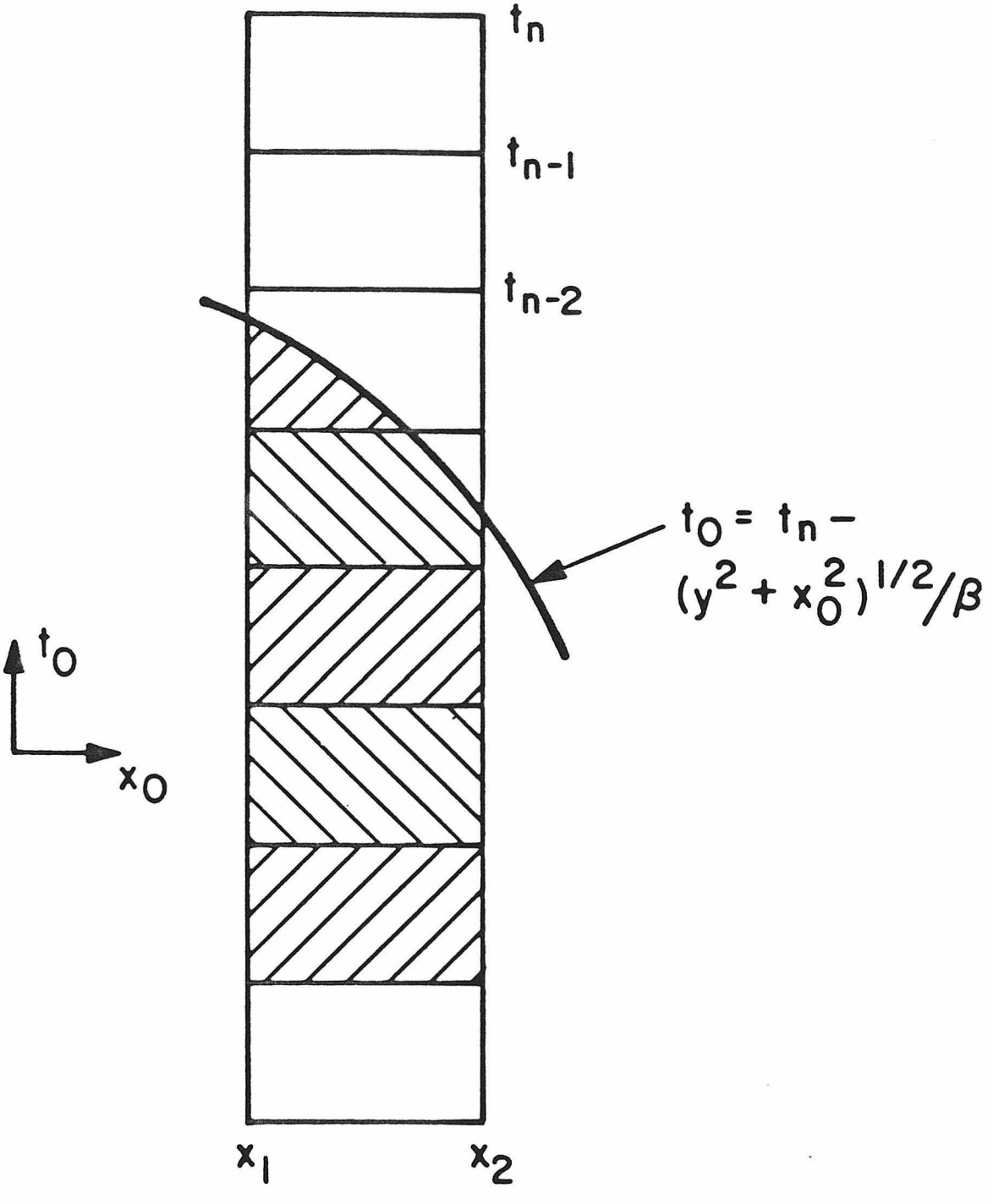

Figure D.2. Source coordinate integration regions for a surface element.

must be provided to ARBIT is

NSTEPS - number of time steps, equal to N + 1 above

DTSP - single precision value of time step size Δt

CSP - single precision value of shear wave velocity

ANORM - single precision array of dimension 5

ANORM(1), ANORM(2) - components of the position vector of the center of the source. In Figure D.1a these are the components $\underline{r}_i - \underline{r}_j$

ANORM(3) - length of the surface element. $x_2 - x_1$ in Figure D.1b

ANORM(4), ANORM(5) - components of the normal vector of the surface element, in the same coordinate system as ANORM(1), ANORM(2).

The calculation of the discrete kernels is carried out using double precision arithmetic. This is unnecessary if single point estimates are used to calculate DK_{ij}^n for $\beta n\Delta t >> |\underline{r}_i - \underline{r}_j|$. Subroutine ARBIT calls function subroutines FGSH and FKSH, with arguments x, y, t, VEL. These arguments are the same as x, y, t, β appearing in equations (D.5) and (D.6). These subroutines return, respectively, $\pi\mu FG$ and πFK as defined above. These subroutines have the restriction $x \geq 0$. If the value of the function for $x < 0$ is desired, the following relations may be employed

$$FG(x,t) + FG(-x,t) = \frac{1}{\mu} (\beta t - |y|) H(\beta t - |y|)$$

$$FK(x,t) + FK(-x,t) = \text{sgn}(y) \frac{1}{\beta} (\beta t - |y|) H(\beta t - |y|)$$

If it is desired to evaluate DG_{ij}^n or DK_{ij}^n for individual values of n, subroutine FGSH and FKSH may be used for that purpose.

```
      SUBROUTINE ARBIT(IOPT1)
      IMPLICIT REAL*8 (A-H,O-Z)
      REAL*4 SDG,SDK,ANORM,DTSP,CSP
      DIMENSION ANORM(5),DG(1024),DK(1024)
      DIMENSION SDG(1024),SDK(1024)
      COMMON/TIME/NSTEPS,DTSP,CSP
      COMMON/MATX/ANORM,SDG,SDK
C
C
C   IOPT1=0   DG ONLY
C   IOPT1=1   DK ONLY
C   IOPT1=2   BOTH KERNELS
C   THIS ROUTINE CALCULATES COEFFICIENTS
C   FOR THE DISCRETE SH INTEGRAL EQUATION
C   IT USES HISTOGRAM INTERPOLATION
C   AND STAGGERED TIME FOR TRACTIONS
C   DISPLACEMENTS ARE LINEARLY
C   VARYING IN TIME
C   DK IS DIMENSIONLESS
C   DG HAS DIMENSIONS OF LENGTH
C   DG SHOULD BE DIVIDED BY THE SHEAR MODULUS
C   THE DISCRETE KERNELS ARE RETURNED IN REVERSED
C   TIME ORDER , I.E. DG FOR TIME INDEX 0 IS
C   RETURNED IN SDG(NSTEPS) AND DG FOR TIME INDEX
C   (NSTEPS-1) IS RETURNED IN SDG(1).
C
C
C     WRITE(6,401) (N,ANORM(N),N=1,5)
  401 FORMAT(1X,*FROM ARBIT *,5(*ANORM(*,I1,*)=*,E11.4,2X))
      DO 04 I=1,NSTEPS
      SDG(I)=0.
      SDK(I)=0.
      DK(I)=0.
   04 DG(I)=0.
      DT=DTSP
      C=CSP
      PI=3.1415926535897
      X=ANORM(1)
      Y=ANORM(2)
      A=ANORM(3)
      IF(A.LE.0.) GOTO 303
      XN=ANORM(4)
      YN=ANORM(5)
      XNORM=XN*XN+YN*YN
      IF(DABS(XNORM-1.0).LT.0.1) GOTO 301
  303 WRITE(6,302) (N,ANORM(N),N=1,5)
      STOP
```

```
301 CONTINUE
302 FORMAT(///1X,*ARBIT HAS DETECTED A BAD ELEMENT*,5(/1X,
   .*ANORM(*,I1,*)=    *,F13.9,3X))
    PIDT=PI*DT
    NSTPP1=NSTEPS+1
    NSTPP2=NSTEPS+2
    XJNJ=X*XN+Y*YN
    SIGN=1.
    IF(XJNJ.LT.0.) SIGN=-1.
    Y0=DABS(XJNJ)
    X0=X*X+Y*Y-Y0*Y0
    IF(X0.LT.0.) X0=0.
    X0=DSQRT(X0)
    XSM=X0-A/2.
    XLG=X0+A/2.
    X1=XSM
    IF(XSM.LT.0.) X1=-XSM
    X2=XLG
    IF(IOPT1.EQ.1) GOTO 10
    DO 01 N=1,NSTPP1
    T=FLOAT(N-1)*DT
    IF(XSM.GE.0.) DG(N)=(FGSH(X1,Y0,T,C)-FGSH(X2,Y0,T,C))
   ./PI
    IF(XSM.LT.0.) DG(N)=(2.*FGSH(0.,Y0,T,C)
   .-FGSH(X1,Y0,T,C)-FGSH(X2,Y0,T,C))/PI
 01 CONTINUE

    DO 02 N=1,NSTEPS
    I=NSTEPS+1-N
    NP1=N+1
 02 SDG(I)=SNGL(DG(NP1)-DG(N))

 10 IF(Y0.EQ.0.) RETURN
    IF(IOPT1.EQ.0) RETURN

    DO 11 N=1,NSTPP2
    T=FLOAT(N-1)*DT
    IF(XSM.GE.0.) DK(N)=SIGN*
   .(FKSH(X1,Y0,T,C)-FKSH(X2,Y0,T,C))/PIDT
    IF(XSM.LT.0.) DK(N)=SIGN*
   .(2.*FKSH(0.,Y0,T,C)-FKSH(X1,Y0,T,C)-FKSH(X2,Y0,T,C))
   ./PIDT
 11 CONTINUE
    SAVEM1=0.
    SAVE=0.
    SAVEP1=DG(1)
```

```
      DO 12 N=1,NSTEPS
      SAVEM1=SAVE
      SAVE=SAVEP1
      SAVEP1=DK(N+1)
      I=NSTEPS+1-N
   12 SDK(I)=SNGL(SAVEP1-2.*SAVE+SAVEM1)

      RETURN
      END




      DOUBLE PRECISION FUNCTION FGSH(X,Y,T,VEL)
      REAL*8 NU
      IMPLICIT REAL*8 (A-H,O-Z)
      FGSH=0.
      CT=VEL*T
      IF(X.EQ.0.) GOTO 01
      CT2=CT*CT
      R2=X*X+Y*Y
      TES=CT2-R2
      IF(TES.LE.0.) RETURN
      NU=DSQRT(TES)
      Q2=CT2-Y*Y
      Q=DSQRT(Q2)
C
C   DON'T FEED THIS ROUTINE
C   NEGATIVE ARGUMENTS. USE
C   THE SYMMETRY PROPERTIES
C   INSTEAD.
C
      ECKS=DABS(X)
      WIE=DABS(Y)
      IF(Y.EQ.0.) GOTO 02

      ARG=NU/Q
      SAVE=CT*DASIN(ARG)

      R=DSQRT(R2)
      ARG=(CT+NU)/R
      SAVE=SAVE-ECKS*DLOG(ARG)

      ARG=(CT*NU+Q2)/(Q*(CT+NU))
      FGSH=SAVE-WIE*(DASIN(ARG)-DATAN2(ECKS,WIE))
      RETURN
```

```
01 FGSH=1.5707963*(CT-DABS(Y))
   IF(FGSH.LT.0.) FGSH=0.
   RETURN
02 ARG=NU/CT
   SAVE=CT*DASIN(ARG)
   ARG=(NU+CT)/ECKS
   FGSH=SAVE-ECKS*DLOG(ARG)
   RETURN
   END



   DOUBLE PRECISION FUNCTION FKSH(X,Y,T,VEL)
   REAL*8 NU
   IMPLICIT REAL*8 (A-H,O-Z)
   FKSH=0.
   IF(Y.EQ.0.) RETURN
   IF(X.EQ.0.) GOTO 01
   CT=VEL*T
   CT2=CT*CT
   R2=X*X+Y*Y
   TES=CT2-R2
   IF(TES.LE.0.) RETURN
   NU=DSQRT(TES)
   Q2=CT2-Y*Y
   Q=DSQRT(Q2)
   ECKS=DABS(X)
   WIE=DABS(Y)

   ARG=ECKS/Q
   SAVE=(1.5707963-DASIN(ARG))*WIE/VEL
   ARG=(CT*NU+Q2)/(Q*(CT+NU))
   FKSH=T*(DASIN(ARG)-DATAN2(ECKS,WIE))-SAVE
   RETURN
01 FKSH=1.5707963*(T-DABS(Y)/VEL)
   IF(FKSH.LE.0.) FKSH=0.
   RETURN
   END
```

APPENDIX E

DIFFRACTED SH WAVES DUE TO A LINE SOURCE ON A CIRCULAR CAVITY WALL

In this appendix the problem of finding the displacement due to a localized traction on the surface of a circular cavity in an infinite medium in antiplane strain mode is considered. The solution takes a particularly simple form when the displacement at the boundary of the cavity is desired. For purposes of comparison with the BIE solution this is all that is required.

The treatment given here will be closely analogous to those of Miklowitz (1978) and Peck and Miklowitz (1969) in which the diffracted field due to a plane compressional pulse impinging on a traction free circular cylinder was evaluated. The starting point for those solutions was the waveform representation due to Friedlander (1954,1958) in which the solution for $-\pi < \theta < \pi$ is represented by a finite sum of values of an aperiodic function defined for $-\infty < \theta < \infty$.

In cylindrical coordinates the equation of motion is, for $r > a$, $t > 0$, $-\pi < \theta < \pi$

$$\frac{1}{\beta^2}\frac{\partial^2}{\partial t^2}u = \frac{1}{r}\frac{\partial}{\partial r}r\frac{\partial}{\partial r}u + \frac{1}{r^2}\frac{\partial^2}{\partial \theta^2}u \qquad \text{(E.1)}$$

The displacement u must satisfy the initial conditions

$$u(r,\theta,t) = 0$$

$$t = 0 \quad , \quad r > a \quad , \quad -\pi < \theta < \pi \qquad \text{(E.2)}$$

$$\dot{u}(r,\theta,t) = 0$$

and the boundary conditions

$$\lim_{r\to\infty} u(r,\theta,t) = 0$$

$$\left.\frac{\partial}{\partial r} u(r,\theta,t)\right|_{r=a} = f(\theta,t) \quad , \quad t > 0 \quad , \quad -\pi < \theta < \pi \qquad \text{(E.3)}$$

It is also required that the displacement and traction be single valued as a function of θ, i.e.,

$$u(r,\theta t) = u(r,-\theta,t)$$

$$r > a \quad , \quad t > 0 \ .$$

$$\left.\frac{\partial}{\partial\theta} u\right|_{\theta=\pi} = \left.\frac{\partial}{\partial\theta} u\right|_{\theta=-\pi} \qquad \text{(E.4)}$$

Friedlander (1954) represented the solution u as a series

$$u(r,\theta,t) = \sum_{m=-\infty}^{\infty} u^*(r,\theta+2m\pi,t) \qquad \text{(E.5)}$$

where u* satisfies equation (E.1) and the initial conditions (E.2) for $-\infty < \theta < \infty$ and boundary conditions

$$\lim_{r\to\infty} u^*(r,\theta,t) = 0 \qquad -\infty < \theta < \infty \quad , \quad t > 0$$

$$\lim_{|\theta|\to\infty} u^*(r,\theta,t) = 0 \qquad r > a \quad , \quad t > 0$$

and

$$\frac{\partial}{\partial r} u^*(r,\theta,t)\Big|_{r=a} = f^*(\theta,t) \quad , \quad -\infty < \theta < \infty, \quad t > 0 \tag{E.6}$$

where

$$f^*(\theta,t) = \begin{cases} f(\theta,t) & |\theta| \le \pi \\ 0 & |\theta| > \pi \end{cases}$$

Since u^* represents a wave propagating outward from the region $|\theta| \le \pi$, $r = a$ and the equation of motion is hyperbolic, u^* will be causal. Therefore, there will be only a finite number of nonzero terms in the sum of equation (E.5) for any finite time.

For simplicity in subsequent calculations, a specialized Green's function, $G^*(r,\theta,t)$ corresponding to a driving traction $\tau = \mu\,\delta(\theta)\,\delta(t)$, will be evaulated first. The particular solution for a traction f^* can then be evaluated by convolution, i.e.,

$$u^*(r,\theta,t) = \int_{t'}\int_{\theta'} f^*(\theta-\theta' \, , \, t-t')\, G^*(r,\theta',t')\, d\theta'\, dt'$$

The transforms of $G^*(r,\theta,t)$ are denoted by a tilde ($\tilde{}$) and are defined as

$$\tilde{G}(r,\theta,s) = \int_{t=0}^{\infty} e^{-st}\, G^*(r,\theta,t)\, dt$$

$$\tilde{G}(r,\nu,s) = \int_{\theta=-\infty}^{\infty} e^{-i\nu\theta}\, \tilde{G}(r,\theta,s)\, d\theta$$

The transform of equation (E.1) is then

$$\left(\frac{s^2}{\beta^2} + \frac{\nu^2}{r^2}\right) \tilde{G}(r,\nu,s) = \frac{1}{r}\frac{\partial}{\partial r}\left(r \frac{\partial}{\partial r} G(r,\nu,s)\right) \qquad \text{(E.7)}$$

The desired solution of (E.7) is

$$G(r,\nu,s) = A(\nu,s)\, K_\nu(rs/\beta)$$

where $K_\nu(z)$ is the modified Bessel function of order ν and argument z. The boundary condition at $r = a$ is

$$\left.\frac{\partial}{\partial r} \tilde{G}(r,\nu,s)\right|_{r=a} = -1 \qquad \text{(E.8)}$$

and so

$$\tilde{G}(r,\nu,s) = -\frac{\beta}{s} \frac{K_\nu(rs/\beta)}{\dot{K}_\nu(as/\beta)} \qquad \text{(E.9)}$$

where

$$\dot{K}_\nu(z) = \frac{\partial}{\partial z} K_\nu(z)$$

Following Miklowitz (1978), the θ transform is inverted first,

$$\tilde{G}(r,\theta,s) = -\frac{\beta}{2\pi s} \int_{\nu=-\infty}^{\infty} e^{i\nu\theta} \frac{K_\nu(sr/\beta)}{\dot{K}_\nu(sa/\beta)} \, d\nu \tag{E.10}$$

It is known that $K_\nu(z)$ is an entire function of ν for fixed argument $z \neq 0$. If the case $\theta > 0$ is considered and the contour in (E.10) is closed in the $\mathrm{Im}(\nu) > 0$ half plane, the residue theorem may be applied to evaluate the integral. The solution is symmetric in θ so this leads to no loss of generality. The poles of the integrand are located at $\nu = \nu_n(sa/c)$, $n = 1, 2, \cdots$. The functions ν_n are implicitly defined by the relation

$$\dot{K}_\nu \Big|_{\nu=\nu_n(z)} (z) = 0 \qquad , \quad \mathrm{Im}(\nu_n) \geq 0 \tag{E.11}$$

In order to evaluate the residues it is necessary to ascertain the order of the zeroes of $\dot{K}_\nu(z)$ as a function of ν. This may be done by investigating the behavior of $\frac{\partial}{\partial \nu} \dot{K}_\nu(z)$ at $\nu = \nu_n(z)$.

A formula analogous to that of Watson (1958, 5.11.14, p. 135) is

$$\int_{z_1}^{z} \left| \frac{K_\nu(\xi)}{\xi} \right|^2 \overline{\xi} \, d\xi = \frac{\xi}{2\nu} \left\{ \overline{K}_\nu(\xi) \frac{\partial}{\partial \nu} \dot{K}_\nu(\xi) - \overline{\dot{K}}_\nu(\xi) \frac{\partial}{\partial \nu} K_\nu(\xi) \right\} \Bigg|_{\xi=z_1}^{z} \tag{E.12}$$

Where $\overline{\xi}$ denotes the complex conjugate of ξ and the integration path does not include the point $\xi = 0$. Since $K_\nu(x) \sim e^{-x}$ as $x \to \infty$, the quantity in brackets vanishes as $\xi \to \infty + i \cdot 0$ for fixed ν. Therefore

$$\frac{z}{2\nu}\left\{\overline{\dot{K}}_\nu(z)\,\frac{\partial}{\partial\nu}K_\nu(z) - \overline{K}_\nu(z)\,\frac{\partial}{\partial\nu}\dot{K}_\nu(z)\right\} = \int_z^\infty \left|\frac{K_\nu(\xi)}{\xi}\right|^2 \overline{\xi}\,d\xi \qquad (E.13)$$

By examining the value of the integral along contour segments upon which either $\mathrm{Im}(d\xi) = 0$ or $\mathrm{Re}(d\xi) = 0$ it is readily shown that for any finite z the integral is nonzero. Since $K_0(z)$ and $K_1(z)$ have no zeros in the region $|\arg z| \leq \pi/2$ (Watson, 1958, p. 511) we have the result that

$$\overline{\dot{K}}_\nu(z)\,\frac{\partial}{\partial\nu}K_\nu(z) - \overline{K}_\nu(z)\,\frac{\partial}{\partial\nu}\dot{K}_\nu(z) \neq 0 \quad , \quad |\arg z| \leq \pi/2 \quad z \neq 0 \qquad (E.14)$$

Thus, if $\dot{K}_\nu(z) = 0$ it follows that $\overline{K}_\nu(z)\,\frac{\partial}{\partial\nu}\dot{K}_\nu(z) \neq 0$, $|z| > 0$. Since $K_\nu(z)$ has no poles for $\mathrm{Re}(z) \geq 0$, $|z| > 0$ it follows that the zeros of $\dot{K}_\nu(z)$ for fixed z in that region, as a function of ν, are simple.

In evaluating the residue the denominator $\frac{\partial}{\partial\nu}\dot{K}_\nu(z)\Big|_{\nu=\nu_n(z)}$ arises. This will be replaced later by more conventional functions by noting that

$$\frac{d}{dz}\left(\dot{K}_\nu(z)\Big|_{\nu=\nu_n(z)}\right) = \frac{d\nu_n}{dz}\frac{\partial}{\partial\nu}\dot{K}_\nu(z)\Big|_{\nu=\nu_n(z)} + \ddot{K}_{\nu_n}(z)$$

hence

$$\frac{\partial}{\partial \nu} \dot{K}_\nu(z) \Big|_{\nu=\nu_n(z)} = - \left(\frac{d\nu_n}{dz}\right)^{-1} \left(\frac{\nu_n^2 + z^2}{z^2}\right) K_{\nu_n}(z) \tag{E.15}$$

Thus, if $s \neq 0$

$$\tilde{G}(r,\theta,s) = 2\pi i \sum_n \tilde{g}_n(r,\theta,s) \tag{E.16}$$

$$\tilde{g}_n(r,\theta,s) = - \frac{\beta}{2\pi s} e^{i\theta\nu} \frac{K_\nu(sr/\beta)}{\frac{\partial}{\partial \nu} \dot{K}_\nu(sa/\beta)} \Big|_{\nu=\nu_n(sa/\beta)} \tag{E.17}$$

$$\mathrm{Im}(\nu_n) \geq 0$$

The inversion of the Laplace transform in time is given by the Bromwich integral

$$G^*(r,\theta,t) = \frac{1}{2\pi i} \int_{\lambda-i\infty}^{\lambda+i\infty} e^{st} \tilde{G}(r,\theta,s)\, ds \tag{E.18}$$

The value of λ is to be such that positions S_j of the poles of $\tilde{G}(r,\theta,s)$ all have $\mathrm{Re}(S_j) < \lambda$. From the previous result on the zeros of $\frac{\partial}{\partial \nu} \dot{K}_\nu(z)$, it is apparent that λ may be taken to be zero if the s-contour is deformed around the origin into the region $\mathrm{Re}(s) > 0$ (see Figure E.1).

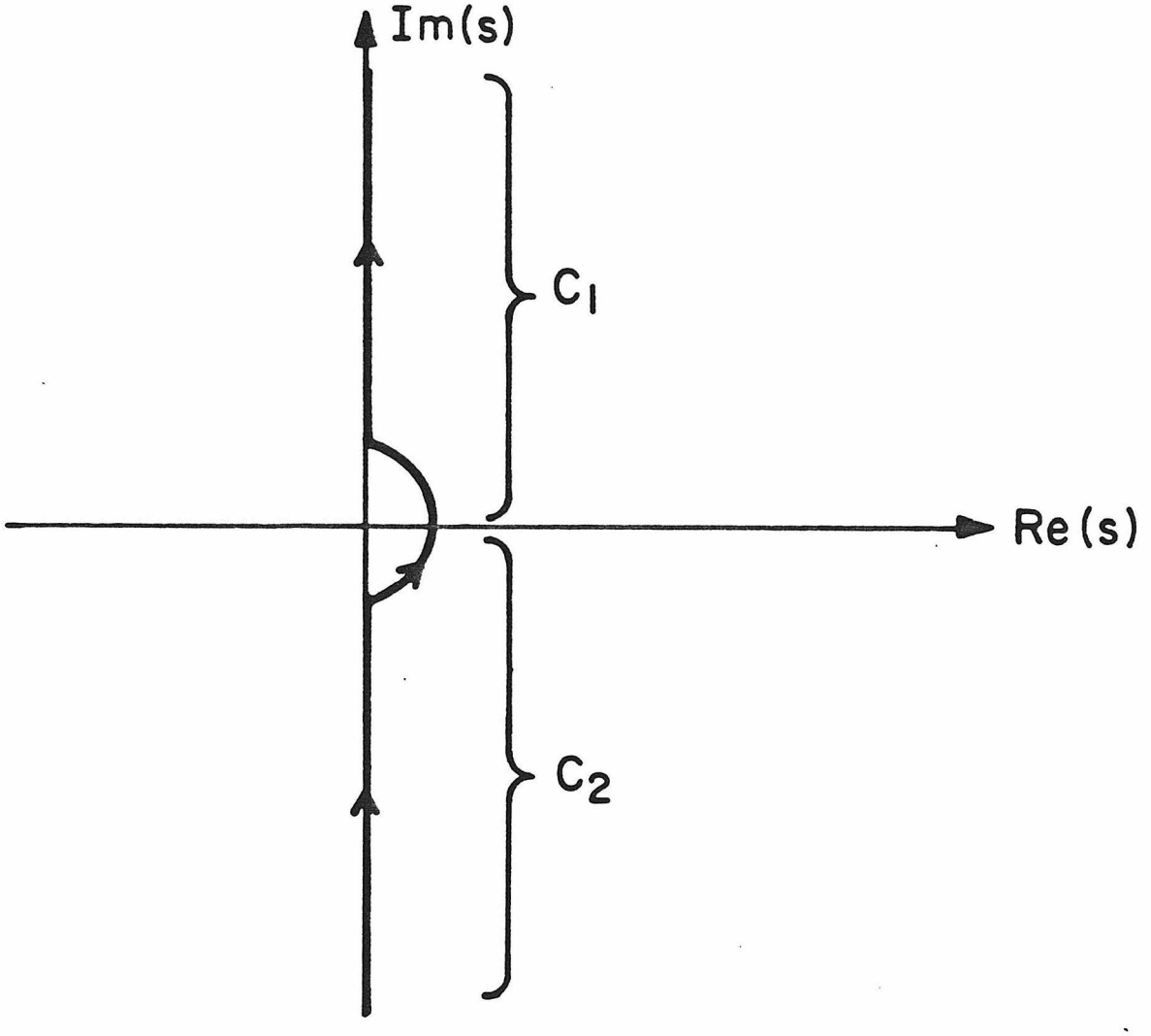

Figure E.1. Inverse Laplace transform integration contour for equation (E.19).

The integral of (E.18) will be carried out numerically for the individual terms $\tilde{g}_n$ of the series in (E.16). Thus, for n = 1, 2, $\cdots$ we wish to evaluate

$$g_n^*(r,\theta,t) = \int_C e^{st}\, \tilde{g}_n(r,\theta,s)\, ds \tag{E.19}$$

Upon substituting equation (E.15) into equation (E.16) we find

$$\tilde{g}_n(r,\theta,s) = \frac{a}{2\pi} e^{i\nu_n\theta} \frac{z\dot{\nu}_n}{z^2 + \nu_n^2} \frac{K_{\nu_n}(zr/a)}{K_{\nu_n}(z)} \tag{E.20}$$

where $z = sa/\beta$, and $\nu_n(z)$ varies with z as defined in equation (E.11).

The modified Bessel function obeys the symmetry relations

$$K_{-\nu}(z) = K_{\nu}(z) \tag{E.21}$$

and

$$\overline{K_{\nu}(z)} = K_{\bar{\nu}}(\bar{z})$$

Therefore we may define

$$\nu_n(\bar{z}) = -\bar{\nu}_n(z)$$

and

$$K_\nu(\bar{z})\Big|_{\nu=\nu_n(\bar{z})} = \overline{K_\nu(z)}\Big|_{\nu=\nu_n(z)}$$

Thus,

$$-\frac{1}{2\pi i}\, e^{\bar{s}t}\, \tilde{g}_n(r,\theta,\bar{s}) = -\overline{\left\{\frac{1}{2\pi i}\, e^{st}\, \tilde{g}_n(r,\theta,s)\right\}}$$

Since the contour C may be taken to be symmetric about Im(s) = 0, the desired transform is given by

$$g_n^*(r,\theta,t) = \frac{\beta}{\pi}\, \mathrm{Re}\left\{\int_{C_2} e^{i\nu_n\theta+z\tau}\, \frac{z\dot{\nu}_n}{z^2+\nu_n^2}\, \frac{K_{\nu_n}(zr/a)}{K_{\nu_n}(z)}\, dz\right\} \quad \text{(E.22)}$$

The contour C_2 is the half of the contour C with Im(s) $\leq$ 0 (see Figure E.1) and $\tau = \beta t/a$.

The modified Bessel function is related to the Hankel function of the first kind by the equation

$$K_\nu(z) = \frac{i\pi}{2}\, e^{i\nu\pi/2}\, H_\nu^{(1)}(ze^{i\pi/2}) \qquad -\pi < \arg z \leq \pi/2$$

If $\mu_n(z)$ is defined by

$$\dot{H}_\mu^{(1)}(z)\Big|_{\mu=\mu_n(z)} = 0$$

we have $\nu_n(z) = \mu_n(ze^{i\pi/2})$; n = 1, 2, $\cdots$.

The roots $\mu_n(z)$ have been investigated by Keller, Rubinow and Goldstein (1963) for real positive values of z. For $|z| << 1$ they give

$$\mu_n = -i\pi(n-\tfrac{1}{2})\, v^{-1} \left\{1 + (vw)^{-1} + (vw)^{-2} + (w^{-3} - \xi(3)\,\pi^2 n^2/3)\, v^{-3} + o(|z|^2/\ell n(z/z)\right\}$$

where $v = \ell n(r/2)$, $z = re^{i\phi}$ (E.23)

$w = i(\pi/2 - \phi) - \gamma$,

γ is Euler's constant, which is approximately equal to 0.577216 and $\xi(n)$ is the Riemann zeta function with $\xi(3) \simeq 1.202057$.

By use of equation (E.23) and the asymptotic expansion as $z \to 0$ for fixed ν

$$K_\nu(z) \sim \frac{1}{2}\,\Gamma(\nu)\,(\tfrac{1}{2}z)^{-\nu} \quad , \quad Re(\nu) > 0$$

it can be shown that the contribution to the integral of equation (E.22) resulting from the small arc of C_2 about the origin from $z = \rho e^{-i\pi/2}$ to $z = \rho$ is

$$\frac{\beta}{\pi^2}\,\frac{\rho}{n-\tfrac{1}{2}} + \theta(\rho^2) \text{ as } \frac{\rho r}{a} \to 0 \quad .$$

Thus C_2 may be taken to lie on the imaginary axis from

$$Im(z) = -0 \quad \text{to} \quad Im(z) = -\infty \quad .$$

Upon setting $z = -i\omega$, equation (E.22) becomes

$$g_n^*(r,\theta,t) = \frac{\beta}{\pi} \int_{\omega=0+}^{\infty} \mathrm{Im} \left\{ e^{i(\mu_n \theta - \tau)} \frac{\omega \dot{\mu}_n}{\mu_n^2 - \omega^2} \frac{H_{\mu_n}^{(1)}(\omega r/a)}{H_{\mu_n}^{(1)}(\omega)} \right\} d\omega \tag{E.24}$$

where

$$\dot{H}_{\mu}^{(1)}(\omega) \Big|_{\mu=\mu_n} = 0 \qquad , \quad \mathrm{Im}(\mu_n) \geq 0 \tag{E.25}$$

For large dimensionless frequency ω the root μ_n is given by Keller (1963) as

$$\mu_n \simeq \omega + 6^{-1/3} e^{i\pi/e} q_n' \omega^{1/3} + 6^{1/3} e^{2i\pi/3} \frac{(q_n')^2}{180} + \frac{1}{10 q_n'} \omega^{-1/3} + o(\omega^{-1}) \quad , \ \omega >> n \tag{E.26}$$

where q_n' is the n^{th} positive real root of the derivative of the Airy function

$$Ai(q) = \int_0^{\infty} \cos(x^3 - qx)\, dx$$

For $n > 5$ q_n' is given approximately by

$$q_n' \simeq (3\,(n - 3/4))^{2/3}\; 6^{1/3}/2$$

and $q_1' \cdots q_5'$ are, respectively, approximately 1.469354, 4.624712, 6.951786, 8.889027, 10.632519. The behavior of the integrand in (E.24) for large ω is then dominated by the factor

$$\exp(-6^{-1/3}\; 3^{1/2}\; q_n'\; \omega^{1/3}\; \theta/2)$$

which causes convergence of the integral for $\theta > 0$.

In order to carry out the integration of (E.24) numerically it is necessary to first evaluate the roots of (E.25) numerically. This was done using the asymptotic results of Keller (1963) for $\omega \leq 0.01$ and $\omega \geq 20.$ and $n = 1, \cdots, 10$. For intermediate values of ω the roots were found from numerical evaluations of $H_\mu^{(1)}(x)$ computed using program C303 of the CERN subroutine library. This algorithm is based on the recursion technique discussed by Goldstein and Thaler (1959). The values of $\dot{H}_\mu^{(1)}(x)$ were found using the standard formula

$$\dot{H}_\mu^{(1)}(z) = \frac{1}{2}\,(H_{\mu-1}^{(1)} - H_{\mu+1}^{(1)})$$

The roots were located successively for decreasing, appropriately spaced, values of $x_1, x_2, \cdots$. The value of x_1 was chosen to be great enough that the asymptotic result (E.26) was applicable for $x > x_1$. Two initial estimates of $\mu_n(x_m)$ were made by extrapolating from $\mu_n(x_{m-1})$, $\mu_n(x_{m-2})$ and $\mu_n(x_{m-3})$ using linear and quadratic fits to the

dependence of μ_n on x. The values of $\dot{H}_\mu^{(1)}(x_m)$ for these two values of μ were calculated. Since the roots as a function of μ are simple,

$$\dot{H}_\mu^{(1)}(x_m) \simeq (\mu - \mu_n(x_m)) \cdot A$$

where $A = \frac{\partial}{\partial \mu} \dot{H}_\mu^{(1)}(x) \Big|_{\mu=\mu_n(x_m)} \neq 0$.

The left hand side is known for two different values of μ, so a new estimate for $\mu_n(x_m)$ may be obtained from the previous two. This procedure was applied iteratively with new estimates of $\mu_n(x_m)$ replacing old estimates, until $\dot{H}_\mu^{(1)}(x_m)$ was sufficiently small and two consecutive estimates of μ were sufficiently close together. Convergence was limited by accuracy of the algorithm used to calculate $H_\mu^{(1)}(x)$ and occurred within four iterations. The estimated error in μ is about $|\mu| \times 10^{-4}$. The composite of numerical and large-x asymptotic evaluations of $\mu_n(x)$ is shown in Figures 2 and 3.

At r/a = 1 equation (E.24) simplifies to

$$g_n^*(a,\theta,t) = -\frac{\beta}{\pi} \int_{\omega=0}^{\infty} \mathrm{Im}\left\{ e^{i(\mu_n\theta - \omega t)} \frac{\omega \dot{\mu}_n}{\mu_n^2 - \omega^2} \right\} d\omega \qquad \text{(E.27)}$$

The numerical integration of (E.27) was carried out by two different

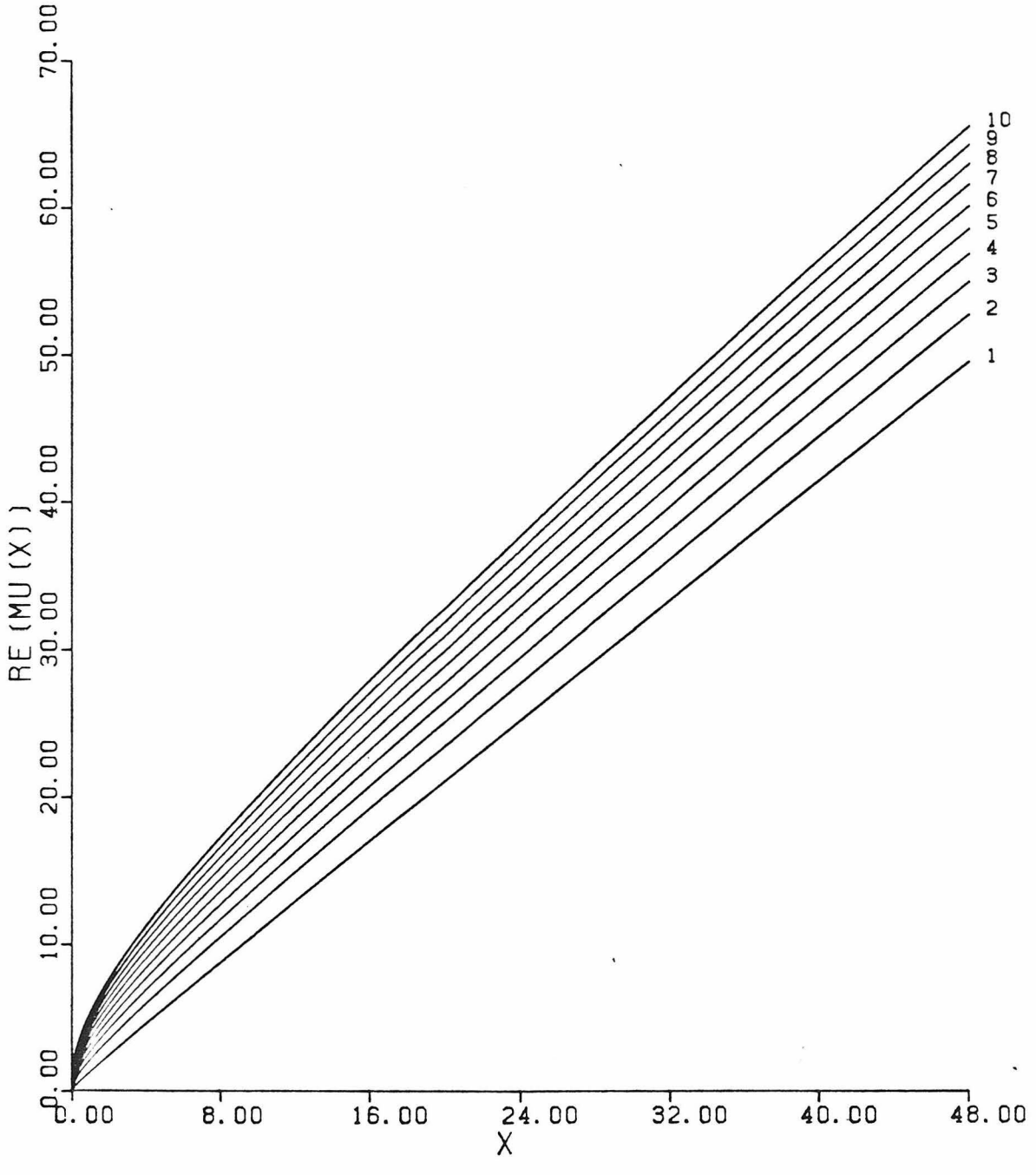

Figure E.2(a). The real part of the roots μ_n (x) for n = 1, $\cdots$, 10 and 0.001 < x < 48.

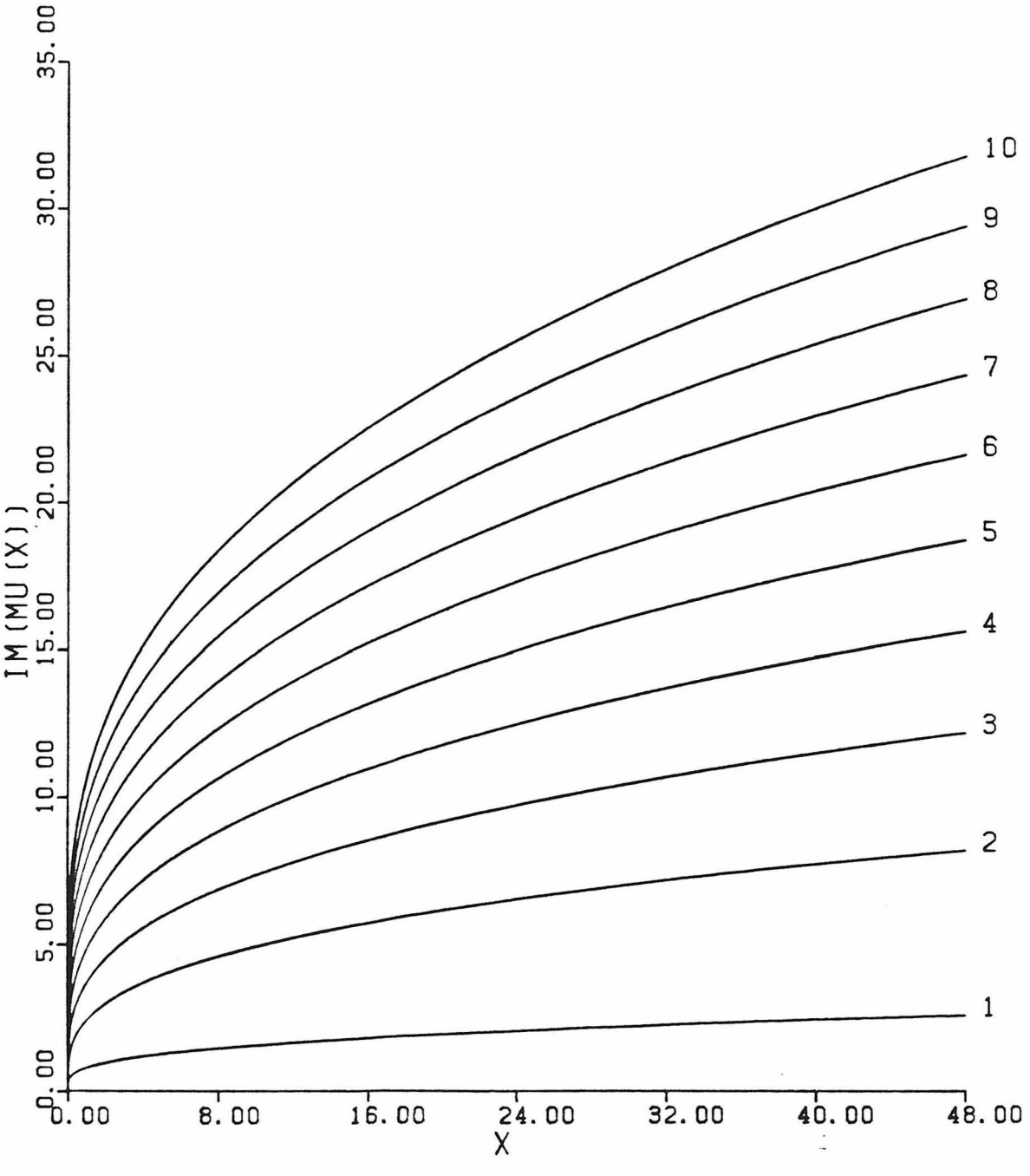

Figure E.2(b). The imaginary part of the roots $\mu_n(x)$ for n = 1, ···, 10 and 0.001 < x < 48.

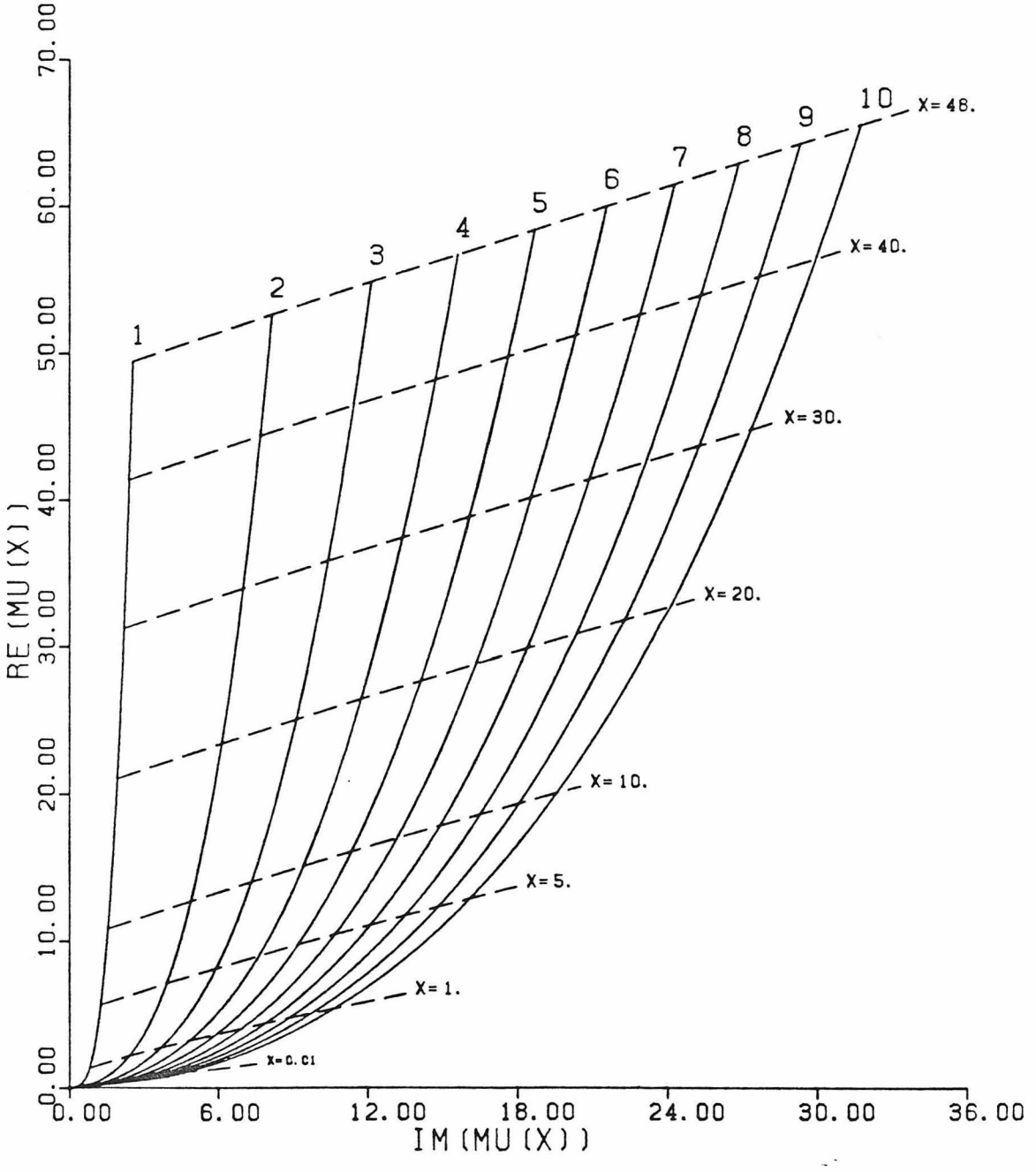

Figure E.2(c). $\mathrm{Re}(\mu_n(x))$ plotted against $\mathrm{Im}(\mu_n(x))$ for n = 1, ···, 10 and $0.001 < x < 48$. The dashed lines indicate approximate values of x.

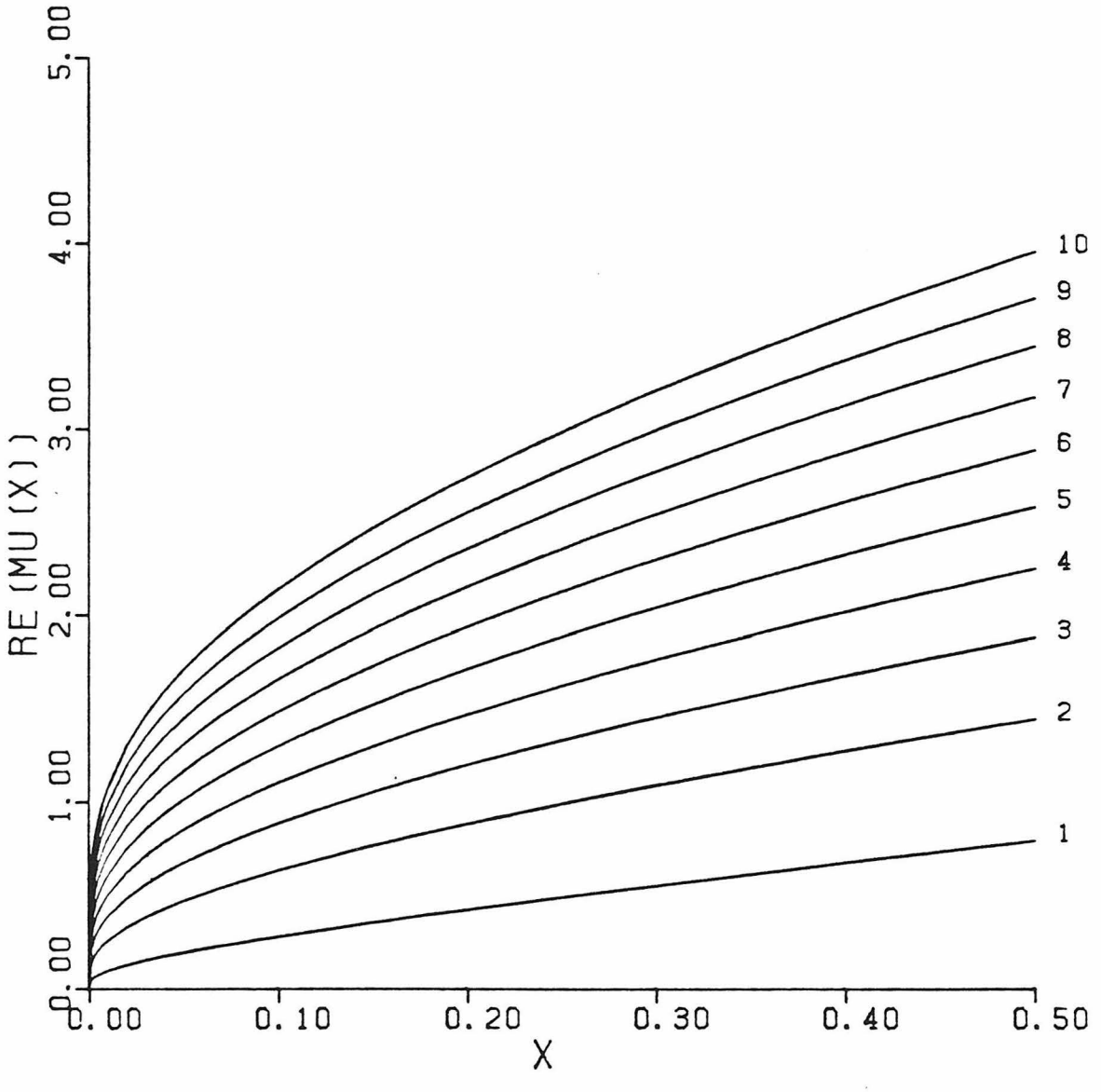

Figure E.3(a). Detail of Figure E.2(a).

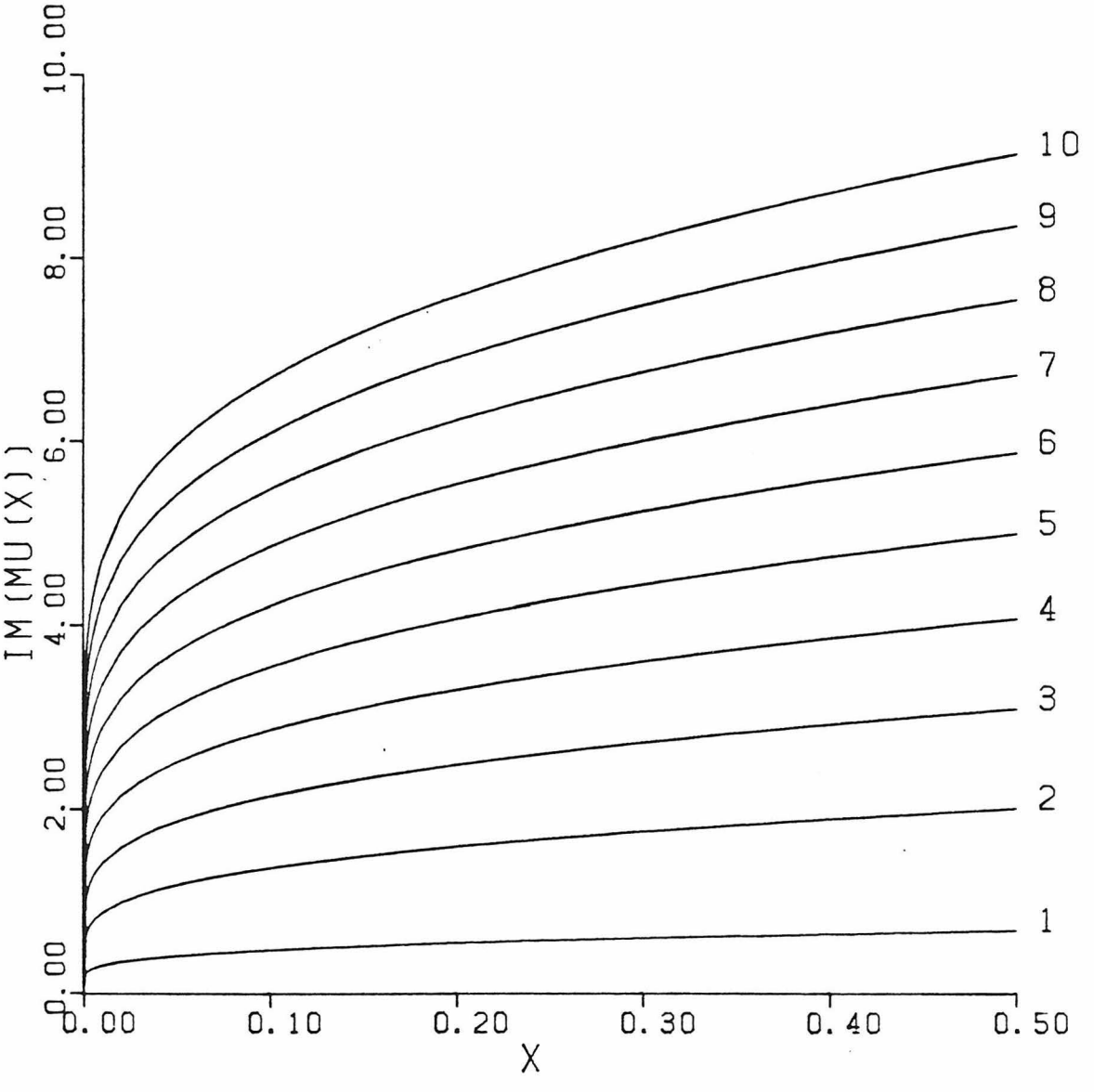

Figure E.3(b). Detail of Figure E.2(b).

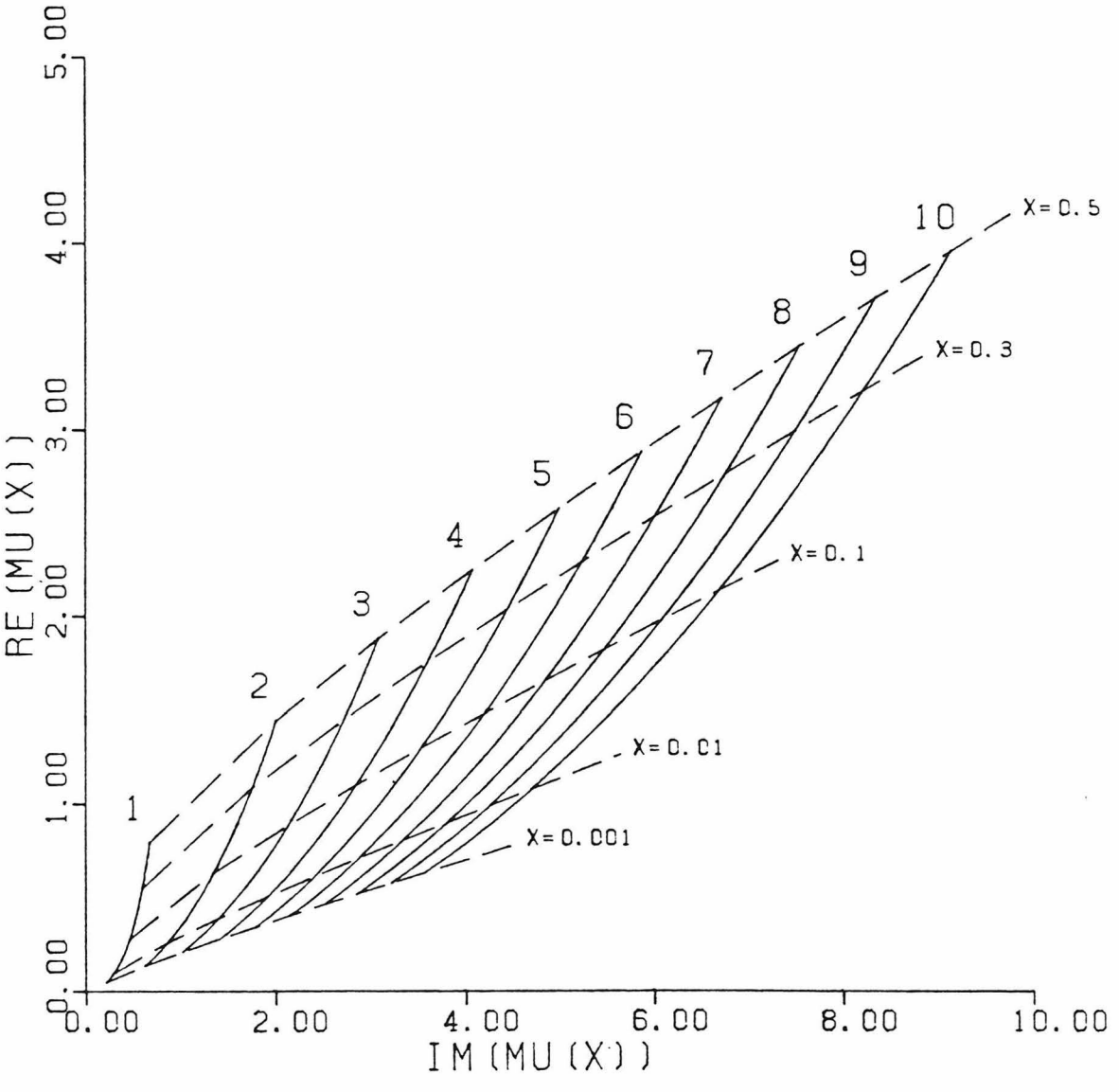

Figure E.3(c). Detail of Figure E.2(c).

methods. In the first method $\mu_n(\omega)$ was approximated over intervals $\omega_m < \omega < \omega_{m+1}$ of varying size by linear interpolation. The factor $(\omega\dot{\mu}_n)/(\mu_n^2 - \omega^2)$ is slowly varying and was also approximated by a piecewise linear function. The resulting approximate analytic integral over (ω_m,ω_{m+1}) was evaluated explicitly and the results were summed for special values of θ and times t. This procedure permitted great flexibility in the selection of time points for comparison with the high frequency saddle point approximations of Friedlander (1954, equation 4.7). The results for the wave form $g_1(a,\theta,t)$ are compared with Friedlander's in Figures E.4. A factor of 2π has been included for consistency with Friedlander's expressions. As can be seen, the results are quite similar when the first motion is dominated by high frequencies; i.e., for the smaller values of θ. At larger values of θ the results differ by progressively greater amounts as the higher frequencies are suppressed by the factor $e^{i\mu_n(\omega)\theta}$. Under these circumstances the dominant contributions to the wave form come from the low frequency portion of the integral, which are not included in the analytic approximation of Friedlander. The different traces have been shifted slightly for legibility.

The second method used to evaluate (E.27) employed the FFT algorithm. The roots $\mu_n(\omega)$ were interpolated to uniform intervals of ω and the values of $(\dot{\mu}_m\omega)/(\mu_n^2 - \omega^2)$ were tabulated at these points. The waveforms for a given value of θ were calculated and stored for succeeding mode numbers until they become insignificant. The higher

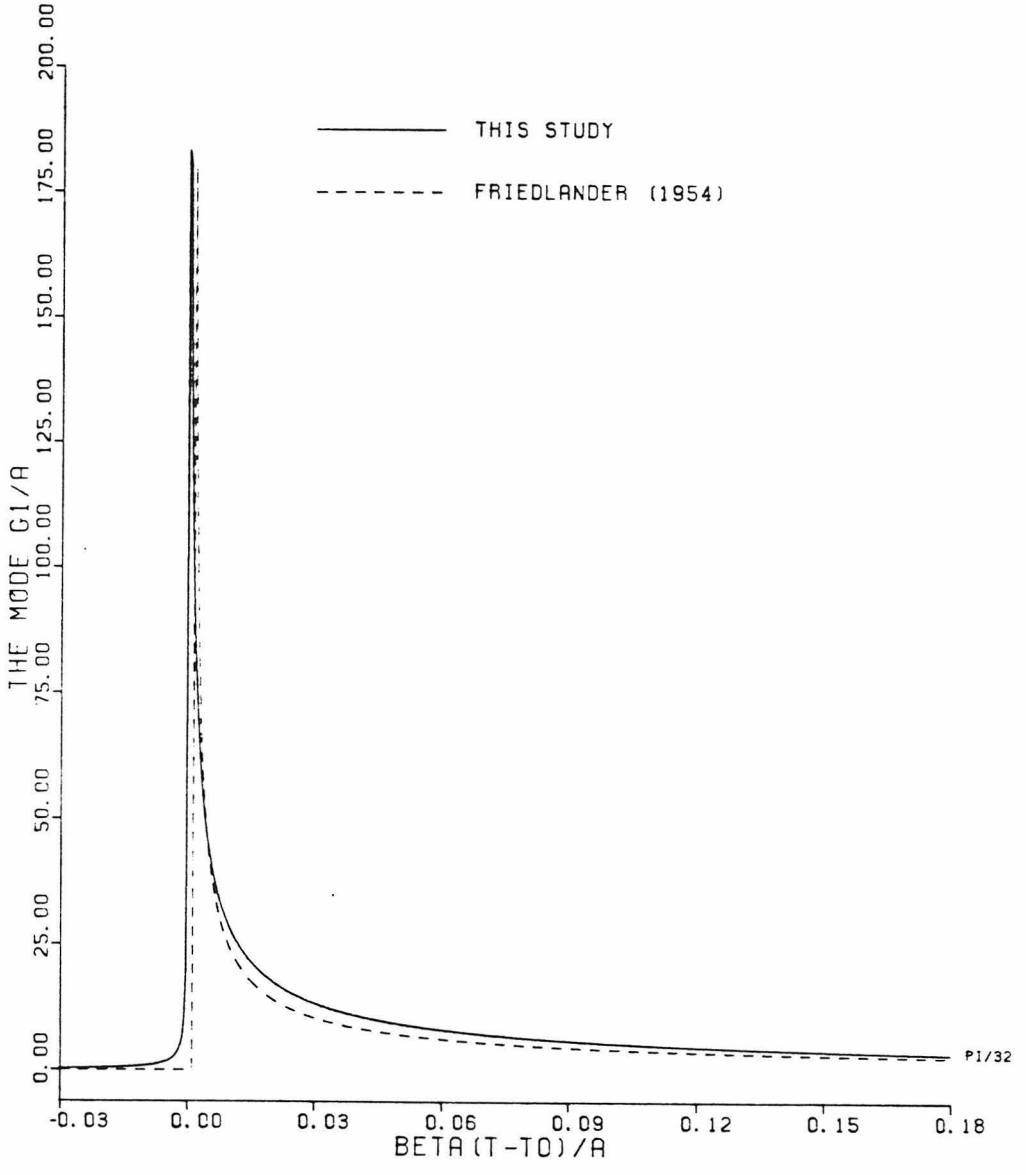

Figure E4(a). The mode 1 impulse response at $\theta = \pi/32$ as evaluated by Friedlander's high frequency saddle point approximation and the numerical ω integration procedure used here. The numerical result has a substantial error at $t = t_0$, the diffracted wave arrival time, due to termination of the integration at a finite frequency. The dashed line has been shifted slightly to improve legibility.

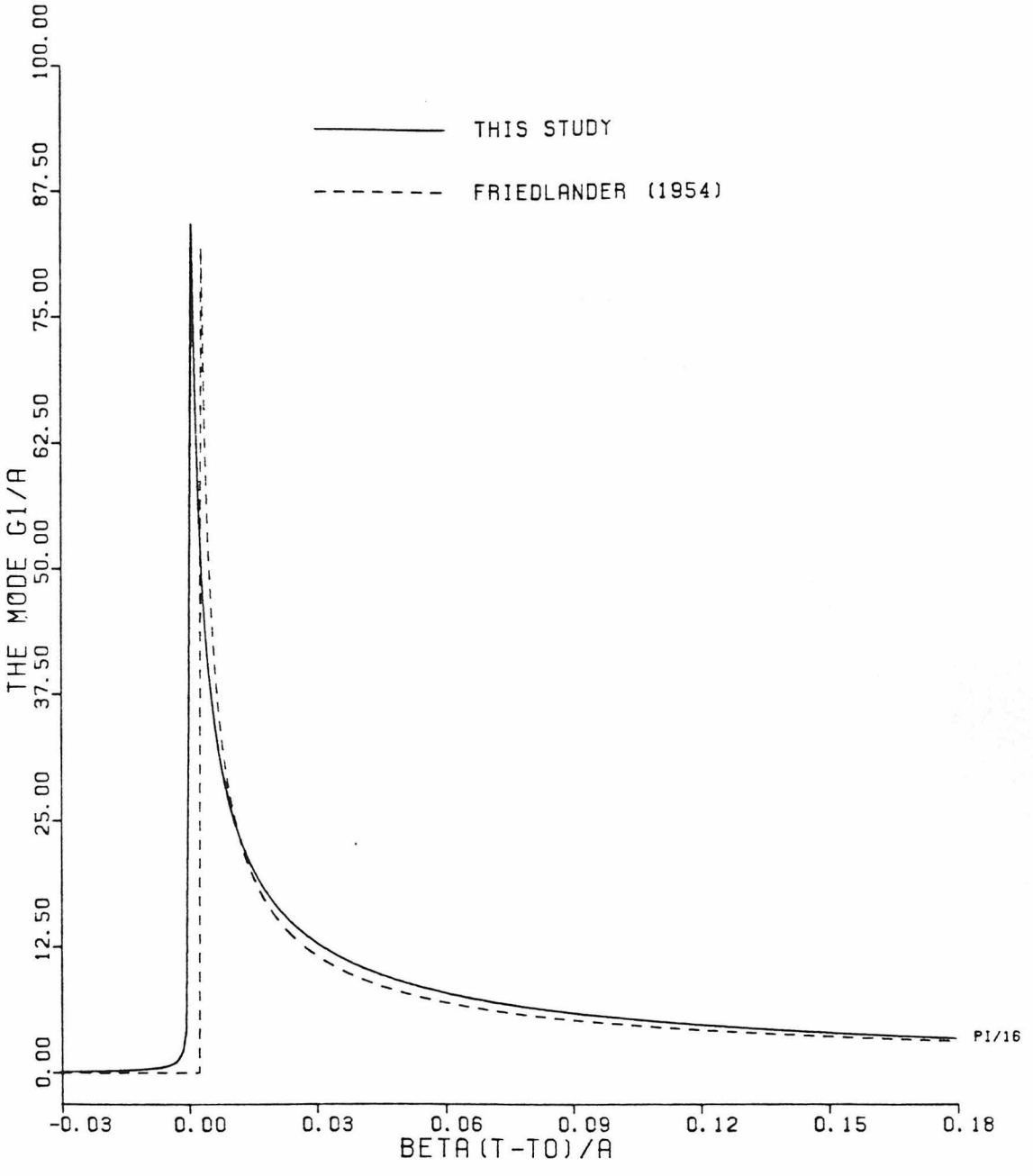

Figure E.4(b). Mode 1 impulse response at $\theta = \pi/16$. The solid line is in error due to truncation of the numerical ω - integration.

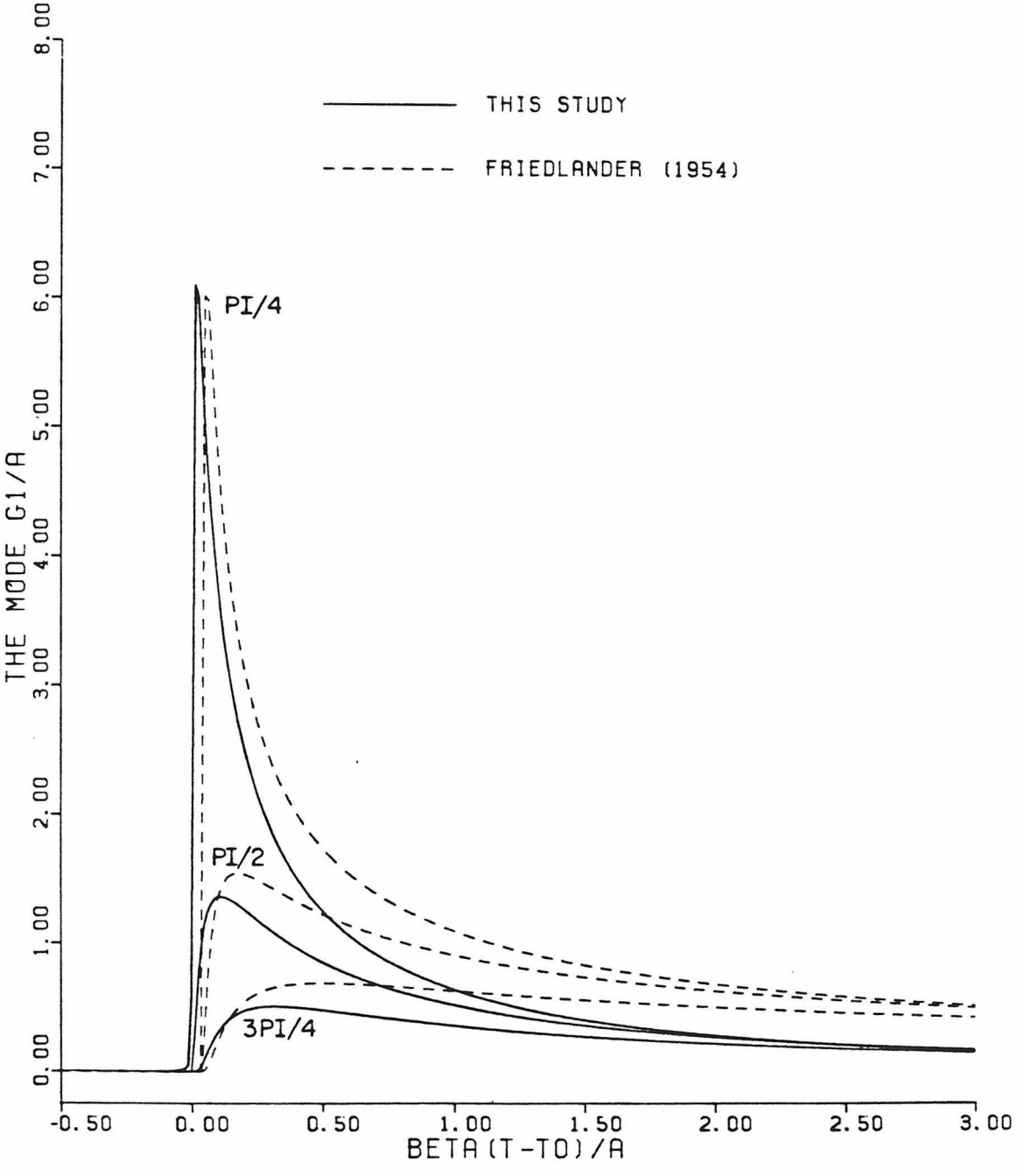

Figure E.4(c). Mode 1 impulse response at $\theta = \pi/4$, $\pi/2$ and $3\pi/4$. The high frequency saddle point approximation is in error for long times.

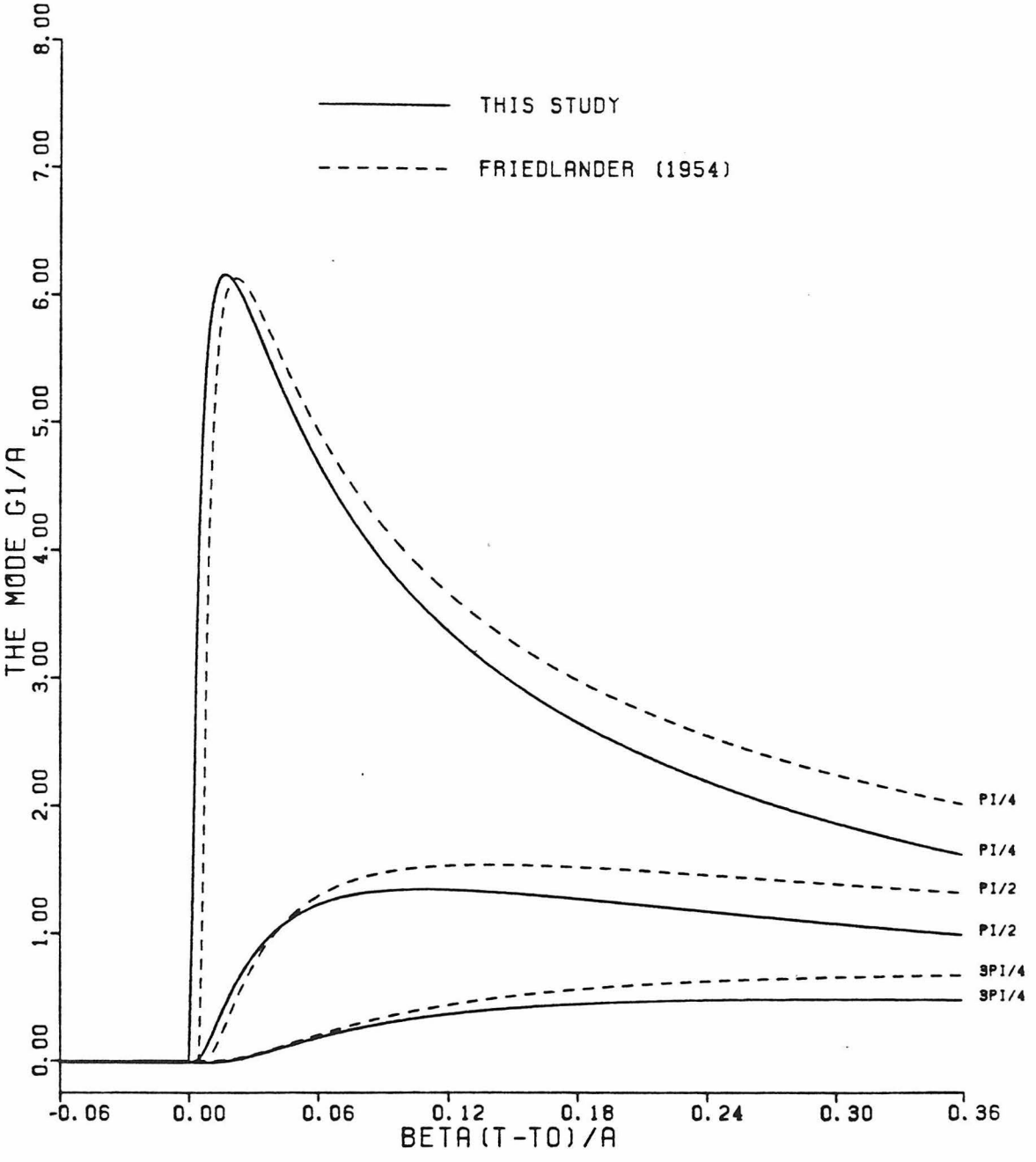

Figure E.4(d). Detail of Figure E.4(c). The two methods are in close agreement for times near the diffracted wave arrival time, when the high frequency contributions are dominant.

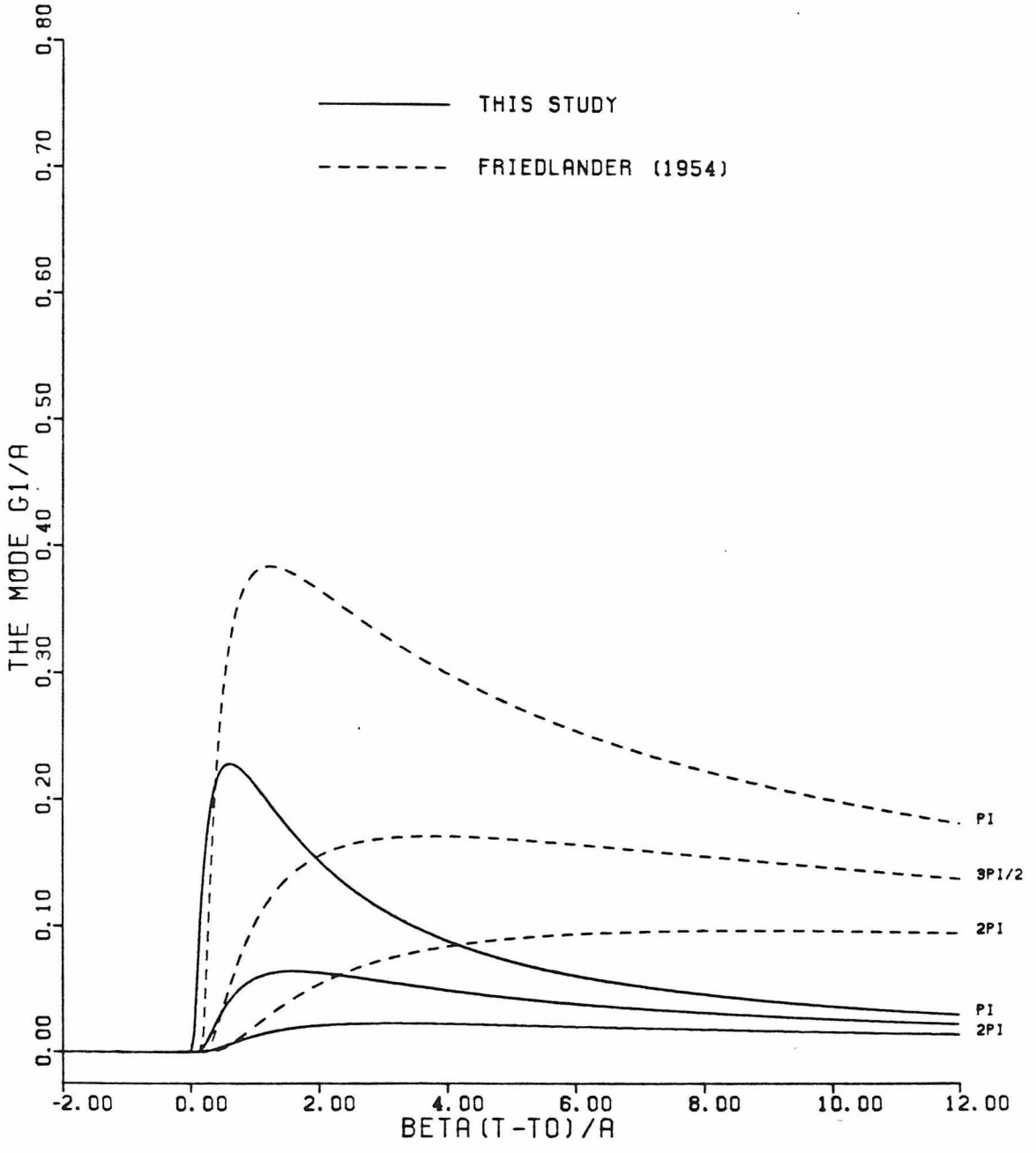

Figure E.4(e). Mode 1 impulse response at $\theta = \pi$, $3\pi/2$ and 2π. There are large errors in the high frequency saddle point approximation.

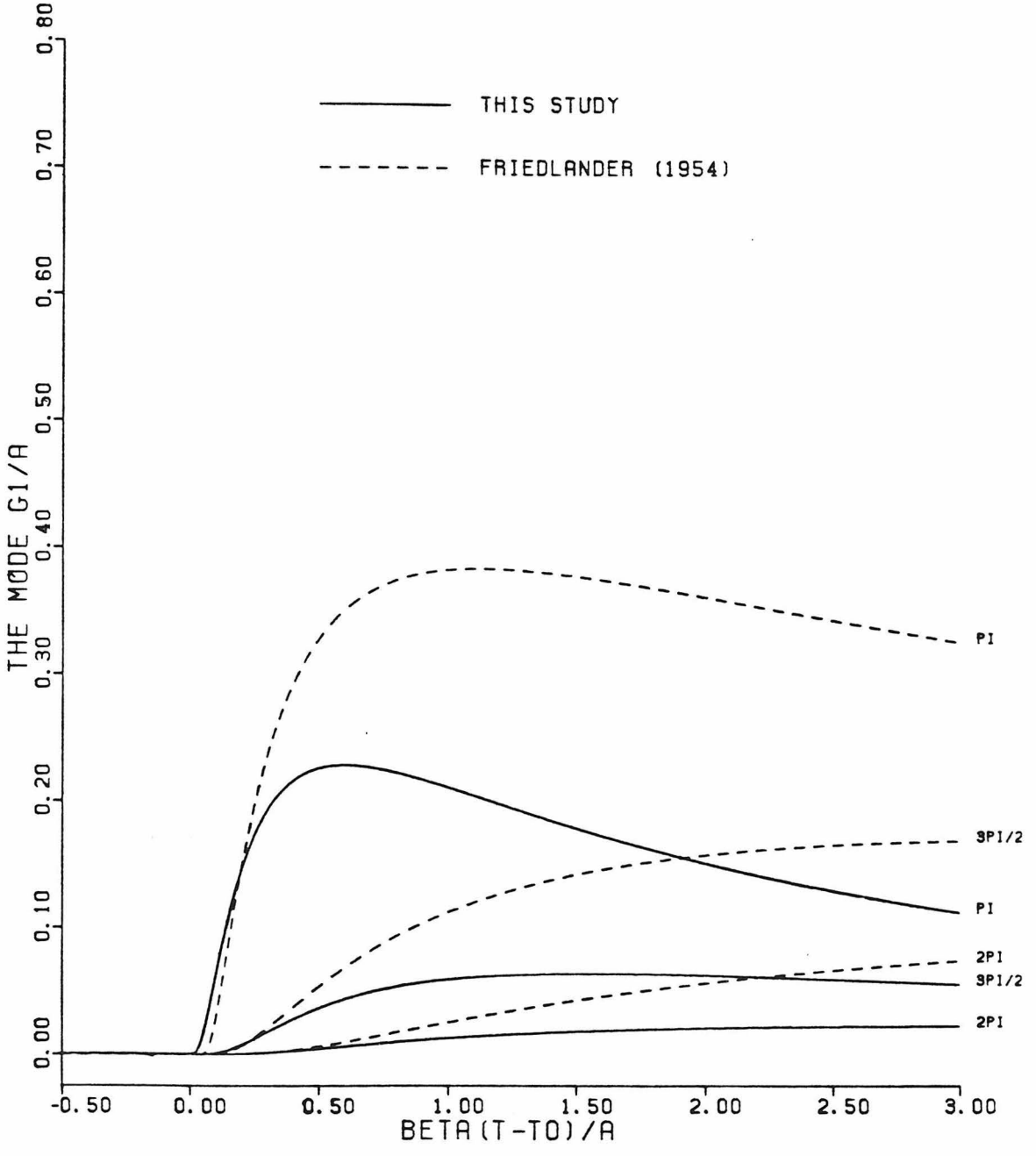

Figure E.4(f). Detail of Figure E.4(e). For times very close to the diffracted wave arrival time the two methods are in rough agreement. The time interval over which Friedlander's approximation is accurate is very short.

order modes fall off more rapidly with θ because $\mathrm{Im}(\mu_n(\omega)) \sim (n - \frac{1}{2})\omega^{1/3}$. Some of these results are shown in Figures E.5.

The delta function responses were not evaluated for $\theta < \pi/32$ because for small values of θ the integrand diminishes as $\omega^{-1/3}$ and the integral (E.27) converges slowly. The poor convergence for small θ is indicated by the acausality of the time series of Figures E.4a and E.4b. For $\theta \leq \pi/16$ high frequency results of Friedlander are probably the more accurate until well after passage of the first impulse.

For comparison to the BIE results of Chapter 3 the delta function results were convolved, in θ and t, with appropriate traction distributions by use of the FFT algorithm.

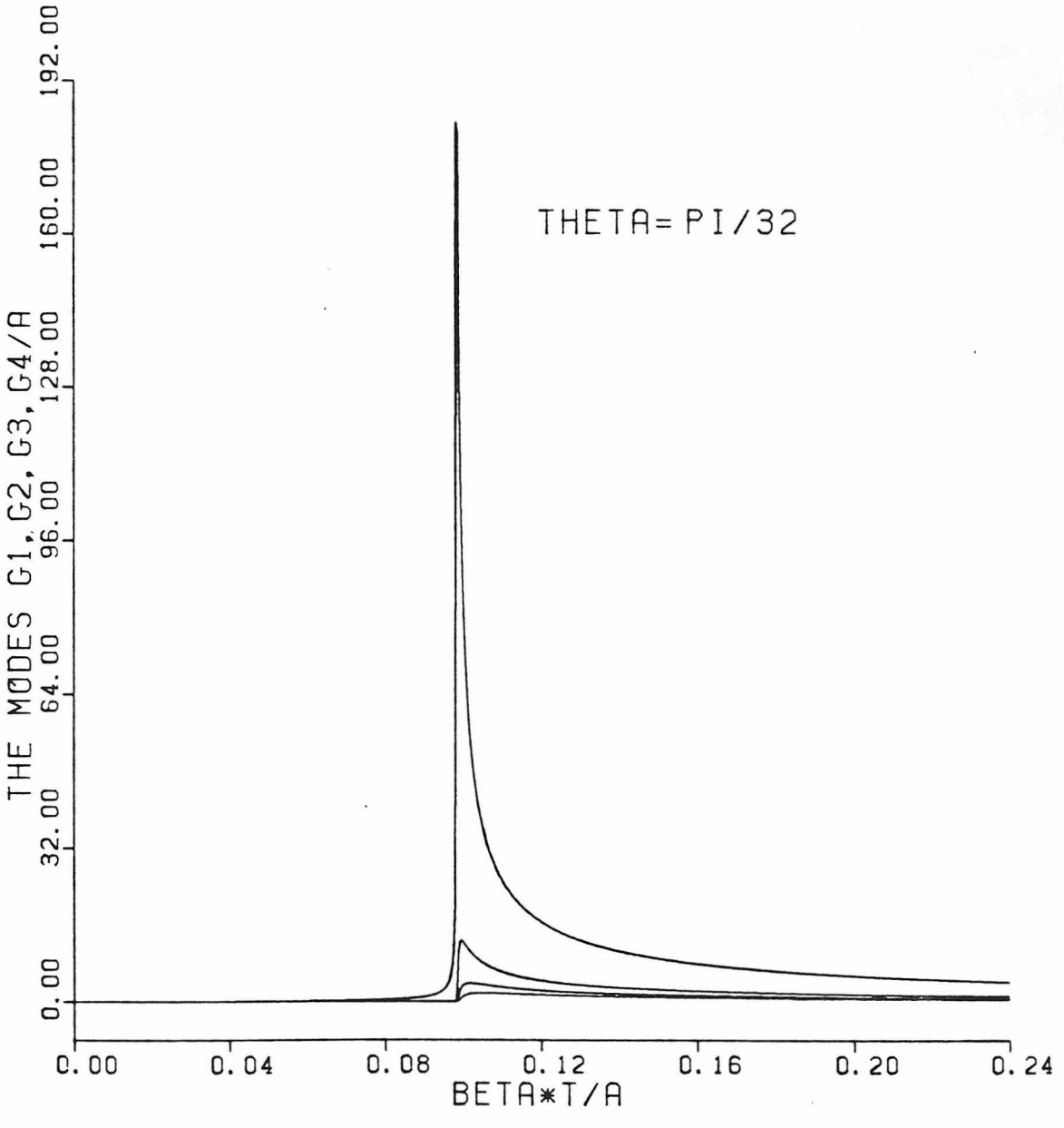

Figure E.5(a) Impulse response for modes 1 to 4 at $\theta = \pi/32$. The amplitudes decrease with increasing mode number. Mode 1 has substantial errors as indicated by its acausality. The mode sum converges slowly at this value of θ.

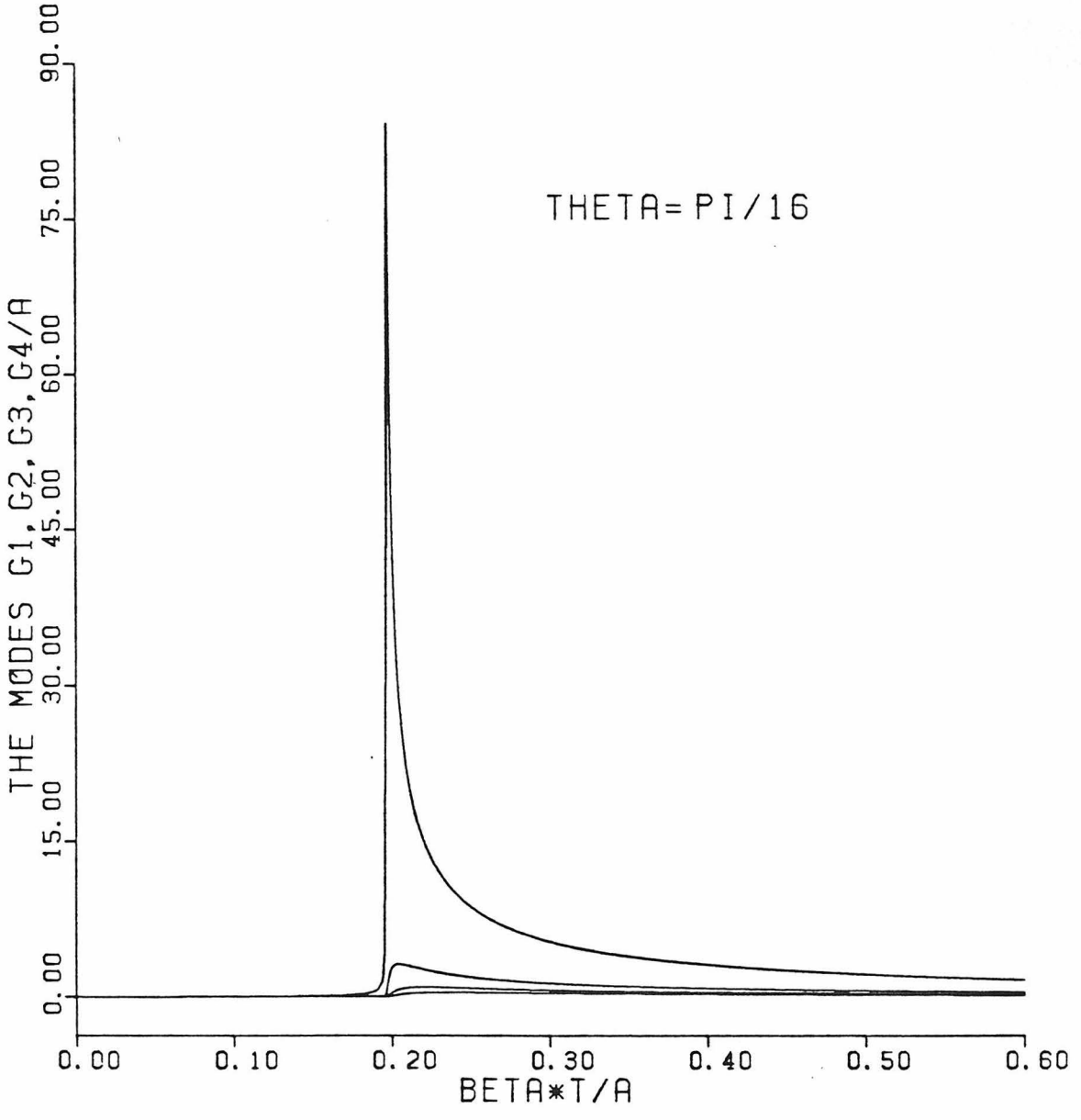

Figure E.5(b). Impulse response for modes 1 to 4 at $\theta = \pi/16$. Mode 1 has observable errors. Mode 4 is very small.

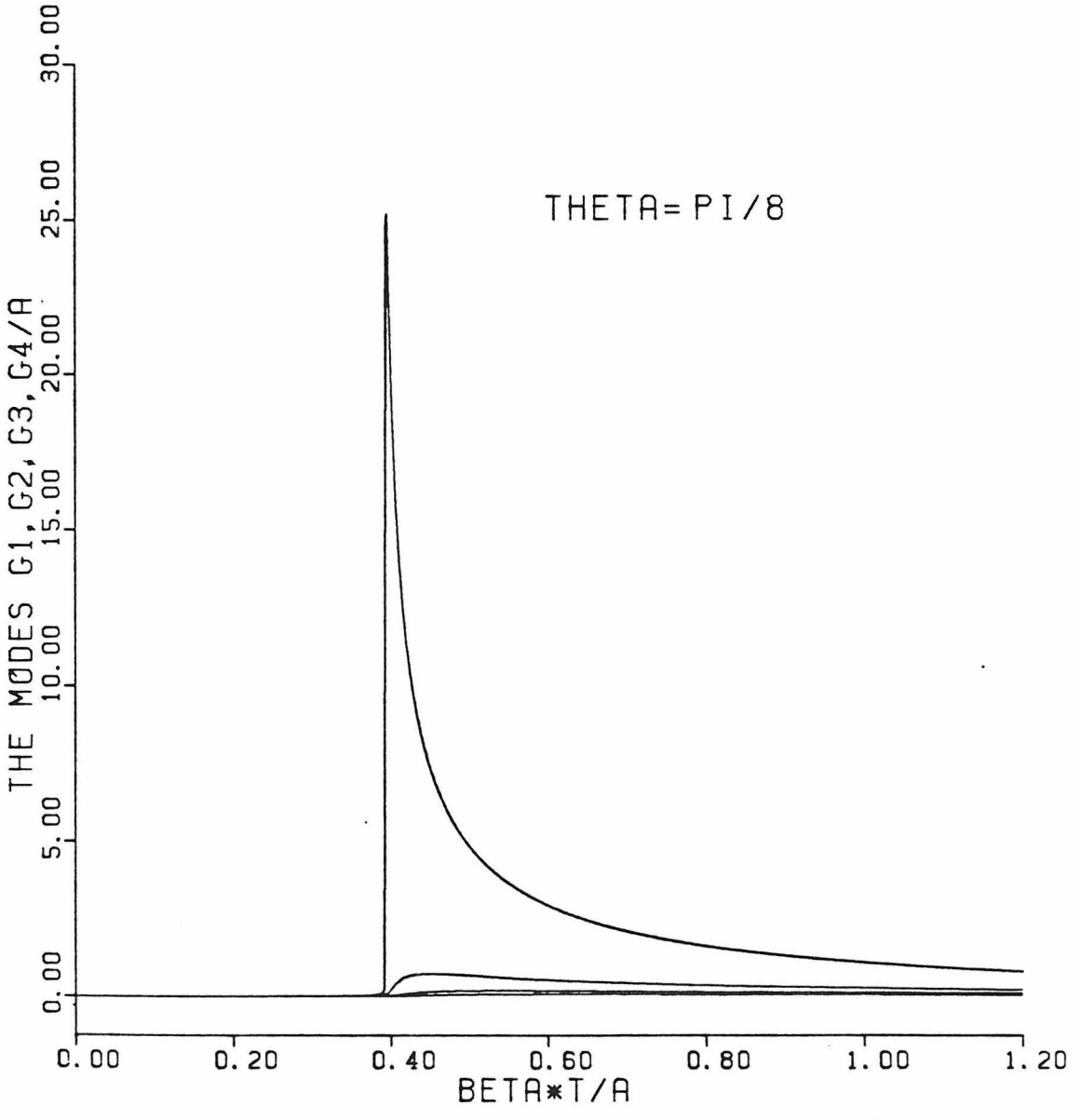

Figure E.5(c). Impulse response for modes 1 to 4 at $\theta = \pi/8$.

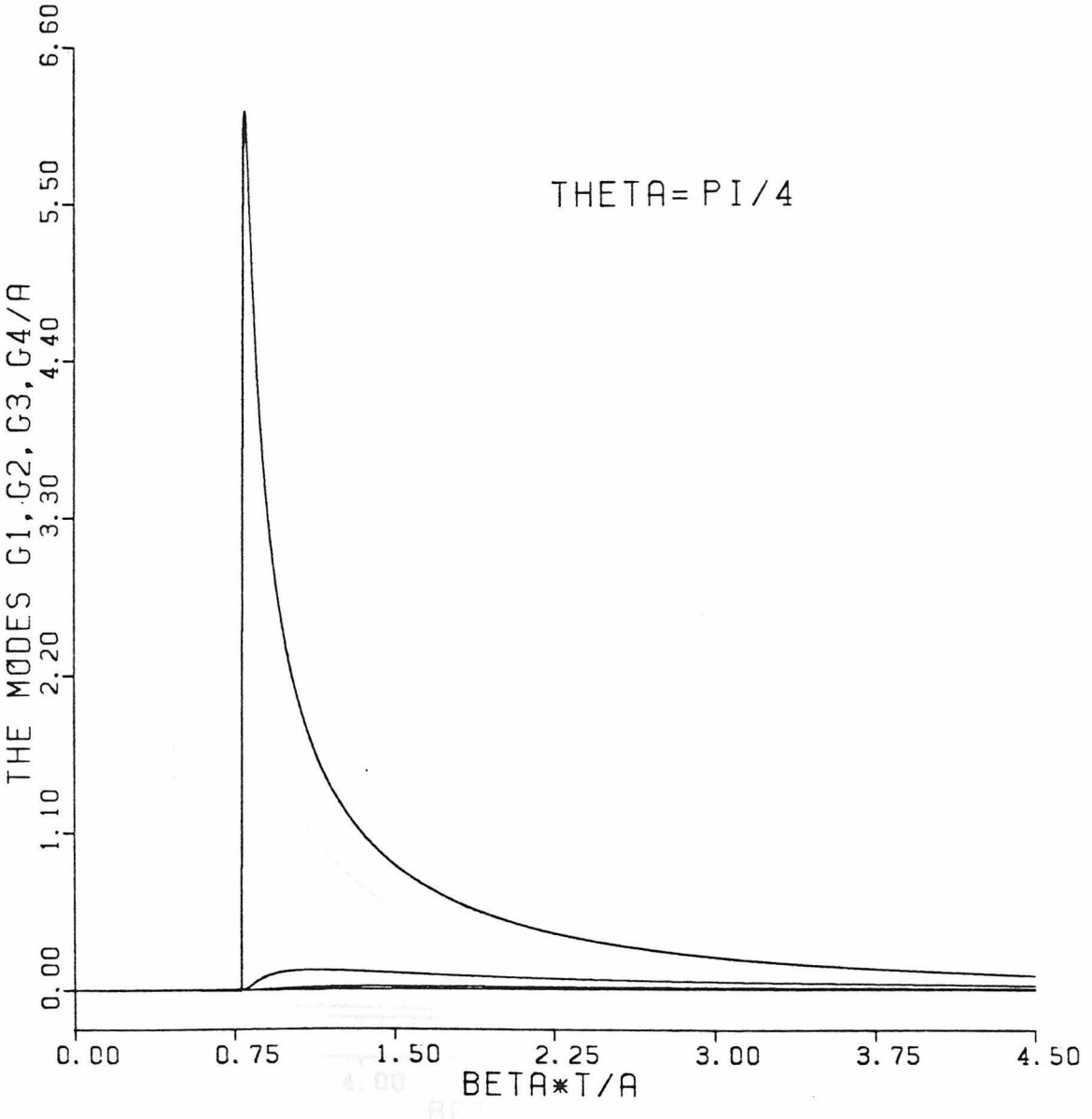

Figure E.5(d). Impulse response for modes 1 to 4 at $\theta = \pi/4$. Modes 3 and 4 are insignificant.

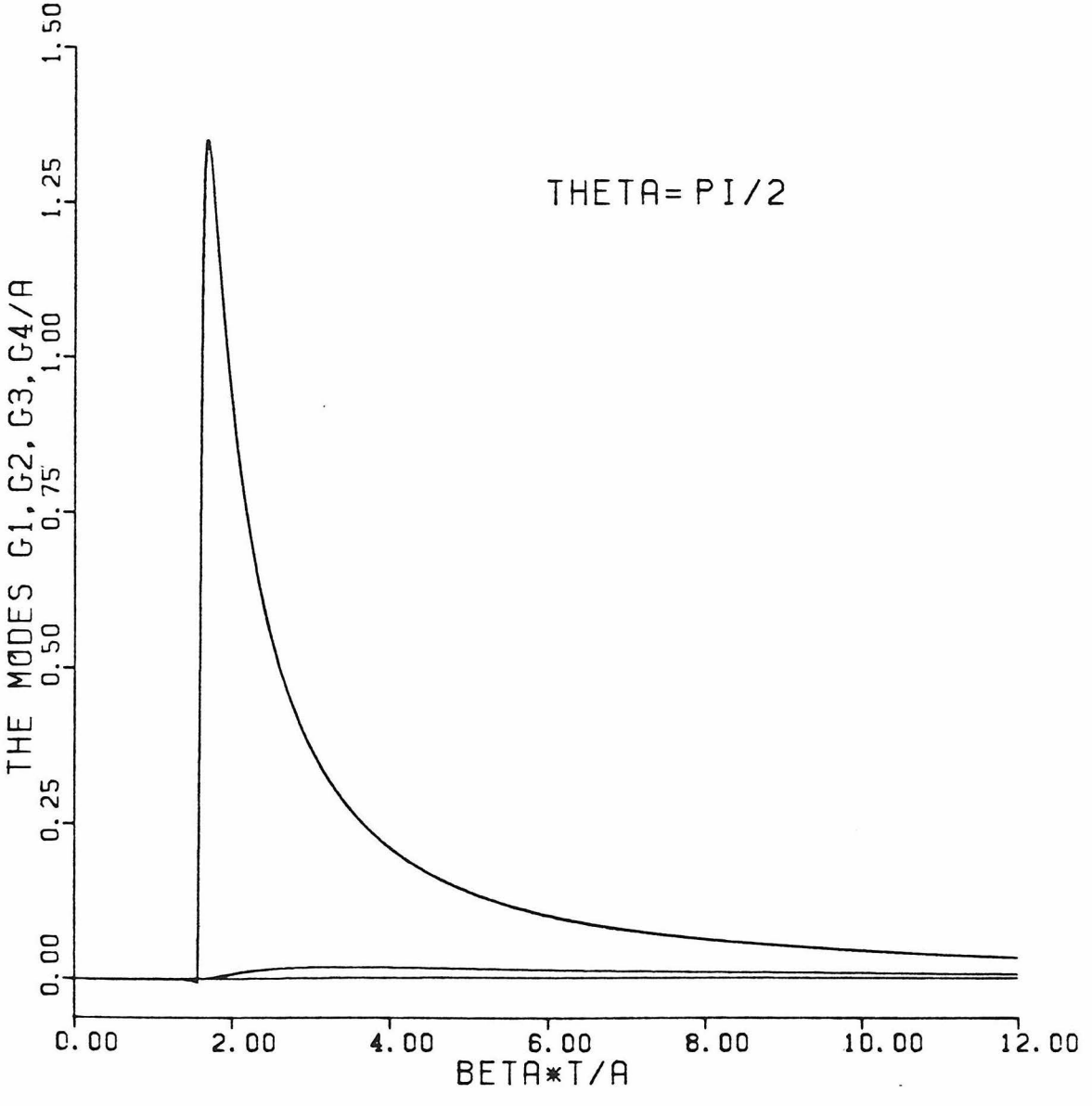

Figure E.5(e). Impulse response for modes 1 to 4 at $\theta = \pi/2$. Modes 2, 3 and 4 are insignificant.

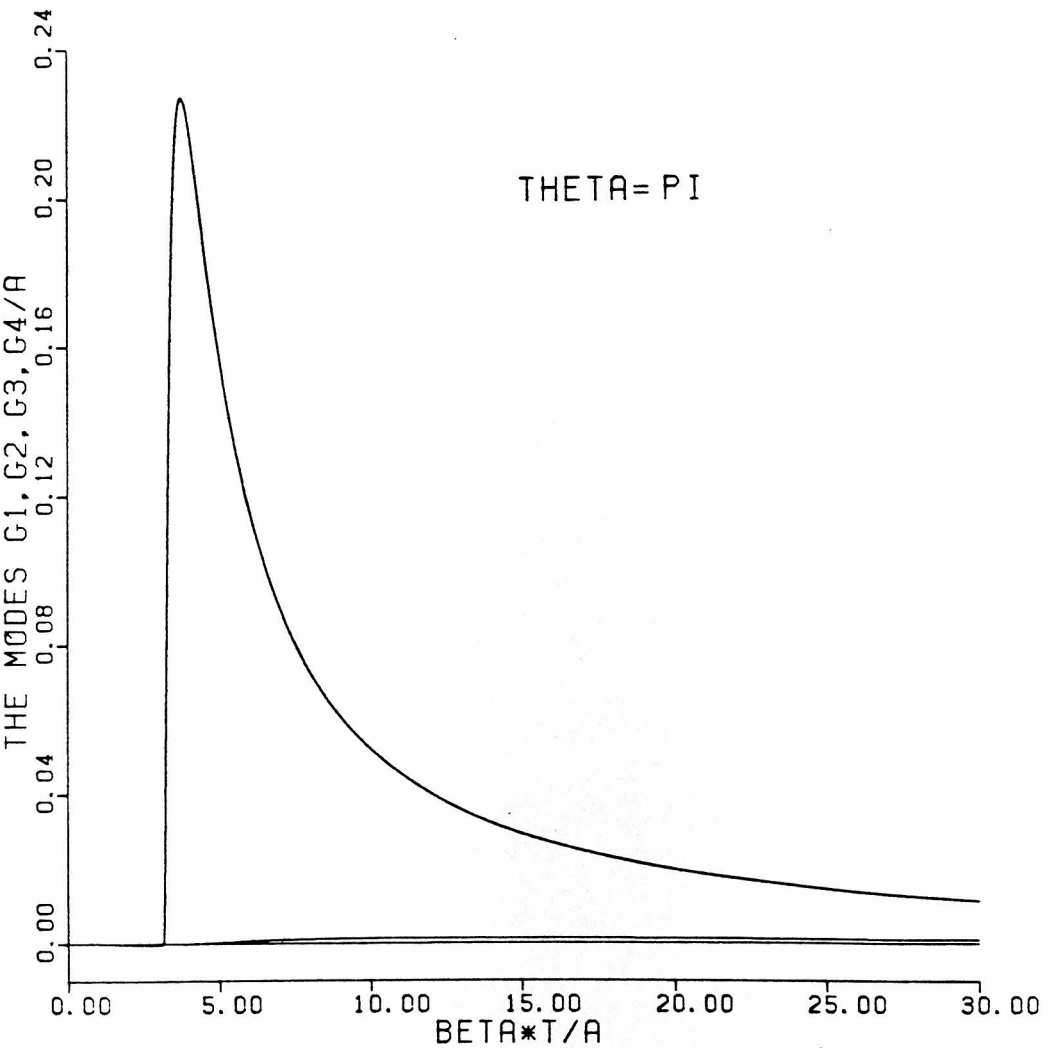

Figure E.5(f). Impulse response for modes 1 to 4 at $\theta = \pi$.